Master's of Science Thesis

Load catalogue for site suitability assessment and design optimization in offshore wind energy

Hadi Hammoud

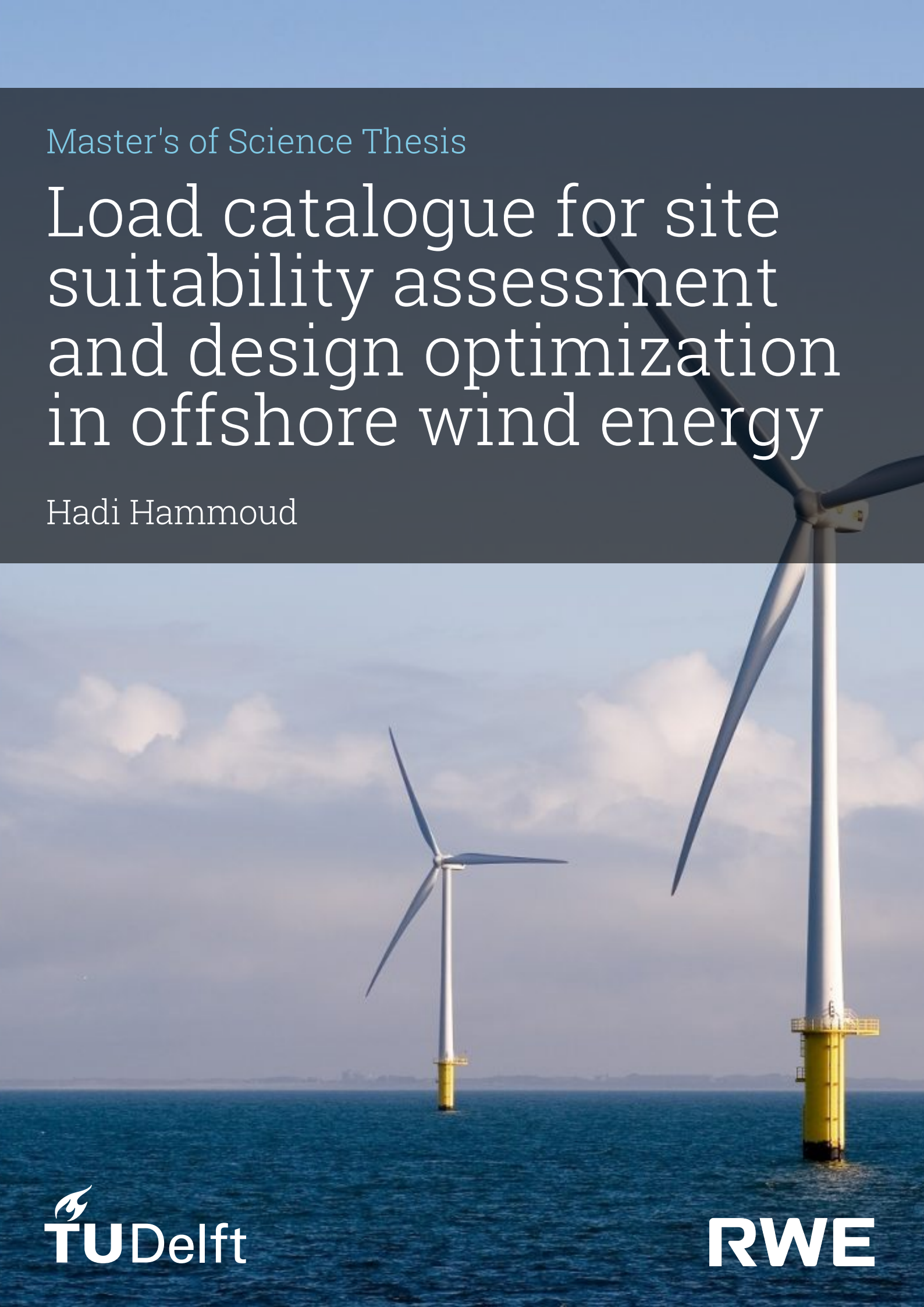

TU Delft

RWE

Load catalogue for site suitability assessment and design optimization in offshore wind energy

Master's of Science Thesis

by

Hadi Hammoud

Student Number:	5777178
University:	Delft University of Technology (TU Delft)
Master's Program:	Sustainable Energy Technology
Faculty:	Faculty of Electrical Engineering, Mathematics and Computer Science
Company:	This thesis was completed in collaboration with RWE
TU Delft Supervisor:	Prof. Dr. Simon Watson
RWE Supervisor:	Dr. Kai Irschik
Project Duration:	December, 2023 - August, 2024

TU Delft RWE

Acknowledgements

This thesis project is the culmination of my enriching two-year journey at TU Delft. This has been a crucial chapter of my life in which I grew immensely and which inspired and empowered me to make an impact in the sustainable energy transition.

The completion of this work would not have been possible without the support of several people and institutions. First and foremost, I extend my appreciation to TU Delft for providing the stimulating intellectual environment necessary for this research. I am also grateful to RWE, the company where I had the privilege to conduct my thesis. The resources that RWE provided were instrumental for the success of this work, and so were the great people that I met there.

A special thank you goes to Dr. Kai Irschik, my company supervisor at RWE. His expertise, mentorship, and cheerful spirit were essential to navigating the daily challenges of this project. I also would like to thank Prof. Simon Watson, my academic supervisor at TU Delft. His insightful feedback and his support have been significant in guiding my research.

Finally, I am grateful to my family and friends for their unwavering support. Their belief in me was the foundation upon which I could build this thesis, and their heart-warming encouragement was the motivation that pushed me through the hard times.

Thank you all for your contributions and support. This thesis stands as a testament to our collective efforts and shared commitment to advancing knowledge in our field.

Hadi Hammoud
Delft, August 2024

Abstract

In recent years, the offshore wind energy industry has been facing significant barriers, ranging from supply chain disruptions to financial challenges due to rising commodity prices and increasing inflation. To keep offshore wind energy competitive, more efforts towards reducing costs and accelerating project timelines are needed. The optimization of load calculation processes, which are central services in the development of any wind energy project, would significantly contribute to the achievement of these goals.

Conventionally, load calculations are performed using high-fidelity numerical models that simulate the dynamic response of the turbine or wind farm. Although this approach is highly reliable, it is computationally intensive. For applications requiring a large number of load evaluations, this translates into high costs and long project timelines. Load response models have been developed as a data-driven alternative to the high-fidelity numerical models, offering sufficiently reliable load estimates at a cheaper computational cost. However, currently-existing load response models suffer from key limitations pertaining to their applicability to modern offshore wind farms.

This thesis aims to develop a load catalogue, consisting of a database of fatigue loads that can serve as a foundation for a load response model, that better represents the loading conditions in modern offshore wind farms. The database is constructed by running dynamic simulations for a variety of operating conditions tailored to represent those observed in offshore sites. In addition, the thesis seeks to use the catalogue to study the impact of employing the different wind and wake models recommended by the IEC 61400-1 standard on calculated loads. Specifically, it does so by comparing the 90^{th} percentile and Weibull distribution turbulence intensity models, the Mann and Kaimal turbulence models, and the Frandsen and DWM wake models with respect to annual equivalent fatigue loads.

The analysis reveals that using a 90^{th} percentile for the turbulence intensity overestimates the annual fatigue loads obtained when sampling the turbulence intensity from a Weibull distribution by an average of 20% for tower base loads and 6% for blade root loads. Moreover, it shows that the Kaimal and Mann turbulence models lead to significantly different fatigue load estimates. Furthermore, it finds that Frandsen's effective turbulence model consistently predicts higher loads than the DWM model for inter-turbine spacings smaller than 5 rotor diameters, but it can predict lower loads for inter-turbine spacings exceeding 5 rotor diameters.

The study concludes that using a 90^{th} percentile turbulence intensity might lead to overly-conservative designs, which can be avoided by using a Weibull distribution that accurately characterizes site turbulence. Also, it suggests that a combined modelling approach to long-term fatigue calculations that selectively toggles between the Kaimal and Mann turbulence models based on the short-term environmental conditions is expected to yield more accurate load estimates compared to employing a single model exclusively. Lastly, it implies that the effective turbulence model might not always be conservative, especially for wind farms with large inter-turbine spacings.

Ultimately, this research culminates in the delivery of a valuable instrument, the load catalogue, that enhances decision-making in the preliminary stages of project development and facilitates the development of better load response models. Additionally, it enriches the theoretical understanding of load calculation methodologies, paving the way for the development of better load calculation techniques.

Contents

List of Figures

List of Tables

Nomenclature

Abbreviations

Abbreviation	Definition
DEL	Damage-Equivalent Load
DLC	Design Load Case
DWM	Dynamic Wake Meandering
IEA	International Energy Agency
IEC	International Electrotechnical Committee
LCOE	Levelized Cost of Electricity
LRM	Load Response Model
NTM	Normal Turbulence Model
NWC	Normal Wind Conditions
PCE	Polynomial Chaos Expansion
PDF	Probability Density Function
RWT	Reference Wind Turbine

Symbols

Symbol	Definition	Unit
U	10-minute mean wind speed	[m/s]
σ_U	10-minute wind speed standard deviation	[m/s]
θ	10-minute mean wind flow direction	[°]
I	10-minute turbulence intensity	[%]
I_{amb}	Annual average 10-minute ambient turbulence intensity	[%]
I_{ref}	Reference turbulence intensity	[%]
α	Wind shear exponent	[-]
ρ	Air density	[kg/m^3]
H_s	Significant wave height	[m]
T_p	Peak spectral period	[s]
m	Wöhler exponent	[-]
S	Load range	[Nm]
DEL	Damage-Equivalent Load	[Nm]
F	Annual equivalent load effect	[Nm]
T_{sim}	Simulation duration	[s]
T_{ref}	Reference time period	[s]
N_{eq}	Equivalent number of cycles	[-]

1

Introduction

1.1 Motivation

During the 28th meeting of the Conference of the Parties (COP28) held in the end of 2023, world governments pledged to triple renewable energy capacity by 2030 [1]. This effort came as a response to the imminent climate crisis as well as concerns about the security of energy supply and aims to accelerate the global transition towards a sustainable energy system. Being one of the most promising sources of renewable electricity, wind energy is expected to play a central role in this endeavor. In fact, according to the latest International Energy Agency (IEA) assessment, global wind energy capacity grew by 66% in 2023 alone. Moreover, based on current trends, renewables are expected to supply around 42% of the world's electricity by 2028, with wind accounting for a considerable 12.5%. Nevertheless, despite the unprecedented growth over the past year and the optimistic future trends, the world needs to do more to meet the COP28 targets [2].

Expanding the wind energy fleet to offshore locations is very promising as it offers a greater electricity generation potential compared to onshore sites while mitigating visual, noise and land use concerns. However, this comes at an additional capital cost due to the challenges involved in dealing with an offshore environment[1]. At the moment, most newly installed utility scale onshore wind capacity has a lower Levelized Cost of Electricity (LCOE) than new fossil fuel plants [2],[3]. The same cannot be said about offshore wind, for which the situation is more nuanced. Indeed, the offshore wind industry is facing several challenges, mainly in the supply chain [4]. The most notable of these are inflation and the increasing cost of the materials needed for offshore wind farm components, which led to a 20% rise in the capital cost of offshore wind between 2020 and 2023 [2]. Hence, to facilitate the growth of the offshore wind fleet, it is crucial to intensify efforts in cost reduction.

Optimizing the design of wind turbines and wind farms ultimately results in a lower LCOE. Load calculation is a core service within that process. With interfaces to almost all disciplines, load calculation feeds into the design of most wind turbine components and support structures. Moreover, site suitability assessment for potential wind farm projects and farm layout optimization are impossible without a precise estimate of the expected loads. Consequently, optimizing load calculation methods translates into a lower LCOE and a reduced environmental footprint from a life-cycle perspective. In addition, a streamlined load calculation work flow can help accelerate wind power project timelines. To these ends, this thesis seeks to contribute to the improvement of load calculation methods for offshore wind energy.

1.2 Problem Statement

Conventionally, load calculations in the wind energy industry are carried out with the aid of specialized aero-hydro-servo-elastic software. These computer programs implement multi-physics models of the wind turbine or wind farm and solve the corresponding differential equations in a step-by-step, time-marching manner. Throughout the years, numerous commercial simulation tools of that sort have been developed and rigorously validated, establishing them as widely trusted industry-standard solutions. However, even the most advanced of these tools are computationally intensive, despite the capabilities of modern computers. This becomes problematic in practical applications requiring numerous load evaluations, as the sheer number of simulations needed can quickly become intractable with a

[1] The challenges include harsh environmental conditions, more complex installation and maintenance, larger transmission distances and more.

compute-heavy approach. Effectively, this translates into increased costs and greater demands on human resources and time.

In practice, site suitability assessment is an application whereby project developers need to repeatedly evaluate structural integrity for various considered turbine designs and wind farm layouts. Other applications requiring iterative load calculations are any type of optimization problem where turbine loads are considered as constraints. These include the optimization of wind farm layouts, component designs and support structure designs. Another important application is wind turbine and wind farm control, where load estimates are factored into control strategies and their design. Thus, for all these applications, it is important to develop a faster, yet sufficiently reliable approach for load calculations that does not require the performance of many computationally-demanding simulations. Besides reducing costs and saving time, such a method would lessen the need for specialized expertise to perform advanced simulations and enhance decision making, especially in the early stages of project development.

1.3 Current Solutions and their Limitations

Over the years, many attempts have been made to address the aforementioned problem. The most prominent solutions fall under the umbrella of so-called Load Response Models (LRMs). Essentially, LRMs are surrogate models adapted for the purpose of load calculations. In the context of wind energy applications, this means that they can predict site-specific wind farm loads from operating conditions at a much lower computational cost as compared to the conventional load calculation approach, effectively addressing the problem raised in Section 1.2. These models are obtained by applying data-driven techniques to the results of high-fidelity aero-hydro-servo-elastic simulations. LRMs can therefore only approximate the precise solutions obtained through the standard load calculation method, but at a much cheaper computational cost. Fortunately, this trade-off turns out to be extremely favorable for many practical applications, particularly the ones described in Section 1.2.

The first step in LRM construction is to design an experiment whereby a set of input points is to be mapped to a corresponding set of outputs through direct evaluation of an accurate numerical model. In the context of this thesis, the inputs would be a set of parameters characterizing the operating conditions (i.e. wind climate, sea state, wind farm layout, etc.) at the considered site and the outputs would be ultimate loads, or fatigue loads or both. As for the numerical model, it would consist of a representative aero-hydro-servo-elastic turbine or farm model, typically integrated into a comprehensive software tool. Once the experiment is set up, it is launched, and data points start being generated. This process continues until a sufficient number of data points is obtained, forming a dataset of loads, or a load catalogue. After that, various mathematical techniques can be applied to this catalogue to identify the relationship that exists between its input and output data. This relationship is captured by a surrogate model, in this case the LRM, which approximates the original numerical model used to establish the dataset, in this case the aero-hydro-servo-elastic model. The concept of a surrogate model is illustrated for a 2D input space in Figure 1.1 below. In this illustration, the surrogate model takes the form of an analytical expression. However, this is not always the case as surrogate models can take many forms.

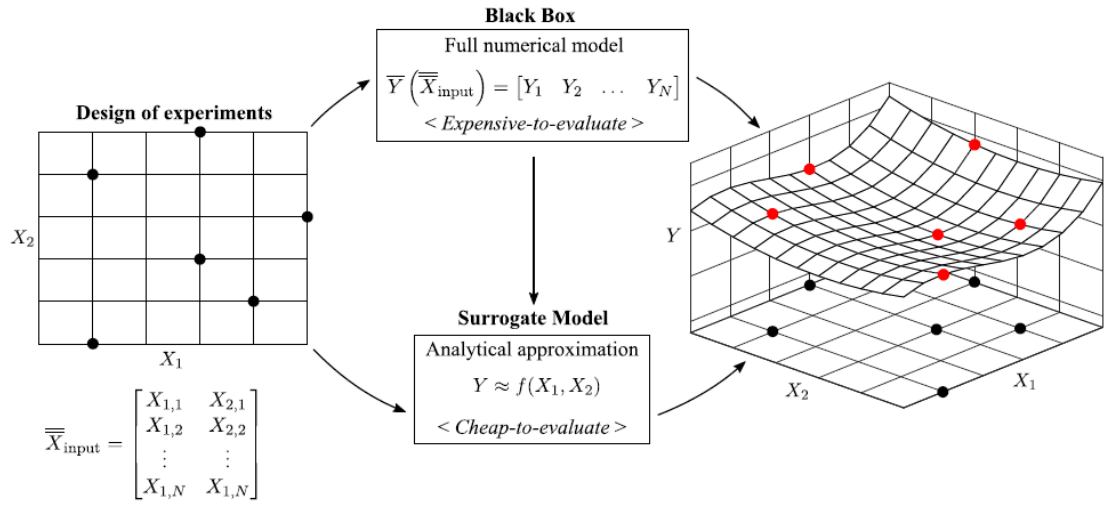

Figure 1.1: Illustration of the surrogate model concept (adapted from [5])

Up to this moment, numerous LRMs have been developed for wind energy applications. Moreover, many of them have been proven to quickly and reliably predict loads. Consequently, they have been integrated into commercial software tools, such as the site suitability tool offered by DNV [6] or the *LOAD RESPONSE* module of the *WindPro* software [7], which have been extensively utilized in the industry. Nevertheless, based on an extensive literature review (refer to Chapter 2), these LRMs still suffer from several key limitations. The most pertinent of these are that:

- They were established based on reference wind turbines with ratings that do not exceed 10MW, meaning that they may not be suitable for modern offshore turbines with power ratings reaching up to 20MW.
- They employ either the Kaimal model or the Mann model for turbulence modelling in the construction of the high-fidelity database. Given that one performs better than the other depending on the prevailing environmental conditions, the selection of a single model for the construction of the entire database might be a sub-optimal choice.
- They (most of them) model turbulence intensity as a 90^{th} percentile rather than sampling it from a Weibull distribution as per the latest IEC[2] recommendation. The latter might lead to overly-conservative load estimates.
- They (most of them) model wake effects based on Frandsen's effective turbulence model rather than the more accurate DWM model recently recommended by the IEC, which might consequently hinder the accuracy of load estimates.

Rather than proposing a novel solution to the problem raised in Section 1.2, this thesis attempts to contribute to the improvement of an existing one: LRMs. For this purpose, the limitations listed above are addressed in this thesis as part of its endeavor towards the development of better load calculation methods in offshore wind energy. In particular, this research focuses on the intermediate building block of an LRM: the load catalogue.

1.4 Objectives and Research Questions

The aim of this thesis is to contribute to the development of a fast and reliable load calculation process for site suitability assessment and design optimization in offshore wind energy. This is achieved through the establishment of a comprehensive, high-fidelity load catalogue tailored to represent fatigue loading conditions in offshore wind farms. The catalogue consists of an extensive database that maps wind farm operating conditions to the corresponding fatigue loads, quantified by damage-equivalent loads, for a variety of site conditions and farm layouts. The latter are defined by a combination of wind climate parameters and a parameter defining the wind farm's configuration, namely the inter-turbine spacing. As for the corresponding loads, they are calculated based on precise aero-hydro-servo-elastic simulations performed using high-fidelity numerical tools. Consequently, given that the turbine model employed in the simulations is representative of modern offshore turbines, the obtained database would reliably capture the fatigue loading situation across a considerable range of offshore sites. This means that the load catalogue has the potential to be used for the calibration of LRMs that do not suffer from the limitations outlined in Section 1.3.

This thesis therefore seeks to address the limitations of currently-existing LRMs and fulfill its broader aim through two main objectives, each supported by several sub-objectives:

1. To deliver a comprehensive, high-fidelity fatigue load catalogue tailored for offshore applications, built based on the latest modelling methods, and that can be used as a basis for the calibration of LRMs. This entails:
    i. Employing a reference wind turbine model that represents the characteristics of modern offshore wind turbines.
    ii. Choosing the catalogue's input parameters to ensure they are robust predictors of fatigue loads while representing a wide range of offshore site conditions.
    iii. Identifying and applying state-of-the-art wind and wake modelling methods in the load calculation process.
    iv. Providing tools and guidelines that facilitate the use of the load catalogue for LRM calibration.

[2] The International Electrotechnical Commission (IEC) is an international regulatory organization that sets standards respected throughout the wind energy industry. Refer to [8] for more information.

2. To use the catalogue to investigate the influence of employing different IEC wind and wake models on calculated loads. This entails:
    i. Comparing load results obtained using a Weibull distribution for turbulence intensity to those obtained with a turbulence intensity conventionally taken as the 90^{th} percentile of the distribution.
    ii. Comparing load results obtained using the Kaimal turbulence model to those obtained using the Mann turbulence model.
    iii. Comparing load results obtained using the DWM wake model to those obtained using the conventional effective turbulence model.

Based on the above, the main research question that guides this study is:

How can the compilation of a comprehensive, high-fidelity fatigue load catalogue contribute to the development of a fast and reliable load calculation methodology for site suitability assessment and design optimization in offshore wind energy?

This overarching question is supported by several sub-questions:

1. How can the load catalogue be designed to represent fatigue loading conditions across a wide range of offshore sites?

2. What wind and wake modelling methods should be employed in the establishment of the load catalogue to ensure a reliable estimation of fatigue loads that complies with the latest industry standards?

3. What is the impact of employing different wind and wake models on load predictions? How can the findings of this analysis be leveraged to better understand and interpret load calculation results and to develop better load calculation methods?

4. How can the obtained load catalogue be adapted for the calibration of practical LRMs?

5. What is the relevance of the obtained load catalogue to the improvement of load calculation methods for site suitability assessment and design optimization in offshore wind energy?

By addressing the outlined research questions, this thesis aims to bridge the gap in current methodologies, setting a foundation for improved approaches to load calculation within the offshore wind energy sector. Moreover, it seeks to enhance the understanding of load calculation methodologies and their impact on predicted loads. The research is anticipated to contribute valuable insights in an endeavor to reduce costs and facilitate the development of wind energy projects. Ultimately, the findings of this study are expected to support the expansion of the offshore wind energy fleet in alignment with global renewable energy targets.

1.5 Thesis Outline

This thesis is organized as follows. Chapter 2 is a literature review that examines several preliminary topics providing a comprehensive background for what follows. Then, Chapter 3 presents the methods employed in this thesis, describing the used methods and tools, the simulation setup, the load calculation framework, the process of load catalogue construction, and the validation methodology. After that, Chapter 4 presents the findings of the thesis and discusses their implications. Finally, Chapter 5 summarizes the study's outcomes and suggests directions for future research and practical work.

2

Literature Review

This chapter systematically reviews the essential literature laying the groundwork for this thesis. Section 2.1 begins by discussing wind turbine design standards, focusing on the type certification framework established by the International Electrotechnical Commission (IEC). Section 2.2 follows by describing the process of site suitability assessment, the practical application most relevant to this thesis. Subsequently, conventional load calculation practices are explored in Section 2.3 in the context of site suitability assessment. After that, Section 2.4 and Section 2.5 review the climate and wake modelling approaches, respectively, employed in load calculations. The chapter concludes with Section 2.6, which gives an extensive and critical overview of the load response models that have been developed throughout the years.

2.1 Wind Turbine Design Standards

Standards are at the core of modern-day engineering practices. They provide guidelines and set strict requirements that are intended to promote the safety, reliability, efficiency and scalability of engineering applications. The last point is particularly important for the wind power industry, whose growth is crucial to meet global renewable energy targets. This is illustrated in Section 2.1.1, which explains the important role of design standards in ramping up wind energy capacity. Then, Section 2.1.2 discusses the IEC 61400-1 standard, which is the globally-accepted reference for wind turbine design.

2.1.1 The Importance of Standards for Wind Energy Scalability

Design standards are essential for the expansion of the wind energy sector. In practice, it is inefficient to tailor wind turbine designs for a specific project site as this would not allow for large-scale manufacturing. Instead, standards introduce a unified classification system for wind turbine designs based on their resilience to well-defined environmental conditions (naturally, the turbine classes reflect their size and power rating). This enables manufacturers to mass-produce wind turbines, which would then be assigned a specific design class. Project developers would then select the most suitable turbine class for their project based on their assessment of the considered site. Having selected the right class, developers can then choose the most convenient turbine model from catalogues provided by different manufacturers.

Besides boosting WTG manufacturing scalability, standardization leads to more optimal WTG designs as manufacturers can focus on improving a few turbine models instead of many custom-made machines. For the same reason, this also has benefits for WTG modelling as efforts are concentrated on a small set of systems. Consequently, improvements in these two areas lead to faster strides towards the growth of the wind energy base.

2.1.2 The IEC 61400-1 Standard

The IEC 61400 standards, in their various editions, are the most well-known and trusted standards in the wind power industry. Although not necessarily mandated by law, compliance with the IEC standards is generally regarded as good industry practice and is respected by most industry players. Lack of compliance, on the other hand, hinders the credi-

bility of the wind turbine manufacturer or the wind farm developer and may even be legally prohibited.

The IEC 61400-1 standard [9] provides guidelines and recommendations regarding wind turbine design. The central, and perhaps most important component of the standard is the type certification framework that it introduces for the classification of wind turbine systems. In this framework, the IEC begins by defining a set of 13 wind turbine classes based on a corresponding set of reference wind climate parameters as tabulated in Table 2.1. In particular, the classification is based on two major wind climate parameters, namely the mean wind speed and the turbulence intensity. In addition, the reference parameters in Table 2.1 were chosen such as to represent a broad range of potential wind farm sites. Furthermore, the 13th IEC wind turbine class, Class S, allows manufacturers to define their own reference wind climate parameters for special applications.

Table 2.1: Wind turbine design classes defined in IEC 61400-1 ed.4 [9]

Wind Turbine Class		I	II	III	S
U_{ave}	[m/s]	10.0	8.5	7.5	Values specified by manufacturer
U_{ref}	[m/s]	50.0	42.5	37 .5	
$U_{ref,T}$	[m/s]	57.0	57.0	57.0	
A+	I_{ref} [-]		0.18		
A	I_{ref} [-]		0.16		
B	I_{ref} [-]		0.14		
C	I_{ref} [-]		0.12		

U_{ave}: Average annual 10 min. mean wind speed
U_{ref}: Reference 10 min. mean wind speed
I_{ref}: Reference value for turbulence intensity at 15m/s
Note: all values evaluated at hub height

After establishing the classification system, the framework defines a series of Design Load Cases (DLCs), each characterized by a specific combination of operating conditions (normal operating, startup, fault, idling, etc.) and environmental conditions (normal wind speed, extreme wind speed, extreme turbulence, etc.). The DLCs can be divided into two main categories based on the loading state of the wind turbine under investigation: Fatigue Limit State (FLS) DLCs and Ultimate Limit State (ULS) DLCs. As shown by research and proven in practice, the FLS is often the most decisive when it comes to wind turbine structural integrity [5]. Consequently, it is the focus of this thesis and its corresponding DLCs are listed in Table 2.2.

Table 2.2: DLCs in FLS defined in IEC 61400-1 ed.4 [9]

Design Load Case	Operating Conditions	Environmental Conditions	Wind Speed Range
DLC 1.2	Power Production	NTM	$U_{in} < U < U_{out}$
DLC 2.4	Power Production with Fault	NTM	$U_{in} < U < U_{out}$
DLC 3.1	Startup	NWP	$U_{in} < U < U_{out}$
DLC 4.1	Normal Shutdown	NWP	$U_{in} < U < U_{out}$
DLC 6.4	Idling	NTM	$U < U_{ref}$

NTM: Normal Turbulence Model
NWP: Normal Wind Profile
U_{in}: Cut-in hub-height mean wind speed
U_{out}: Cut-out hub-height mean wind speed

When a wind turbine manufacturer applies for type certification, he must prove that his turbine meets well-defined performance, structural integrity, safety, environmental impact and grid compliance criteria among others. This should be done for every single DLC and under the reference wind climate conditions corresponding to the class that the manufacturer is applying for. If the considered turbine fulfills the certification criteria, it is awarded a certificate assigning it a given class and thereby documenting its compliance with the IEC standards. In practice, independent certification bodies are in charge of certifying newly manufactured turbines and of ensuring compliance with the IEC standards

through continuous monitoring, auditing and inspection. Some of the most widely recognized certification bodies in the industry are DNV GL, UL and TÜV SÜD.

As will become clear in Section 2.2, the IEC type certification framework plays a central role in wind farm development as it helps in standardizing procedures and facilitating cooperation between manufacturers and project developers. By the same token, the classification system introduced in this section will be used in the definition of the load catalogue developed in this thesis.

2.2 Site Suitability Assessment

The first step in the development of a wind power project is the identification of a potential site having favorable wind climate conditions. After that, one or multiple commercial wind turbines must be selected for the project. In general, to maximize energy density at the lowest cost, developers will seek the highest-rated turbine that is precisely strong enough to withstand the site's environmental conditions. The question that arises then is the following: is the considered wind turbine suitable for the project site? Suitability in this context hinges on one specific assurance: the turbine's ability to endure without failure throughout its entire operational life at the designated site. Site suitability assessment is therefore about evaluating whether or not a considered commercial wind turbine will survive for the target project duration under the suggested site's environmental conditions.

The IEC type certification framework is particularly useful for answering the question raised above. In fact, based on this framework, the IEC standard 61400-1 [9] suggests a systematic procedure for site suitability assessment. Particularly, the standard states that the following two approaches may be applied to assess the suitability of a given site:

1. A demonstration that site-specific wind climate conditions are no more severe than those assumed for the design of the certified wind turbine. In the remainder of the text, this approach shall be referred to as 'site suitability assessment with reference to wind climate'.

2. A demonstration of structural integrity for wind climate conditions each equivalent to or more severe than those observed at the site. This approach shall be referred to as 'site suitability assessment with reference to loads'.

For both of these methodologies, the IEC specifies the relevant wind climate parameters required for the analysis. This selection is informed by thorough research and practical expertise concerning the impact of various wind climate metrics on wind turbine loads. The six required parameters are the following, all evaluated at hub height:

1. 10 min. mean wind speed (U) distribution (Weibull distributed)
2. 10 min. extreme mean wind speed (U_{ref}) (50 year recurrence period)
3. 10 min. wind speed standard deviation (σ_U) (90% quantile)
4. 10 min. wind shear exponent (α) (mean value)
5. Air density (ρ) (mean value)
6. Wind inflow inclination angle (ϕ) (maximum value)

In addition to defining the required wind climate parameters, the IEC standard provides guidelines for performing the on-site measurements and data processing required to derive these parameters. For instance, the standard requires that each parameter, except air density, must be evaluated across all directions within sectors of 30° or less. Moreover, it is stated that wind speed bins no wider than 2m/s shall be used for the computation of the Weibull distribution parameters as well as the turbulence (σ_U). Many more instructions are given in the standard. For further details, readers are advised to consult the document directly.

Two other important aspects affecting site suitability assessment are addressed by the IEC standard, namely the influence of wakes and surrounding terrain complexity. Wake effects are typically treated according to the effective turbulence approximation developed by Fransden[1] [10], although an alternative model has been recently suggested in the latest edition of the standard. The effective turbulence model accounts for wake effects by modifying the ambi-

[1] Details on the application of the model can be found in Annex E of the IEC 614000-1 standard [9].

ent turbulence intensity based on the distance from surrounding turbines and their respective thrust coefficients. The corrected turbulence intensity is then used for site suitability assessment, whether with reference to reference to wind climate or with reference to loads. As for the terrain complexity, it should be evaluated by investigating the deviation of the surrounding terrain topography from a horizontal plane. The specific details of this analysis are out of the scope of this thesis.

Additional site conditions must also be examined during site suitability assessment as per the IEC. These include environmental conditions such as temperature, icing, humidity and solar radiation among others. Also, soil conditions and earthquake risk must be assessed. Furthermore, the electrical network conditions around the designated site must be carefully qualified. Nonetheless, these facets of site suitability assessment are less important than the aforementioned ones and will therefore not be addressed in this thesis.

In site suitability assessment with reference to wind climate, the site-specific wind climate parameters are first derived from on-site measurements according to the IEC guidelines. Then, these are compared to the reference wind climate parameters corresponding to the class of the wind turbine considered for the project (see Table 2.1). Guidelines for performing the comparison are also provided in the standard. If all of the site-specific wind climate parameters pass the IEC checks, the turbine class is deemed suitable for the designated site.

Referring to Table 2.1, it can be seen that not all the IEC reference wind climate parameters are explicitly listed. However, the standard provides all the information needed to derive the missing parameters from the classification table. Indeed, to obtain the reference Weibull distribution, the shape parameter is taken as 2.0 and the scale parameter is determined directly from U_{ave}. U_{ref} is in turn calculated from the Weibull distribution. Moreover, the wind speed standard deviation is computed from I_{ref} as a function of mean wind speed and the wind shear exponent is simply taken as 0.14 for offshore locations. As for the air density, it is given a reference value of 1.225kg/m^3. Finally, the reference flow inclination is given an absolute value of 8°.

The utility of the type certification framework becomes evident when considering site suitability assessment with reference to wind climate. Indeed, the rationale behind this is clear: if the turbine was proven to withstand a given wind climate (i.e. the reference wind climate), then it must be capable of withstanding a less harsh wind climate (i.e. the site-specific wind climate). This spares project developers the need to perform site-specific load calculations, leading to notable time and cost reductions. Thus, this approach is almost always preferred. Nevertheless, for most realistic projects, at least one wind climate parameter will be in violation of the reference climate [5]. In that case, developers must resort to direct site suitability assessment with reference to loads, which is the subject of Section 2.3.

2.3 Load Calculations for Site Suitability

When site suitability cannot be established through a comparison of wind climates, it needs to be demonstrated through direct load calculation. In that case, it must be shown that, for a given commercial turbine, the site-specific loads do not exceed the reference values documented during the type certification of that turbine. This requires an accurate estimation of the operational loads on each of the turbine's main structural components and throughout its entire lifetime. In the industry, this is typically carried out with the aid of specialized computer models. These models take as input a timeseries describing the evolution of the incident wind field as a function of time at the considered site. Based on that and the turbine's specifications, the models predict the resulting loads on the different turbine components over a given timeframe. The resulting loading history is then analyzed and converted into a smaller set of Ultimate Loads (ULs) and Damage-Equivalent Loads (DELs), which are representative of the turbine's loading situation in the ULS and FLS respectively. These ULs and DELs are then compared to those obtained during the type certification of the turbine to verify site suitability.

In most cases, DELs are the decisive determinants of wind turbine structural integrity [5]. Hence, further elaboration is due on the DEL framework for fatigue load calculations. Before that, Subection 2.3.1 briefly describes wind turbine modelling and provides some examples of popular software tools in the industry. Then, Subection 2.3.2 introduces the concept of reference wind turbines and highlights their importance for research and site suitability assessment. Finally, the DEL framework is discussed in Subection 2.3.3, focusing on how it facilitates the process of site suitability assessment with reference to loads.

2.3.1 Wind Turbine Modelling

As the name suggests, aero-hydro-servo-elastic models are a set of computer codes divided into several modules. Two of these modules are particularly crucial for load calculations: the aerodynamics module and the elastic module. The aerodynamics module captures the interaction between the in-flowing wind field and the turbine, while the elastic module translates that into the resulting loading state of the different turbine components. Naturally, these numerical models are based on corresponding physics models. Nowadays, most aerodynamic modules rely on Blade-Element Momentum (BEM) theory to compute wind forces on turbine blades [11],[12]. Then, different techniques can be applied to calculate the resulting internal loads. The most popular methods are multi-body dynamics and finite-element methods [11],[12].

Wind turbine modelling is now a relatively mature science. Indeed, the underlying theory is advanced and numerous modelling tools have been developed and repeatedly validated. For instance, the design and simulation software *Bladed* developed by DNV [13] has now become very popular in the industry and has been validated against field data in multiple studies [14],[15]. However, Bladed is a relatively costly commercial product mainly intended for wind turbine manufacturers, project engineers, consultants, and certification agencies. Nevertheless, other modelling tools are available for a wider audience. A notable example is *OpenFAST*, developed by the National Renewable Energy Laboratory (NREL) [16]. The distinctive features of this software is that it is publicly available, free of charge, and open-sourced, meaning that anyone can contribute to its debugging and improvement. OpenFAST is also renowned in academia and in the industry and has been extensively validated for both onshore and offshore applications [17], [18], [19], [20]. For these reasons, OpenFAST was chosen for performing the simulations involved in this thesis.

2.3.2 Reference Wind Turbines

In addition to wind climate data, simulation tools need to be fed the specifications of the considered turbine (blade and tower geometry, component masses and stiffnesses, damping coefficients, controller gains, etc.) in order to compute useful results. For commercial turbines, this data is held as exclusive property of manufacturers and is thereby inaccessible to the general public. This is problematic for both researchers and other industry parties, including, in many cases, site suitability assessors.

To address this issue, generic Reference Wind Turbines (RWTs) have been developed. These RWTs are deliberately designed to be representative of a certain range of commercial machines by employing standardized components having carefully selected properties. However, unlike commercial turbines, RWT specifications are made available to the public. This makes RWTs extremely valuable as they provide benchmarks for design, analysis and modelling for a wide range of applications [21],[22]. Moreover, they foster collaboration between academia, research institutes and industry [21],[22]. Furthermore, numerical models based on the publicly-accessible specifications of RWTs can be utilized when the proprietary data of commercial turbines is unavailable. In fact, this generic approach has been shown to accurately model the behavior of real turbine and can therefore be reliably employed [5], [23]. This is particularly important for site suitability assessment as developers might not have access to the exact specifications of commercial turbine models, especially at the early stages of project development.

A single RWT cannot be representative of all the wind turbines available on the market. Thus, different RWTs have been established for different rotor sizes and power ratings. Some prominent examples developed by the NREL are the four WindPACT turbines (750kW, 1.5MW, 3MW and 5MW) [24] and the 5MW reference turbine [25]. Higher-rated RWTs have also been established, such as the 8MW LEANWIND turbine [26] and the 10MW turbine by the Technical University of Denmark (DTU) [27]. All of these RWTs have a similar architecture, which is uncoincidentally typical of commercial wind turbines. They all have three blades and a gearbox, face upwind, operate at variable speed, and employ conventional pitch and torque control strategies for rotor speed and power output regulation. Moreover, their cut-in, rated and cut-out wind speeds are around 3m/s, 12m/s and 25m/s respectively. Evidently, this is also not a coincidence as these values were shown to be optimal from an economical perspective [28].

The RWTs mentioned so far are well-known and have been extensively utilized in academia. Nevertheless, these RWTs are starting to become outdated as the industry shifts towards higher-rated turbines and as direct-drive architectures become more prevalent [22]. As a response, the International Energy Agency (IEA) proposed two revised designs for RWTs that reflect newer wind turbine technology [22]. The suggested RWTs are rated 3.4MW and 10MW and are intended for onshore locations with moderate winds (Class III) and offshore locations (Class I) respectively. In addition, both geared and direct-drive configurations were proposed for the 10MW RWT. In a more recent publication, the IEA outlines the design of an even higher rated RWT with a power rating of 15MW [21]. This RWT is a direct-drive machine having a 240m rotor diameter and is intended to represent state-of-the-art large offshore machines resting on a monopile support structure. Since this thesis is focused on current and future offshore applications, the IEA 15MW

turbine was selected as RWT.

2.3.3 The DEL Framework for Fatigue Load Analysis

Site suitability assessment with reference to loads entails the comparison of site-specific DELs (DEL_{site}) to type certification DELs (DEL_{ref}) for a given wind turbine. These two DEL sets are derived from load data obtained through extensive aero-hydro-servo-elastic simulations under the site-specific wind climate and the reference wind climate respectively. The performance of the simulations and the processing of the load data into DELs are both subject to IEC guidelines [9].

The main requirement of the standard is that all prescribed DLCs must be covered in the generation of the load data. Moreover, it is required to carry out the simulations with reliable aero-hydro-servo-elastic models that have been validated by measurements and to thoroughly document the employed calculation methods, preferably with references to verification studies. Several criteria are also imposed on the characteristics of the simulated wind field and on the loading sources accounted for in the calculations. Furthermore, restrictions are imposed on the minimum size of wind speed bins and, for some DLCs, on the minimum number of simulations carried out for a given mean wind speed.

Once a loading history is obtained, it is converted into a corresponding set of DELs through a standardized process. The first step is to apply *Rainflow Counting* [29] to identify distinct load cycles in the loading history. Then, Miner's rule [30] is applied to calculate the resulting fatigue damage of these loading cycles based on a component-specific SN-curve [31]. Finally, the fatigue damage is converted into a DEL with an associated equivalent number of cycles via a simple formula. This methodology was applied in the fatigue calculations presented in this thesis and is therefore described in more detail in Chapter 3.

Ultimately, a DEL is a single number quantifying the intensity of the fatigue loading subjected to a given turbine component over its entire operational lifetime in a specific wind climate. This makes DELs ideal metrics for reporton loads in a load catalogue, justifying their use in this thesis. For the same reason, the benefit of the DEL framework for site suitability assessment becomes clear: instead of comparing entire load histories across sites, it is sufficient to compare a small set of DELs. In fact, for each major turbine component (indexed by i), a Load Index (LI_i) can be defined as in Equation 2.1. Subsequently, a site can be deemed suitable with respect to the FLS only when $LI_i \leq 1 \, \forall \, i$, that is for all turbine components. Furthermore, it can be easily inferred that LI_i reflects the relative component lifetime across sites. This insight is particularly informative for lifetime extension decisions whereby a certain turbine component can be replaced to extend the machine's lifetime.

$$LI_i = \frac{DEL_{site,i}}{DEL_{ref,i}} \tag{2.1}$$

Although it is recommended by the IEC standard, the DEL framework is not flawless and suffers some limitations. The first major limitation is due to the use of Miner's rule. The latter was derived from test results based on aluminum alloys and might not be suitable for other materials, especially the modern composite utilized in turbine blades [5]. Another shortcoming of the framework is its reliance on SN-curves, which are only an approximation of material fatigue behavior [5]. Nevertheless, the DEL framework is still standard industry practice, mainly by virtue of its simplicity. This makes it instrumental for streamlining load calculations and facilitating cross-site load comparisons. Besides that, the fact that it can reduce entire loading histories into a small set of scalars makes it crucial for the application of surrogate techniques. More on this follows in Section 2.6.

On a final note, the load calculation practices described in this section are by no means restricted to site suitability assessment. They are rather prevalent in the wind energy industry across applications ranging from support structure design to wind farm control. The discussion on site suitability assessment serves to underscore the practical significance of these load calculations.

2.4 Climate Modelling

In Section 2.3, it was established that DELs are associated to a specific wind climate. In particular, they are derived based on aero-hydro-servo-elastic simulations taking wind field timeseries as input. Two major questions arise at this point: What is a wind climate and how is it related to wind field realizations?

A wind climate is inferred from on-site measurements of certain physical quantities, namely wind speed and direction, wind shear, and air density. To be reliable, these measurements must be carried out over a long enough period of time and must also be compared to measurements from nearby weather stations [9]. This results in a huge dataset that precisely reflects the site's wind climate. This data can thus be reasonably used as input material for simulations. However, it would be unpractical to store years-worth of wind climate data for use in simulations. Moreover, as wind is driven by stochastic forces, it would be unreasonable to expect future wind fields to be identical to historical ones. This calls for the need to model the wind climate based on the historical data in a way that enables the simulation of realistic wind fields.

The same characteristic wind climate parameters introduced in Section 2.2 in the context of site suitability serve as the parameters of a site-specific wind model. This means that, knowing these parameters, a wind field timeseries can be simulated for the considered site. Nonetheless, there are different ways to do that. Although the hub-height mean wind speed is always modelled by a Weibull distribution, there are various ways to model wind shear and turbulence. These are explored in Subsection 2.4.1 and Subsection 2.4.2 respectively.

Besides the wind, in offshore locations, waves and currents exert loads on wind turbines. Yet, as can be deduced from Section 2.2, the IEC does not require the consideration of waves and currents for site suitability assessment. This is because, compared to the wind, they have a small influence on loads. However, this thesis still accounts for the influence of waves in its load calculations. Thus, an overview of wave modelling is given in Subsection 2.4.3.

2.4.1 Wind Shear Modelling

Wind turbines lie in the surface layer (up to 200m in altitude [32]) of earth's Atmospheric Boundary Layer (ABL). The vertical wind profile in this region, also referred to as the wind shear, is influenced by a complex interaction between geostrophic winds in the free atmosphere, surface friction and heat fluxes [32]. Consequently, wind shear is strongly dependent on ABL stability [32], [33],[5], [34], [35]. This effect is adequately captured by Monin-Obukhov Similarity Theory (MOST) [36], based on which an analytical model for the wind profile can be derived [33],[35]. The model is based on a logarithmic wind profile, which is observed under neutral ABL conditions. A correction is then applied to account for stability effects [33],[35]. The latter is parameterized by empirically-determined coefficients (derived in [37]) and is generally accepted in literature [33],[35].

The complexity of atmospheric stability makes it variable and difficult to assess [32]. Therefore, for practicality, the IEC 61400-1 standard prescribes the use of simpler wind shear models that neglect stability effects [9]. The two wind shear models proposed in the standard are the log-law profile and the power-law profile given by Equation 2.2 and Equation 2.3 respectively. Moreover, the IEC defines the Normal Wind Profile (NWP) for use in DLCs by a power law with $\alpha = 0.2$ and $z_{ref} = z_{hub}$. This is mainly due to the superior reliably of the power-law as compared to the log-law, especially for altitudes exceeding 50m [33].

$$U(z) = U(z_{ref}) \frac{ln(z/z_0)}{ln(z_{ref}/z_0)} \tag{2.2}$$

$$U(z) = U(z_{ref}) \left(\frac{z}{z_{ref}}\right)^{\alpha} \tag{2.3}$$

where:

- z is the height above ground
- $U(z)$ is the wind speed at height z
- z_{ref} is the reference height used for fitting the profile (usually where the anemometer is located)
- z_0 is the roughness length
- α is the wind shear exponent

Both the log-law and the power-law are founded on an empirical basis. While the log-law follows from the MOST model [36] for a neutral atmosphere, the power-law formula was first suggested by Hellman [38]. As for the model parameters, z_0 for the log-law and α for the power-law, they are determined empirically based on fitting to field measurements [33]. The value of z_0 strongly depends on the nature of the terrain and can vary greatly (from 0.0002

m for sea surface to more than 2 m for an urban environment) [32]. In contrast, while the value of α is correlated to z_0, it is not as sensitive to surface conditions and is typically taken as $\alpha = 1/7$ for a flat and open terrain like a body of water [33].

Naturally, neglecting atmospheric stability hinders the accuracy of IEC wind shear models. In fact, several studies have shown that accounting for atmospheric stability is necessary to accurately predict wind turbine loads [35],[39],[40]. In response to that, several methodologies were suggested to incorporate stability effects into wind shear models. In [35], different methods to predict atmospheric stability based on site wind speed and temperature measurements were proposed. Then, various models based on MOST were suggested to correct the log-law according to the assessed stability conditions. On another hand, [40] presents an indirect approach whereby stability effects are captured by conditioning the wind shear exponent of the power-law on both turbulence and wind speed. An even simpler approach is proposed in [41], where the wind shear exponent is taken as a directional, wind speed dependent 60% quantile of annual 10-min measurements instead of the omnidirectional mean value proposed by the IEC (see Section 2.2). All of these approaches were shown to effectively improve the accuracy of load estimates. However, none of them were adopted by the IEC. Thus, since this thesis is concerned with practical applications, the IEC recommendation was followed and only the conventional power law was employed.

2.4.2 Turbulence Modelling

Turbulence is one of the most complex physical phenomena characterized by irregularity, unpredictability and non-linearity [32],[42]. Consequently, turbulent winds are highly stochastic in nature and are correlated in both time and space [5],[43],[44]. Nevertheless, with the development of computers and numerical techniques, turbulent wind fields could still be simulated to great degree of accuracy through direct numerical simulations that solve the Navier-Stokes equations [43], [45]. However, this comes at an enormous computational cost. Simpler, computationally cheaper methods have therefore been developed over time. Notable examples are large-eddy simulations and engineering models based on the Reynolds-Averaged Navier-Stokes framework (e.g. $k-\epsilon$ and $k-\omega$ models) [45]. Other attempts to simulate three dimensional wind fields for wind energy applications have also been made. These are spectral methods based on *Taylor's Frozen Turbulence Hypothesis* and have been pioneered by Veers [44] and Mann [43].

Unfortunately, for practical applications, even the simplest methods presented above require significant computational power. As a result, the IEC turbulence models represent turbulence by a stationary Gaussian process with zero mean and standard deviation derived from empirical measurements. In these models, random turbulent fluctuations are superimposed on the time-invariant (within a 10-min interval) mean wind speed field and then spatially corrected for wind shear and spatial correlation.

Two turbulence models are suggested by the IEC standard (Annex C in [9]), namely the Kaimal spectral and exponential coherence model [46] and the Mann uniform shear model [47]. Both of these are founded on the study of turbulence power spectra in the atmospheric surface layer, with Kaimal approaching the subject from an empirical perspective and Mann taking a more theoretical approach [48]. In particular, turbulence timeseries are generated based on the Kaimal spectrum [46] for the Kaimal model and the Von Karman spectrum [49] for the Mann model. Then, to represent real turbulence structures, the timeseries are made spatially coherent based on different coherence functions derived from measured turbulence cross-spectra.

Like for wind shear models, the simplifications introduced in the IEC turbulence models result in accuracy losses in the predicted results. The main driver behind that shortcoming is, again, the models' failure to account for atmospheric stability [48], [50], [51]. In particular, by implicitly assuming neutral atmospheric conditions in their formulation, both models do not adequately depict stable and unstable conditions [50], [52]. Comparing the Kaimal and Mann models, it seems that the two yield wind fields with similar turbulence spectra, turbulence intensities and wind shear [51], [52]. However, the two models exhibit significant differences in their representation of coherent structures, leading to conflicting predictions of wind turbine response, and therefore of wind turbine loads [50], [51], [52], [53], [54]. Nonetheless, the question of which model gives a more realistic depiction of turbulence, and consequently of loads, remains open and seems to depend on the prevailing environmental conditions [48], [50], [51], [52], [53], [54]. Thus, to ensure a comprehensive depiction of turbulence that aligns with industry practices, both the IEC Kaimal and Mann models were employed for compiling the load catalogue of this thesis.

Another reason to use both the Kaimal and Mann models in this thesis is to compare them in terms of their fatigue load predictions. This was done in numerous previous studies including [48], [51], [52], [53], and [54]. However, the highest-rated RWT employed in these studies was the DTU 10 MW turbine, which may not reflect the features of current higher-rated offshore turbines. Moreover, these studies only evaluated the differences between the Kaimal and Mann models with respect to short-term DELs and for a relatively small set of wind climate parameters. This thesis

therefore extends the current body of knowledge by comparing the IEC turbulence models with respect to long-term fatigue loads, for a wider range of operating conditions, and using a 15 MW RWT.

2.4.3 Wave Modelling

In offshore locations, considering waves is not only important for load calculations, but also for planning the installation, maintenance and operation of a wind farm. Waves are driven by the wind and are an inherently stochastic phenomenon that occurs over the span of several time and length scales [55],[56]. In practice, the most common approach to capture the random character of waves is through wave spectra, which describe the distribution of wave energy across frequency and propagation direction. Like wind spectra, wave spectra are derived from empirical wave height measurements and have similar shapes under a wide range of environmental conditions. However, the total energy content of these spectra is time and location dependent. To account for that, for a given direction, the spectra are parameterized by two variables that characterize the wave climate and consequently the spectral energy content. These variables are the significant wave height H_s, defined as the mean of the highest third of wave height measurements, and the mean zero-crossing period T_z. Together, these variables define the directional wave spectrum at a given time and location. The directional spectra can then be used to recreate wave time-series having properties that are consistent with observations. This is achieved through a methodology similar to the one employed in wind field simulations, whereby an inverse Fourier transform is applied to the energy spectrum to retrieve harmonic amplitudes. These amplitudes are then used to generate wave timeseries based on Airy theory [57] for linear wave kinematics, whereby stochastic waves are modelled as a superposition of independent sinusoidal components having different frequencies and travelling in different directions.

Several spectra have been suggested over the years to describe wave energy distribution. A well-known example is the Pierson-Moskowitz spectrum [58], which was derived based on several measurement campaigns in the Atlantic ocean. The main limitation of this spectrum is that it is only suitable for fully-developed sea conditions, which is a rather rare situation. Accordingly, the Pierson-Moskowitz spectrum was adjusted to account for developing sea conditions. This was done as part of the JONSWAP (JOint North Sea WAve Project) initiative and culminated in the development of the JONSWAP wave spectrum, which is applicable for both developing and fully-developed conditions. Currently, the Pierson-Moskowitz and the JONSWAP spectra are the most prevalent in the industry. Nevertheless, when detailed long-term measurements are available for a specific site, a wave spectrum can be fine-tuned to best fit the wave conditions at that site [55].

Wave spectra can only capture the short-term characteristics of waves. Specifically, during periods where the spectra's parameters, H_s and T_z, are constant. These variables define the wave conditions at a specific time and location, that is the sea state, and depend on a variety of conditions. Thus, to describe the long-term wave climate at a certain site, it is necessary to understand how H_s and T_z vary over time. Observations have shown that wave conditions typically remain the same for 3-hour periods, meaning that H_s and T_z change every 3 hours [55]. Moreover, the driving forces behind sea state variations are inherently complex and stochastic. Therefore, like for the mean wind speed, statistical methods are employed to characterize the long-term wave climate at the location of interest. Particularly, H_s and T_z are measured during 3-hour intervals over a sufficiently long period, and the measurements are binned to construct a so-called scatter diagram. The diagram quantifies the occurrence of different (H_s, T_z) values, thereby representing the joint probability distribution of these variables. Wind climate measurements can then be combined with the wave climate measurements to create a wind-wave scatter diagram, giving a comprehensive description of long-term environmental conditions at the considered site.

2.5 Wake Effects

Solitary wind turbines are a rare occurrence in practical applications. Instead, turbines are packed into dense clusters to make the most efficient use of land and wind resource. As a result, the proximity of the turbines to one another causes them to interfere with each other. In fact, as the wind flows over the blades of a given turbine, it loses energy and gets disturbed. Consequently, downstream of the turbine, this results in a region characterized by reduced wind speeds and increased turbulence intensity [59], [60], [61]; the latter is called the wake. In a wind farm, some turbines will inevitably lie in the wakes of others. Therefore, it is essential to understand the effects of wakes on power production and fatigue loads through reliable wake models.

Modern computational resources allow for the detailed modelling of wake flows based on the Navier-Stokes equations [59], [60], [61]. However, a mentioned before, these solutions come at a tremendous computational cost, thereby

making them unpractical. As an alternative, simpler, yet less accurate analytical models have been suggested in the literature [59], [60], [61]. On one hand, wake deficit models have been proposed to model mean wind speed reduction in wakes. These semi-empirical models rely on fundamental physical laws, such as momentum and energy conservation, in combination with empirical observations of the similar character of far-wakes [59]. Among wake deficit models, the most important are the Larsen model [62], the Jensen model [63] and the Frandsen model [64]. Due to their reasonable accuracy and low computational costs, these models, the Jensen model in particular, have been extensively employed by the industry mainly for power output calculations in wind farm layout optimization [59]. On another hand, since wake deficit models do not consider the influence of wakes on turbulence and therefore on fatigue loads, analytical models have been developed to fill this gap. The most prominent example of these is the previously discussed wake-added turbulence model developed by Frandsen [10] and adopted by the IEC (refer to Section 2.2).

Although the analytical models discussed above are widely used in the industry, they suffer from two major drawbacks: they fail to account for the dynamic meandering of wakes[2] and they are tailored to capture a single aspect of wake effects (either velocity deficit or turbulence increase) [5]. This issue was addressed by the Dynamic Wake Meandering (DWM) model first introduced by the Risø Technical University of Denmark in [65] and [66], then validated in [67] and [68]. The DWM model effectively accounts for wake deficit, wake-added turbulence and wake meandering through a simplified computational framework that is compatible with conventional aero-hydro-servo-elastic code [59],[66],[67]. For this reason, the IEC 61400-1 [9] adopted the DWM model as an additional alternative to the Frandsen model[3]. Furthermore, for research as well as practical applications, the DWM model was integrated into wind farm modelling software such as FAST.Farm [69] and HAWC2Farm [70]. Nevertheless, the DWM model remains much more costly to evaluate in comparison to the Frandsen model, especially when the latter is combined with the effective turbulence approximation as suggested in the IEC standard [5]. However, since this thesis involves the one-time effort of developing a load catalogue, computational cost is not a major consideration and therefore the high-fidelity DWM model will be utilized in addition to the effective turbulence model.

There exists numerous variants of the Frandsen and DWM wake models. However, the versions adopted by the IEC are of particular interest as they are predominantly applied in practice. Since these models are fundamentally different, they are expected to yield differing load estimates. These differences were quantified in multiple previous studies by comparing the IEC Frandsen and DWM models with respect to their load predictions under a variety of circumstances. In [71] and [72], the models were assessed against field load measurements. These studies found that the Frandsen model generally tends to overestimate loads, while the DWM model is in more agreement with measured values [71], [72]. Other studies comparing the two wake models without validation against measurements also concluded that the Frandsen model consistently leads to higher load estimates than DWM [73], [74]. Nevertheless, this was not the case in [75] and [76], which found that Frandsen's model might underestimate DWM results in some cases, especially for large inter-turbine spacings.

Like for the case of studies comparing the IEC turbulence models, the aforementioned work on the IEC wake models was carried out based on RWTs with ratings that do not exceed 5 MW, which therefore do not reflect the characteristics of modern offshore technology. Moreover, all the aforementioned research, except [74], compares the models with respect to short-term DELs rather than long-term loads. Furthermore, even when the long-term loads were considered like in [74], the assessment was done for a specific wind farm layout characterized by fixed inter-turbine spacings. Thus, this thesis addresses these knowledge gaps by comparing the IEC wake models under a complete setup relevant to offshore conditions. More specifically, the comparison is carried out with respect to annual equivalent loads under a realistic wind climate corresponding to an actual wind farm site in the North Sea and for multiple values of the inter-turbine spacing.

2.6 Load Response Models

As pointed out in Section 1.2, load assessment through aero-hydro-servo-elastic simulations is costly and time consuming. Load Response Models (LRMs) have therefore been developed as a solution to this problem. The concept of an LRM and its construction procedure were explained in Section 1.3. In this section, a critical overview of advancements in LRM development for wind energy applications is provided. The culmination of this review was the identification of the limitations of current LRMs as listed in Section 1.3.

Many LRMs have been developed throughout the years for both commercial and academic purposes. The first LRMs were build in an indirect manner by regressing the statistical moments defining three-parameter load spectra over

[2] Refer to [65] and [66] for a detailed description of dynamic wake meandering and to [59] and [60] for a review of wake meandering modelling
[3] Details on both models can be found in Annex E of the IEC 614000-1 standard [9]

mean wind speed and turbulence intensity [77],[78]. However, these models were intended for sensitivity analysis and uncertainty assessment rather than accurate load estimation and only accounted for two wind climate parameters. A more comprehensive LRM was developed in [79] using linear regression based on a larger set of environmental inputs, with the purpose of understanding load sensitivity to different inputs. A similar approach was followed in [28] in the context of reliability assessment, where an LRM based on linear regression combined with a product approximation was compared to another one based on a Taylor series approximation. The conclusion was that the first LRM yielded better results. Nevertheless, by employing a linear model, both of the LRMs developed in [79] and [28] implicitly made the unrealistic assumption that wind climate parameters are independent. An attempt to address this issue was made in [80] for the purpose of simplifying structural analysis for offshore turbines. To achieve that, second and third order regression models were fitted to reliable simulation results, accounting for both the wind and wave climate. Yet, the predictions of these LRMs were not satisfying when considering accuracy and the computational cost of developing the models. Better results were obtained in [81], also in the context of structural optimization for offshore turbines. The LRM suggested in this study employs first and second order linear regression to predict fatigue loads based on high-fidelity simulations of only a few wind speed bins. This effectively reduces the number of aero-hydro-servo-elastic simulations required to estimate loads, but does not eliminate them. Furthermore, all the aforementioned LRMs are not tailored for site suitability assessment, where both speed and accuracy are needed. This is addressed in [82], where two LRMs based on the IEC wind climate parameters of Section 2.2 (with the exception of the extreme wind speed) and intended for site suitability assessment are proposed. The study compares a quadratic regression model based on central composite design to a model based on a Taylor approximating, finding that the former yields better load estimates.

Although the approach presented in [82] is promising for site suitability assessment, it suffers from several drawbacks. Firstly, it is only applicable to a relatively small range of site conditions, which have to be similar to the reference conditions based on which the LRM was established. Secondly, it does not explicitly account for the correlations between environmental inputs during the construction of the model. Thirdly, it requires a relatively large number of simulations to establish the LRMs. These limitations are addressed in [83], where an LRM based on Polynomial Chaos Expansion (PCE) is proposed. This approach considerably reduces the amount of simulations required to establish the LRM and explicitly accounts for the correlations between the inputs by sampling the training points from their joint Probability Density Function (PDF). Moreover, the sampling variable ranges are specified such as to represent a large set of possible site conditions. Furthermore, the use of PCE enables the LRM to explicitly estimate the uncertainties in the predicted loads as well as the individual contributions of the various input variables to the total uncertainty. The latter is extremely useful for uncertainty propagation and sensitivity analysis. In [84], the work presented in [83] is extended by considering a PCE model with more environmental input parameters and based on an extensive database of high-fidelity simulations covering a wide range of potential site conditions. In addition, the PCE model was compared to four other models based on nearest-neighbor interpolation, Kriging interpolation, importance sampling and quadratic regression. It was found that the PCE-based LRM achieves the best accuracy to computational cost ratio. In a different approach presented in [85], Artificial Neural Networks (ANNs) were trained for load estimation in an offshore environment. However, the results were not satisfying as the model predictions exhibited large uncertainties. A better ANN model was presented in [86] and was compared to a PCE model and a quadratic regression model under the same setup considered in [84] and based on the same database. The study showed that the ANN can predict loads more accurately and faster than the PCE model, which in turn performs better than the quadratic model.

All the LRMs discussed so far were designed for a singular turbine. This means that they overlook the significant influence of wakes on the loading situation in a realistic wind farm. The latter has been considered in [87], where the DWM model was incorporated into the development of an LRM for load prediction in an offshore wind farm. The LRM was based on Kriging interpolation, meaning that it has a high evaluation cost. Moreover, it is attuned for a specific wind farm and might not be suitable for other ones. Two alternative LRMs that also employ the DWM model but do not suffer from these limitations were proposed in [88]. Specifically, building on the work of [84] and [86], it was shown that a PCE model and an ANN model can accurately predict wind farm loads, with the ANN model outperforming the PCE model with respect to both speed and accuracy. Additionally, these LRMs can readily provide analytical derivatives of the outputs of interest, making them instrumental for gradient-based optimization or sensitivity analysis. On the other hand, the main drawback of these LRMs is that they require a relatively large training dataset.

To mitigate the adverse effects of wakes on power production and loading in a wind farm setting, control strategies can be applied. To improve these strategies, the operating conditions of wind turbines in a farm, mainly characterized by their individual controller setpoints, were incorporated as inputs to LRMs for use in optimization routines. This was done in [89] using ANNs for an onshore two-turbine wind farm. A similar ANN-based LRM was also developed in [90], but for an onshore wind farm with an arbitrary number of turbines (greater than two). In that same context, [91] showed that, for a small high-fidelity dataset (with less than 825 samples), an LRM based on Gaussian process regression performs better than an ANN. Further work on the topic was presented in [92], where a novel approach for LRM construction was suggested. The authors proposed that better results can be obtained by treating the individual

environmental conditions contributing to wind turbine loads separately. In particular, in this approach, a different LRM is tailored to calculate the load contributions of each individual input parameter, and the contributions are then combined. The employed LRMs consist of a mixture of DC gains, transfer function and empirical fits. Although promising, the potential of this method is yet to be explored.

3

Methods

In this chapter, the methodology followed to achieve the objectives of this thesis is presented. Firstly, the various models and tools used to establish the dynamic simulation environment for load calculations are presented in Section 3.1. Following this, the Damage-Equivalent Load (DEL) framework applied to post-process the dynamic simulation outputs for fatigue analysis is discussed in Section 3.2. Section 3.3 subsequently defines the structure and contents of the load catalogue developed in this thesis, in addition to the underlying load calculation parameters, cases, and operating conditions. Section 3.4 follows by describing the population process of the load catalogue as well as the validation study performed to ensure the reliability of the applied load calculation pipeline. Lastly, the chapter is concluded in Section 3.5 with a description of the analysis methods employed to extract valuable insights from the load catalogue data.

3.1 Models and Tools

3.1.1 Reference Wind Turbine: The IEA 15 MW Offshore Turbine

The utilization of Reference Wind Turbines (RWTs) is a critical strategy in the context of advancing wind energy research. As delineated in Section 2.3.2, RWTs provide publicly-accessible wind turbine models that foster research reproducibility while offering a valuable resource for both academia and industry stakeholders. In particular, by standardizing turbine specifications and making them publicly available, RWTs not only facilitate the validation and comparison of different methodologies but also ensure the transparency and integrity of research outcomes. Consequently, this thesis employs an RWT to leverage these advantages.

In the dynamic landscape of offshore wind energy, wind turbine technology is constantly evolving. This necessitates the selection of an RWT that accurately reflects the characteristics of modern offshore turbines. As offshore turbines grow in size and power rating, surpassing the 15 MW threshold, it is essential to align the RWT selection with these advancements. Moreover, the prevalence of monopile support structures in the offshore industry and the increased adoption of direct-drive technology underscores the need for an RWT that reflects these features.

In light of these considerations, the IEA 15 MW offshore turbine, with a fixed-bottom monopile support structure, emerges as an ideal RWT choice for this thesis. Designed through a collaborative effort between the National Renewable Energy Laboratory (NREL) and the Technical University of Denmark (DTU) under IEA Wind Task 37 [93], the IEA 15 MW, sketched in Figure 3.1, turbine reflects the technology and scale characteristic of modern offshore turbines [21]. With a 240m rotor diameter and a direct-drive configuration, this turbine stands as a testament to the latest advancements in offshore wind energy. The overall specifications of IEA 15 MW RWT are provided in Table 3.1 below and the full design definition of the RWT can be found in [21].

For the purpose of this thesis, the design definition data of the IEA 15 MW RWT was retrieved from the publicly-accessible GitHub repository [94] of IEA Wind Task 37 in addition to some performance assessment data used for the validation of Section 3.4.3.

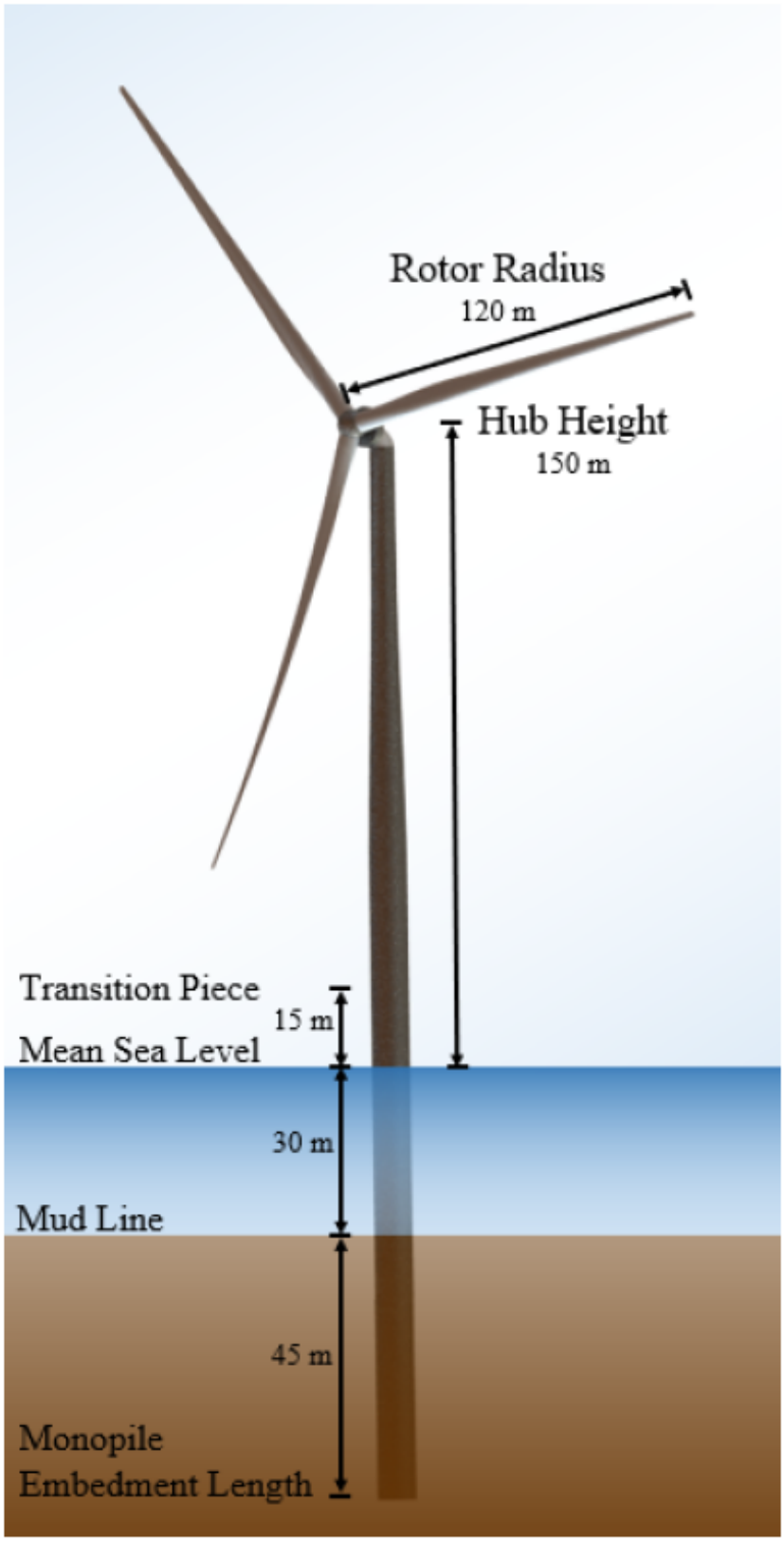

Figure 3.1: The IEA 15 MW offshore RWT with fixed-bottom monopile support structure (adapted from [21])

Parameter	Units	Value
Power rating	MW	15
Turbine class	-	IEC Class 1B
Specific rating	W/m^2	332
Rotor orientation	-	Upwind
Number of blades	-	3
Control	-	Variable speed Collective pitch
Cut-in wind speed	m/s	3
Rated wind speed	m/s	10.59
Cut-out wind speed	m/s	25
Design tip-speed ratio	-	90
Minimum rotor speed	rpm	5.0
Maximum rotor speed	rpm	7.56
Maximum tip speed	m/s	95
Rotor diameter	m	240
Airfoil series	-	FFA-W3
Hub height	m	150
Hub diameter	m	7.94
Hub overhang	m	11.35
Rotor precone angle	deg	-4.0
Blade prebend	m	4
Blade mass	t	65
Drivetrain	-	Direct drive
Shaft tilt angle	deg	6
Rotor nacelle assembly mass	t	1,017
Transition piece height	m	15
Monopile embedment depth	m	45
Monopile base diameter	m	10
Tower mass	t	860
Monopile mass	t	1,318

deg	degrees	rpm	revolutions per minute
m	meters	t	metric tons
m/s	meters per second	W/m^2	watts per square meter

Table 3.1: Overall specifications of the IEA 15 MW RWT (adapted from [21])

3.1.2 Simulation Tools: OpenFAST and FAST.Farm

In this thesis, load calculations were performed for both a solitary turbine and a wind farm. This necessitates the use of numerical simulation tools capable of handling both of these scenarios while being suitable for modelling modern offshore turbine technology. As outlined in Section 2.3.1, there are numerous software tools available that meet these criteria and that have been validated for reliability.

OpenFAST [16] was selected for the simulation of a single turbine. OpenFAST is an open-source, multi-physics tool specifically designed for simulating the coupled dynamic response of wind turbines. It relies on a modular framework, as illustrated in Figure 3.2, integrating computational modules for aerodynamics, hydrodynamics for offshore structures, control and electrical system dynamics, and structural dynamics. This enables the performance of comprehensive aero-hydro-servo-elastic simulations in the time domain. Moreover, OpenFAST supports a variety of wind turbine configurations for both onshore and offshore environments. Evidently, the IEA 15 MW RWT has compatible characteristics.

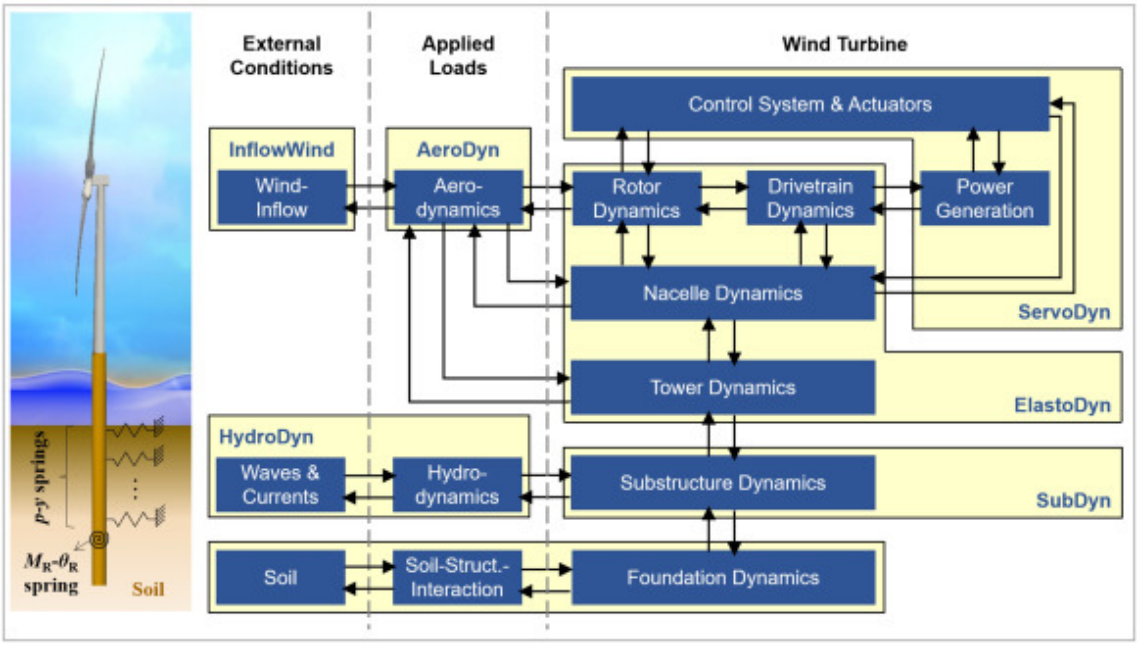

Figure 3.2: The OpenFAST modularization framework (adapted from [16])

Several reasons justify the choice of OpenFAST for this thesis:

1. **Accessibility**: As an open-source tool, OpenFAST is freely accessible, facilitating access to a valuable resource as well as reproducibility in research.

2. **Reliability**: OpenFAST has been extensively used in the literature and validated in multiple studies [17], [18], [19], [20], ensuring its reliability.

3. **Compatibility**: The tool supports the implementation of the climate models adopted in this thesis, which will be described in the subsequent subsections.

4. **Integration with IEA 15 MW RWT Model**: The design definition of the IEA 15 MW turbine is available in a version compatible with OpenFAST, with input files accessible from the IEA Wind Task 37 GitHub repository [94]. This direct compatibility streamlines the simulation process and ensures accurate modeling of the RWT.

FAST.Farm [95] was chosen for the wind farm simulations. FAST.Farm is also an open-source tool that builds upon the capabilities of OpenFAST to extend its application to wind farms. As illustrated in Figure 3.3, it follows a similar modularization framework to that of OpenFAST, where the latter is integrated with additional physics modules that account for wind farm-wide ambient wind, wake dynamics, and wind farm control.

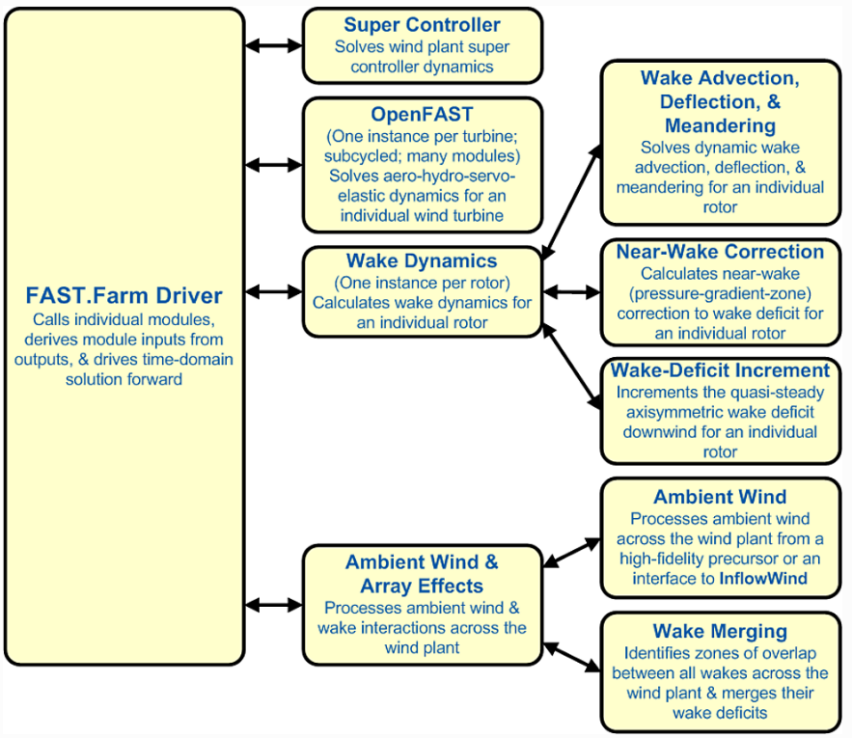

Figure 3.3: The FAST.Farm modularization framework (adapted from [95])

The choice of FAST.Farm is supported by several key factors:

1. **Consistency and Efficiency**: FAST.Farm is built on top of OpenFAST, thus inheriting its desirable features outlined above and ensuring seamless integration. In addition, FAST.Farm is based on a similar architecture to that of OpenFAST and employs the same input and output file formats. This enables the establishment of an efficient workflow and simplifies the comparison of results between solitary turbine and wind farm simulations.

2. **Advanced Wake Modeling**: FAST.Farm supports the Dynamic Wake Meandering (DWM) model, which is crucial for achieving the objectives of this thesis. Furthermore, the tool addresses many limitations of previous DWM implementations in a computationally-efficient manner [95].

3.1.3 Wind Models and Simulation

Wind Models

Wind turbine loads are mainly driven by the inflowing wind. Thus, to obtain accurate load estimates, a realistic representation of the wind field over the operational lifetime of the turbine is needed. As discussed in Section 2.4, this can be achieved by dividing the operational lifetime into 10-minute intervals and treating the wind field as a superposition of a mean wind speed field and a turbulence field.

The mean wind speed field is defined on a 10-minute basis, and thus remains invariant, with respect to both speed and direction, over a given 10-minute interval. The field is established by first determining the mean wind speed and direction at hub-height, then using them to construct the full field based on a wind shear model. The hub-height mean wind speed (U_{hub}) and mean flow direction (θ_{hub}) are sampled from site-specific probability distributions obtained from on-site measurements. The hub-height mean wind speed follows a Weibull distribution, with a Probability Density Function (PDF) given by Equation 3.1 and defined by two site-specific parameters k and a. The distribution is illustrated in Figure 3.4a for different values of k. As for the hub-height mean flow direction distribution, it is represented by a wind rose (Figure 3.4b) that captures the probability of the wind flowing from a given angular sector, typically 30 degrees wide.

On the other hand, the turbulence field fluctuates constantly in both speed and direction within the 10-minute interval. Moreover, it is inherently stochastic and is constructed according to a turbulence model based on normalized energy spectra, as discussed in Section 2.4.2. The parameters of this turbulence model are site-specific and are conditioned

on the mean wind speed.

$$f(U_{hub}) = \frac{k}{a}\left(\frac{U_{hub}}{a}\right)^{k-1} e^{-\left(\frac{U_{hub}}{a}\right)^{k}} \tag{3.1}$$

where:

k is the shape parameter

a is the scale parameter

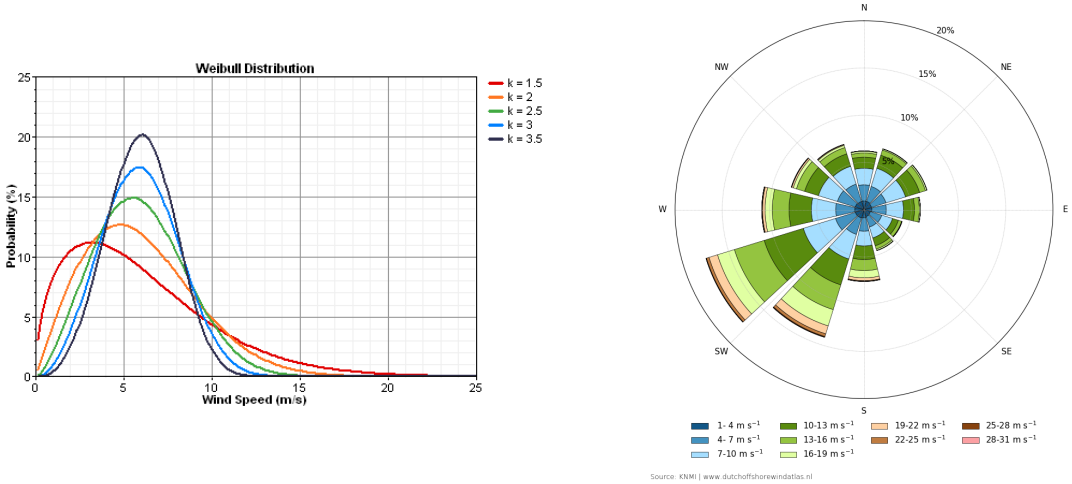

(a) Weibull distribution for mean wind speed

(b) Wind rose

Figure 3.4: Mean wind speed distribution and wind rose

Since the objective of this thesis is to provide insights into practical load calculation methods, it is important to consider the wind modelling practices applied in the wind energy industry. For this reason, the Normal Wind Conditions (NWC) model suggested in Section 6.3.2 of the IEC 61400-1 standard [9] was adopted in this thesis. In this model, the hub-height mean wind speed is normally modelled by a site-specific Weibull distribution. However, for design load calculations in the context of turbine type certification, a value of 2 is assumed for the shape parameter (k) and the Weibull distribution reduces to a Rayleigh distribution (Equation 3.2), parameterized by the average hub-height 10-minute mean wind speed (U_{ave}) of the considered wind turbine class (refer to Table 2.1). Additionally, the hub-height mean flow direction is still given by a site-specific wind rose. But, for design calculations, the distribution is often assumed uniform as directional loading effects are often neglected. Furthermore, zero yaw misalignment and flow inclination are assumed, implying that the mean wind always flows perpendicularly to the untilted rotor plane.

$$f(U_{hub}) = \frac{\pi U_{hub}}{U_{ave}^2} e^{-\pi\left(\frac{U_{hub}}{2U_{ave}}\right)^2} \tag{3.2}$$

Knowing the hub-height mean wind speed (U_{hub}) and flow direction (θ_{hub}), the NWC mean wind speed field is obtained using the power law wind shear model given by Equation 3.3a. Also, wind veer is neglected, meaning that mean flow direction is assumed to remain constant with height (Equation 3.3b).

$$U(z) = U_{hub}\left(\frac{z}{z_{hub}}\right)^{\alpha} \tag{3.3a}$$

$$\theta(z) = \theta_{hub} \tag{3.3b}$$

where:

$U(z)$ is the mean wind speed at height z

$\theta(z)$ is the mean flow direction at height z

z is the height above ground

z_{hub} is the hub-height

α is the wind shear exponent

In the NWC model, the turbulence field is computed based on one of the two suggested turbulence models described in Annex C of the IEC 61400-1 standard [9]: the Kaimal spectral and exponential coherence model or the Mann uniform shear model. Both of these models were employed in this thesis and they are both parameterized by the hub-height turbulence intensity (I). In NWC, the latter is computed based on the Normal Turbulence Model (NTM). In this model, turbulence intensity is taken as the 90% quantile of a mean wind speed dependent Weibull distribution fitted to site turbulence intensity measurements. Alternatively, the turbulence intensity can be directly sampled from the Weibull distribution.

For design load calculations, the 90$^{\text{th}}$ percentile U_{hub}-dependent turbulence intensity is computed from the reference turbulence intensity (I_{ref}) of the relevant turbine class using Equation 3.4. In this case, the alternative would be to sample the turbulence intensity from the Weibull distribution with PDF given by Equation 3.5, whose shape and scale parameters depend on the hub-height mean wind speed and the reference turbulence intensity. Both of these approaches were considered in this thesis and shall be referred to as the 90$^{\text{th}}$ Percentile NTM and the Distribution NTM respectively in the remainder of this report. Additionally, more details on the application of these models in the construction of this thesis' load catalogue are provided in Appendix E.

$$I = I_{ref}\frac{0.75U_{hub} + 5.6}{U_{hub}} \tag{3.4}$$

$$f(I) = \frac{kU_{hub}^{k}}{a}\left(\frac{I}{a}\right)^{k-1} e^{-\left(\frac{U_{hub}I}{a}\right)^{k}} \tag{3.5}$$

where:

$k = 0.27U_{hub} + 1.4$ is the shape parameter

$a = I_{ref}(0.75U_{hub} + 3.3)$ is the scale parameter

Wind Field Simulation

For the purpose of this thesis, 10-minute wind fields need to be simulated based on the NWC wind models discussed in the previous subsection. In addition, the generated wind files, containing the simulated wind field data, must have a format compatible with OpenFAST and FAST.Farm. Wind simulators must therefore be selected accordingly. Consequently, NREL's *TurbSim* [96] was used to simulate Kaimal wind fields and the built-in turbulence simulator of DNV Bladed [14] was used to simulate Mann wind fields. These tools satisfy the required criteria and are widely used in the industry.

To simulate wind fields, a grid of points at which wind velocities are to be calculated first needs to be defined. For solitary turbine simulations, the defined grid was a uniform, two-dimensional, vertical square grid that covers the rotor span as illustrated in Figure 3.5. The grid's side length was set to approximately 1.25 times the rotor diameter to also cover most of the tower, and the grid's resolution was set in accordance with the guidelines of Section 7.5 of the IEC standard [9]. The full grid definition is provided in Table 3.2. Once the wind grid is defined and the simulator is configured according to the NWC wind models, it can be launched to sequentially compute wind fields in a time-marching manner. The wind simulator frequency was set to 13 Hz, corresponding to a timestep of 0.077 s, which is a typical value used in the industry.

For wind farm simulations, the wind grid definition is significantly different. Particularly, two types of three-dimensional wind grids must be defined: a low-resolution grid that covers the whole farm and multiple high-resolution grids, one per wind turbine, covering a small volume of space centred at the corresponding rotor and enclosing it. To illustrate this, a top-view of a FAST.Farm wind grid is shown in Figure 3.6 for a two-turbine wind farm example. In FAST.Farm, the parameters of the low and high resolution grids are not fixed. They are rather conditioned on the mean wind speed and wind farm dimensions among other variables. These parameters were determined based on the modelling guidelines found in the software's documentation [95]. In addition, TurbSim was utilized to generate Kaimal wind files for

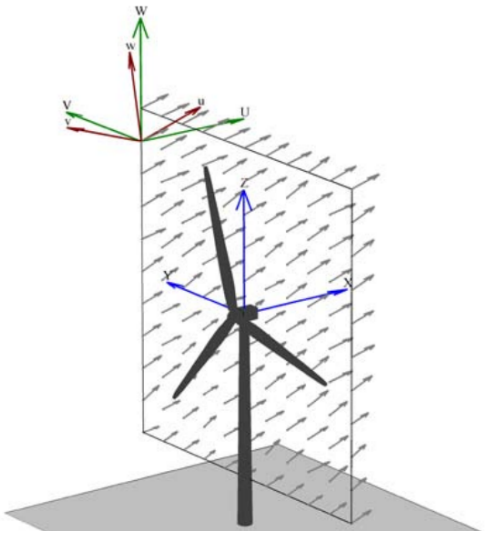

Figure 3.5: Wind grid illustration for OpenFAST simulations (adapted from [96])

Parameter	Value
Frequency [Hz]	13
Dimensions [m]	299x299
Discretization [-]	49x49
Resolution [m]	6.23x6.23

Table 3.2: Wind grid definition for OpenFAST simulations

farm simulations, while no Mann wind files were employed. Furthermore, the simulator frequency was set to 0.5s, as calculated for the IEA 15 MW RWT per the modelling guidance. Finally, templates for the TurbSim input files used for both single turbine and farm simulations are provided in Appendix A, in addition to the configuration settings of the Bladed turbulence simulator used for Mann wind fields in single turbine simulations.

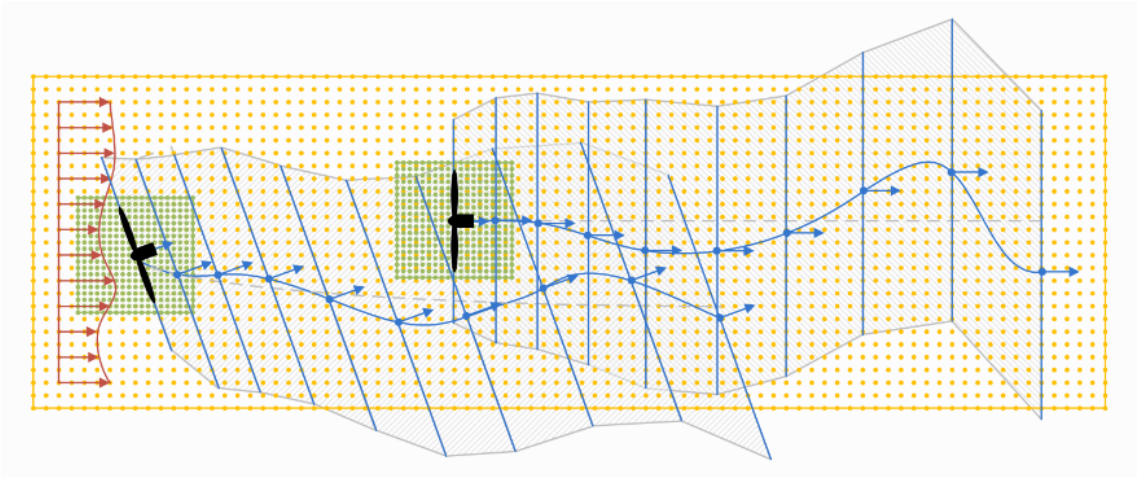

Figure 3.6: Wind grid illustration for FAST.Farm simulations; the low-resolution grid is represented in yellow while the high-resolution grids are represented in green (adapted from [95])

For both single turbine and farm wind fields, the NTM turbulence intensity, discussed in the previous subsection, corresponds to that of the longitudinal component (u) of the turbulent velocity. The latter is directed along the mean wind velocity. The lateral and vertical components, v and w respectively, exhibit different turbulence intensities. These values are dictated by the IEC standard based on the employed turbulence model as per Table 3.3.

Table 3.3: Turbulence intensity for the different turbulence components by turbulence model (adapted from [9], Annex C)

Turbulence Model	I_u	I_v	I_w
Kaimal	I	$0.8I$	$0.5I$
Mann	I	$0.7I$	$0.5I$

3.1.4 Wave Model

Waves also contribute to offshore turbine loading and must therefore be considered in the load analysis of this thesis. Section 2.4.3 discussed wave modelling and explained that it involves two time scales: short-term and long-term. In this framework, long-term sea states define the parameters of short-term wave spectra. The spectra in turn dictate the behaviour of short-term waves.

In this study, short-term waves were modelled as irregular waves relying on first-order Airy theory based on the JONSWAP spectrum. Additionally, the waves were assumed unidirectional, propagating along the mean wind flow direction, and no wave stretching was considered. These choices are justified as they represent common industry practices. Moreover, the internal wave simulator of OpenFAST's *HydroDyn* module (see Figure 3.2) was utilized to conveniently simulate 10-minute wave timeseries. Templates of the HydroDyn input files used for wave simulation are provided in Appendix B.

The parameters of the JONSWAP spectrum, H_s and T_p[1], depend on the long-term sea-state. The latter changes approximately every 3 hours and is described by a site-specific wind-wave scatter distribution, which is derived from site measurements. In this thesis, H_s and T_p are treated deterministically as dependent variables. They are determined directly from the mean wind speed as dictated by a wind-wave lookup table, presented in Section 3.3.1. On a final note, loading due to currents was not considered in this research.

3.1.5 Wake Models

Wind turbines rarely stand alone in practical wind energy projects. Thus, any realistic load assessment must account for wake effects, arising from the proximity of wind turbines to each other in a wind farm. Like for the wind models, the wake models adopted in this research were selected in alignment with latest industry practices. Accordingly, Frandsen's effective turbulence model and the Dynamic Wake Meandering (DWM) model as formulated in the IEC 614000-1 standard were employed in this thesis. The models are briefly described in this section. For more details on the theory behind each model and their implementation, the reader is urged to consult Annex E of the IEC standard [9]. In addition, a general discussion of wake models and their differences can be found in Section 2.5.

Frandsen's Effective Turbulence Model

In Frandsen's effective turbulence model [10], fatigue loading is assumed to be proportional to the turbulence intensity, allowing the definition of a fatigue-equivalent effective turbulence turbulence intensity (I_{eff}). In other words, the fatigue loading contribution of each surrounding turbine wake translates into an increased turbulence intensity. For given hub-height mean wind speed (U_{hub}) and flow direction (θ_{hub}), the contribution to the total turbulence intensity of the nearest turbine lying at distance $d(\theta)$ from the considered turbine, is given by Equation 3.6. The wake-added turbulence intensity (I_{wake}) is then combined through Equation 3.8 with the characteristic turbulence intensity of the undisturbed flow (I_c), given as a 90$^{\text{th}}$ percentile by Equation 3.7. This yields the total turbulence intensity (I_{total}) in the direction specified by θ. The total turbulence intensities in the different directions are then weighed by the conditional PDF of flow direction $f(\theta|U_{hub})$ and combined into a wind speed-dependent effective turbulence intensity as per Equation 3.9. I_{eff} is then used as input parameter in load calculation simulations, thus effectively capturing wake effects on fatigue loading.

$$I_{wake}(U_{hub},\theta) = \frac{U_{hub}}{1.5 + \frac{0.8d(\theta)}{\sqrt{C_T(U_{hub},\theta)}}} \tag{3.6}$$

$$I_c(U_{hub}) = I_{amb}(U_{hub}) + 1.28\sigma_{I_{amb}}(U_{hub}) \tag{3.7}$$

$$I_{total}(U_{hub},\theta) = \sqrt{I_c^2(U_{hub},\theta) + I_{wake}^2(U_{hub},\theta)} \tag{3.8}$$

$$I_{eff}(U_{hub}) = \Big(\int_0^{2\pi} f(\theta|U_{hub}) I_{total}^m(U_{hub},\theta) d\theta \Big)^{1/m} \tag{3.9}$$

[1]The peak spectral period T_p, defined as the inverse of the frequency at which the spectrum peaks, is a function of the mean zero-crossing period T_z and the peak shape parameter γ: $\frac{T_p}{T_z} \approx 0.327e^{-0.315\gamma} + 1.17$ [55].

where:

d is the distance in rotor diameters to the nearest neighbouring turbine in direction θ

C_T is the thrust coefficient of the nearest neighbouring turbine in direction θ

I_{amb} is the mean ambient turbulence intensity

$\sigma_{I_{amb}}$ is the standard deviation of the ambient turbulence intensity

To perform farm simulations with Frandsen's effective turbulence model, FAST.Farm is not needed. Instead, the effective turbulence intensity is calculated for the turbine selected for load calculations based on the farm's layout and the mean flow direction distribution. This turbulence intensity is then used as input to the turbulence simulator to generate wind fields accounting for the influence of nearby wakes. These wind fields are then fed to OpenFAST for a single turbine simulation.

Dynamic Wake Meandering Model

A more realistic representation of wakes is given by the DWM model. In contrast to the Frandsen model, it accounts for all the key aspects of wakes, namely wake deficit, wake-added turbulence and wake meandering. The model applies fundamental fluid dynamics theory along with several key assumptions and simplifications that make it computationally efficient. However, discussing the theoretical details of the DWM model is beyond the scope of this thesis.

There are many different implementations of the DWM model. The one employed in this thesis is the one implemented in FAST.Farm's *Wake Dynamics* module (see Figure 3.3). This version is compliant with the IEC formulation while addressing several limitations found in conventional DWM implementations in an attempt to improve the model's accuracy and computational cost. A detailed description of the DWM version implemented in FAST.Farm in addition to a list of the addressed limitations can be found in [95].

In this research, the DWM wake model was applied by default in wind farm simulations with FAST.Farm. The wake was modelled as a polar wake and default values were taken for the DWM model parameters. These default values are provided by the NREL and were computed by calibrating the wake model using a high-fidelity computational fluid dynamics simulation [95]. For completeness, the wake model configuration employed in this thesis, specified in the FAST.Farm main input file, can be found in Section D.1.

3.1.6 Programming Language: Python

Achieving the objectives of this thesis requires the establishment of a seamless computational workflow for load calculations, involving a series of pre-processing, simulation and post-processing steps. The Python programming language was chosen for the implementation of this workflow. Multiple reasons justify this choice:

1. **Simplicity and Versatility**: Python is simple and easy to learn, read and use, while its versatility allows it to handle a wide range of applications, from basic scripting to advanced scientific computing. This makes it ideal for developing and maintaining the workflow described above.

2. **Availability of Extensive Libraries**: Python offers a rich ecosystem of libraries such as *NumPy*, *Pandas*, and *SciPy*, which are instrumental for performing the mathematical computations and data manipulation tasks involved in the load calculation pipeline. Moreover, these libraries enable the efficient processing and analysis of large datasets, which is critical for creating the load catalogue being developed in this study.

3. **Integration with OpenFAST and FAST.Farm**: Python is highly compatible with the simulation tools OpenFAST and FAST.Farm. In fact, the NREL provides an extensive library of Python scripts[2] specifically designed to work with these tools, facilitating the execution of simulations and the pre- and post-processing of simulation data. This seamless integration ensures the development of a fast and robust workflow.

4. **Integration with RWE Software**: Python is extensively used by RWE, the company collaborating on this thesis, making it a strategic choice for this research. This alignment with RWE's existing software infrastructure promotes easier collaboration, integration, and application of the thesis findings within the company's operations.

[2] The *openfast_toolbox* can be found in OpenFAST's GitHub repository [97].

3.2 The DEL Framework for Fatigue Load Analysis

In wind turbine fatigue analysis, the fatigue behaviour of materials is described by the conventional SN model. In this framework, for a fully-reversed (i.e. zero-mean) regular cyclic loading (i.e. sinusoidal loading timeseries), the stress range (S) is related to the number of cycles to failure (N) by a so-called SN-curve given by Equation 3.10. The parameters K and m of the SN-curve are determined experimentally and are documented in standardized material codes. Moreover, the parameter m is referred to as the Wöhler exponent and is important in wind turbine fatigue analysis.

$$N(S) = KS^{-m} \tag{3.10}$$

As discussed in Section 2.3, reliable wind turbine loading histories are typically obtained through performing a set of dynamic simulations. However, these loading histories are complex and highly irregular. This means that no unique cycle period or load range can be identified. Instead, the loading history consists of a multitude of fatigue cycles and corresponding load ranges. Accordingly, *Rainflow Counting* [29] is applied to identify the different fatigue cycles and load ranges found in the loading history. This data is then used to construct a load spectrum, depicting the frequency of occurrence (in number of cycles) of each load range. After that, Miner's rule is applied on the spectrum to compute the resulting fatigue damage of the loading history as given by Equation 3.11. The obtained fatigue damage effectively quantifies the loading situation of the structure over the considered time period and can be used to estimate its lifetime or predict its failure, which occurs when $D \geq 1$.

$$D = \sum_i \frac{n_i}{N(S_i)} = \sum_i n_i \frac{S_i^m}{K} \tag{3.11}$$

In practical applications, it is often simpler and more convenient to report and compare loads rather than fatigue damages. Nevertheless, working with load histories or load spectra is cumbersome and confusing. To address this issue, the concept of a Damage-Equivalent Load (DEL) was introduced. The DEL (S_{eq}) is defined as the single equivalent load range that results in the same fatigue damage as the full loading history when applied over an arbitrary equivalent number of cycles (N_{eq}). Given the component-specific Wöhler exponent m, a DEL can be calculated for any loading history using Equation 3.12.

$$S_{eq} = \Big(\frac{1}{N_{eq}} \sum_i n_i S_i^m\Big)^{1/m} \tag{3.12}$$

Since turbulence is a stochastic process, many realizations of the turbulent wind field are required to minimize the statistical uncertainty associated with a given load computation. This means that any accurate load evaluation requires the performance of multiple simulations for different turbulence simulator seeds under the same operating conditions. The result is multiple DEL values, one for each seed (i.e. a total of N_{seeds} DELs, each denoted by $S_{eq,j}$). These DELs are combined using Equation 3.13 to obtain a single representative DEL value for the considered operating conditions. This representative DEL is associated with the same equivalent number of cycles N_{eq} from Equation 3.12 and with the length of the load history, corresponding to the effective simulation time T_{sim} which is typically 10 minutes.

$$DEL = \Big(\frac{1}{N_{seeds}} \sum_{j=1}^{N_{seeds}} S_{eq,j}^m\Big)^{1/m} \tag{3.13}$$

Equation 3.13 yields the representative DEL for a given set of operating conditions. Evidently, operating conditions change over time and this must be taken into account to obtain a significant DEL that reflects the fatigue damage accumulated over a reference period of time T_{ref}, which can be, for example, the turbine's lifetime or a typical year. Assuming that the only independent operating conditions are the hub-height mean wind speed (U_{hub}) and flow direction (θ), the DELs can be combined into an equivalent load effect F over the period T_{ref} via Equation 3.14. The formula uses the PDFs $f(U_{hub}|\theta)$ and $f(\theta)$ to weight the DELs calculated under the corresponding operating conditions.

$$F = \Big(\frac{T_{ref}}{T_{sim}} \int_\theta f_\theta(\theta) \int_{U_{hub}} f_{U_{hub}}(U_{hub}|\theta) DEL^m(U_{hub},\theta) dU_{hub} d\theta\Big)^{1/m} \tag{3.14}$$

In the fatigue load calculations of this thesis, the DEL framework was applied as described in this section. Again, the choice of this framework was made in accordance with contemporary industry practices. Besides that, the methodology was implemented in a set of Python scripts which, were integrated into a comprehensive load calculation workflow further described in Section 3.4.2. Finally, note that no mean stress corrections were considered in the fatigue analysis of this research.

3.3 Load Catalogue Design

3.3.1 Reference Site Conditions

The load catalogue developed in this thesis is intended to represent loading conditions in modern offshore wind farms. Based on the Global Wind Atlas [98] [99], site conditions suitable for IEC Class IC turbines (refer to Table 2.1) are the most prevalent in offshore locations, particularly in the North Sea, which is a global hotspot for offshore wind energy projects. Accordingly, Class IC was selected as a reference for the definition of the environmental conditions considered in part of the load catalogue. In other words, in a portion of the catalogue, the wind climate inputs were selected in accordance with the reference conditions of Class IC. These are presented in Table 3.4. One important note to make here is that the reference wind climate parameters for Class IC are higher than those observed in offshore sites, which are typically characterized by low turbulence intensity and wind shear exponent values. However, Class IC turbines are still selected for most offshore sites to guarantee safety, accounting for wake effects and design uncertainties.

Table 3.4: Reference environmental conditions for IEC design Class IC

Mean wind speed distribution	Rayleigh (Equation 3.2)
Average 10-min mean wind speed (U_{ave}^{IC})	10 m/s
Reference turbulence intensity (I_{ref}^{IC})	12%
Wind shear exponent in NWC	0.14

For the remainder of the load catalogue, an actual wind farm site was considered. The site is located in the Danish North Sea, 22 kilometers off of the west coast of Thorsminde, Denmark, and is the home to one of the wind farms currently being constructed by RWE. The wind farm shall be referred to as the *RWE wind farm* in the remainder of this report.

Wind climate measurements from a floating LiDAR collected at the site between 2020 and 2021 were provided by RWE. The data consists of mean wind speed, mean wind direction, turbulence intensity, and wind shear values measured over 10-minute intervals for a period of one year. Moreover, the dataset was processed to obtain a Weibull distribution for the mean wind speed and a wind rose for the mean wind direction, in addition to other relevant wind climate statistics. Summary information about the wind climate at the RWE wind farm site is provided in Figure 3.5. As for the full dataset, it is not provided for confidentiality reasons.

Mean wind speed distribution	Weibull (Equation 3.1)
Weibull shape parameter (k)	2.45
Weibull scale parameter (a)	11.68 m/s
Mean turbulence intensity (I_{amb})	9.5%
Mean wind shear exponent	0.07
Air density	1.225 kg/m^3

Table 3.5: Ambient environmental conditions at RWE wind farm site

Long-term sea state data for the RWE wind farm site could not be acquired for the purpose of this thesis. Instead, metocean data was adapted from Table 3.2 of the IEA 15 MW RWT documentation [21], where it was used to conduct an ultimate load analysis with OpenFAST. The data tabulates the significant wave height (H_s) and peak spectral period (T_p) against the hub-height mean wind speed (U_{hub}), and is presented in Table 3.6. This wind-wave lookup table was used for all the load calculations of this thesis, including those of Class IC. On a final note, the division of the load catalogue between Class IC conditions and RWE wind farm conditions is explained in Section 3.3.5.

Table 3.6: Wind-wave lookup table used to determine wave model parameters based on the mean wind speed (adapted from [21], Table 3.2)

U_{hub} [m/s]	H_s [m]	T_p [s]
4	1.102	8.515
6	1.179	8.310
8	1.316	8.006
10	1.537	7.651
12	1.836	7.441
14	2.188	7.461
16	2.598	7.643
18	3.061	8.047
20	3.617	8.521
22	4.027	8.987
24	4.516	9.542

3.3.2 Load Analysis Framework

Fatigue is a major risk factor for wind turbine failure. Therefore, fatigue loading, as reflected by DELs, is the focus of this thesis. Accordingly, the DEL framework described in Section 3.2 was applied for the load calculations of this research. Moreover, no directional load analysis was performed for tower components. That is, the DELs corresponding to the same loading component, e.g. the tower base fore-aft bending moment, were added up regardless of wind flow direction, even thought the stresses resulting from these loads would be distributed differently over the tower's circumference across the different flow directions.

Since fatigue damage builds up over relatively long timescales and since wind turbines operate under normal operating conditions for most of their lifetimes, the load catalogue established in this thesis is based entirely on load calculations for DLC 1.2 (refer to Table 2.2), namely power production under normal operating conditions. Fatigue load contributions from other operating modes, such as startups (DLC 3.1) and shutdowns (DLC 4.1), can be accounted for by properly applying a correction margin to the DEL results. However, this was not done in this research.

As explained in Section 3.2, DEL results must be reported along with an associated equivalent number of cycles (N_{eq}) and simulation time (T_{sim}). The values used in this study are 600 cycles and 10 minutes for N_{eq} and T_{sim} respectively. To wrap up, the parameters of the load analysis performed in the construction of this thesis' load catalogue are summarized in Table 3.7.

Table 3.7: Load analysis parameters used for the load calculations of this thesis

Loading type	Fatigue
DLC	1.2
N_{eq}	600 cycles
T_{sim}	10 minutes

3.3.3 Input Space Design

Wind Climate Parameters

The main function of the load catalogue built in this thesis is to map wind climate parameters to wind turbine fatigue loads. To be practically valuable, the catalogue must be representative of a wide range of offshore site conditions. This means that, first and foremost, the catalogue must account for as many relevant wind climate parameters as possible, whereby relevance is measured with respect to influence on fatigue loads. Second, the values of each considered wind climate parameter must vary over a range wide enough to reflect a variety of possible offshore climates. Third, by the same token, many combinations of the selected wind climate parameters must be considered.

The considerations above lead to a trade-off between the catalogue's size, complexity, and development effort on one hand and its comprehensiveness on the other. Indeed, a balanced selection of wind climate parameters is crucial to ensure the catalogue's practical utility without making it overly complex to use or excessively labor-intensive to develop. Accordingly, the wind climate parameters selected for the load catalogue of this thesis are the mean wind speed, the turbulence intensity, and the wind shear exponent. The rationale behind this choice is that numerous studies have shown these wind climate parameters to be the most influential on fatigue loads [5], [100], [84], [101].

As discussed in Section 3.3.1, part of this thesis' load catalogue is intended for operation near Class IC reference environmental conditions. For this catalogue subset, the selected wind climate parameters can assume values within the ranges given in Table 3.8. The mean wind speed varies between 3 m/s and 25 m/s, covering the operational range of typical modern offshore turbines. The range for the turbulence intensity is centred around the reference value for IEC design Class IC, namely $I_{ref}^{IC} = 12\%$, and stretches to $I_{ref}^{IC} \pm 0.1 I_{ref}^{IC}$. Likewise, the wind shear exponent is approximately centred at the reference value and goes from 0.1 to 0.2. The specific values and combinations of the wind climate parameters found in this portion of the load catalogue are discussed in Section 3.3.6.

Table 3.8: Ranges of variation for the selected wind climate parameters centred around IEC Class IC reference conditions; applicable for LS1 only (refer to Figure 3.8)

Wind Climate Parameter	Lower Bound	Upper Bound
Mean wind speed [m/s]	3	25
Reference Turbulence intensity [%]	10.8	13.2
Wind shear exponent [-]	0.10	0.20

For the remaining portion of the catalogue, intended for operation under environmental conditions similar to those of the RWE wind farm, the wind climate parameters were directly derived from the site measurements. Specifically, the mean wind speed range was divided into eleven 2 m/s-wide bins between 3 m/s and 25 m/s, and the 360-degree range was divided into twelve 30-degree angular sectors. The site data was then used to compute the ambient turbulence intensity for each wind speed bin and angular sector. This was done using Equation 3.7 to calculate the 90th percentile ambient turbulence intensity from the mean value and standard deviation for each bin and sector. As for the wind shear exponent, it was taken as the energy-weighted average value of 0.07, independent of mean wind speed and direction.

Wind Farm Configuration Parameters

Offshore wind farms are typically densely packed to make efficient use of land. However, the farm's layout is optimized to maximize power production and farm lifetime, resulting in a site-specific configuration that might not always exhibit a regular pattern. Thus, there is no such thing as a characteristic or universal wind farm layout. Nevertheless, the impact of surrounding turbines on loads is predominantly dictated by the turbines in close proximity to the turbine being assessed. Therefore, the number of neighbouring turbines and the distance to each one of them are more important than the exact wind farm layout. Building on this reasoning, in the farm load calculations performed in this study, a regular rectangular layout like the one sketched in Figure 3.7 was assumed. Moreover, it was assumed that the farm comprises more than two rows, implying that each interior turbine in the farm has eight neighbouring turbines (see Table 3.9). Furthermore, it was assumed that the spacing between rows is equal to the inter-turbine spacing within each row.

The points discussed above imply that the relevant wind farm unit for load calculations is a 3x3 square grid with uniform spacing in all directions. Evidently, in this setup, the relevant turbine for load calculations is the central turbine. Additionally, a single degree parameter is needed to define the farm's layout, namely the spacing s, measured in turbine diameters. The latter is regarded as an independent input parameter in the load catalogue and ranges from 4 to 8. Another consideration is the farm's orientation. The latter was optimized based on the site's energy rose, resulting in a compass orientation of 30 degrees measured counterclockwise.

Before further proceeding, it is important to note that the wind farm loads documented in this thesis' load catalogue do not exactly reflect the loading conditions at the actual RWE wind farm. Instead, the listed loads represent various hypothetical wind farms, each characterized by a regular square layout and differentiated solely by their inter-turbine spacing, operating at the RWE wind farm site.

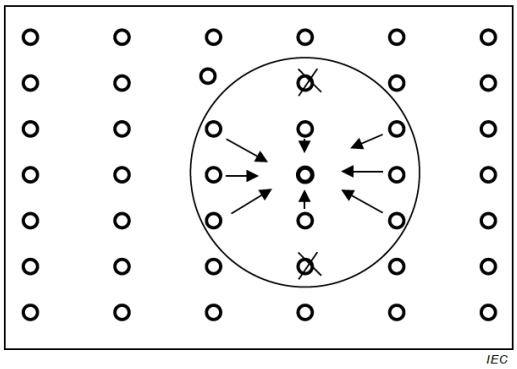

Figure 3.7: Wind farm with a regular rectangular layout and more than two rows (adapted from [9])

Wind Farm Configuration	N
2 wind turbines	1
1 row	2
2 rows	5
more than 2 rows	8

Table 3.9: Number of neighbouring turbines for different rectangular wind farm configurations (adapted from [9])

Since directional loading effects are neglected in this study, mean flow direction is not important for solitary turbine load calculations. However, this is not the case for wind farm load calculations where the mean flow direction together with the wind farm layout and compass orientation define the wake characteristics. Consequently, mean flow direction should be considered in farm load calculations. This means that, to obtain a representative DEL value for a given combination of input parameters, twelve simulations must be performed, one per 30-degree angular sector. However, the symmetric nature of the wind farm layout was exploited to reduce the number of required simulation. Indeed, it can be observed from Figure 3.7 that the considered layout consists of 4 identical quadrants. It follows that considering a single quadrant is sufficient to capture all possible wake states. Therefore, only three simulations corresponding to three angular sectors, centred at 0, 30 and 60 degrees respectively, were needed. Conservatively, the turbulence intensity values corresponding to each of the three sectors were taken as the maximum values across the 4 symmetrical sectors per wind bin[3].

The directional considerations above were relevant for farm load calculations with the DWM wake model. In this case, for a given input parameter combination, three FAST.Farm simulations were performed and the corresponding DELs were computed. These results were then extrapolated to the full 360-degree range and combined into a single representative DEL using the site's wind rose. This was not required for farm load calculations with Frandsen's wake model. In fact, in this case, directional effects were taken into account by the effective turbulence intensity, and only a single OpenFAST simulation was needed. Nonetheless, directional considerations were necessary for the calculation of effective turbulence intensity values. This was done for each wind speed bin according to the procedure described in Section 3.1.5, with the aid of the site's wind rose. Lastly, note that multiple sets of effective turbulence intensities were computed, one for each considered combination of the inter-turbine spacing and Wöhler exponent.

[3] For example, for a given wind speed bin, the turbulence intensity for the sector centred at 0 degrees would be the maximum of the turbulence intensities for the sectors centred at 0, 90, 180 and 270 degrees.

3.3.4 Selected Load Sensors and Metrics

In this research, fatigue loads are quantified in terms of DELs. The load catalogue of this thesis displays DELs for various loading types affecting different turbine structural components. These designated load sensors are listed in Table 3.10 along with the Wöhler exponent (m) of the corresponding structural component. The selection was mainly based on the importance of the load sensors in wind farm design and site suitability assessment. As for the Wöhler exponents, they were taken as generic values following common industry practices.

Table 3.10: Selected load sensors and corresponding Wöhler exponents

Component	Label	Description	Wöhler exponent
Blade	BldRtMedg	Edgewise bending moment at blade root	10
Blade	BldRtMflp	Flapwise bending moment at blade root	10
Blade	BldMdMedg	Edgewise bending moment at 50% of the blade span	10
Blade	BldMdMflp	Flapwise bending moment at 50% of the blade span	10
Blade	BldTpMedg	Edgewise bending moment at 75% of the blade span	10
Blade	BldTpMflp	Flapwise bending moment at 75% of the blade span	10
Tower	TwrBsMss	Side-to-side bending moment at tower base	4
Tower	TwrBsMfa	Fore-aft bending moment at tower base	4
Tower	TwrBsTor	Torsional moment at tower base	4
Tower	TwrMdMss	Side-to-side bending moment at tower midpoint	4
Tower	TwrMdMfa	Fore-aft bending moment at tower midpoint	4
Tower	TwrMdTor	Torsional moment at tower midpoint	4
Tower	TwrTpMss	Side-to-side bending moment at tower top	4
Tower	TwrTpMfa	Fore-aft bending moment at tower top	4
Tower	TwrTpTor	Torsional moment at tower top	4

3.3.5 Load Catalogue Structure

The load catalogue delivered alongside this thesis is organized as illustrated in Figure 3.8. The catalogue is divided into two main load databases, load sets 1 and 2. Load Set 1 (LS1) contains load data for a solitary turbine operating under Class IC reference environmental conditions (Table 3.4). On the other hand, the data in LS2 is for a turbine in a wind farm operating under the environmental conditions at the RWE wind farm site (Figure 3.5). Based on the rationale of Section 3.3.3, the load data is reported for the central turbine in a 3x3 wind farm having a regular square grid layout with three rows.

Each load set is further divided into subsets, whereby LS1 consists of four subsets and LS2 consists of two subsets. These subsets are all identical in structure and consist of load databases in tabular format. These tables map the selected input parameters of Section 3.3.3 to the corresponding DELs, obtained by applying the load calculation workflow described in Section 3.4.2, for the load sensors defined in Section 3.3.4. In particular, each table row is regarded as a catalogue entry and presents the DEL results for a given operational scenario, defined by a specific combination of input parameters listed alongside the outputs. Moreover, the operational scenarios remain consistent across all the subsets of a given load set, but they differ between LS1 and LS2.

For LS1, the input parameters are the wind climate parameters. While the same operational scenarios are considered for all subsets of LS1, the subsets are distinguished by the selection of turbulence and turbulence intensity models employed in their load calculations. The combinations of turbulence and turbulence intensity models used for each subset are presented in Figure 3.8. As will become clearer in Section 3.5, the structure of the load catalogue was designed to facilitate the comparison of DEL results obtained using different wind models.

In LS2, the wind climate parameters are not considered as input parameters since they are implicitly specified by the wind climate at the RWE wind farm site. Hence, since the layout geometry is also implicitly specified, the inter-turbine spacing is the only input parameter. As opposed to LS1, the same turbulence and turbulence intensity models, namely the Kaimal model and the 90^{th} Percentile NTM respectively, are applied in the load calculations of each subset of LS2. These models are applied based on the site turbulence intensity data described in Section 3.3.3. The only difference between the subsets of LS2 is the utilized wake model, whereby the Frandsen model is applied for LS2.1 and the DWM

model is applied for LS2.2.

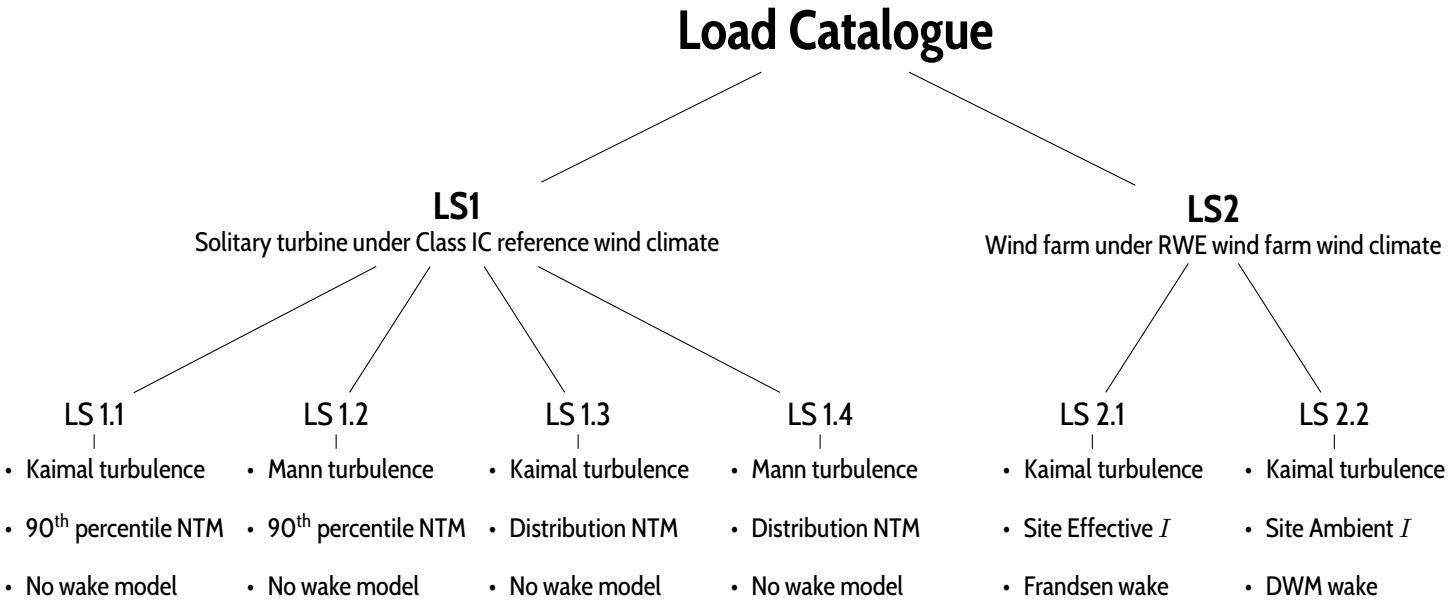

Figure 3.8: Load catalogue hierarchical diagram

3.3.6 Load Catalogue Contents

In total, the load catalogue has 462 entries and requires 6,732 simulations to compile. As explained in Section 3.3.5, each entry corresponds to a specific operational scenario, defined by a unique combination of input parameters. For each load set, the combinations are drawn from a predefined set of possible parameter values. The input parameters are treated as independent variables, and the sampling is exhaustive, meaning that all possible combinations of input parameters are considered.

The considered sets of input parameter values for each load set are given in Table 3.11, along with the corresponding number of entries and required simulations. For LS1, the wind climate parameter values are selected to effectively cover the variation ranges specified in Table 3.8, thereby reflecting the wind conditions at sites with climates similar to the Class IC reference climate. In contrast, LS2 focuses on the environmental conditions at the RWE wind farm site and only considers the wind climate parameters observed there. The operating conditions in this case are thus defined by a single variable: the inter-turbine spacing (s) in the wind farm. In addition, it is noteworthy that the reference turbulence intensity is not defined for LS2, just like the turbine spacing is undefined for LS1.

As pointed out in Section 3.3.5, the subsets of each load set list the same operational scenarios. Considering the parameter value sets[4] for LS1 and LS2 and given that they have 4 and 2 subsets respectively, the result is 396 total entries for LS1 and 66 total entries for LS2. Since 12 random number generator seeds are used in the load calculations, 12 simulations are required per catalogue entry (refer to Section 3.2 and Section 3.4 for more details). This means that LS1 requires 4,752 simulations to complete. For LS2, more simulations are needed per operational scenario. This is because, for LS2.1, the application of Frandsen's effective turbulence model (Section 3.1.5) requires the performance of two separate simulations, one for each Wöhler exponent, per operational scenario per turbulence seed. For 33 operating cases, this results in 792 simulations needed. This number is even larger for LS2.2. In this case, no separate simulations are needed for components having different Wöhler exponents. Nevertheless, since the DWM simulations are inherently directional, each load calculation requires three simulations (more details in Section 3.3.3) per operating case per turbulence seed. Overall, this amounts to 1,188 simulations for LS2.2.

[4] These imply a total of 11x3x3=99 possible combinations/scenarios for LS1, and 11x3=33 possible combinations/scenarios for LS2.

Table 3.11: Load catalogue contents and simulation requirements

	LS1	LS2
Mean wind speed values[5] [m/s]	4:2:24	4:2:24
Reference Turbulence intensity values [%]	(10.8, 12.0, 13.2)	-
Wind shear exponent values [-]	(0.10, 0.15, 0.20)	0.07
Normalized inter-turbine spacing values [-]	-	(4, 6, 8)
Subset entries [-]	99	33
Load set entries [-]	396	66
Simulations required [-]	4,752	1,980

3.4 Load Catalogue Population

3.4.1 Simulation Setup

Once the load catalogue's structure is established and the operational scenarios are defined, the data population process can start. This entails iteratively performing load calculations for every operational scenario of every load set. To do that, the simulation environment employed in these calculations first needs to be defined.

The simulation setups used for each load set are presented in Table 3.12. All performed simulations have a duration of 700 seconds, out of which the first 100 seconds are discarded from the output record to eliminate the transient response, resulting in 10-minute output timeseries. The wind timeseries required for the simulations match the simulation duration and are generated using the turbulence simulators of Section 3.1.3, where their settings are described. Moreover, 12 different random number generator seeds[6] are used for every load calculation run. This means that, for each load catalogue entry, 12 wind file realizations and 12 corresponding simulations are needed. Furthermore, the same seeds are fed to the turbulence simulator, the HydroDyn wave simulator, and the random number generator employed to sample from the Weibull distribution for turbulence intensity (when applicable).

For completeness, all the OpenFAST and FAST.Farm input files defining the simulation setup of this study are provided in Appendix C and Appendix D respectively.

Table 3.12: Simulation setups used for the load calculations of each catalogue load set

	LS1.1	LS1.2	LS1.3	LS1.4	LS2.1	LS2.2
Simulation duration	700 s					
Output record start time	100 s					
Number of seeds (N_{seeds})	12					
Simulation tool	OpenFAST					FAST.Farm
Solver timestep	0.005 s					Variable[7]
Turbulence simulator	TurbSim	Bladed	TurbSim	Bladed	TurbSim	TurbSim

3.4.2 Load Calculation Workflow

Having set up the simulation environment, the load calculation iterations can begin. Each iteration fills the output section of a single catalogue entry and follows the workflow illustrated in Figure 3.9. First, based on the catalogue load

[5] The notation 4:2:24 means that the load set ranges from 4 m/s to 24 m/s inclusive with steps of 2 m/s. The resulting mean wind speed values can thus be thought of as the centers of 11 2m/s-wide wind bins between 3 m/s and 25 m/s. Full set: (4, 6, 8, 10, 12, 14, 16, 18, 20, 22, 24).

[6] The same set of seeds is used for all the operational scenarios in both LS1 and LS2. The seed values are provided in Appendix A.

[7] The FAST.Farm driver timestep is variable and depends on the mean wind speed as per the modelling guidance in [95]. The timestep for the OpenFAST modules in farm simulations remains 0.005 seconds.

set being populated, the appropriate simulation setup is determined. Then, the input parameters are extracted from the input section of the first load set entry. The turbulence simulator is then invoked to generate the wind files required for the dynamic simulations. Since 12 seeds are used, 12 turbulence timeseries realizations are produced. The wind data is subsequently fed to the relevant numerical model, which simulates the response of the wind turbine or wind farm for each wind timeseries. The outcome is 12 sets of output data, each containing 10-minute loading histories for each of the load sensors listed in Table 3.10. The loading histories must then be converted into DELs through a series of post-processing steps. Applying the framework described in Section 3.2, the loading histories are rainflow-counted to construct load spectra, from which a damage-equivalent load range can be computed for each load sensor based on Equation 3.12. This is done for all 12 output datasets, reducing them to 12 sets of damage-equivalent load ranges. After that, the damage-equivalent load ranges for the different seeds are combined into a single set of DELs using Equation 3.13. Lastly, the DELs are stored in the output section of the relevant entry and the iteration is completed. The described process is then repeated for all load set entries and all load sets until the database is fully populated.

For the purpose of this research, the workflow described above was fully implemented in a Python code pipeline. NREL's *openfast_toolbox* [97] was instrumental in the establishment of the pipeline. Most notably, the toolbox's *equivalent_load* function greatly facilitated the computation of DELs directly from OpenFAST/FAST.Farm simulation output files.

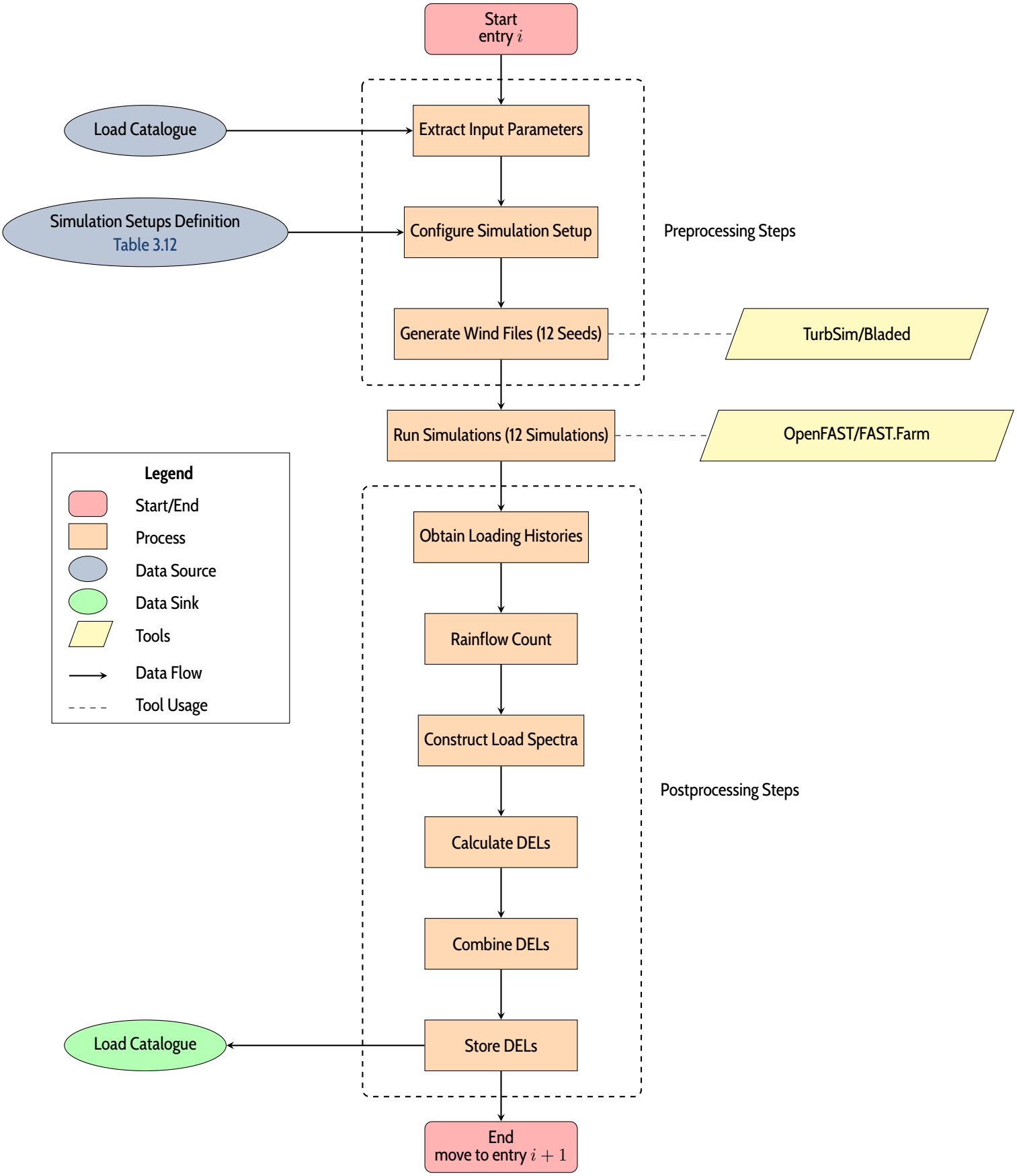

Figure 3.9: Load calculation workflow applied for load catalogue population

3.4.3 Workflow Validation

One of the main objectives of this thesis is to deliver a reliable load catalogue. To ensure the fulfillment of this goal, a validation study was conducted to evaluate the reliability of the load calculation pipeline used to compile the catalogue. Unfortunately, no DEL data for the IEA 15 MW RWT could be found in the literature. Thus, the entire load calculation workflow could not be validated directly by benchmarking against known DEL results. Instead, an alternative approach was considered.

First, the OpenFAST model of the IEA 15 MW RWT was validated by running a steady-state analysis. Specifically, the response of the RWT was simulated under uniform, steady wind conditions for multiple mean wind speed values covering the turbine's operational range and the steady-state values of several characteristic response variables were recorded. Subsequently, the rotor performance curve and the controller regulation curve of the RWT were constructed. The curves were then benchmarked against the reference curves found in the documentation of the IEA 15 MW RWT [21], which were reproduced using the tabular data found in the GitHub repository of IEA Wind Task 37 [102]. The results are shown in Figure 3.10, in which a good agreement between the results can be observed. Therefore, it can be concluded that the OpenFAST RWT model employed in this thesis is reliable with respect to the one defined in the RWT's documentation. It follows that the used FAST.Farm model, which employs the same OpenFAST RWT model for the farm's constituent turbines, is also reliable, provided that the employed FAST.Farm glue-code passed NREL's diagnostic regressions tests [103].

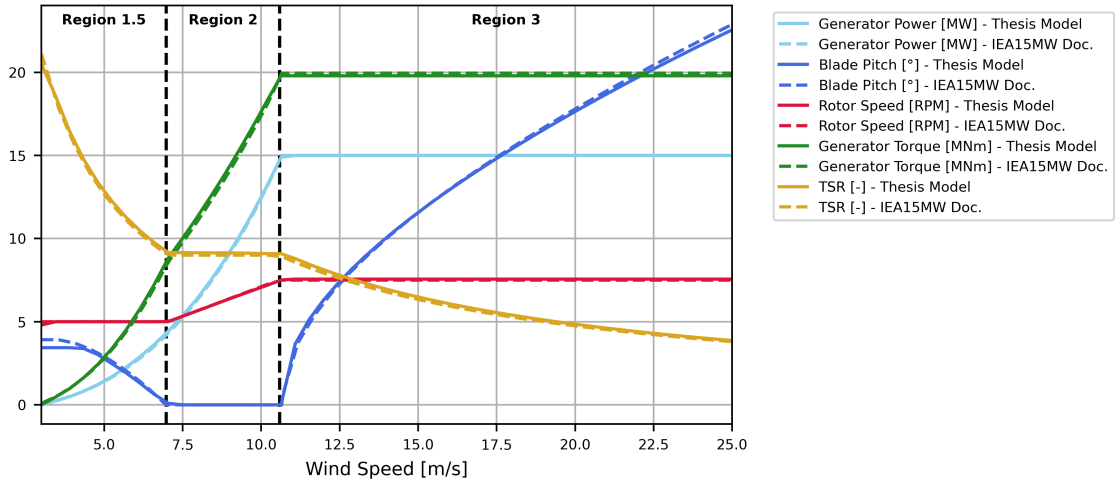

Figure 3.10: Steady-state response validation for IEA 15 MW RWT model used in this thesis

Since the load catalogue is designed for turbulent operating conditions, it is not enough to verify the steady-state response of the RWT model. To address that, an extreme load validation study was conducted under turbulent wind conditions. Particularly, 700-second turbulent simulations of the IEA 15 MW RWT were performed with IEC Class B turbulence (90$^{\text{th}}$ percentile NTM, $I_{ref} = 14\%$) for a variety of mean wind speeds within the operational range. Moreover, the Kaimal turbulence model was employed, the wind shear exponent was taken as $\alpha = 0.14$ and 6 turbulence seeds were used. The 10-minute ultimate loads were then calculated for each of the performed simulations after discarding the first 100 seconds of the output records. After that, the obtained results, presented in Figure 3.11, were benchmarked against those reported in Figure 7 of [104], which conducted a validation study for the IEA 15 MW turbine model using various software tools including OpenFAST, and under the same conditions of this study. Unfortunately, the data used to plot the response graphs of [104] could not be obtained. Hence, the results are not presented explicitly and the comparison was made by inspection of the plots found in the paper. Close agreement was observed in the results, providing further evidence into the reliability of the employed numerical model as well as the involved pre-processing code pipeline.

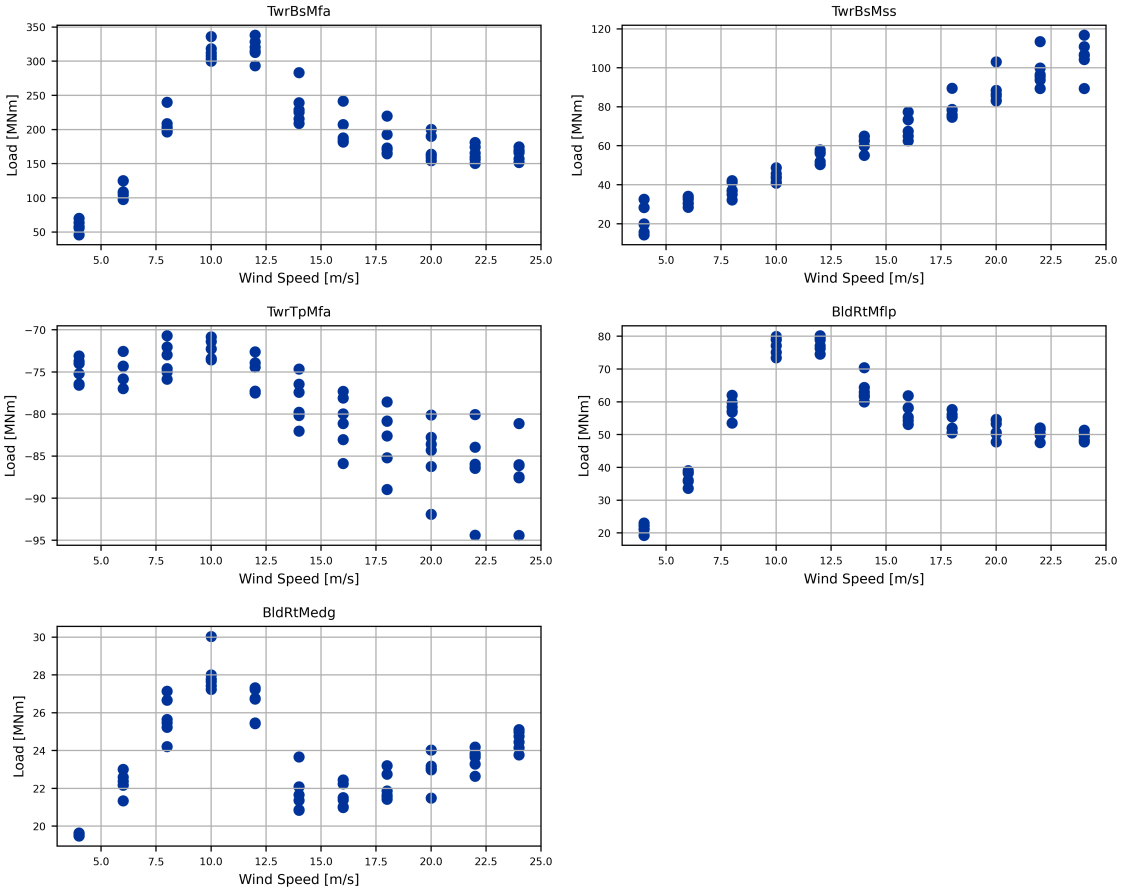

Figure 3.11: Extreme load results for the IEA 15 MW RWT obtained through OpenFAST simulations for normal operation under Class IB environmental conditions

Although the conducted validation study does not certify the reliability of the post-processing pipeline utilized to compute DELs, there is a good reason to assume its reliability regardless. The reason is that the *equivalent_load* function of NREL's *openfast_toolbox* was used without modification to calculate DELs directly from OpenFAST/FAST.Farm simulation output data. Hence, provided that this code has been developed by a reliable party and has been extensively used for fatigue analysis in the literature, the load calculation pipeline employed in this research can be regarded as reliable.

3.5 Load Catalogue Analysis

3.5.1 Analysis Objectives and Focus Areas

As outlined in Section 1.4, besides delivering a high-fidelity fatigue load catalogue, this thesis aims to evaluate the impact of employing different wind and wake models on DEL results. To achieve that, the catalogue data was analyzed in an attempt to answer the following two questions:

1. What is the impact of employing different wind and wake models on DEL predictions?
2. How does this impact vary as a function of the different wind climate parameters?

Based on these questions, three analysis Focus Areas (FAs) were identified to isolate the different aspects under investigation in this study. These are described in Table 3.13. The three FAs address the influence of changing the turbulence intensity model, the turbulence model, and the wake model respectively. For each FA, two different models among the ones described in Section 3.1 are compared, as reflected by the FA's designation. Moreover, each FA is concerned with specific operating conditions, as reflected by the load set used for its analysis. Particularly, since FA1 and FA2 analyse LS1, these involve a solitary wind turbine operating under Class IC reference environmental conditions. In contrast,

since FA3 analyses LS2, it involves a wind farm operating under the environmental conditions at the RWE wind farm site.

Table 3.13: Description of the analysis focus areas of this thesis

Focus Area	Designation	Investigated Model	Load Set
1	90th Percentile NTM vs Distribution NTM	Turbulence Intensity	LS1
2	Kaimal Turbulence vs Mann Turbulence	Turbulence	LS1
3	Frandsen Wake vs DWM Wake	Wake	LS2

3.5.2 Analysis Methods

Equivalent Load Effect and Load Deviation

For each FA, the impact of swapping the considered models was quantified by the resulting deviation in the annual equivalent load effect. This metric is calculated as follows. First, the pair of load sets to be compared is identified based on the considered FA. For example, for FA1, this pair could either be LS1.1 and LS1.3 or LS1.2 and LS1.4. Notice that, in accordance with the analysis objectives of FA1, only the considered NTM model varies within each of these load set pairs, with all other modelling choices remaining consistent. The same reasoning applies to FA2 and FA3.

Once the analysis load sets are identified, a specific combination of input parameters, excluding the mean wind speed, is selected. For LS1, this would be a specific combination (I_{ref}, α). While for LS2, this would be a specific value of s. After that, all the entries of the analysis load sets corresponding to the selected input parameter values are collected. Referring back to Table 3.11, this results in two sets of 11 entries each, one for every mean wind speed value. In other words, each of the analysis load sets would be reduced into a set of 11 entries, with one DEL value (per load sensor) for each 2 m/s wide wind speed bin between the cut-in and cut-out wind speeds. Also, it must be noted that these reduced sets correspond to specific values of I_{ref} and α for LS1, and s for LS2, drawn from their respective sets of possible values presented in Table 3.11.

After the load sets are reduced, the annual equivalent load effects are calculated for all load sensors based on Equation 3.14. To do that, for LS1, the mean wind speed distribution is used to determine the occurrence probabilities $p(U_i)$ of each of the 11 mean wind speed values U_i. In this case, the distribution is a Rayleigh distribution (Equation 3.2) with $U_{ave} = U^C_{ave} = 10\,m/s$. As for the mean flow direction distribution, it is assumed uniform since directional loading effects are neglected in this study. Thus, Equation 3.14 reduces to Equation 3.15, with $T_{ref} = 1\,year$.

$$F_{LS1} = \left(\frac{T_{ref}}{T_{sim}} \sum_{i=1}^{11} p(U_i) DEL^m(U_i)\right)^{1/m} \tag{3.15}$$

In contrast, for LS2, the occurrence probabilities $p(U_i|\theta_j)$ and $p(\theta_j)$ are determined from the site-specific data described in Section 3.3.1. In this case, Equation 3.14 translates to Equation 3.16.

$$F_{LS2} = \left(\frac{T_{ref}}{T_{sim}} \sum_{j=1}^{12} p(\theta_j) \sum_{i=1}^{11} p(U_i|\theta_j) DEL^m(U_i, \theta_j)\right)^{1/m} \tag{3.16}$$

The procedure so far yields two sets of values, one for each of the initially-selected analysis load sets, containing the annual equivalent load effects for each load sensor. The final step is to compute the deviations between these two sets. For each load sensor, this deviation is computed through Equation 3.17. This results in a single set of load effect deviations, one for each load sensor. Importantly, these deviations are associated to a pair of analysis load sets as well as a set of input parameters, namely (I_{ref}, α) for LS1 and s for LS2.

$$\Delta F_l = \frac{F_{l,2} - F_{l,1}}{F_{l,1}} \tag{3.17}$$

where:

l is an index designating a specific load sensor

$F_{l,1}$ is the annual equivalent load effect for load sensor l calculated based on the first analysis load set

$F_{l,2}$ is the annual equivalent load effect for load sensor l calculated based on the second analysis load set

Sensitivity Analysis

In addition to assessing the effect of interchanging two specific models on load results, it is important to investigate how this effect varies as a function of the wind climate parameters, the wind farm layout and other modelling choices. This was achieved by conducting a sensitivity analysis for the load effect deviation. To that end, the procedure described in the previous subsection was applied for different combinations of the input parameters and the results were compared. For FA1 and FA2, sensitivity was assessed with respect to I_{ref} and α as well as the choice of turbulence and turbulence intensity models. As for FA3, only the sensitivity to inter-turbine spacing was assessed. Moreover, for FA2, the load deviation sensitivity to the mean wind speed was investigated. However, the 10-minute DEL deviation was considered for this analysis rather than the annual load effect deviation to preserve dependence on the mean wind speed. This was done by applying the procedure described in the previous subsection, but only up to the point just before calculating the load effect.

4

Results and Discussion

4.1 Results

4.1.1 The Load Catalogue

In accordance with the foremost objective of this research, the culmination of this thesis' work was the development of a high-fidelity fatigue load catalogue tailored for offshore applications. This was achieved by applying the methods described in Chapter 3 to design the load database, setup a load calculation workflow, and then use the workflow to populate the database. The resulting catalogue was delivered alongside this thesis as a set of two Excel files, each subdivided into multiple sheets according to the diagram in Figure 3.8, such that each file contains one load set and each sheet contains one load subset. In total, the catalogue has 462 entries and required 6,732 simulations to populate, among which 5,544 were performed using OpenFAST and 1,188 were performed using FAST.Farm. Regarding the specific contents of the database, these are described in Section 3.3.6. As for the associated environmental conditions, load calculation framework and simulation setup, refer to Section 3.3.1, Section 3.3.2 and Section 3.4.1 respectively.

To illustrate the organization of the elementary catalogue unit, the load subset, samples from LS1.1 and LS2.1 are presented in Figure 4.1a and Figure 4.1b respectively. The load sets are not shown in full for convenience. For both subsets, the first column contains integer numbers indexing the various operational scenarios. For LS1.1, the next three columns contain the wind climate parameter values. The subsequent two columns define the employed turbulence and turbulence intensity models, forming the input section along with the wind parameter columns and the index column. Subsequently, the last 15 columns define the output section, tabulating the DEL results with one column per load sensor listed in Table 3.10. For LS2.1, only three input columns are required. The first one is the index column, while the second one contains the inter-turbine spacing values and the third one specifies the used wake model. Conversely, the turbulence and turbulence intensity models need not be specified as they are consistent across LS2. This is also the case for the turbulence intensity and wind shear exponent values, which are similarly consistent across LS2. Furthermore, the output section of LS2.1 follows the same structure as for LS1.1. Finally, all the subsets of LS1 follow the same organization as LS1.1, and the same applies for the subsets of LS2 in relation to LS2.1.

Input Section						Output Section			
Op. Scenario	U [m/s]	Ref. TI [%]	Wind Shear Exp. [-]	Turbulence Model [-]	TI Model [-]	BldRtMedg [MNm]	BldRtMflp [MNm]	...	TwrTpTor [MNm]
1	4	10.8	0.1	Kaimal	Percentile	30	30	...	9
2	6	10.8	0.1	Kaimal	Percentile	28	29	...	15
3	8	10.8	0.1	Kaimal	Percentile	29	32	...	15
4	10	10.8	0.1	Kaimal	Percentile	31	31	...	5
5	12	10.8	0.1	Kaimal	Percentile	29	32	...	5
6	14	10.8	0.1	Kaimal	Percentile	31	28	...	13
7	16	10.8	0.1	Kaimal	Percentile	29	32	...	9
8	18	10.8	0.1	Kaimal	Percentile	28	31	...	10
9	20	10.8	0.1	Kaimal	Percentile	30	31	...	8
10	22	10.8	0.1	Kaimal	Percentile	31	28	...	10
11	24	10.8	0.1	Kaimal	Percentile	31	31	...	4
12	4	10.8	0.15	Kaimal	Percentile	32	30	...	5
13	6	10.8	0.15	Kaimal	Percentile	30	29	...	12
14	8	10.8	0.15	Kaimal	Percentile	30	31	...	14
15	10	10.8	0.15	Kaimal	Percentile	29	32	...	5
16	12	10.8	0.15	Kaimal	Percentile	30	32	...	11
17	14	10.8	0.15	Kaimal	Percentile	32	29	...	5
18	16	10.8	0.15	Kaimal	Percentile	31	29	...	5
19	18	10.8	0.15	Kaimal	Percentile	32	30	...	7
20	20	10.8	0.15	Kaimal	Percentile	32	28	...	4
21	22	10.8	0.15	Kaimal	Percentile	29	28	...	15
22	24	10.8	0.15	Kaimal	Percentile	30	28	...	15
⋮	⋮	⋮	⋮	⋮	⋮	⋮	⋮	⋮	⋮

(a) Load catalogue sample from LS1.1

Input Section				Output Section			
Op. Scenario	U [m/s]	Spacing [-]	Wake Model [-]	BldRtMedg [MNm]	BldRtMflp [MNm]	...	TwrTpTor [MNm]
1	4	4	Frandsen	32	28	...	9
2	6	4	Frandsen	31	29	...	11
3	8	4	Frandsen	29	32	...	5
4	10	4	Frandsen	29	32	...	15
5	12	4	Frandsen	32	31	...	15
6	14	4	Frandsen	29	32	...	6
7	16	4	Frandsen	30	29	...	4
8	18	4	Frandsen	32	32	...	14
9	20	4	Frandsen	32	31	...	15
10	22	4	Frandsen	32	29	...	15
11	24	4	Frandsen	32	32	...	5
12	4	5	Frandsen	30	31	...	6
13	6	5	Frandsen	31	30	...	13
14	8	5	Frandsen	31	30	...	6
15	10	5	Frandsen	31	29	...	5
16	12	5	Frandsen	29	30	...	14
17	14	5	Frandsen	30	28	...	5
18	16	5	Frandsen	29	28	...	12
19	18	5	Frandsen	30	29	...	4
20	20	5	Frandsen	30	32	...	8
21	22	5	Frandsen	31	28	...	4
22	24	5	Frandsen	32	28	...	13
⋮	⋮	⋮	⋮	⋮	⋮	⋮	⋮

(b) Load catalogue sample from LS2.1

Figure 4.1: Load catalogue samples illustrating the organization of load subsets

In addition to the load data, the load catalogue is equipped with functional features for data analysis and visualization. These features have been implemented in Excel and integrated into each of the two Excel files constituting the load catalogue. The offered tools include:

1. An interpolation tool that estimates DELs for a custom (restricted) combination of input parameters based on the catalogue entries.

2. A load effect calculation tool that allows the calculation of the equivalent load effect for any Weibull distribution parameters (k and a), reference period (T_{ref}) and equivalent number of cycles (N_{eq}).

3. A data visualization tool that provides a visual comparison of DELs corresponding to different wind or wake models for a given operational scenario.

In order to develop the load catalogue, this thesis involved the establishment of an efficient and reliable computational pipeline for fatigue load calculations. This pipeline was implemented in a series of Python scripts assisted by a set of libraries and executable applications. The whole pipeline was packaged into a self-contained Python virtual environment that is extremely easy to install and use. However, the load catalogue and the code are not shared with this publicly-available report.

4.1.2 Focus Area 1: 90th Percentile NTM vs Distribution NTM

This section and the subsequent two relate to the second main objective of this thesis: to investigate the effects of employing different wind and wake models on load calculation results. To accomplish that, three analysis Focus Areas (FAs) were introduced in Section 3.5.1. These serve to focus the analysis lens on evaluating the influence of one specific modelling choice at a time. In particular, the three FAs assess the effect of changing the turbulence intensity model, the turbulence model and the wake model respectively, all else being equal[1]. In each case, a portion of the load catalogue is isolated, and its data is analyzed based on the methods described in Section 3.5.2. The results of this analysis are presented in this chapter.

This section presents the results of comparing fatigue loads calculated using two different turbulence intensity models: the 90th Percentile NTM and the Distribution NTM. The fatigue loads were compared in terms of the annual equivalent load effect[2] for the different tower and blade sensors listed in Table 3.10. Moreover, LS1 was used for the analysis[3], meaning that the results are for a solitary wind turbine operating under environmental conditions close to the reference conditions of IEC Class IC. Particularly, LS1.1 and LS1.3 were compared to assess the influence of changing the turbulence intensity model when the Kaimal turbulence model is utilized. On the other hand, LS1.2 and LS1.4 were compared to conduct the same assessment when the Mann model is utilized. The results are presented below for tower loads and blade loads respectively. Lastly, it is important to note that although some of the presented results correspond to specific wind climate parameter values, the insights that they provide are valid for all the other parameter combinations considered in this study.

FA1 - Tower Loads

Figure 4.2a shows a comparison of annual equivalent tower load effects calculated with a 90th Percentile NTM (LS1.1) and a Distribution NTM (LS1.3) under the Kaimal turbulence model. In contrast, Figure 4.2b shows the same comparison made under the Mann turbulence model. In both cases, the values for the reference turbulence intensity and the wind shear exponent are $I_{ref} = 12\%$ and $\alpha = 0.15$. In Figure 4.2c, the deviations in the load effects presented in Figure 4.2a and Figure 4.2b are shown alongside each other. These deviations are measured in percent relative to the load effect values obtained with the 90th Percentile NTM. Moreover, Table 4.1 provides summary statistics for the load effect deviations observed at the tower base, the point exhibiting the maximum tower loads. In contrast to the figures, these statistics are derived from the entirety of LS1 rather than only the entries for $I_{ref} = 12\%$ and $\alpha = 0.15$. In other words, the load effect deviations computed for all possible combinations of I_{ref} and α and for the two turbulence models were considered. Furthermore, when computing the statistics across all loading components, the absolute values of the relative deviations were taken.

[1] Refer to Section 3.1.3 and Section 3.1.5 for a detailed description of the wind and wake models respectively.
[2] Refer to Section 3.5.2 for a description of the calculation procedure.
[3] Refer to Figure 3.8 for an overview of the catalogue's organization and contents.

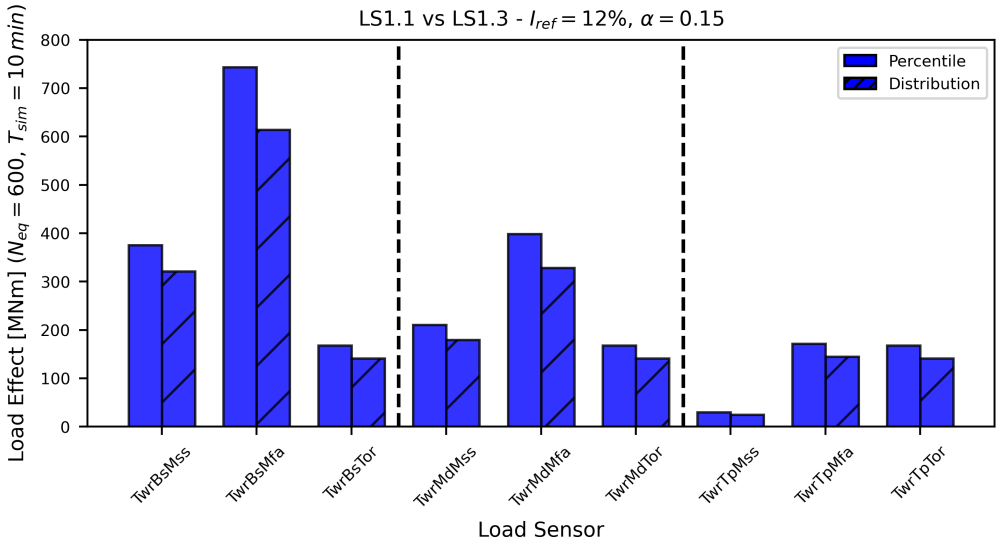

(a) Annual equivalent load effect at multiple tower sensors for different turbulence intensity models under Kaimal turbulence model.

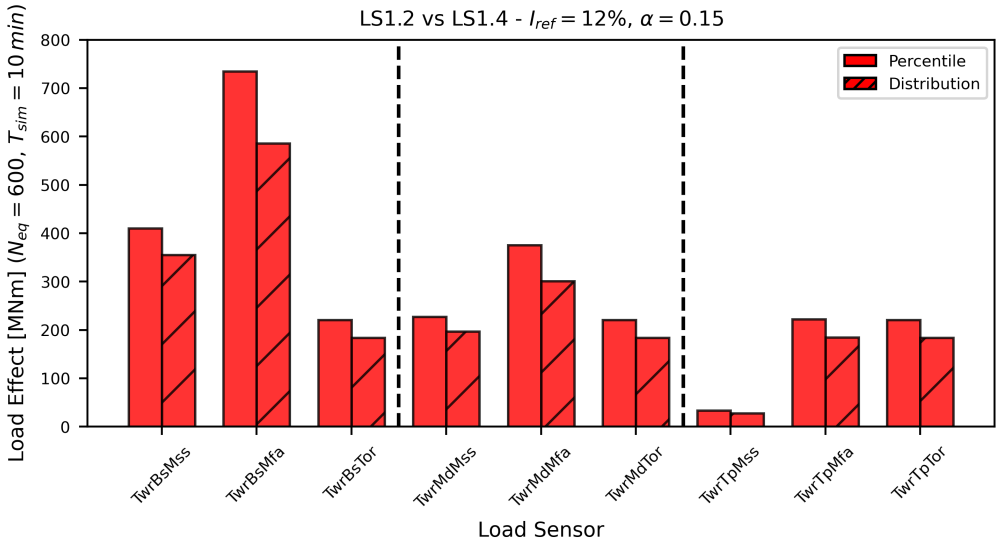

(b) Annual equivalent load effect at multiple tower sensors for different turbulence intensity models under Mann turbulence model.

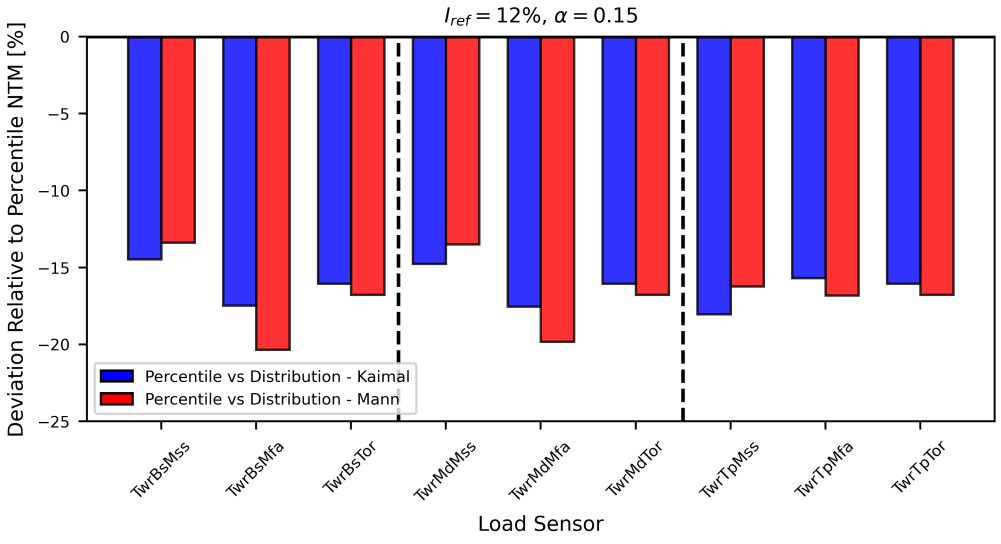

(c) Annual equivalent load effect deviations between 90^{th} Percentile NTM loads and Distribution NTM loads at multiple tower sensors for different turbulence models.

Figure 4.2: Tower load results in Focus Area 1: 90^{th} Percentile NTM vs Distribution NTM.

Table 4.1: Summary statistics for tower base load deviations in Focus Area 1: 90^{th} Percentile NTM vs Distribution NTM.

Load Component	Mean [%]	Std.Dev. [%]	Max. [%]	Min. [%]
Side-to-Side	-13.48	5.92	-6.07	-21.30
Fore-Aft	-19.71	6.19	-11.72	-27.07
Torsional	-16.25	6.71	-7.72	-24.36
Overall (abs. values)	16.48	6.78	27.07	6.07

The following observations can be drawn from the results above:

1. Using a Weibull distribution for the turbulence intensity consistently results in substantially lower fatigue loads than when the turbulence intensity is taken as a 90^{th} percentile. In particular, the load effects decrease by 16.48% on average.

2. For constant I_{ref} and α, the load deviations do not vary significantly across the different tower locations. This holds for all the considered values of I_{ref} and α, although only the results for $I_{ref} = 12\%$ and $\alpha = 0.15$ are presented in this report.

3. Among the different loading components, the fore-aft bending moment exhibits the largest load effect deviations, with an average deviation of -19.71% at the tower base. Conversely, the side-to-side bending moment exhibits the smallest deviations, with an average deviation of -13.48% at the tower base.

4. For the fore-aft bending moment and the torsional moment, the load effect deviations are larger when the Mann model is employed as compared to when the Kaimal model is employed. The opposite is true for the side-to-side bending moment. This holds for all the considered values of I_{ref} and α.

FA1 - Blade Loads

Following the same rationale as for tower loads, blade load results are presented in Figure 4.3. In the same fashion, blade load effects are shown in Figure 4.3a and Figure 4.3b for the Kaimal turbulence model (LS1.1) and the Mann turbulence model (LS1.3) respectively. The corresponding deviations are subsequently presented in Figure 4.3c, followed by summary statistics for blade root deviations in Table 4.2.

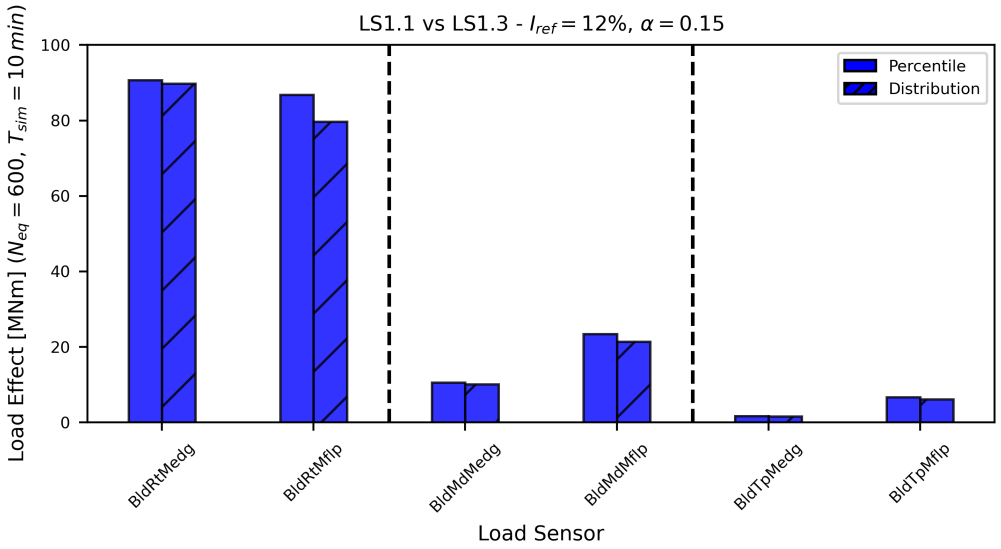

(a) Annual equivalent load effect at multiple blade sensors for different turbulence intensity models under Kaimal turbulence model.

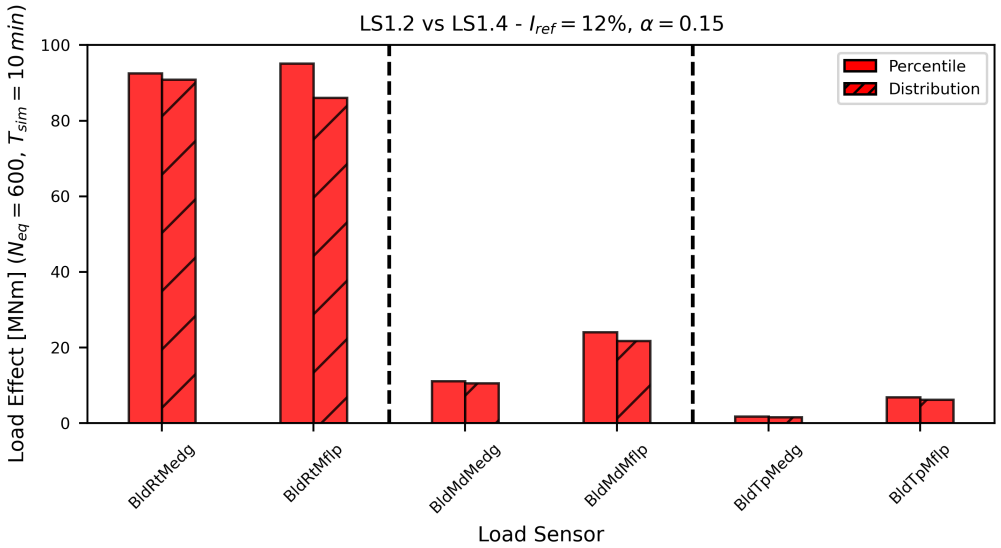

(b) Annual equivalent load effect at multiple blade sensors for different turbulence intensity models under Mann turbulence model.

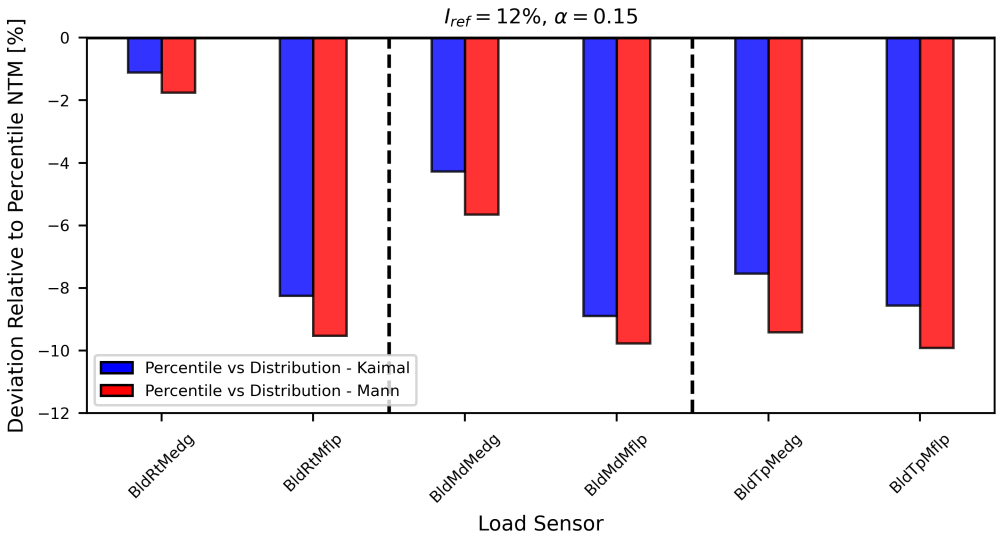

(c) Annual equivalent load effect deviations between 90^{th} Percentile NTM loads and Distribution NTM loads at multiple blade sensors for different turbulence models.

Figure 4.3: Blade load results in Focus Area 1: 90^{th} Percentile NTM vs Distribution NTM.

Table 4.2: Summary statistics for blade root load deviations in Focus Area 1: 90^{th} Percentile NTM vs Distribution NTM.

Load Component	Mean [%]	Std.Dev. [%]	Max. [%]	Min. [%]
Edgewise	-1.78	0.72	-0.89	-2.75
Flapwise	-9.37	5.13	-2.92	-17.12
Overall (abs. deviations)	5.58	5.28	17.12	0.89

The following observations can be drawn from the results above:

1. Like for tower loads, using a Weibull distribution for the turbulence intensity consistently results in lower fatigue loads (by 5.58% on average) than when the turbulence intensity is taken as 90^{th} percentile. However, the deviations are notably smaller in magnitude for the blade loads, for which the average deviation is -5.58% at the blade root compared to -16.48% at the tower base.

2. For constant I_{ref} and α, deviations for both loading components increase from blade root to blade tip. Nonetheless, this trend is more significant for the edgewise component. This applies for all the considered values of I_{ref} and α.

3. Deviations for the flapwise bending component are substantially larger in magnitude than deviations for the edgewise component at all blade stations, particularly at the blade root where the average deviation is -1.78% for the edgewise component and -9.37% for the flapwise component.

4. Like for tower loads, blade load effect deviations are larger when the Mann model is employed as compared to when the Kaimal model is employed. This applies for all blade stations and loading components, but the discrepancies are more substantial towards the blade tip. This is true for all the considered values of I_{ref} and α.

5. The choice of turbulence model has more influence on load effect deviations for blade loads than for tower loads. This applies for all the considered values of I_{ref} and α.

FA1 - Sensitivity Analysis

The results presented thus far have shown how the choice of the turbulence intensity model impacts calculated load effects for different turbulence models. However, the data presented in the figures was associated with specific values of the reference turbulence intensity and the wind shear exponent. Nonetheless, this research seeks to quantify how the influence of modelling choices varies for different values of these parameters. As discussed in Section 3.5.2, this objective was fulfilled by conducting a sensitivity analysis with respect to the load effect deviation, with the results for $I_{ref} = 12\%$ and $\alpha = 0.15$ regarded as a base case. The analysis findings are showcased below.

While the mentioned sensitivity analysis can be applied to any load sensor, only the sensors at the tower base and the blade root were considered. Moreover, sensitivity was assessed separately for the case where Kaimal turbulence model is employed and the case where the Mann turbulence model is employed. Accordingly, Figure 4.4a shows how the load effect deviations at the tower base vary as a function of the reference turbulence intensity and wind shear exponent for both the side-to-side and fore-aft bending moments when the Kaimal turbulence model is used. Subsequently, the corresponding sensitivity plots are presented in Figure 4.4b for the case where the Mann model is used. Likewise, Figure 4.5 presents the findings of the sensitivity analysis applied to blade root load deviations. In all the sensitivity plots below, the load effect deviation values were normalized with respect to the value obtained for the base case.

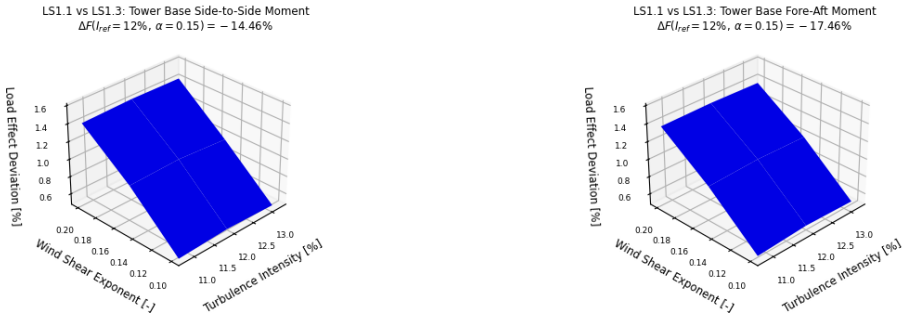

(a) Sensitivity of tower base load effect deviation between 90^{th} Percentile NTM loads and Distribution NTM loads under Kaimal turbulence model.

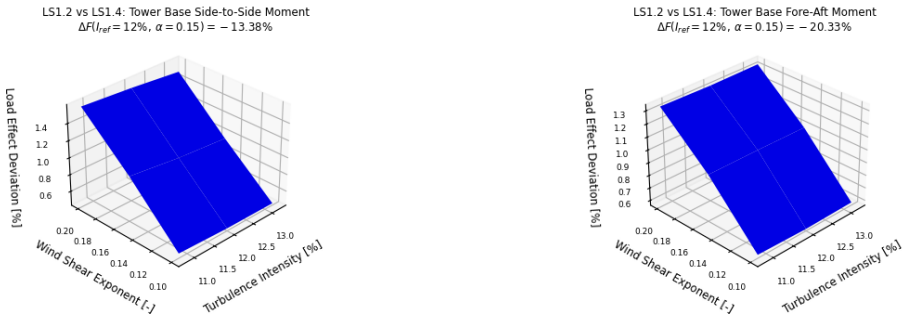

(b) Sensitivity of tower base load effect deviation between 90^{th} Percentile NTM loads and Distribution NTM loads under Mann turbulence model.

Figure 4.4: Sensitivity analysis results for tower base load deviations in Focus Area 1: 90^{th} Percentile NTM vs Distribution NTM.

The figures above lead to the following observations:

1. Load effect deviations consistently increase in magnitude as the wind shear exponent increases.
2. There is no consistent variation trend for load effect deviations with respect to the reference turbulence intensity.
3. For the considered parameter value ranges, the load effect deviations are more sensitive to the wind shear exponent than to the turbulence intensity.
4. Sensitivity to the turbulence intensity tends to increase as the wind shear exponent decreases, while sensitivity to the wind shear exponent remains relatively the same for different values of the turbulence intensity.
5. As reflected by the figures above and the comparable standard deviations in Table 4.1, the load effect deviations

for the two loading components display similar sensitivities to the wind climate parameters.

6. For the side-to-side bending moment, sensitivity to both the wind shear exponent and the turbulence intensity increases when using the Mann model instead of the Kaimal model. The reverse is true for the fore-aft bending moment.

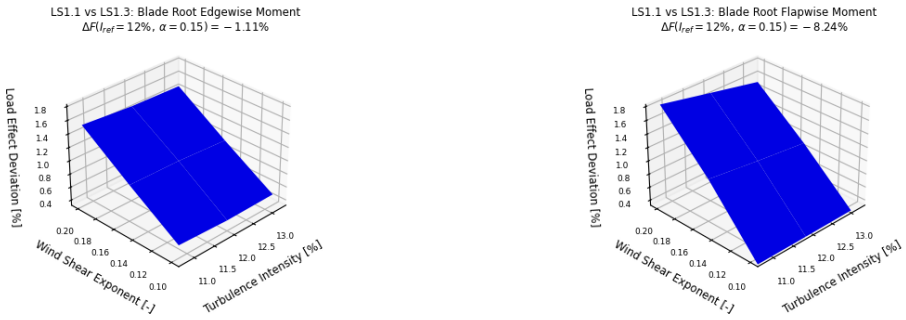

(a) Sensitivity of blade root load effect deviation between 90^{th} Percentile NTM loads and Distribution NTM loads under Kaimal turbulence model.

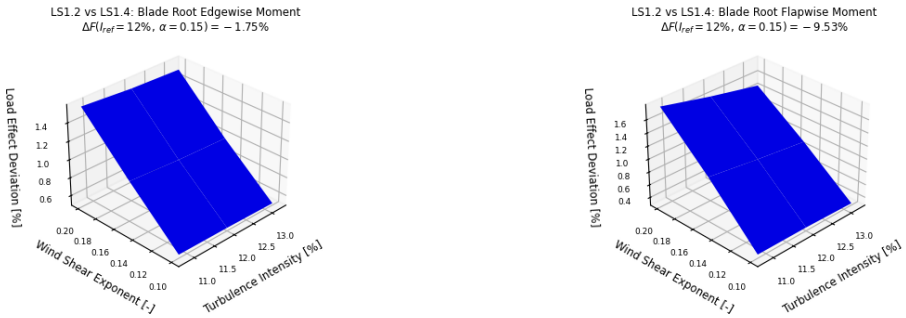

(b) Sensitivity of blade root load effect deviation between 90^{th} Percentile NTM loads and Distribution NTM loads under Mann turbulence model.

Figure 4.5: Sensitivity analysis results for blade root load deviations in Focus Area 1: 90^{th} Percentile NTM vs Distribution NTM.

The figures above lead to the following observations:

1. Like for the tower, blade load effect deviations consistently increase in magnitude as the wind shear exponent increases.

2. Also, there is no consistent variation trend for blade load effect deviations with respect to the reference turbulence intensity.

3. Similarly to the tower case, the blade load effect deviations are more sensitive to the wind shear exponent than to the turbulence intensity.

4. The load effect deviation sensitivity is substantially higher for the flapwise bending moment than for the edgewise bending moment, as also reflected by the standard deviations in Table 4.2.

5. Among all tower and blade loading components, the load effect deviation for the flapwise bending moment at the blade root is the most sensitive to both the wind shear exponent and the turbulence intensity.

6. Blade load effect deviations are more sensitive to the turbulence intensity than tower load effect deviations, especially for the blade flapwise bending moment.

7. Swapping the turbulence model has a smaller effect on sensitivity for blade load deviations than for tower load deviations.

4.1.3 Focus Area 2: Kaimal Turbulence vs Mann Turbulence

Section 4.1.2 investigated the load effect deviations resulting from interchanging two turbulence intensity models under two different turbulence models. The converse is done in this section, which looks into the effect of swapping two turbulence models under two different turbulence intensity models. This was also done based on LS1. However, in this case, load effects computed from LS1.1 were compared to those computed from LS1.2 to capture the influence of changing the turbulence model when a 90th Percentile NTM is used. Alternatively, LS1.3 and LS1.4 were considered to assess the same effect when a Distribution NTM is used. The findings are showcased below for tower loads and blade loads respectively, following the same structure as in Section 4.1.2. Also, it is important to note that, like for FA1, the presented results provide insights that are generalizable to all the wind climate parameter values considered in this study.

FA2 - Tower Loads

A comparison of annual equivalent fatigue load effects calculated from LS1.1 and LS1.2 for various tower load sensors is presented in Figure 4.6a. On the other hand, load effects based on LS1.3 and LS1.4 are compared in Figure 4.6b. The distinction between these two comparison cases is the employed turbulence intensity model, whereby the 90th Percentile NTM was applied for LS1.1 and LS1.2 while the Distribution NTM was applied for LS1.3 and LS1.4. Also, both comparisons are made for the base case defined in the previous section, namely $I_{ref} = 12\%$ and $\alpha = 0.15$. Moreover, the corresponding load effect deviations are displayed in Figure 4.6c, with the deviations measured relative to the values obtained with the Kaimal turbulence model. Furthermore, Table 4.3 displays summary statistics for tower base load effect deviations calculated for all possible combinations of I_{ref} and α. However, it is important to note that, in the calculation of these statistics, only the data for the Distribution NTM was considered, i.e. the data in LS1.3 and LS1.4.

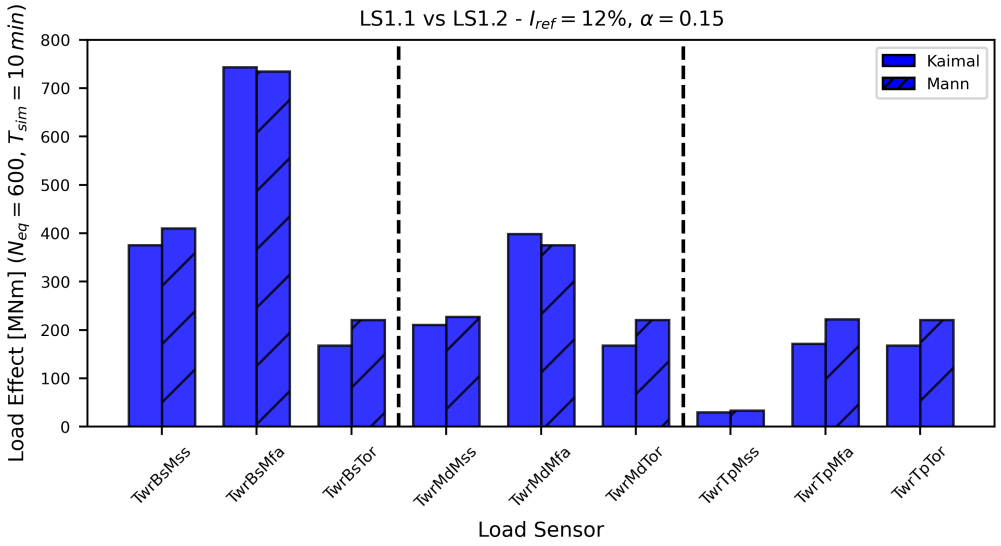

(a) Annual equivalent load effect at multiple tower sensors for different turbulence models under 90th Percentile NTM.

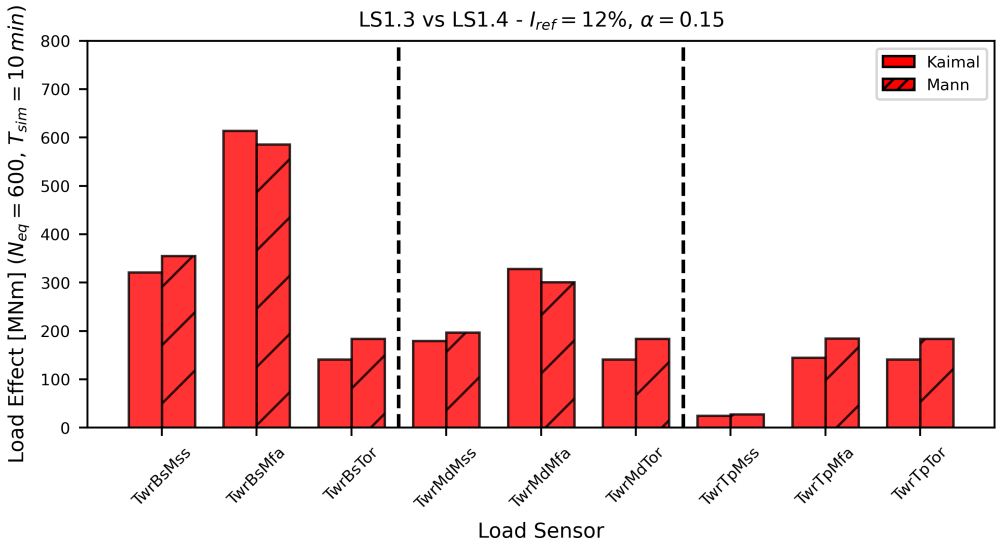

(b) Annual equivalent load effect at multiple tower sensors for different turbulence models under Distribution NTM.

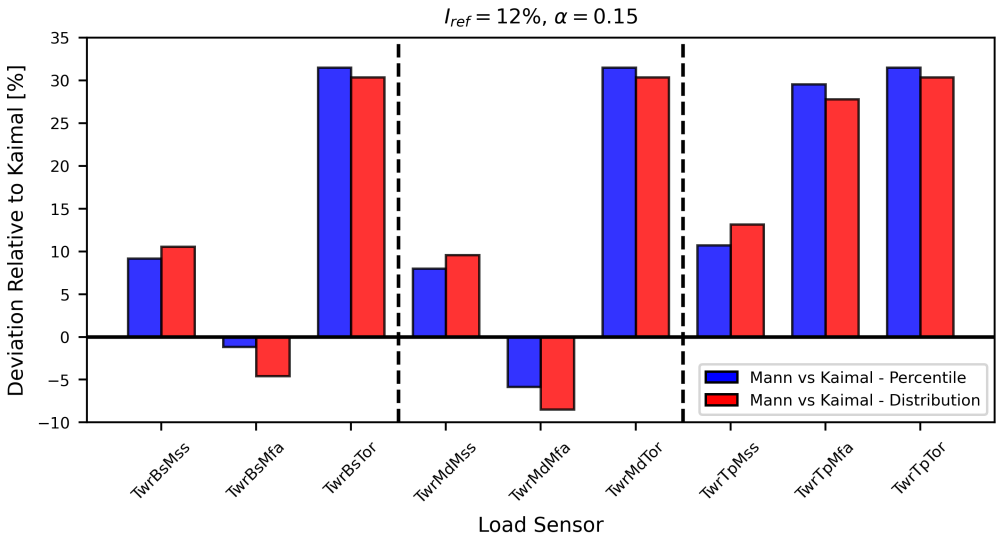

(c) Annual equivalent load effect deviations between Kaimal loads and Mann loads at multiple tower sensors for different turbulence intensity models.

Figure 4.6: Tower load results for Focus Area 2: Kaimal Turbulence vs Mann Turbulence.

Table 4.3: Summary statistics for tower base load deviations in Focus Area 2: Kaimal Turbulence vs Mann Turbulence.

Load Component	Mean [%]	Std.Dev. [%]	Max. [%]	Min. [%]
Side-to-Side	10.27	0.81	11.07	9.17
Fore-Aft	-4.81	0.25	-4.59	-5.16
Torsional	30.28	0.33	30.64	29.84
Overall (abs. deviations)	15.12	10.96	30.64	4.59

The following observations can be drawn from the results above:

1. For the side-to-side and torsional moments, using the Mann turbulence model consistently yields higher fatigue load effects than using the Kaimal turbulence model, with an average overestimation of 10.27% and 30.28% respectively at the tower base.

2. This is not the case for the fore-aft component, for which using the Mann model results in lower load effects at the tower base (by 4.81% on average). This is also true at the midpoint, but not at the top, where using the Mann model yields considerably higher load effects with deviations reaching up to 30%.

3. The deviations for the side-to-side and torsional moments do not vary considerably across the different tower stations. The opposite is true for the fore-aft moment, which varies substantially and even changes sign between the tower midpoint and top. This is true for all the considered values of I_{ref} and α.

4. The most substantial absolute tower base deviations correspond to the torsional moment, with an average deviation of 30.28%. On the other hand, the smallest absolute tower base deviations are observed for the side-to-side moment, with an average deviation of -4.81%,

5. When considering all tower locations, the absolute deviations for the torsional moment remain the largest, but the deviations for the side-to-side bending moment become the smallest. This is true for all the considered values of I_{ref} and α.

6. On average, the effect of swapping the turbulence model on the side-to-side and fore-aft load effects is more significant when a Weibull distribution is used for the turbulence intensity. An exception can be made at the tower top, where the opposite is true. This holds for all the considered values of I_{ref} and α.

7. The opposite is also true for the torsional load effect, for which using the 90th Percentile NTM results in higher deviations. This holds for all the considered values of I_{ref} and α.

FA2 - Blade Loads

In accordance with tower load results, blade load results are presented in Figure 4.7. Figure 4.7a and Figure 4.7b show the blade load effects for the 90th Percentile NTM (LS1.1) and the Distribution NTM (LS1.3) respectively. The corresponding deviations are then presented in Figure 4.7c, followed by summary statistics for blade root deviations in Table 4.4.

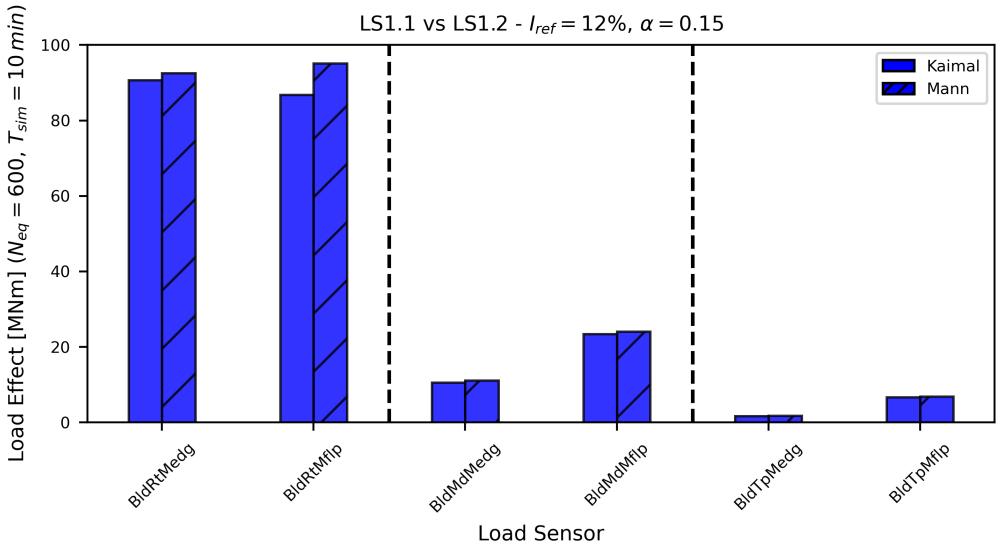

(a) Annual equivalent load effect at multiple blade sensors for different turbulence models under 90th Percentile NTM.

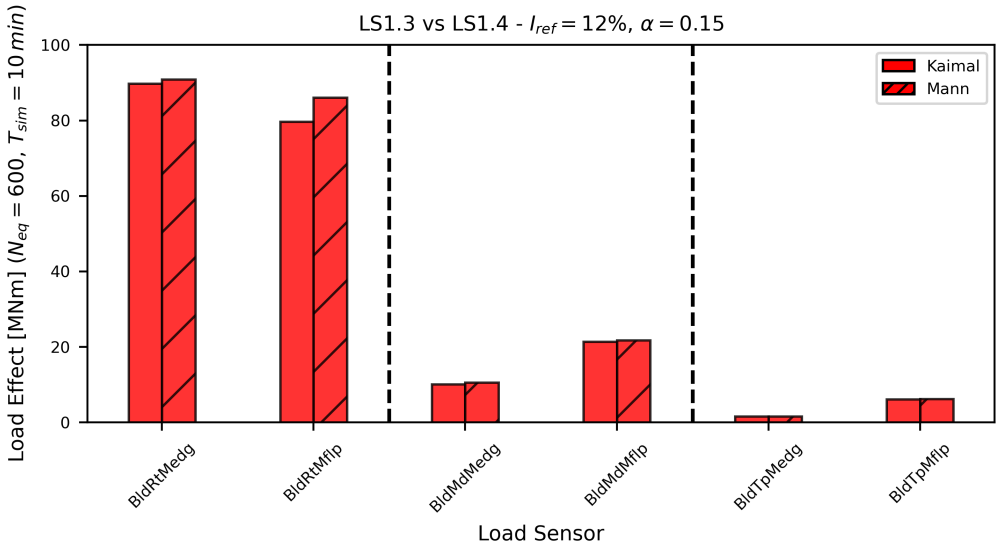

(b) Annual equivalent load effect at multiple blade sensors for different turbulence models under Distribution NTM.

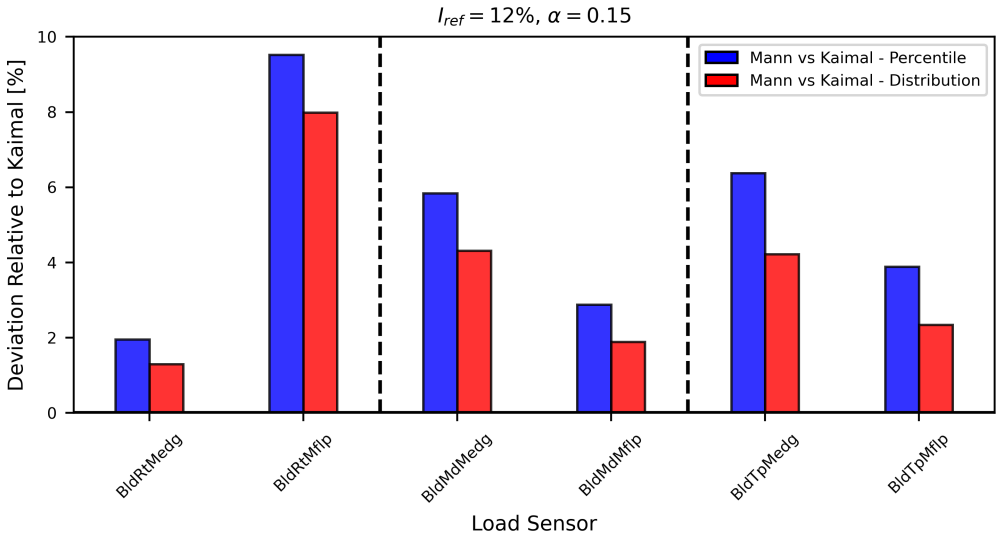

(c) Annual equivalent load effect deviations between Kaimal loads and Mann loads at multiple blade sensors for different turbulence intensity models.

Figure 4.7: Blade load results for Focus Area 2: Kaimal Turbulence vs Mann Turbulence.

Table 4.4: Summary statistics for blade root load deviations in Focus Area 2: Kaimal Turbulence vs Mann Turbulence.

Load Component	Mean [%]	Std.Dev. [%]	Max. [%]	Min. [%]
Edgewise	1.29	0.01	1.30	1.29
Flapwise	8.04	0.68	8.89	7.24
Overall (abs. deviations)	4.67	3.41	8.89	1.29

The following observations can be drawn from the results above:

1. Unlike for tower loads, utilizing the Mann turbulence model consistently yields higher blade load effects than utilizing the Kaimal turbulence model. However, the deviations are smaller in magnitude for the blade loads, for which the average absolute deviation is 4.67% at the blade root compared to 15.12% at the tower base.

2. Deviations for the edgewise bending moment tend to increase from blade root to blade tip, while no clear trend can be identified for the flapwise component. This holds for all the considered values of I_{ref} and α.

3. Deviations for the flapwise bending component are significantly larger than deviations for the edgewise component at the blade root, with average deviations of 1.29% and 8.04% respectively. The reverse is true at the blade midpoint and 75%-span, at which the deviations for the edgewise component are larger.

4. Unlike for tower loads, blade load effect deviations are consistently larger when the 90th Percentile NTM is employed as compared to when the Distribution NTM is employed. Moreover, this effect tends to become more substantial towards the blade tip. This applies for all the considered values of I_{ref} and α.

5. Similar to the observation made for FA1 (Section 4.1.2), the choice of turbulence intensity model has more influence on load effect deviations for blade loads than for tower loads. This applies for all the considered values of I_{ref} and α.

FA2 - Sensitivity Analysis

Sensitivity to Turbulence Intensity and Wind Shear Exponent

The same sensitivity analysis conducted for FA1 (Section 4.1.2) was also conducted for FA2. For this FA, the sensitivity of the load effect deviation due to changing the turbulence model was investigated. The same base case considered for FA1 was also considered for FA2, namely the case corresponding to $I_{ref} = 12\%$ and $\alpha = 0.15$. The analysis results are presented in Figure 4.8 for tower loads and in Figure 4.9 for blade loads. For both figures, the deviation values are normalized with respect to the base case value.

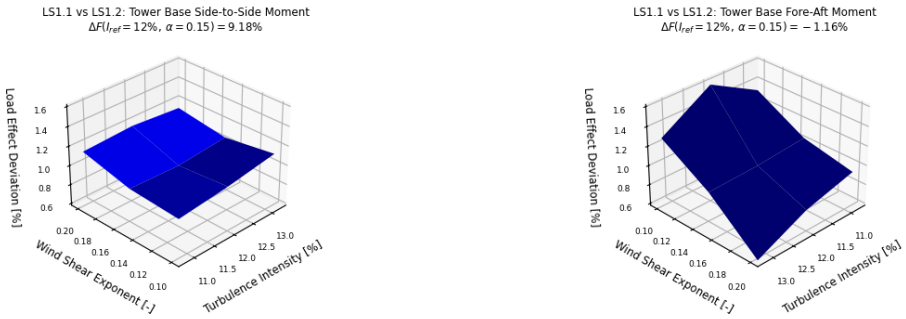

(a) Sensitivity of tower base load effect deviation between Kaimal loads and Mann loads under 90th Percentile NTM.

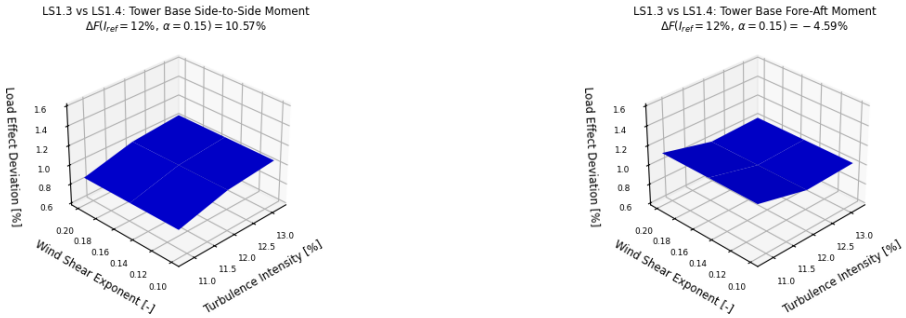

(b) Sensitivity of tower base load effect deviation between Kaimal loads and Mann loads under Distribution NTM.

Figure 4.8: Sensitivity analysis results for tower base load deviations in Focus Area 2: Kaimal Turbulence vs Mann Turbulence.

The figures above lead to the following observations:

1. Tower load effect deviations exhibit little variability across the different wind climate conditions, as also reflected by the standard deviations in Table 4.3.

2. The sensitivity of tower load effect deviations is smaller when the turbulence model is varied (FA2) than when the turbulence intensity model is varied (FA1). This can also be deduced by comparing the standard deviations in Table 4.3 to those in Table 4.1.

3. Sensitivity to the turbulence intensity is higher when the turbulence model is varied (FA2) as compared to when the turbulence intensity model is varied (FA1). Conversely, the sensitivity to the wind shear exponent is lower when the turbulence model is varied (FA2) as compared to when the turbulence intensity model is varied (FA1).

4. For the side-to-side loading component, load effect deviations increase as the wind shear exponent or the turbulence intensity increase. The converse is true for the fore-aft component, for which the deviations increase with decreasing wind shear exponent or turbulence intensity.

5. Sensitivity to both the wind shear exponent and the turbulence intensity decreases when using the Distribution NTM instead of the 90th Percentile NTM, particularly for the fore-aft bending moment.

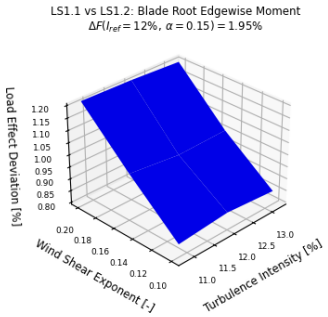

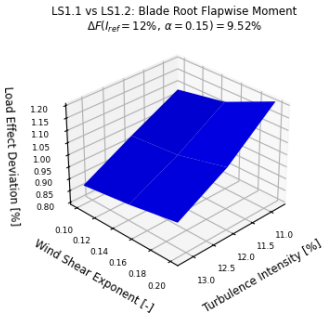

(a) Sensitivity of blade root load effect deviation between Kaimal loads and Mann loads under 90th Percentile NTM.

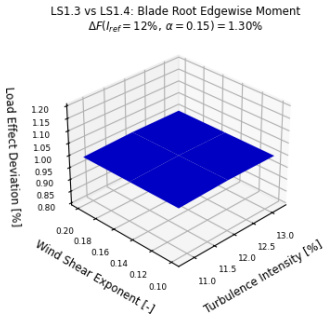

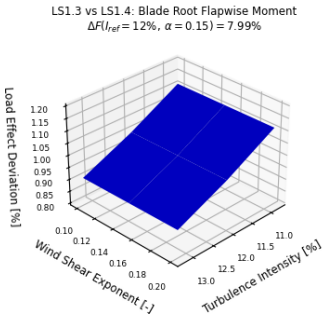

(b) Sensitivity of blade root load effect deviation between Kaimal loads and Mann loads under Distribution NTM.

Figure 4.9: Sensitivity analysis results for blade root load deviations in Focus Area 2: Kaimal Turbulence vs Mann Turbulence.

The figures above lead to the following observations:

1. Like for the tower, blade load effect deviations show a small variability with wind climate parameters, as also reflected by the standard deviations in Table 4.4.
2. Like for the tower, blade load effect deviation sensitivity is smaller when the turbulence model is varied (FA2) than when the turbulence intensity model is varied (FA1).
3. Generally, blade load effect deviations are more sensitive to both the turbulence intensity and the wind shear exponent than tower load effect deviations.
4. For the edgewise bending moment, load effect deviations are more sensitive to the wind shear exponent than to the turbulence intensity. The opposite is true for the flapwise bending moment.
5. Unlike for the tower, blade load effect deviations consistently increase in magnitude as the wind shear exponent increases.
6. The relationship with the turbulence intensity is more complex. For the flapwise component, deviations increase with decreasing turbulence intensity. For the edgewise component, deviations remain relatively constant as the turbulence intensity changes (at constant wind shear exponent).
7. In consistence with the observation made in FA1, the flapwise bending moment exhibits higher sensitivity than the edgewise bending moment, as also reflected by the standard deviations in Table 4.4.
8. Similar to the tower case, replacing the 90th Percentile NTM by the Distribution NTM reduces sensitivity. However, the reduction is more substantial for the blade case, especially for the edgewise bending moment.

Sensitivity to Mean Wind Speed

For this FA, the sensitivity of fatigue loads to the mean wind speed was also investigated. However, instead of considering the deviation in the annual equivalent load effect, the deviation in the 10-minute DEL was considered to preserve dependence on the mean wind speed. The results are presented in Figure 4.10 and Figure 4.11 for tower base loads and blade root loads respectively, where the deviations were computed for $I_{ref} = 12\%$ and $\alpha = 0.15$ under a Distribution NTM. That is, the deviations were calculated based on LS1.3 and LS1.4. On a final note, the same trends observed in the figures below can be identified for different values of I_{ref} and α.

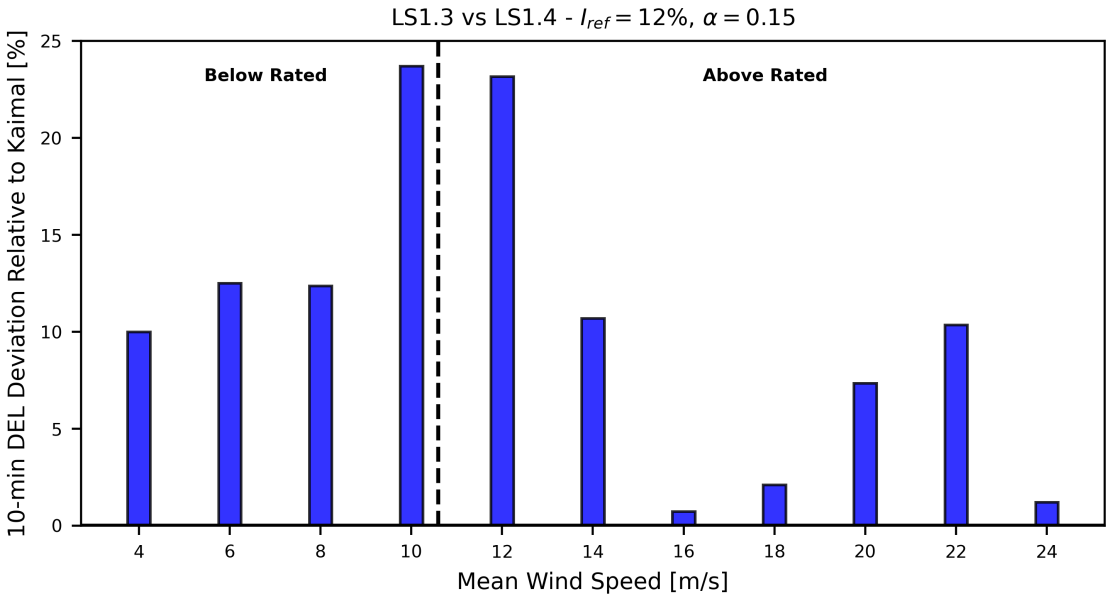

(a) Tower base side-to-side moment.

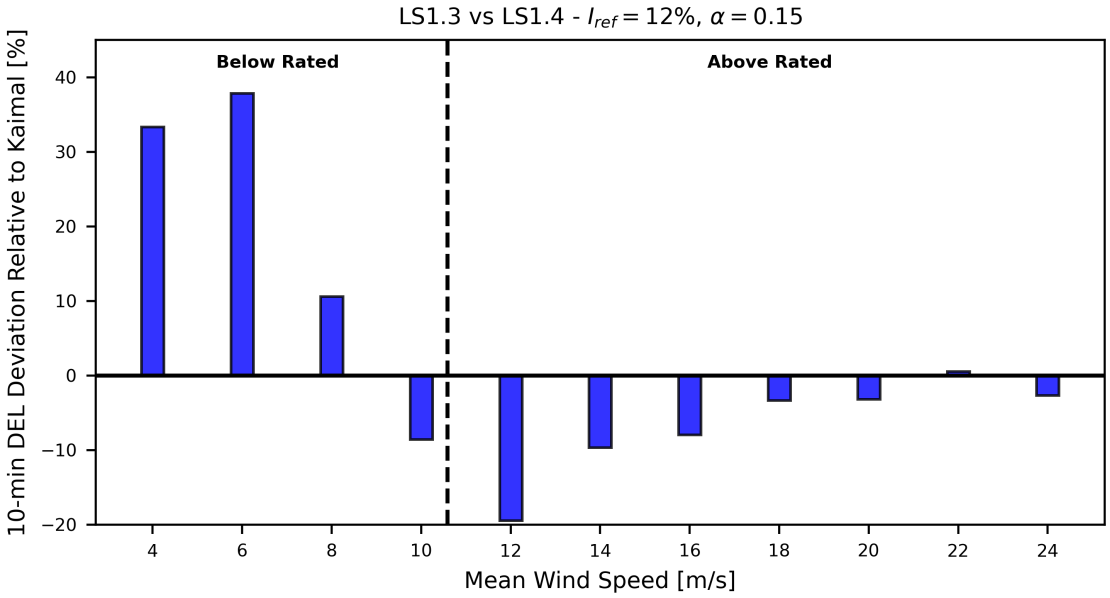

(b) Tower base fore-aft moment.

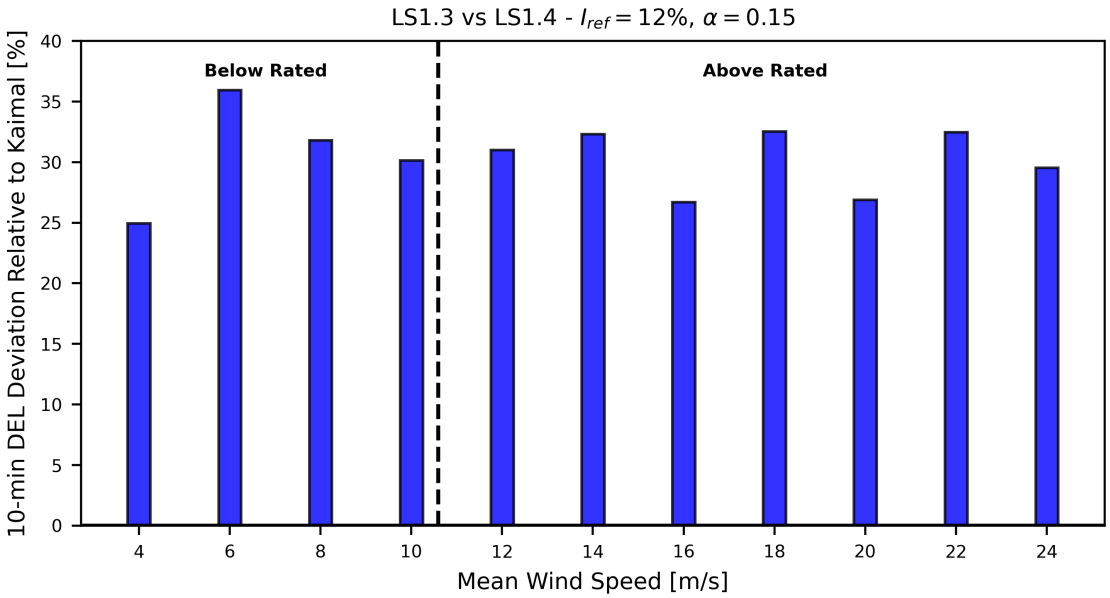

(c) Tower base torsional moment.

Figure 4.10: Tower base 10-minute DEL deviations between Kaimal loads and Mann loads versus mean wind speed under Distribution NTM.

Based on the figures above, the following observations can be made:

1. Using the Mann model consistently yields higher fatigue load effects than using the Kaimal model for the side-to-side and torsional moments.
2. For the fore-aft moment, the Mann model overestimates the loads calculated with the Kaimal model in the below rated region, and vice versa in the above rated region.
3. The DEL deviations for the torsional moment are relatively consistent across the operation mean wind speed range. The same cannot be said about the side-to-side and fore-aft moments.
4. For both the side-to-side and fore-aft moments, the deviations are larger in magnitude in the below rated region than in the above rated region.
5. For the fore-aft moment, the deviations flip sign near the rated wind speed and notably decrease in magnitude towards the cut-out wind speed, where the Kaimal and Mann models are in closer agreement.
6. A clear trend is more difficult to identify for the side-to-side moment, but a notable spike in deviations can be observed near the rated wind speed.

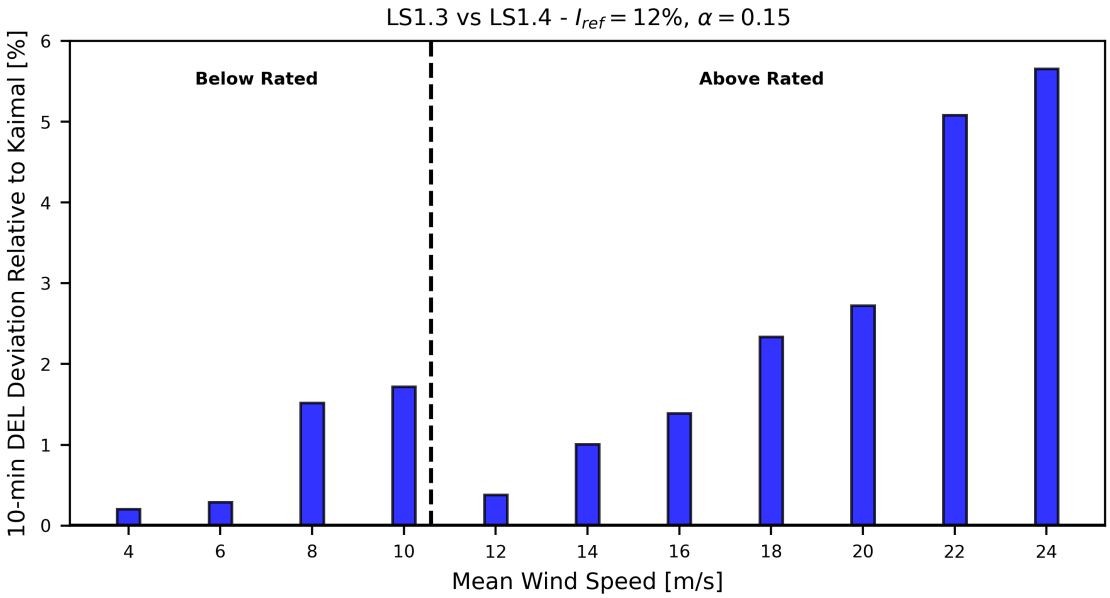

(a) Blade root edgewise moment.

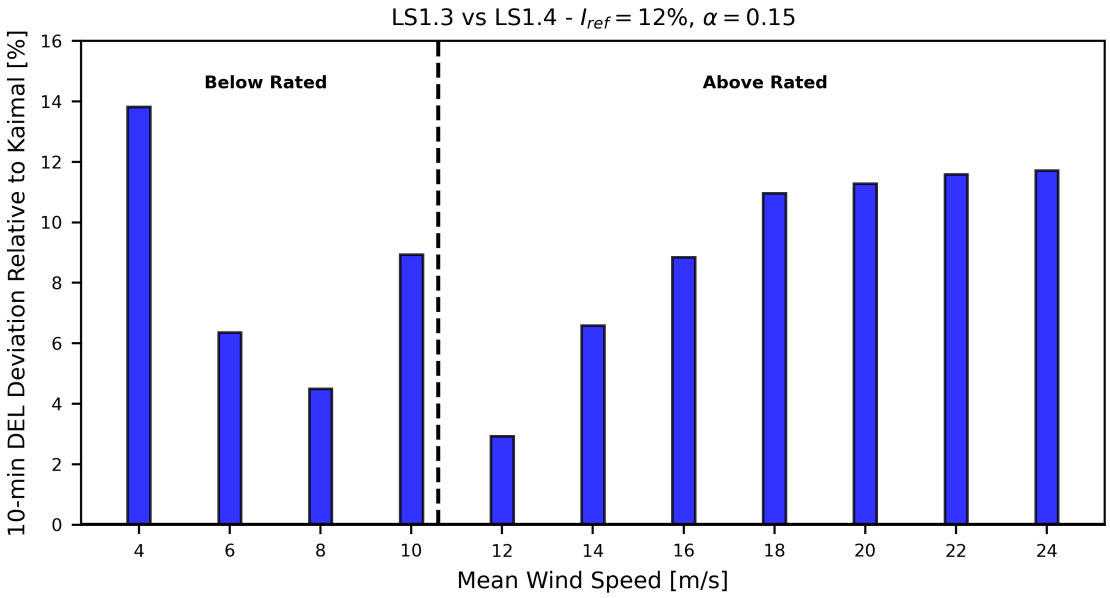

(b) Blade root flapwise moment.

Figure 4.11: Blade root 10-minute DEL deviations between Kaimal loads and Mann loads versus mean wind speed under Distribution NTM.

Based on the figures above, the following observations can be made:

1. Using the Mann model consistently yields higher fatigue load effects than using the Kaimal model for the both the edgewise and flapwise moments.

2. For the edgewise moment, the deviations are larger in magnitude in the above rated region than in the below rated region. Moreover, the deviations tend to increase towards higher wind speeds.

3. For the flapwise moment, the deviations tend to increase moving away from the rated region, and tend to more or less stabilize towards the cut-out wind speed.

4. For both components, a notable dip in the DEL deviation occurs directly after the rated wind speed.

4.1.4 Focus Area 3: Frandsen Wake vs DWM Wake

In Section 4.1.2 and Section 4.1.3, the influence of wind model choices on fatigue loads was explored for a single turbine operating under environmental conditions close to the reference conditions for IEC Class IC. In this section, the attention is shifted to the effect of the wake model choice on load response. In particular, annual equivalent load effects computed using Frandsen's effective turbulence model are compared to those computed using the DWM model. The analysis is done based on LS2. That is, as explained in Section 3.3, in the context of a 3x3 square grid wind farm operating under the wind climate observed at the RWE wind farm site, whereby the reported loads correspond to the central turbine. The comparison results for an inter-turbine spacing of 6 rotor diameters ($s = 6$) are presented below for tower and blade loads respectively. Finally, it is important to note that, unless indicated otherwise, the results for $s = 6$ may not be generalized for other values of s.

FA3 - Tower Loads

Figure 4.12a presents a comparison of annual equivalent fatigue load effects calculated from LS2.1 (Frandsen) and LS2.2 (DWM) for various tower load sensors. Then, the corresponding load effect deviations are shown in Figure 4.12b, with the deviations measured relative to the values obtained with the DWM model.

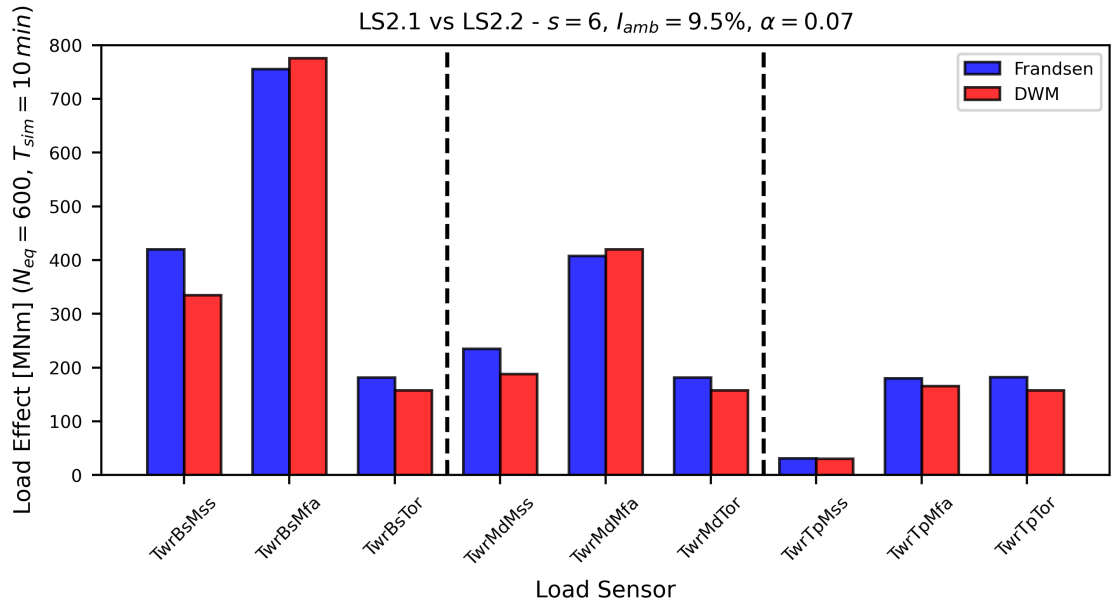

(a) Comparison of annual equivalent load effects computed with the Frandsen and DWM wake models at multiple tower sensors.

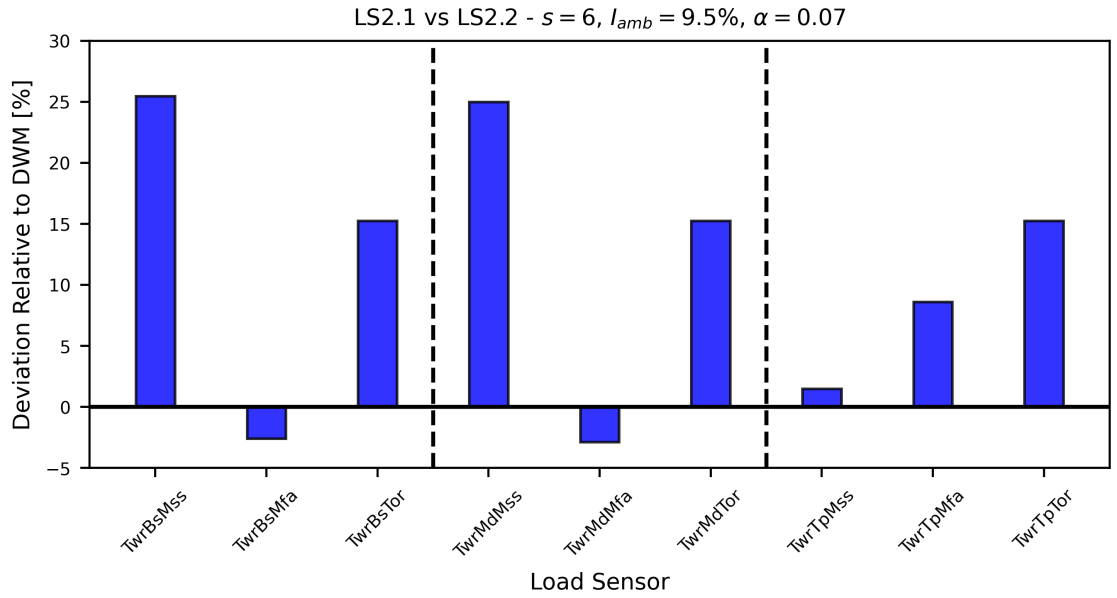

(b) Annual equivalent load effect deviations between Frandsen loads and DWM loads at multiple tower sensors.

Figure 4.12: Tower load results for Focus Area 3: Frandsen Wake vs DWM Wake.

The following observations can be drawn from the results above:

1. For the side-to-side and torsional moments, using the Frandsen wake model consistently yields higher fatigue load effects than using the DWM wake model.

2. This does not apply for the fore-aft component, for which using the DWM model results in higher load effects at the tower base and at the midpoint, but not at the top.

3. In magnitude, the largest tower base deviation corresponds to the side-to-side bending moment (25%), while the smallest corresponds to the fore-aft bending moment (2.5%). The maximum and minimum deviations correspond to these same components for all the considered values of s, namely 4, 6 and 8.

4. The deviations for the side-to-side and fore-aft components change negligibly between the tower base and the tower midpoint, but they change significantly at the tower top. At this point, the deviation for the fore-aft component changes increases significantly, while the deviation for the side-to-side component decreases significantly. This holds for all the considered values of s, namely 4, 6 and 8.

FA3 - Blade Loads

In consistence with tower load results, blade load effects calculated from LS2.1 (Frandsen) and LS2.2 (DWM) are presented in Figure 4.13a, followed by the corresponding deviations, measured relative to the values obtained with the DWM wake model, in Figure 4.13b.

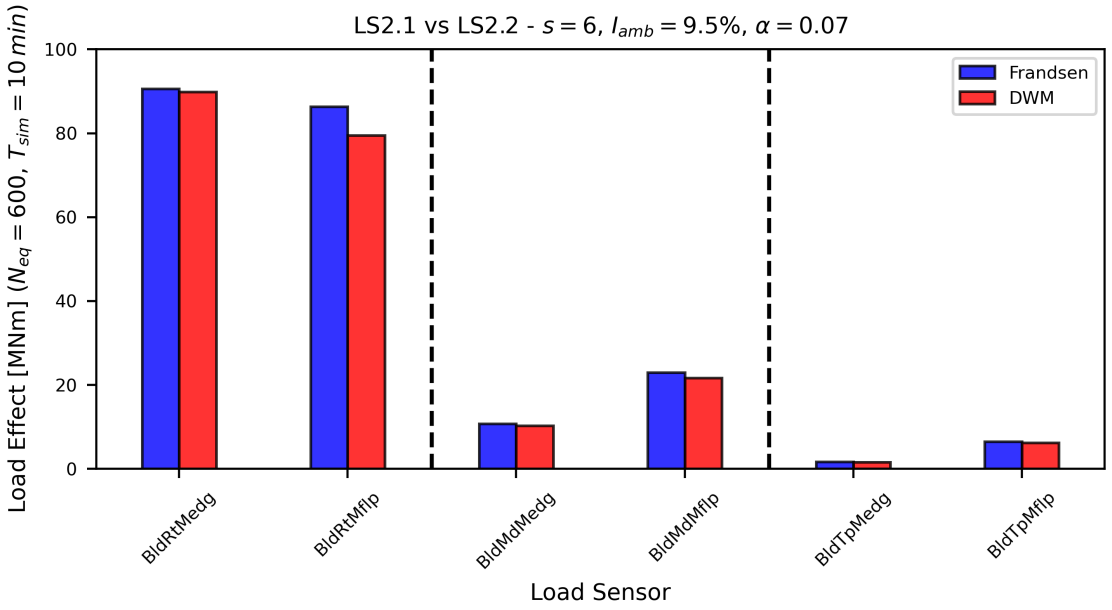

(a) Comparison of annual equivalent load effects computed with the Frandsen and DWM wake models at multiple blade sensors.

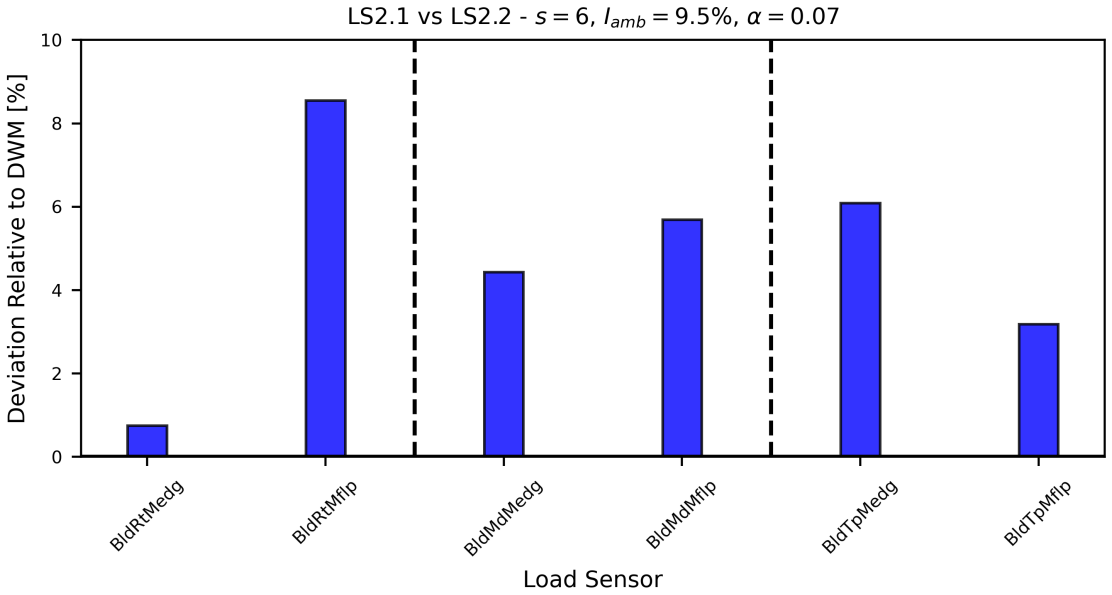

(b) Annual equivalent load effect deviations between Frandsen loads and DWM loads at multiple blade sensors.

Figure 4.13: Blade load results for Focus Area 3: Frandsen Wake vs DWM Wake.

The following observations can be drawn from the results above:

1. Unlike for tower loads, regardless of the loading component, utilizing the Frandsen wake model consistently yields higher blade load effects than utilizing the DWM wake model.

2. The largest deviation is observed for the flapwise bending moment at the blade root (8.5%), while the smallest corresponds to the edgewise bending moment at the blade root (0.75%).

3. Deviations for the edgewise bending moment tend to increase from blade root to blade tip. The opposite is true for the flapwise bending moment.

4. On average, deviations for the blade loads are smaller than deviations for the tower loads. However, an exception can be made for the tower fore-aft component, for which deviations are in the range of blade load deviations.

FA3 - Sensitivity Analysis

Up to this point, load effects computed with the Frandsen and DWM wake models have been compared for an inter-turbine spacing of 6 rotor diameters. In Figure 4.14a and Figure 4.14b below, they are compared for different values of s, namely 4, 6 and 8 rotor diameters. Again, the comparison is made based on the annual load effect deviation relative to the value obtained with the Frandsen model.

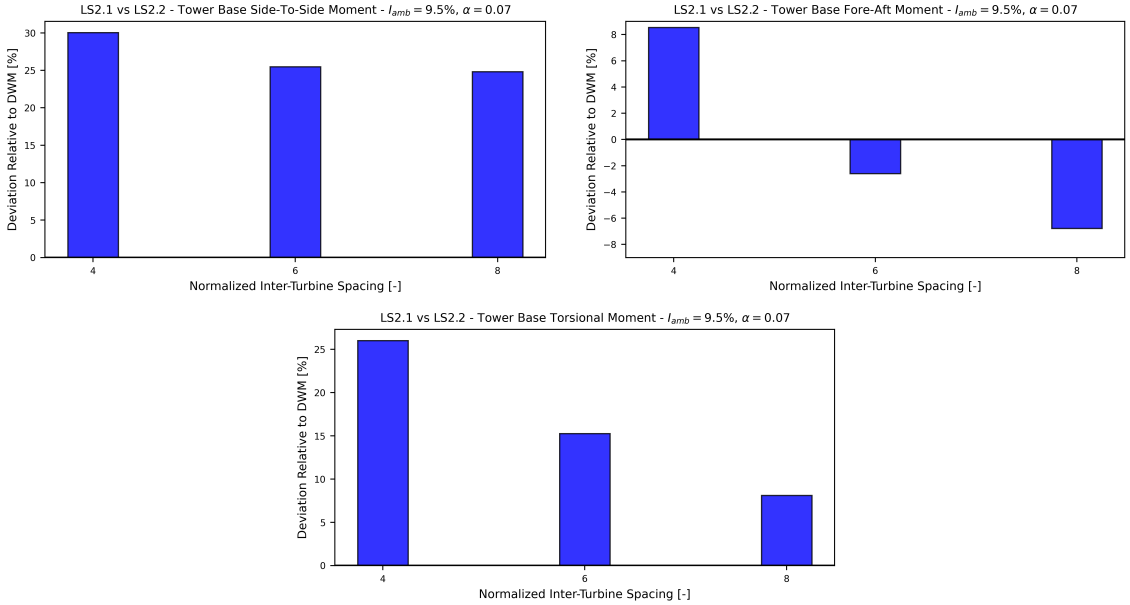

(a) Annual tower base equivalent load effect deviations between Frandsen loads and DWM loads for different inter-turbine spacings.

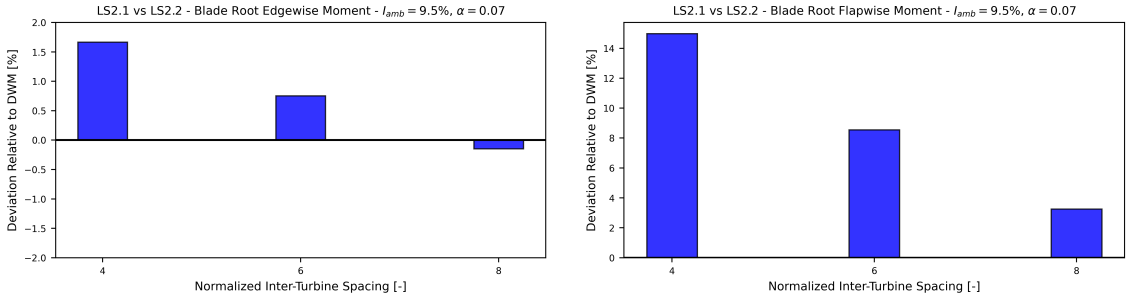

(b) Annual blade root equivalent load effect deviations between Frandsen loads and DWM loads for different inter-turbine spacings.

Figure 4.14: Sensitivity analysis results in Focus Area 3: Frandsen Wake vs DWM Wake.

The figures above lead to the following observations:

1. The Frandsen model consistently yields higher load values than the DWM model for the tower base side-to-side and torsional moments and the blade root flapwise moment, but not for the tower base fore-aft moment and the blade root edgewise moment.

2. For all considered loads, the load effect deviations consistently decrease as the inter-turbine spacing increases. In other words, the Frandsen model overestimates the DWM model by a larger amount for lower values of the inter-turbine spacing.

3. Distinctively, deviations for the tower base fore-aft moment and the blade root edgewise moment change sign at $s = 6$ and $s = 8$ respectively, meaning that the DWM model starts yielding lower load results than the Frandsen model after these spacing values.

4. Deviations for the fore-aft, torsional and flapwise components are more sensitive to the inter-turbine spacing than deviations for the side-to-side and edgewise components.

4.2 Discussion

To address the need for a fast and reliable load calculation method for site suitability assessment and design optimization in offshore wind energy, a load catalogue was developed in this thesis. The catalogue was developed with the intention to answer the following research question:

How can the compilation of a comprehensive, high-fidelity fatigue load catalogue contribute to the development of a fast and reliable load calculation methodology for site suitability assessment and design optimization in offshore wind energy?

Chapter 3 of this report described the design and development process of the load catalogue. It showcased how the load calculation methodology applied to populate the catalogue was carefully tailored to represent the load response of modern offshore turbines. This was achieved by adopting the IEA 15 MW offshore turbine as a reference wind turbine, capturing the characteristics of current offshore technology. Moreover, by interchangeably employing both the Kaimal and Mann turbulence models, a comprehensive representation of turbulence was guaranteed. Furthermore, by applying the DWM wake model and using a Weibull distribution for the turbulence intensity, the methodology aligned itself with the latest IEC modelling guidelines, incorporating the latest state of knowledge and industry experience.

Chapter 3 also showed how the input parameters defining the operational scenarios found in the load catalogue were curated to make it representative of offshore site conditions. To strike a balance between comprehensiveness and complexity, only the wind climate parameters with the highest influence on fatigue loads were considered, namely the mean wind speed, turbulence intensity and wind shear exponent. Additionally, given that the Class IC wind climate is the most prevalent in offshore sites, sampling the wind climate parameters from ranges centred on the reference values for Class IC ensured the representation of a considerable range of offshore environments.

By implementing these design strategies in its construction, the load catalogue effectively offers a fast and reliable method to estimate fatigue loads in offshore wind farms. Also, since this method only involves looking up load values within a database, it is notably faster than the conventional approach, making it suitable for practical applications such as site suitability assessment and design optimization. In addition, by addressing the limitations of currently-existing LRMs and by employing state-of-the-art modelling techniques, the catalogue provides a reference for benchmarking calculated fatigue loads, fostering reliability in the offshore wind energy industry. Furthermore, it can provide a solid basis for the calibration of better LRMs, further contributing to the improvement of practical load calculation methods. Nevertheless, this requires the catalogue to be further extended and improved, as discussed in Section 5.2.1.

Besides its direct use, the catalogue also indirectly contributes to the improvement of load calculation methods by contrasting fatigue load results obtained using the different IEC wind and wake models. In fact, these contrasts were explored in Chapter 4 and important observations were made. The latter provide valuable insights, further discussed in Section 4.2.1, into the impact of modelling choices on calculated fatigue loads. These insights can in turn be incorporated into the design of better load calculation methods, or exploited to make better use of existing ones.

The remainder of this section elaborates on the discussion of the thesis findings. Section 4.2.1 begins by discussing the key theoretical findings of this research, relating them to the existing body of knowledge and highlighting their implications, to then reveal the theoretical significance of this study. Subsequently, Section 4.2.2 shifts the attention to the practical value of this work. It discusses the current capabilities of the load catalogue and its use value in practical applications, to later describe the practical significance of this research. Finally, Section 4.2.3 critically reflects on the methods and outcomes of this research, shedding light on its limitations.

4.2.1 Theoretical Insights

The theoretical aspect of this thesis involved exploring the impact of different wind and wake modelling choices on calculated fatigue loads. The results of this investigation were presented in Section 4.1, where many interesting features were identified in the data. Analyzing these features leads to several key findings. These are discussed below for each of the focus areas of Section 4.1.

Focus Area 1: 90th Percentile NTM vs Distribution NTM

The results of Section 4.1.2 show that using a 90^{th} percentile for the turbulence intensity consistently overestimates the fatigue loads obtained when sampling the turbulence intensity from a Weibull distribution. This result is expected, as a 90^{th} percentile inherently assumes more severe turbulence conditions to ensure conservative load estimates.

However, this might lead to overly-conservative designs that are economically sub-optimal. Given that direct sampling from the turbulence intensity distribution may be more representative of actual site conditions, the load deviations computed in this study reflect the magnitude of the safety margin introduced by using a 90^{th} percentile. Specifically, this margin was found to be more substantial for tower loads than for blade loads, with average annual equivalent load effect deviations of 16.48% at the tower base and 5.58% at the blade root measured relative to the 90^{th} percentile value. Nevertheless, the question of whether this margin is necessary remains open and warrants validation with field load data.

It was also demonstrated that the impact of swapping the NTM model, i.e. the resulting load overestimation, is more pronounced when the Mann model is employed than when the Kaimal model is employed. This means that, in the assessment of safety margins introduced by using a more conservative NTM model, attention should also be given to the choice of turbulence model. Another relevant finding is that the choice of turbulence model has a greater influence on load effect deviations for blade loads than for tower loads, and this should also be taken into account.

Furthermore, it was found that the magnitude of fatigue load overestimation for both blade and tower loads is strongly dependent on the wind shear exponent and weakly dependent on the reference turbulence intensity. This suggests that safety margins calculated for a specific site could potentially be extrapolated to other sites with similar wind shear exponents but varying reference turbulence intensities. Nonetheless, this should be done with caution as other wind climate parameters should also be taken into account, especially the mean wind speed distribution. The current study does not account for the sensitivity of fatigue load deviations to these other parameters, highlighting the need for more research into the matter.

Focus Area 2: Kaimal Turbulence vs Mann Turbulence

The findings of Section 4.1.3 reveal that, although both models are recommended by the IEC, significant discrepancies exist in the fatigue loads computed using the Kaimal turbulence model and those computed using the Mann turbulence model. This aligns with the conclusions of [48], [50], [53], [51], [54], and [52], which suggest that such discrepancies are expected due to the different representation of the coherent structures of turbulence between the two models. In [48], [50], [53], [51], and [52], the performance of the IEC Kaimal and Mann models was assessed against high-fidelity LES flow simulations or wind fields generated based on offshore field measurements. The common verdict was that none of the models consistently represents turbulence structures better than the other. With that in mind, the findings of this thesis imply the existence of a non-negligible uncertainty margin associated with the annual fatigue loads calculated using either of the Kaimal or Mann models alone. This suggests that relying on a single turbulence model in the calculation of annual fatigue loads, which reflect estimated component lifetimes, may lead to sub-optimal design choices, hindering safety and cost-effectiveness. Therefore, further research into combined modelling approaches to practical lifetime fatigue load calculation is needed. It is also noteworthy that the load catalogue of this thesis serves to estimate the uncertainty margins associated with the use of either the Kaimal or the Mann models for various site conditions. Nevertheless, to effectively use this information, it is crucial to identify the specific conditions under which the Kaimal model outperforms the Mann model, and vice versa. Fortunately, this an active area of research with many ongoing investigations into the performance of the IEC turbulence models, building upon the aforementioned studies.

Among the aforementioned studies, [48] provides particularly useful insights into the conditions under which the Kaimal model outperforms the Mann model and vice versa. Specifically, the study found that the Kaimal model better matches high-fidelity LES wind fields for high wind speeds, whereas the Mann model is a better match for low wind speeds. Armed with this understanding, the previously discussed uncertainty margins can be better interpreted. More importantly, in practical load calculations, insights like those of [48] can be utilized to select the better-performing turbulence model based on the input wind climate parameters on a case-by-case basis. Such a strategy can be employed to construct a load catalogue following a similar methodology to the one applied in this thesis, or even to filter the current load catalogue, keeping the entries corresponding to the better-performing turbulence model. It follows that the resulting database would provide a better representation of turbulence. Consequently, an LRM calibrated based on such a database is expected to predict loads more accurately. Unfortunately, the current understanding of the dependence of turbulence model performance on wind climate parameters is insufficient to develop such a combined modelling scheme. Nevertheless, this is certainly a promising research avenue, calling for a deeper exploration of the IEC turbulence models' performance under various wind climate conditions.

In accordance with the findings of [48] and [52], tower loads were found to exhibit larger deviations than blade loads, with average absolute deviations of 15.12% at the tower base and 4.67% at the blade root. Moreover, [52] found that loads calculated using the Kaimal and Mann models were in closer agreement with loads calculated based on a wind field constructed from measured offshore wind data for blade components as compared to tower components. This observation was also made by [48] for the tower torsional (yaw) moment and the blade flapwise moment. These considerations suggest that there is generally less uncertainty in the blade loads calculated using either the Kaimal or

Mann models compared to tower loads, but also that the choice of turbulence model matters more for tower design, in addition to support structure design, than for blade design.

Taking a closer look at tower loads, but now considering signed rather than absolute deviations, no consistent trend was detected, implying the absence of a statistically-significant systematic bias in load predictions between the Mann and Kaimal models. However, clearer trends were detected when considering each loading component separately, showing that the Mann model consistently overestimates loads for side-to-side and torsional moments and underestimates them for the fore-aft moment. This is consistent with the findings of [52], which investigated load deviations for the fore-aft component. The results also align with those of [48], which considered deviations in the torsional moment. Nonetheless, [48] and [52] identified those trends solely in short-term DEL results. This research extends the findings to annual load effects as well. Moreover, the previous studies only considered a small set of wind climate parameters, while the current work accounts for a wider range of conditions. The implication of this is that, for the side-to-side and torsional moments, fatigue load estimates obtained using the Mann model can be safely assumed to be larger than those expected for the Kaimal model under most offshore site conditions. The opposite is true for the fore-aft component.

On another note, the results for one particular tower loading component stood out from the rest, namely the torsional moment. This component showed disproportionately large deviations compared to the other two, reaching up 30% at the tower base under certain conditions. Interestingly, similar observations were made in [48] and [53]. According to these studies, this is due to significant differences in the modelling of the lateral coherence of the longitudinal velocity component between the Kaimal and Mann models, which translates into significant load deviations for yaw loads in particular. Yet again, it remains unclear which of the two turbulence models represents this coherence component more accurately. Hence, supported by the findings of [48] and [53], the results of this thesis imply the existence of substantial uncertainties in torsional moments calculated using either the Kaimal or Mann models, which can be problematic for safety considerations. Furthermore, these uncertainties are expected to be more significant for floating turbines than for fixed-bottom ones, since torsional moments are known to have a strong influence on the design of mooring systems [48].

In contrast to the case of tower loads, the results of this study indicate that the Mann model consistently overestimates blade loads obtained with the Kaimal model for both the flapwise and edgewise components. Moreover, it overestimates the flapwise moment by a considerably larger amount compared to the edgewise moment, with average deviations of 1.29% and 8.04% respectively at the blade root. This can be explained by the fact that edgewise moments are mainly gravity-driven, while flapwise moments are turbulence-driven. As for the obtained magnitude of the flapwise deviation, it was notably larger than that observed in [52], where the Mann and Kaimal models were found to be in closer agreement. This could be due to the fact that the comparison in [52] was made for short-term DELs and for a small set of environmental conditions, while this thesis compares annual load effects for a wider range of conditions. Overall, the findings of this research suggest that, although lower than for tower loads, the uncertainty in blade loads calculated with either the Kaimal or Mann models is non-negligible, especially for the turbulence-dominated flapwise moment.

Another interesting observation made in Section 4.1.3 was that using a Weibull distribution for the turbulence intensity reduces the discrepancies observed when toggling between the Kaimal and Mann models. This is likely due to the smoothing effect of sampling from a probabilistic distribution. Given that the relative performance of the Kaimal and Mann models depends on the specific wind climate parameter values, this suggests that employing a Weibull distribution for the turbulence intensity may reduce the uncertainty in lifetime fatigue load results calculated using either the Kaimal or Mann models. Nevertheless, this would come at the expense of the safety margin introduced by employing a 90^{th} percentile turbulence intensity.

Besides the choice of turbulence intensity model, the values of the wind shear exponent and reference turbulence intensity also affect the observed discrepancies between the Kaimal and Mann models. Particularly, the observed load effect deviations were found to exhibit a low sensitivity to variations in the wind shear exponent and the reference turbulence intensity. This means that the uncertainties associated with the selection of the turbulence model may be safely extrapolated from one site to the other, further underscoring the importance of assessing these uncertainties through field measurements. Nonetheless, as noted in the previous section for the choice of turbulence intensity model, attention should be given to the other wind climate parameters, mainly the mean wind speed distribution.

The dependence of deviations in the short-term DEL, rather than the annual load effect, on the mean wind speed was also investigated in Section 4.1.3. Among the various findings, some were especially noteworthy. Indeed, it was noted that, for the tower base fore-aft moment, the Mann model overestimates DEL values calculated with the Kaimal model in the below rated region, and underestimates them in the above rated region. This contradicts the results of [52], where the Mann model was found to consistently overestimate the Kaimal DEL values for this loading component throughout the wind speed range. Moreover, this thesis showed that, for the blade root flapwise moment, the Mann

model consistently overestimates Kaimal DELs. This conflicts with the findings of [48], where it was observed that the Mann model only overestimates Kaimal DELs in the below rated and rated regions, and underestimates them in the above rated region. The discrepancies between the findings of this thesis and those of [48] and [52] may be explained by the NTM models employed in the current research. In fact, these NTM models are characterized by a higher variability in the turbulence intensity across the wind speed range. In contrast, in [48] and [52], the turbulence intensity does not vary considerably across the different wind speeds. Essentially, these conflicting findings call for more research into the matter.

A final point to note follows from the insights of [48], indicating that the Kaimal model is a better match for LES wind fields at high wind speeds. Since high wind speeds are more relevant than lower ones from a loading point of view, this suggests that, in the load catalogue of this thesis, annual load effects computed with the Kaimal model may be more reliable than those obtained with the Mann model. This claim is further supported by [52], which found that the Kaimal model is in better agreement with wind fields constructed from measured timeseries. However, the existing body of evidence is insufficient to assert the superiority of Kaimal model. Moreover, there is compelling evidence that the Mann model outperforms the Kaimal model under certain conditions. Hence, extensive performance assessments of the IEC turbulence models with respect to long-term fatigue predictions are particularly needed, especially against field measurements rather than high-fidelity simulations. In addition, regardless of that, it may be best to follow a combined modelling approach in future endeavors towards the improvement of practical load calculations in wind energy, especially in the context of LRMs and associated load catalogues.

Focus Area 3: Frandsen Wake vs DWM Wake

The main takeaway from Section 4.1.4 is that deviations in fatigue loads computed with the Frandsen and DWM wake models strongly depend on the inter-turbine spacing. More specifically, the deviations measured relative to the Frandsen loads tend to decrease as the inter-turbine spacing increases. Moreover, the Frandsen model overestimates the loads predicted by DWM across all load sensors for an inter-turbine spacing of 4 rotor diameters. These findings are consistent with those of [75] and [76], which also compared the IEC Frandsen and DWM models with respect to fatigue loads for different turbine separations in the range of 3 to 10 rotor diameters. In [75], the analysis was made for a two-turbine case with the NREL 5MW RWT. In addition, only a single 10-minute mean wind speed value was considered, and therefore the reported loads were short-term DELs. On the other hand, [76] assessed long-term equivalent loads for 3x3 wind farm layout like the one considered in this thesis, accounting for a wider range of mean wind speeds and directions and their distributions. Nevertheless, the study was based on turbines with a rating of only 2MW. Therefore, by employing a 15 MW offshore RWT and assessing long-term load effects under offshore operating conditions, this thesis effectively extends the conclusions made in previous work to a context more relevant to modern offshore wind farms. Given that loads predicted by the DWM model have been proven to match measured loads more accurately [71] [72], the general implication of these conclusions is that the Frandsen model will most likely lead to conservative designs for tightly-packed wind farms with inter-turbines spacings smaller than 5 rotor diameters.

For the tower base torsional moment and the blade root flapwise moment, the Frandsen model was found to overestimate the DWM loads for all inter-turbine spacings, with deviations in the range of 16% and 9% respectively. This general trend is consistent with the findings of [75] and [76]. However, the deviation magnitudes vary considerably across the different studies, with the deviations reported in this thesis being the lowest. Hence, it can be inferred that, for the aforementioned loading components, loads computed using the Frandsen model are likely to be conservative regardless of the inter-turbine spacing.

The previous claim cannot be made for the tower base fore-aft moment and the blade root edgewise moment. In fact, Section 4.1.4 revealed that, for certain values of the inter-turbine spacing, the Frandsen model underestimates the DWM results for the tower base fore-aft moment and the blade root edgewise moment. In particular, this occurs at spacings of 6 and 8 rotor diameters for the fore-aft component, and at a spacing of 8 rotor diameters for the edgewise component. Supposing that the DWM model better predicts the true load values, this implies that the Frandsen model might not be conservative in the aforementioned cases. Not only that, but it might underestimate the actual fatigue loads. This finding is critical for practical applications, as most practical load calculations are currently based on the IEC Frandsen model. Specifically, since the tower base fore-aft moment is typically design-driving in site suitability assessment and support structure design, the possible lack of conservatism of the effective turbulence approach might be problematic for these applications as it might pose a safety concern or over-predict project lifetimes. Thus, care should be taken when applying this modelling method in practical load calculations, especially for wind farm with inter-turbine spacings exceeding 5 rotor diameters.

Although the result discussed above has important implications, it is at odds with the expectation that the effective turbulence model is a conservative approach with regard to loads. This calls for more scrutiny into the plausibility of this finding. Looking into previous work, the findings of [75] and [76] corroborate the evidence presented in this work.

Indeed, [75] found that the DWM model can overestimate the tower base fore-aft 10-minute DEL relative to Frandsen for spacings greater than 5 rotor diameters, while [76] made the same observation for the lifetime load effect at a spacing of 8 rotor diameters.

On another hand, more recent studies like [71] and [73] comparing the IEC wake models have concluded that the Frandsen model consistently leads to more conservative load estimates. However, [71] only evaluated short-term DELs for a single mean wind speed and for two turbines separated by distances smaller than 4 rotor diameters. In contrast, the analysis in [73] was more comprehensive as it considered multiple mean wind wind speeds and flow directions in the context of a 4x4 wind farm with inter-turbine spacings of 5 and 8 rotor diameters. Yet, the conclusion drawn in this study was based on a comparison of median load standard deviations obtained with the Frandsen and DWM models. Since this thesis compares annual equivalent loads, this might explain the diverging conclusions. In fact, [73] found that the Frandsen model underestimates the 10-minute DWM DELs for specific values of the mean wind speed and mean flow direction. Given that the annual equivalent load calculation involves weighting the 10-minute DELs based on the probability distributions of the mean wind speed and mean flow direction, this suggests that it is possible to obtain lower annual load effects with the Frandsen model, despite it leading to higher DELs on average. This highlights the importance of the site-specific distributions of the mean wind speed and mean flow direction in the comparison of the IEC turbulence models, calling for more research into their influence.

Another potential explanation for the conflicting results is the size and technology of the studied RWTs. While this research employs the IEA 15 MW turbine, [73] considered the NREL 5 MW turbine and [71] studied 3.3 MW turbines. One more interesting contrast can be made with [74], which compared the 20-year fatigue equivalent loads in the Horns Rev wind farm characterized by inter-turbine spacings exceeding 7 rotor diameters. The study still concluded that the Frandsen model consistently overestimates the DWM loads, even for such large spacings and despite the fact that it accounted for the site-specific wind speed and direction distributions in a comparable offshore site. Nevertheless, the Horns Rev wind farm has turbines rated at 2 MW, considerably smaller than that of the IEA 15 MW turbine considered in this work. This further underscores the importance of accounting for the turbine technology in future research into this matter.

Regarding the magnitudes of the observed deviations relative to the Frandsen result, Section 4.1.4 showed that they are in the range of 27%, 18% and 9% for the tower base side-to-side moment, the tower base torsional moment, and the blade root flapwise moment respectively. Deviations in the tower base fore-aft moment and the blade root edgewise moment were found to be significantly smaller in magnitude, amounting to 5% and 1% on average, respectively. This indicates that the Frandsen and DWM predictions are in more agreement for the latter components than for the former. Another interesting observation is that, in consistence with the results of [73], negative deviations were not only less prevalent than positive ones, but they were also notably smaller. This suggests that these negative deviations may not have enough statistical significance to assert that the Frandsen model underestimates DWM predictions. Nonetheless, they suggest that the Frandsen model can be non-conservative relative to DWM for large inter-turbine spacings.

As noted for the previous wind model comparisons, tower loads were also found to generally exhibit larger deviations than blade loads in this case, except for the fore-aft component which showed deviations comparable to those of the blade components. This aligns with the findings of [71], [76] and [74], but contradicts the findings of [73], which found the opposite result. Hence, an interesting avenue for future work would be to investigate the origin of these discrepancies and to shed more light into the reason behind the differences in blade and tower load deviations.

Theoretical Significance

Ultimately, the comparative analysis of wind and wake models conducted in this study extends the existing literature by highlighting the implications of model selection on load predictions in a context relevant to modern offshore wind farms. By doing that, this research contributes to the theoretical understanding of load calculation methodologies, particularly in the context of offshore wind energy. This is in turn expected to promote the development of better load calculation techniques, leading to more efficient design processes in wind energy. Essentially, this potentially translates into lower LCOEs, aligning with the overarching objectives of this work.

4.2.2 Practical Value

Aside from its theoretical exploration of load calculation methodologies, this thesis aimed to deliver a tool that provides value in practice. To appreciate its practical utility, the capabilities of the load catalogue are first explored. Section 4.1.1 described the organization of the load catalogue and introduced its functional features. These features capitalize on the catalogue's data, processing it to provide useful services. Practically, the catalogue, equipped with its functional features, can serve the following purposes:

- To provide a preliminary estimate of fatigue loads in offshore wind farms.
- To benchmark calculated load results against a reliable reference.
- To estimate the uncertainty in a calculated load value associated with making a specific modelling choice.
- To compute the expected change in the value of a calculated load resulting from making a different modelling choice.
- To infer the expected variation in a calculated load value resulting from a change in environmental conditions.

By supplying the services outlined above, the load catalogue can be instrumental in practical applications. Indeed, it offers a data-driven basis for decision-making that project developers or designers can use, particularly in early design stages. For instance, by providing preliminary estimates of fatigue loads, the load catalogue enables developers to anticipate structural demands and act accordingly, without investing substantial time and effort in the load calculation process at an early design phase. This is particularly relevant for applications like site suitability assessment, which can be facilitated by guidance from the load catalogue. The catalogue also facilitates the comparison and conversion of load results obtained using different modelling methods. Furthermore, it provides a reliable reference for validating load calculation methods and results, in addition to assessing their sensitivity to different modelling choices and wind climate parameters. Lastly, and most importantly, it provides a basis that facilitates the development of better LRMs, as further discussed in Section 5.2.1.

Overall, this thesis delivers a valuable instrument that can guide turbine and farm developers, especially in the early design stages. Additionally, it provides a validated approach for integrating modern offshore turbine models and advanced modelling techniques into a comprehensive load calculation pipeline. Consequently, this research contributes to increasing the efficiency of the load calculation process, helping to reduce the costs and human resource expenditures associated with it. In addition, the catalogue aids in accelerating the development of wind energy projects. Moreover, it is expected to facilitate collaboration among industry players and between them and research institutions. Ultimately, these benefits translate into a lower LCOE for the generated wind power, in alignment with the global objective of boosting the growth of the offshore wind energy industry.

4.2.3 Limitations

Although this thesis makes valuable practical and theoretical contributions, it is important to acknowledge its limitations. These limitations can be classified into three main areas: limitations in the design on the load catalogue, limitations in the load calculation methodology employed for its construction, and general limitations in the overall scope of this study. Each of these limitations is discussed below.

Limitations in the Catalogue Design

The load catalogue of this thesis was tailored to represent loading conditions for sites with wind climates similar to either the reference wind climate for Class IC or the conditions observed at the RWE wind farm site. This means that the applicability of the catalogue is restricted to sites that fit those criteria. Moreover, the catalogue's range of validity around these reference site conditions is relatively narrow. This is due to the narrow ranges considered for the wind climate parameter values of the catalogue, in addition to the limited number of combinations of these parameters that were evaluated. Besides that, for the farm load sets, a single simplified layout was considered and only the wake influence of direct-neighbour turbines was accounted for. Additionally, given the complexity of characterizing the wind climate at a specific site, considering three wind climate parameters only may lead to an incomplete description, and more variables, such as the ones listed in Section 2.2, may be required. Furthermore, in the sampling of the wind climate parameters, the statistical correlations existing between them were ignored as they were assumed to be independent. This is of course a simplification of the relationships between the wind climate variables observed in actual sites.

All the considerations above imply that the load catalogue in its current form is by no means a replacement for current LRMs, and should not be used as a basis for design decisions. Nevertheless, as demonstrated in Section 4.2.2, it is still a valuable instrument that can provide useful guidance to designers, particularly in early design stages. Most importantly, this thesis provides the blueprint and the tools required to address the aforementioned limitations and improve the current load catalogue, making it suitable for the calibration of better LRMs. Moreover, recommendations regarding this extension process are provided in Section 5.2.1. Unfortunately, this could not be done in the current work, mainly due to limitations in time and in computational resources.

Limitations in the Load Calculation Methodology

The population of this thesis' load catalogue relied on a calculation methodology involving the modelling of complex physics. Evidently, this involves simplifications that hinder the accuracy of the predicted loads. Identifying these simplifications is therefore crucial for the improvement of load calculation methods.

Firstly, it is important to acknowledge the inherent limitations in the IEC wind shear and turbulence models employed in the load calculation workflow, which do not account for atmospheric stability, limiting their predictive accuracy. The applied DEL framework also suffers from inherent limitations relating to its reliance on Miner's rule and SN-curves, which involve engineering simplifications.

More specific modelling limitations involve the consideration of only DLC 1.2 for the dynamic simulations, which fails to capture the full range of conditions under which a turbine operates throughout its lifetime. Additionally, the DEL framework was applied without mean stress corrections in this thesis, which is another simplification. In addition, generic values for the Wöhler exponent were assumed for the turbine components, which might not be representative of the full range of specific turbine components in the market. Also, DELs were computed separately for each orthogonal loading component, which when combined would lead to a rather conservative fatigue life estimate, as opposed to a directional calculation approach. Furthermore, in farm simulations, the considered angular increments were rather coarse (30°). Lastly, the load calculation pipeline could only be validated partially (refer to Section 3.4.3) due to the unavailability of reliable DEL data for the IEA 15 MW RWT model.

General Limitations

Naturally, the generalizability of the theoretical findings of Section 4.2.1 is limited by the catalogue data from which they were inferred. Therefore, care should be taken when generalizing the findings of FA1 and FA2 for sites with wind climates diverging from that of Class IC. Likewise, the findings of FA3 should not be generalized to sites with wind climates diverging from that of the RWE wind farm site. Moreover, a complete assessment of the impact of modelling choices on fatigue loads is impossible without benchmarking these loads against measured field data, a luxury that could not be afforded in this thesis. Finally, it is important to consider that this study only considered fatigue loading. Although crucial, the loading situation of a wind farm cannot be fully characterized without the consideration of ultimate loads as well.

5

Conclusion and Recommendations

5.1 Conclusion

In the offshore wind energy industry, load calculations are conventionally carried out through high-fidelity aero-hydro-servo-elastic simulations. Despite being highly reliable, this approach is computationally expensive. For applications requiring a large number of load evaluations, such as site suitability assessment, support structure design and wind farm layout optimization, this translates into substantial costs and significant human resource and time expenditures. To address this issue, Load Response Models (LRMs) have been developed as an approximate, computationally cheaper alternative to numerical simulations that can provide sufficiently reliable load estimates. While many of the currently-existing LRMs have proven to be effective solutions to the aforementioned problem, they still suffer from several limitations, particularly in their applicability to offshore environments. Therefore, this thesis set out to develop a load catalogue that better represents the fatigue loading conditions in modern offshore wind farms, and that can be used as a basis for the calibration of better LRMs. Additionally, it sought to utilize this catalogue to assess the influence of employing different wind and wake models on calculated fatigue loads.

By adopting the IEA 15 MW fixed-bottom turbine as a reference wind turbine, employing both the Kaimal and Mann turbulence models, and incorporating the latest IEC guidelines entailing the use of the DWM wake model and a Weibull distribution for the turbulence intensity, this thesis started by setting up a state-of-the-art load calculation methodology tailored for offshore environments. Then, it achieved its first objective by applying this methodology to an input space that was designed to represent a variety of potential offshore sites. The outcome of that was the delivery of a valuable instrument, the load catalogue, which can guide designers and project developers by providing them with preliminary load estimates and informing them about the uncertainties in their load calculations. More importantly, this thesis provides the tools and knowledge necessary to extend the current load catalogue to make it suitable for the calibration of improved LRMs, which in turn would be instrumental for offshore applications like site suitability assessment. Guidelines for future work aiming towards that end are provided in Section 5.2.1.

Once the catalogue was fully compiled, its data was analyzed to investigate the effects of employing different wind and wake models on load results. From this analysis, the following main conclusions can be drawn:

- Using a 90^{th} percentile for the turbulence intensity consistently overestimates the fatigue loads obtained when sampling the turbulence intensity from a Weibull distribution by an average of 20% for tower base loads and 6% for blade root loads. Consequently, taking the turbulence intensity as a 90^{th} percentile might lead to overly-conservative designs if other safety measures are considered as well. To avoid that while guaranteeing safety, direct sampling from the Weibull distribution is advised, provided that it accurately characterizes site turbulence.

- Care should be taken when modelling turbulence using either the IEC Kaimal or Mann models as they lead to significantly different lifetime fatigue load predictions, while none of them consistently outperforms the other across the whole range of lifetime operating conditions. Thus, a combined modelling approach that selectively toggles between the IEC models based on the short-term environmental conditions is expected to yield more accurate fatigue load estimates compared to using a single model exclusively.

- Frandsen's effective turbulence model can be safely considered conservative for lifetime fatigue load calculations in wind farms with inter-turbine spacings not exceeding 5 rotor diameters. However, it may not be conservative for wind farms with spacings in excess of 5 rotor diameters, especially for the tower base fore-aft

moment. Furthermore, this degree of conservativeness greatly depends on the site-specific mean wind speed and mean flow direction distributions, to which special attention should be given.

In conclusion, by enhancing the theoretical understanding of load calculation methodologies and by providing a practical tool that supports their application, this research promotes more efficient design and development processes in offshore wind energy. This contributes to the reduction of the Levelized Cost of Energy (LCOE) of offshore wind power and to the acceleration of the industry's expansion. Ultimately, this comes as an endeavor to further advance the sustainable energy transition.

However, this study is not without its limitations. In fact, the load catalogue of this thesis is, in its current form, not representative enough of the plethora of possible scenarios encountered in offshore environments, making it unsuitable for the calibration of a practical LRM. Moreover, the generalizability of this research's findings is restricted to the range of validity of the load catalogue upon which they are based. In addition, the load calculation methodology employed in this thesis has its inherent limitations and was not validated against field data. In light of these considerations, further research is required to improve this thesis' load catalogue and expand the findings of this study. To that end, Section 5.2 below outlines specific areas for future work to address these limitations and build upon the contributions of this thesis.

5.2 Recommendations

Based on the findings of this research and its limitations, this section provides recommendations intended to ensure that the contributions of this study translate into practical improvements and novel research directions. Recommendations regarding the improvement of the load catalogue and its optimization for LRM calibration are first given in Section 5.2.1. Then, Section 5.2.2 follows with recommendations for future work related to the topic of this thesis.

5.2.1 Recommendations for Load Catalogue Improvement

Although the load catalogue in its current form has practical value, its full potential can be realized by adapting it for the calibration of an LRM that represents loading conditions in offshore sites better than currently-existing ones. This requires both extending and improving the catalogue's input space design such that it becomes comprehensive and representative enough to serve as a basis for an LRM. This entails:

- Considering additional characteristic climate parameters such as mean inflow inclination, wind veer, air density, and wave spectrum parameters (H_s and T_p).
- Expanding the sampling ranges of the wind climate parameters to capture a broader range of variability for offshore site conditions.
- Increasing the number of operational scenarios (i.e. wind climate parameter combinations) to represent a wider range of potential offshore sites.
- Implementing a sampling scheme that accounts for the statistical correlations between the wind climate parameters observed in offshore sites.
- Including a larger set of load sensors, including the drive train loads for example.
- Accounting for the influence of the wind farm controller by incorporating controller set points into the catalogue as input parameters.
- Devising and applying a case-by-case selection scheme that determines and employs the best turbulence model between the IEC Kaimal and Mann models depending on the input climate parameters. With this combined modelling approach, each catalogue entry would be populated using the most suitable turbulence model.

This research facilitates this improvement process by providing the basic building block and the tools required to establish the improved load catalogue. The current load catalogue serves as the basic building block on top of which the improved catalogue can be built. On the other hand, the load calculation workflow developed in this thesis provides the tools, all encapsulated in a ready-to-use package. In fact, once the input space of the new load catalogue is defined and tabulated, the code pipeline can be readily used to seamlessly compute the corresponding fatigue loads, populat-

ing the catalogue and making it ready for LRM calibration. On a final note, the current load calculation workflow can also be easily adapted to compute ultimate loads in addition to fatigue loads, which would result in a more complete LRM.

5.2.2 Recommendations for Future Work

The following recommendations are put forward for future work aligned with this thesis:

- To validate the use of a Weibull distribution for turbulence intensity as a less conservative alternative to the 90^{th} percentile model through field tests.
- To assess the performance of the IEC turbulence models with respect to long-term fatigue loads against field data under different site conditions.
- To determine the specific short-term environmental conditions under which the Kaimal model outperforms the Mann model, and vice versa.
- Based on this knowledge, to explore the potential of combined modelling approaches employing both the Kaimal and Mann turbulence models in the development of future LRMs.
- To improve the IEC turbulence models in order to reduce the discrepancies observed in their predictions.
- To evaluate the performance of the IEC Frandsen and DWM models:
  - Against on-site load measurements in real wind farms.
  - With respect to long-term fatigue loads.
  - Under a variety of site conditions.
  - For different wind farm layouts.
  - When the Mann model is employed instead of the Kaimal model.
- To explore the influence of wind and wake models on loads for larger wind turbines, like the IEA 22 MW offshore reference wind turbine.
- To improve the computational efficiency of the DWM model in order to enable its use in practical applications like site suitability assessment and design optimization.

References

[1] European Council. *COP28*. Available at https://www.consilium.europa.eu/en/policies/climate-change/paris-agreement/cop28/#:~:text=The%20stocktake%20highlighted%20the%20need,meeting%20their%20Paris%20Agreement%20goals. (31-01-2024).

[2] IEA. *Renewables 2023*. Tech. rep. 2024.

[3] G. Bilicic and S. Scroggins. *LCOE+*. Tech. rep. Lazard, 2023.

[4] Global Wind Energy Council. *Global Wind Report 2023*. Tech. rep. 2023.

[5] René Slot. "From Wind Climate to Wind Turbine Loads: efficient and accurate decision support and reliability analysis". PhD thesis. Aalborg University, 2019.

[6] DNV. *Wind turbine site suitability tool*. Available at https://www.dnv.com/services/wind-turbine-site-suitability-tool-99122 (30-01-2024).

[7] EMD International. *LOAD RESPONSE - WindPro*. Available at https://www.emd-international.com/windpro/windpro-modules/load-modules/load-response/ (30-01-2024).

[8] International Electrotechnical Commission. *IEC Homepage*. Accessed: 2024-07-29. 2024. URL: https://www.iec.ch/homepage.

[9] IEC. *International Standard IEC 61400-1 ed. 4: 'Wind Turbines - Part 1 Design Requirements'*. 2019.

[10] Sten Frandsen. "Turbulence and turbulence-generated structural loading in wind turbine clusters". In: (2007).

[11] Mesfin Belayneh Ageze, Yefa Hu, and Huachun Wu. "Wind turbine aeroelastic modeling: basics and cutting edge trends". In: *International Journal of Aerospace Engineering* (2017).

[12] Lin Wang, Xiongwei Liu, and Athanasios Kolios. "State of the art in the aeroelasticity of wind turbine blades: Aeroelastic modelling". In: *Renewable and Sustainable Energy Reviews* 64 (2016), pp. 195–210.

[13] DNV. *Wind turbine design software - Bladed*. Available at https://www.dnv.com/services/wind-turbine-design-software-bladed-3775 (16-01-2024).

[14] DNV. *Bladed Documentation*. Available at https://renewableenergysoftwareportal.dnv.com/Documentation?ProductID=1 (16-01-2024).

[15] DNV. *Bladed List of Publications*. Available at https://renewableenergysoftwareportal.dnv.com/Documentation?ProductID=1 under *Publications* (16-01-2024).

[16] NREL. *OpenFAST*. Available at https://www.nrel.gov/wind/nwtc/openfast.html#:~:text=OpenFAST%20is%20an%20open%2Dsource,now%20take%20place%20in%20OpenFAST. (16-01-2024).

[17] Srinivas Guntur et al. "A validation and code-to-code verification of FAST for a megawatt-scale wind turbine with aeroelastically tailored blades". In: *Wind Energy Science* 2.2 (2017), pp. 443–468.

[18] Alexander J Coulling et al. "Validation of a FAST semi-submersible floating wind turbine numerical model with DeepCwind test data". In: *Journal of Renewable and Sustainable Energy* 5.2 (2013).

[19] Jieyan Chen, Chungkuk Jin, and Moo-Hyun Kim. "Systematic comparisons among OpenFAST, Charm3D-FAST simulations and DeepCWind model test for 5 MW OC4 semisubmersible offshore wind turbine". In: *Ocean Systems Engineering* 13.2 (2023), pp. 173–193.

[20] Frederick Driscoll et al. "Validation of a FAST model of the statoil-hywind demo floating wind turbine". In: *Energy Procedia* 94 (2016), pp. 3–19.

[21] Evan Gaertner et al. *Definition of the IEA 15-Megawatt Offshore Reference Wind Turbine*. Tech. rep. International Energy Agency, 2020. URL: https://www.nrel.gov/docs/fy20osti/75698.pdf.

[22] Pietro Bortolotti et al. "IEA Wind Task 37 on systems engineering in wind energy". In: *WP2-Reference Wind Turbines.: IEA Wind Task* 37 (2019).

[23] David Malcolm, Kevin Lybarger, and Gordon Randall. "Advances in Wind Turbine Site Assessment". In: *49th AIAA Aerospace Sciences Meeting including the New Horizons Forum and Aerospace Exposition*. 2011, p. 456.

[24] Katherine L Dykes and Jennifer Rinker. *Windpact reference wind turbines*. Tech. rep. National Renewable Energy Lab.(NREL), Golden, CO (United States), 2018.

[25] Jason Jonkman et al. *Definition of a 5-MW reference wind turbine for offshore system development*. Tech. rep. National Renewable Energy Lab.(NREL), Golden, CO (United States), 2009.

[26] Cian Desmond et al. "Description of an 8 MW reference wind turbine". In: *Journal of Physics: Conference Series*. Vol. 753. 9. IOP Publishing. 2016, p. 092013.

[27] Christian Bak et al. "The DTU 10-MW reference wind turbine". In: *Danish wind power research 2013*. 2013.

[28] Dick Veldkamp. "Chances in Wind Energy: A probabilistic approach to wind turbine fatigue design". PhD thesis. Delft University of Technology, 2006.

[29] ASTM. *ASTM No. E1049-85: 'Standard Practice for Cycle Counting in Fatigue Analysis'*. 2011.

[30] Milton A. Miner. "Cumulative damage in fatigue". In: *Journal of Applied Mechanics* (1945).

[31] European Standard. "Eurocode 3 — Design of steel structures — Part 1-9: Fatigue". In: *BS EN* (2005).

[32] Roland Stull. *Practical Meteorology: An Algebra-based Survey of Atmospheric Science*. University of British Columbia, 2017.

[33] Giovanni Gualtieri. "A comprehensive review on wind resource extrapolation models applied in wind energy". In: *Renewable and Sustainable Energy Reviews* 102 (2019), pp. 215–233.

[34] Jiale Li, Xuefei Wang, and Xiong Bill Yu. "Use of spatio-temporal calibrated wind shear model to improve accuracy of wind resource assessment". In: *Applied energy* (2018).

[35] W. A. A. M. Bierbooms M. C. Holtslag and G. J. W. van Bussel. "Estimating atmospheric stability from observations and correcting wind shear models accordingly". In: *Wind Energy* (2014).

[36] AS Monin and AM Obukhov. "Dimensionless characteristics of turbulence in the surface layer". In: *Akad. Nauk SSSR, Geofiz. Inst., Tr* (1954).

[37] Joost A Businger et al. "Flux-profile relationships in the atmospheric surface layer". In: *Journal of the atmospheric Sciences* (1971).

[38] Gustav Hellmann. *Über die Bewegung der Luft in den untersten Schichten der Atmosphäre*. Kgl. Akademie der Wissenschaften [G.] Reimer, 1914.

[39] AR Sathe et al. "Influence of atmospheric stability on wind turbine loads". In: *Wind Energy* (2012). DOI: 10.1002/we.1528.

[40] Nikolay Dimitrov, Anand Natarajan, and Mark Kelly. "Model of wind shear conditional on turbulence and its impact on wind turbine loads". In: *Wind Energy* (2015).

[41] René MM Slot et al. "Importance of shear in site assessment of wind turbine fatigue loads". In: *Journal of Solar Energy Engineering* 140.4 (2018), p. 041012.

[42] P. K. Kundu. *Fluid mechanics*. Elsevier Science, 2013.

[43] Jakob Mann. "Wind field simulation". In: *Probabilistic engineering mechanics* 13.4 (1998), pp. 269–282.

[44] Paul S Veers. *Three-dimensional wind simulation*. Tech. rep. Sandia National Labs., Albuquerque, NM (USA), 1988.

[45] Karthik Duraisamy, Gianluca Iaccarino, and Heng Xiao. "Turbulence modeling in the age of data". In: *Annual review of fluid mechanics* 51 (2019), pp. 357–377.

[46] J. C. Kaimal et al. "Spectral characteristics of surface-layer turbulence". In: *Journal of the Royal Meteorological Society* (1972).

[47] J. Mann. "The spatial structure of neutral atmospheric surface-layer turbulence". In: *Journal of Fluid Mechanics* (1994).

[48] Paula Doubrawa et al. "Load response of a floating wind turbine to turbulent atmospheric flow". In: *Applied Energy* 242 (2019), pp. 1588–1599.

[49] Theodore Von Karman. "Progress in the statistical theory of turbulence". In: *Proceedings of the National Academy of Sciences* 34.11 (1948), pp. 530–539.

[50] Astrid Nybø et al. "Evaluation of different wind fields for the investigation of the dynamic response of offshore wind turbines". In: *Wind Energy* 23.9 (2020), pp. 1810–1830.

[51] Astrid Nybø, Finn Gunnar Nielsen, and Marte Godvik. "Sensitivity of the dynamic response of a multimegawatt floating wind turbine to the choice of turbulence model". In: *Wind Energy* 25.6 (2022), pp. 1013–1029.

[52] Maylinn Haaskjold Myrtvedt. "Investigation of the importance of wind field modelling for loads on a bottom fixed and a spar floater wind turbine". MA thesis. The University of Bergen, 2019.

[53] Astrid Nybø, Finn Gunnar Nielsen, and Marte Godvik. "Quasi-static response of a bottom-fixed wind turbine subject to various incident wind fields". In: *Wind Energy* 24.12 (2021), pp. 1482–1500.

[54] Erin E Bachynski and Lene Eliassen. "The effects of coherent structures on the global response of floating offshore wind turbines". In: *Wind Energy* 22.2 (2019), pp. 219–238.

[55] Jan Van Der Tempel. *Design of support structures for offshore wind turbines*. Published and distributed by the author, 2006.

[56] HL Tolman. "Practical wind wave modeling". In: *Water Waves: Theory and Experiment*. World Scientific, 2010, pp. 79–92.

[57] George B Airy. "Tides and waves. encyclopaedia metropolitana (1817–1845)". In: *Mixed Sciences, edited by HJ Rose* 3 (1841), p. 1841.

[58] Willard J Pierson Jr and Lionel Moskowitz. "A proposed spectral form for fully developed wind seas based on the similarity theory of SA Kitaigorodskii". In: *Journal of geophysical research* 69.24 (1964), pp. 5181–5190.

[59] Mojtaba Maali Amiri, Milad Shadman, and Segen F Estefen. "A review of physical and numerical modeling techniques for horizontal-axis wind turbine wakes". In: *Renewable and Sustainable Energy Reviews* 193 (2024), p. 114279.

[60] Fernando Porté-Agel, Majid Bastankhah, and Sina Shamsoddin. "Wind-turbine and wind-farm flows: A review". In: *Boundary-layer meteorology* 174.1 (2020), pp. 1–59.

[61] Cristina L Archer et al. "Review and evaluation of wake loss models for wind energy applications". In: *Applied Energy* 226 (2018), pp. 1187–1207.

[62] G. C. Larsen. *A simple stationary semi-analytical wake model*. Tech. rep. Risø National Laboratory, 2009.

[63] N. O. Jensen. *A Note on Wind Generator Interaction*. Tech. rep. Risø National Laboratory, 1983.

[64] S. Frandsen et al. "Analytical modelling of wind speed deficit in large offshore wind farms". In: *Wind Energy* (2006).

[65] G. C. Larsen et al. "A new method for prediction of detailed wake loads". In: *IEA Annex XI joint action meeting# 16 on the 'Aerodynamics of wind turbines'* (2003).

[66] H.A. Madsen, K. Thomsen, and G.C. Larsen. "Wake meandering: a pragmatic approach". In: *Wind Energy* (2008).

[67] H.A. Madsen et al. "Calibration and validation of the dynamic wake meandering model for implementation in an aeroelastic code". In: *J Sol Energy Eng* (2010).

[68] Torben J Larsen et al. "Validation of the Dynamic Wake Meander model with focus on tower loads". In: *Journal of Physics: Conference Series*. Vol. 854. 1. IOP Publishing. 2017, p. 012027.

[69] Jason Mark Jonkman and Kelsey Shaler. *FAST.Farm User's Guide and Theory Manual*. National Renewable Energy Laboratory, Golden, CO, USA, 2021.

[70] Jaime Liew et al. "LES verification of HAWC2Farm aeroelastic wind farm simulations with wake steering and load analysis". In: *Journal of Physics: Conference Series*. Vol. 2265. 2. IOP Publishing. 2022, p. 022069.

[71] Inga Reinwardt et al. "Validation of wind turbine wake models with focus on the dynamic wake meandering model". In: *Journal of Physics: Conference Series*. Vol. 1037. 7. IOP Publishing. 2018, p. 072028.

[72] V Bernard et al. "Observation and modelling of asymmetric loading on large offshore wind turbines in wake conditions". In: *Journal of Physics: Conference Series*. Vol. 2767. 9. IOP Publishing. 2024, p. 092092.

[73] Paula Doubrawa, Kelsey Shaler, and Jason Jonkman. "Difference in load predictions obtained with effective turbulence vs. a dynamic wake meandering modeling approach". In: *Wind Energy Science Discussions* 2023 (2023), pp. 1–28.

[74] Björn Schmidt et al. "Wake loads and fatigue load certification in offshore wind farms". In: *Offshore EWEA proceedings* (2011).

[75] Björn Schmidt et al. "Load validation and comparison versus certification approaches of the Risø Dynamic Wake Meandering model implementation in GH Bladed". In: *EWEA Annual Event 2011*. European Wind Energy Association (EWEA). 2011, pp. 249–254.

[76] Torben J Larsen, Helge Madsen Aagaard, and Gunner Chr Larsen. "Comparison of design methods for turbines in wake". In: *Research in aeroelasticity EFP-2007*. Danmarks Tekniske Universitet, Risø Nationallaboratoriet for Bæredygtig Energi, 2008, pp. 83–92.

[77] Tina Kashef and Steven R Winterstein. "Relating turbulence to wind turbine blade loads: Parametric study with multiple regression analysis". In: (1999).

[78] Lance Manuel, Paul S Veers, and Steven R Winterstein. "Parametric models for estimating wind turbine fatigue loads for design". In: *J. Sol. Energy Eng.* 123.4 (2001), pp. 346–355.

[79] F Mouzakis, E Morfiadakis, and P Dellaportas. "Fatigue loading parameter identification of a wind turbine operating in complex terrain". In: *Journal of Wind Engineering and Industrial Aerodynamics* 82.1-3 (1999), pp. 69–88.

[80] Gordon M Stewart. "Design load analysis of two floating offshore wind turbine concepts". PhD thesis. University of Massachusetts Amherst, 2016.

[81] Daniel Zwick and Michael Muskulus. "Simplified fatigue load assessment in offshore wind turbine structural analysis". In: *Wind Energy* 19.2 (2016), pp. 265–278.

[82] Henrik Stensgaard Toft et al. "Assessment of wind turbine structural integrity using response surface methodology". In: *Engineering Structures* 106 (2016), pp. 471–483.

[83] Juan Pablo Murcia et al. "Uncertainty propagation through an aeroelastic wind turbine model using polynomial surrogates". In: *Renewable Energy* 119 (2018), pp. 910–922.

[84] Nikolay Dimitrov et al. "From wind to loads: wind turbine site-specific load estimation using databases with high-fidelity load simulations". In: *Wind Energ. Sci. Discuss* 375 (2018), pp. 767–790.

[85] Kolja Müller, Martin Dazer, and Po Wen Cheng. "Damage assessment of floating offshore wind turbines using response surface modeling". In: *Energy Procedia* 137 (2017), pp. 119–133.

[86] Laura Schröder et al. "Wind turbine site-specific load estimation using artificial neural networks calibrated by means of high-fidelity load simulations". In: *Journal of Physics: Conference Series*. Vol. 1037. 6. IOP Publishing. 2018, p. 062027.

[87] Christos Galinos et al. "Mapping wind farm loads and power production-a case study on horns rev 1". In: *Journal of Physics: Conference Series*. Vol. 753. 3. IOP Publishing. 2016, p. 032010.

[88] Nikolay Dimitrov. "Surrogate models for parameterized representation of wake-induced loads in wind farms". In: *Wind Energy* 22.10 (2019), pp. 1371–1389.

[89] Christos Galinos et al. "T2FL: An efficient model for wind turbine fatigue damage prediction for the two-turbine case". In: *Energies* 13.6 (2020), p. 1306.

[90] Nikolay Dimitrov and Anand Natarajan. "Wind farm set point optimization with surrogate models for load and power output targets". In: *Journal of Physics: Conference Series*. Vol. 2018. 1. IOP Publishing. 2021, p. 012013.

[91] Georgios Gasparis, Wai Hou Lio, and Fanzhong Meng. "Surrogate models for wind turbine electrical power and fatigue loads in wind farm". In: *Energies* 13.23 (2020), p. 6360.

[92] Ervin Bossanyi. "Surrogate model for fast simulation of turbine loads in wind farms". In: *Journal of Physics: Conference Series*. Vol. 2265. 4. IOP Publishing. 2022, p. 042038.

[93] IEA. *Wind Task 37*. Available at https://iea-wind.org/task37/ (23-05-2024).

[94] IEA. *IEAWindTask37/IEA-15-240-RWT*. Available at https://github.com/IEAWindTask37/IEA-15-240-RWT (23-05-2024).

[95] NREL. *FAST.Farm Documentation*. Available at https://openfast.readthedocs.io/en/dev/source/user/fast.farm/Introduction.html (16-01-2024).

[96] NREL. *TurbSim Documentation*. Available at https://www.nrel.gov/docs/fy09osti/46198.pdf (16-01-2024).

[97] NREL. *openfast_toolbox*. Available at https://github.com/OpenFAST/openfast_toolbox/tree/main (23-05-2024).

[98] Neil N Davis et al. "The Global Wind Atlas: A high-resolution dataset of climatologies and associated web-based application". In: *Bulletin of the American Meteorological Society* 104.8 (2023), E1507–E1525.

[99] DTU. *IEC Class Wind Map*. Obtained from the Global Wind Atlas version 3.3, a free, web-based application accessible at https://globalwindatlas.info/en. The Global Wind Atlas version 3.3 is developed, owned and operated by the Technical University of Denmark (DTU) and is released in partnership with the World Bank Group, utilizing data provided by Vortex, using funding provided by the Energy Sector Management Assistance Program (ESMAP). (16-07-2024).

[100] Henrik Stensgaard Toft et al. "Uncertainty in wind climate parameters and their influence on wind turbine fatigue loads". In: *Renewable Energy* 90 (2016), pp. 352–361.

[101] Henrik Stensgaard Toft et al. "Wind climate parameters for wind turbine fatigue load assessment". In: *Journal of Solar Energy Engineering* 138.3 (2016), p. 031010.

[102] IEA. *IEAWindTask37/IEA-15-240-RWT/Documentation*. Available at https://github.com/IEAWindTask37/IEA-15-240-RWT/tree/master/Documentation (23-05-2024).

[103] NREL. *r-test*. Available at https://github.com/OpenFAST/r-test (11-06-2024)).

[104] Jennifer Rinker et al. “Comparison of loads from HAWC2 and OpenFAST for the IEA Wind 15 MW Reference Wind Turbine”. In: *Journal of Physics: Conference Series*. Vol. 1618. 5. IOP Publishing. 2020, p. 052052.

A

Wind Simulator Configuration

A.1 TurbSim input file used for OpenFAST simulation wind files

```
---------TurbSim v2.00.* Input File------------------------
Example TurbSim input file for OpenFAST simulations with the IEA 15MW RWT.
---------Runtime Options-----------------------------------
False         Echo            - Echo input data to <RootName>.ech (flag)
60362647      RandSeed1       - First random seed  (-2147483648 to 2147483647)
"RANLUX"      RandSeed2       - Second random seed (-2147483648 to 2147483647)
     for intrinsic pRNG, or an alternative pRNG: "RanLux" or "RNSNLW"
False         WrBHHTP         - Output hub-height turbulence parameters in
    binary form?  (Generates RootName.bin)
False         WrFHHTP         - Output hub-height turbulence parameters in
    formatted form?  (Generates RootName.dat)
False         WrADHH          - Output hub-height time-series data in AeroDyn
    form?  (Generates RootName.hh)
True          WrADFF          - Output full-field time-series data in TurbSim/
    AeroDyn form? (Generates RootName.bts)
False         WrBLFF          - Output full-field time-series data in BLADED/
    AeroDyn form?  (Generates RootName.wnd)
False         WrADTWR         - Output tower time-series data? (Generates
    RootName.twr)
False         WrHAWCFF        - Output full-field time-series data in HAWC
    form?  (Generates RootName-u.bin, RootName-v.bin, RootName-w.bin, RootName
    .hawc)
False         WrFMTFF         - Output full-field time-series data in
    formatted (readable) form?  (Generates RootName.u, RootName.v, RootName.w)
False         WrACT           - Output coherent turbulence time steps in
    AeroDyn form? (Generates RootName.cts)
1             ScaleIEC        - Scale IEC turbulence models to exact target
    standard deviation? [0=no additional scaling; 1=use hub scale uniformly;
    2=use individual scales]

--------Turbine/Model Specifications-----------------------
49            NumGrid_Z       - Vertical grid-point matrix dimension
49            NumGrid_Y       - Horizontal grid-point matrix dimension
0.07692       TimeStep        - Time step [seconds]
700           AnalysisTime    - Length of analysis time series [seconds] (
    program will add time if necessary: AnalysisTime = MAX(AnalysisTime,
    UsableTime+GridWidth/MeanHHWS) )
"ALL"         UsableTime      - Usable length of output time series [seconds]
    (program will add GridWidth/MeanHHWS seconds unless UsableTime is "ALL")
150.0         HubHt           - Hub height [m] (should be > 0.5*GridHeight)
299.0         GridHeight      - Grid height [m]
299.0         GridWidth       - Grid width [m] (should be >= 2*(RotorRadius+
    ShaftLength))
0.0           VFlowAng        - Vertical mean flow (uptilt) angle [degrees]
0.0           HFlowAng        - Horizontal mean flow (skew) angle [degrees]
```

```
--------Meteorological Boundary Conditions-------------------
"IECKAI"      TurbModel       - Turbulence model ("IECKAI","IECVKM","GP_LLJ","
    NWTCUP","SMOOTH","WF_UPW","WF_07D","WF_14D","TIDAL","API","USRINP","TIMESR
    ", or "NONE")
"unused"      UserFile        - Name of the file that contains inputs for user
    -defined spectra or time series inputs (used only for "USRINP" and "TIMESR
    " models)
"1-ED3"       IECstandard     - Number of IEC 61400-x standard (x=1,2, or 3
    with optional 61400-1 edition number (i.e. "1-Ed2") )
0.12          IECturbc        - IEC turbulence characteristic ("A", "B", "C"
    or the turbulence intensity in percent) ("KHTEST" option with NWTCUP model
    , not used for other models)
NTM          IEC_WindType     - IEC turbulence type ("NTM"=normal, "xETM"=
    extreme turbulence, "xEWM1"=extreme 1-year wind, "xEWM50"=extreme 50-year
    wind, where x=wind turbine class 1, 2, or 3)
"default"     ETMc            - IEC Extreme Turbulence Model "c" parameter [m/
    s]
"PL"          WindProfileType - Velocity profile type ("LOG";"PL"=power law;"
    JET";"H2L"=Log law for TIDAL model;"API";"USR";"TS";"IEC"=PL on rotor disk
    , LOG elsewhere; or "default")
"unused"      ProfileFile     - Name of the file that contains input profiles
    for WindProfileType="USR" and/or TurbModel="USRVKM" [-]
150.0         RefHt           - Height of the reference velocity (URef) [m]
10.59         URef            - Mean (total) velocity at the reference height
    [m/s] (or "default" for JET velocity profile) [must be 1-hr mean for API
    model; otherwise is the mean over AnalysisTime seconds]
"default"     ZJetMax         - Jet height [m] (used only for JET velocity
    profile, valid 70-490 m)
0.14          PLExp           - Power law exponent [-] (or "default")
"default"     Z0              - Surface roughness length [m] (or "default")

--------Non-IEC Meteorological Boundary Conditions------------
"default"     Latitude        - Site latitude [degrees] (or "default")
0.05          RICH_NO         - Gradient Richardson number [-]
"default"     UStar           - Friction or shear velocity [m/s] (or "default
    ")
"default"     ZI              - Mixing layer depth [m] (or "default")
"default"     PC_UW           - Hub mean u'w' Reynolds stress [m^2/s^2] (or "
    default" or "none")
"default"     PC_UV           - Hub mean u'v' Reynolds stress [m^2/s^2] (or "
    default" or "none")
"default"     PC_VW           - Hub mean v'w' Reynolds stress [m^2/s^2] (or "
    default" or "none")

--------Spatial Coherence Parameters----------------------------
"default"     SCMod1          - u-component coherence model ("GENERAL","IEC","
    API","NONE", or "default")
"default"     SCMod2          - v-component coherence model ("GENERAL","IEC","
    NONE", or "default")
"default"     SCMod3          - w-component coherence model ("GENERAL","IEC","
    NONE", or "default")
"default"     InCDec1         - u-component coherence parameters for general
    or IEC models [-, m^-1] (e.g. "10.0  0.3e-3" in quotes) (or "default")
"default"     InCDec2         - v-component coherence parameters for general
    or IEC models [-, m^-1] (e.g. "10.0  0.3e-3" in quotes) (or "default")
"default"     InCDec3         - w-component coherence parameters for general
    or IEC models [-, m^-1] (e.g. "10.0  0.3e-3" in quotes) (or "default")
"default"     CohExp          - Coherence exponent for general model [-] (or "
    default")

--------Coherent Turbulence Scaling Parameters-------------------
"Y:\Wind\Archive\Public\Projects\KH_Billow\EventData"  CTEventPath     - Name
    of the path where event data files are located
"Random"      CTEventFile     - Type of event files ("LES", "DNS", or "RANDOM
    ")
```

```
True          Randomize       - Randomize the disturbance scale and locations?
    (true/false)
1             DistScl         - Disturbance scale [-] (ratio of event dataset
    height to rotor disk). (Ignored when Randomize = true.)
0.5           CTLy            - Fractional location of tower centerline from
    right [-] (looking downwind) to left side of the dataset. (Ignored when
    Randomize = true.)
0.5           CTLz            - Fractional location of hub height from the
    bottom of the dataset. [-] (Ignored when Randomize = true.)
30            CTStartTime     - Minimum start time for coherent structures in
    RootName.cts [seconds]

================================================
! NOTE: Do not add or remove any lines in this file!
================================================
```

Note that in the template input file above, `RandSeed1`, `IECturbc`, `URef` and `PLExp` are variables modified throughout the load calculation iterations.

A.2 Configuration parameters for Bladed turbulence simulator used for OpenFAST simulation wind files

Parameter	Value
Number of points along Y	49
Number of points along Z	49
Volume width Y	299 m
Volume height Z	299 m
Duration of wind file	700 s
Frequency along X	13 Hz
Mean wind speed	Variable, specified as an input
Turbulence seed	Variable, specified as an input
Spectrum type	Mann
Turbulence evolution	Frozen turbulence
Shear parameter (γ)	3.9
Scale length (L)	33.6 m
FFT points	64
Max. lateral/vertical wavelength	320 m

A.3 TurbSim input files used for FAST.Farm simulation wind files

A.3.1 Input file for low-resolution wind files

```
--------TurbSim v2.00.* Input File------------------------
Custom TurbSim file written using openfast_toolbox library
---------Runtime Options-----------------------------------
False   Echo        - Echo input data to <RootName>.ech (flag)
199 RandSeed1       - First random seed  (-2147483648 to 2147483647)
"RanLux"    RandSeed2       - Second random seed (-2147483648 to 2147483647)
    for intrinsic pRNG, or an alternative pRNG: "RanLux" or "RNSNLW"
False   WrBHHTP     - Output hub-height turbulence parameters in binary form?
    (Generates RootName.bin)
```

```
False   WrFHHTP      - Output hub-height turbulence parameters in formatted
    form?  (Generates RootName.dat)
False   WrADHH       - Output hub-height time-series data in AeroDyn form?  (
    Generates RootName.hh)
True    WrADFF       - Output full-field time-series data in TurbSim/AeroDyn
    form? (Generates RootName.bts)
False   WrBLFF       - Output full-field time-series data in BLADED/AeroDyn
    form?  (Generates RootName.wnd)
False   WrADTWR      - Output tower time-series data? (Generates RootName.twr)
False   WrHAWCFF         - Output full-field time-series data in HAWC form?  (
    Generates RootName-u.bin, RootName-v.bin, RootName-w.bin, RootName.hawc)
False   WrFMTFF      - Output full-field time-series data in formatted (
    readable) form?  (Generates RootName.u, RootName.v, RootName.w)
False   WrACT        - Output coherent turbulence time steps in AeroDyn form? (
    Generates RootName.cts)
1   ScaleIEC         - Scale IEC turbulence models to exact target standard
    deviation? [0=no additional scaling; 1=use hub scale uniformly; 2=use
    individual scales]

--------Turbine/Model Specifications-----------------------
27  NumGrid_Z        - Vertical grid-point matrix dimension
99  NumGrid_Y        - Horizontal grid-point matrix dimension
0.5 TimeStep         - Time step [seconds]
700 AnalysisTime         - Length of analysis time series [seconds] (program
    will add time if necessary: AnalysisTime = MAX(AnalysisTime, UsableTime+
    GridWidth/MeanHHWS) )
"ALL"   UsableTime       - Usable length of output time series [seconds] (
    program will add GridWidth/MeanHHWS seconds unless UsableTime is "ALL")
391 HubHt        - Hub height [m] (should be > 0.5*GridHeight)
780 GridHeight       - Grid height [m]
2940    GridWidth        - Grid width [m] (should be >= 2*(RotorRadius+
    ShaftLength))
0   VFlowAng         - Vertical mean flow (uptilt) angle [degrees]
0   HFlowAng         - Horizontal mean flow (skew) angle [degrees]

--------Meteorological Boundary Conditions-------------------
"IECKAI"    TurbModel        - Turbulence model ("IECKAI","IECVKM","GP_LLJ","
    NWTCUP","SMOOTH","WF_UPW","WF_07D","WF_14D","TIDAL","API","IECKAI","TIMESR
    ", or "NONE")
"unused"    UserFile         - Name of the file that contains inputs for user-
    defined spectra or time series inputs (used only for "IECKAI" and "TIMESR"
     models)
"1-ED3" IECstandard      - Number of IEC 61400-x standard (x=1,2, or 3 with
    optional 61400-1 edition number (i.e. "1-Ed2") )
17.700  IECturbc         - IEC turbulence characteristic ("A", "B", "C" or the
    turbulence intensity in percent) ("KHTEST" option with NWTCUP model, not
    used for other models)
"NTM"   IEC_WindType         - IEC turbulence type ("NTM"=normal, "xETM"=
    extreme turbulence, "xEWM1"=extreme 1-year wind, "xEWM50"=extreme 50-year
    wind, where x=wind turbine class 1, 2, or 3)
"default"   ETMc         - IEC Extreme Turbulence Model "c" parameter [m/s]
"PL"    WindProfileType      - Velocity profile type ("LOG";"PL"=power law;"JET
    ";"H2L"=Log law for TIDAL model;"API";"PL";"TS";"IEC"=PL on rotor disk,
    LOG elsewhere; or "default")
"unused"    ProfileFile      - Name of the file that contains input profiles
    for WindProfileType="USR" and/or TurbModel="USRVKM" [-]
150.000 RefHt        - Height of the reference velocity (URef) [m]
6.000   URef         - Mean (total) velocity at the reference height [m/s] (or
    "default" for JET velocity profile) [must be 1-hr mean for API model;
    otherwise is the mean over AnalysisTime seconds]
"default"   ZJetMax      - Jet height [m] (used only for JET velocity profile,
    valid 70-490 m)
0.070   PLExp        - Power law exponent [-] (or "default")
"default"   Z0       - Surface roughness length [m] (or "default")

--------Non-IEC Meteorological Boundary Conditions------------
```

```
"default"   Latitude        - Site latitude [degrees] (or "default")
0.05    RICH_NO     - Gradient Richardson number [-]
"default"   UStar       - Friction or shear velocity [m/s] (or "default")
"default"   ZI      - Mixing layer depth [m] (or "default")
"default"   PC_UW       - Hub mean u'w' Reynolds stress [m^2/s^2] (or "default
    " or "none")
"default"   PC_UV       - Hub mean u'v' Reynolds stress [m^2/s^2] (or "default
    " or "none")
"default"   PC_VW       - Hub mean v'w' Reynolds stress [m^2/s^2] (or "default
    " or "none")

--------Spatial Coherence Parameters----------------------------
"default"   SCMod1      - u-component coherence model ("GENERAL","IEC","API","
    NONE", or "default")
"default"   SCMod2      - v-component coherence model ("GENERAL","IEC","NONE",
     or "default")
"default"   SCMod3      - w-component coherence model ("GENERAL","IEC","NONE",
     or "default")
"default"   InCDec1 - u-component coherence parameters for general or IEC
    models [-, m^-1] (e.g. "10.0  0.3e-3" in quotes) (or "default")
"default"   InCDec2 - v-component coherence parameters for general or IEC
    models [-, m^-1] (e.g. "10.0  0.3e-3" in quotes) (or "default")
"default"   InCDec3 - w-component coherence parameters for general or IEC
    models [-, m^-1] (e.g. "10.0  0.3e-3" in quotes) (or "default")
"default"   CohExp      - Coherence exponent for general model [-] (or "
    default")

--------Coherent Turbulence Scaling Parameters-------------------
".\EventData"   CTEventPath     - Name of the path where event data files are
    located
"Random"    CTEventFile     - Type of event files ("LES", "DNS", or "RANDOM")
true    Randomize       - Randomize the disturbance scale and locations? (true
    /false)
1   DistScl     - Disturbance scale [-] (ratio of event dataset height to
    rotor disk). (Ignored when Randomize = true.)
0.5 CTLy        - Fractional location of tower centerline from right [-] (
    looking downwind) to left side of the dataset. (Ignored when Randomize =
    true.)
0.5 CTLz        - Fractional location of hub height from the bottom of the
    dataset. [-] (Ignored when Randomize = true.)
30  CTStartTime     - Minimum start time for coherent structures in RootName.
    cts [seconds]

======================================================
! NOTE: Do not add or remove any lines in this file!
======================================================
```

Note regarding the input file above:

- This input file is for FAST.Farm simulations with `Mod_AmbWind`=3.
- `RandSeed1`, `IECturbc`, `URef` and `PLExp` are variables modified throughout the load calculation iterations.
- `NumGrid_Y` and `NumGrid_Z` are also variables conditioned on the mean wind speed according to the modelling guidelines in [95].

A.3.2 Input file for high-resolution wind files

```
--------TurbSim v2.00.* Input File------------------------
Custom TurbSim file written using openfast_toolbox library
---------Runtime Options-----------------------------------
False   Echo        - Echo input data to <RootName>.ech (flag)
199 RandSeed1       - First random seed  (-2147483648 to 2147483647)
```

```
"RanLux"    RandSeed2       - Second random seed (-2147483648 to 2147483647)
    for intrinsic pRNG, or an alternative pRNG: "RanLux" or "RNSNLW"
False   WrBHHTP     - Output hub-height turbulence parameters in binary form?
     (Generates RootName.bin)
False   WrFHHTP     - Output hub-height turbulence parameters in formatted
    form?  (Generates RootName.dat)
False   WrADHH      - Output hub-height time-series data in AeroDyn form?  (
    Generates RootName.hh)
True    WrADFF      - Output full-field time-series data in TurbSim/AeroDyn
    form? (Generates RootName.bts)
False   WrBLFF      - Output full-field time-series data in BLADED/AeroDyn
    form?  (Generates RootName.wnd)
False   WrADTWR     - Output tower time-series data? (Generates RootName.twr)
False   WrHAWCFF        - Output full-field time-series data in HAWC form?  (
    Generates RootName-u.bin, RootName-v.bin, RootName-w.bin, RootName.hawc)
False   WrFMTFF     - Output full-field time-series data in formatted (
    readable) form?  (Generates RootName.u, RootName.v, RootName.w)
False   WrACT       - Output coherent turbulence time steps in AeroDyn form? (
    Generates RootName.cts)
1   ScaleIEC        - Scale IEC turbulence models to exact target standard
    deviation? [0=no additional scaling; 1=use hub scale uniformly; 2=use
    individual scales]

--------Turbine/Model Specifications-----------------------
49  NumGrid_Z       - Vertical grid-point matrix dimension
45  NumGrid_Y       - Horizontal grid-point matrix dimension
0.5 TimeStep        - Time step [seconds]
700 AnalysisTime        - Length of analysis time series [seconds] (program
    will add time if necessary: AnalysisTime = MAX(AnalysisTime, UsableTime+
    GridWidth/MeanHHWS) )
"ALL"   UsableTime      - Usable length of output time series [seconds] (
    program will add GridWidth/MeanHHWS seconds unless UsableTime is "ALL")
157 HubHt       - Hub height [m] (should be > 0.5*GridHeight)
288 GridHeight      - Grid height [m]
264 GridWidth       - Grid width [m] (should be >= 2*(RotorRadius+ShaftLength)
    )
0   VFlowAng        - Vertical mean flow (uptilt) angle [degrees]
0   HFlowAng        - Horizontal mean flow (skew) angle [degrees]

--------Meteorological Boundary Conditions-------------------
"TIMESR"    TurbModel       - Turbulence model ("IECKAI","IECVKM","GP_LLJ","
    NWTCUP","SMOOTH","WF_UPW","WF_07D","WF_14D","TIDAL","API","USRINP","TIMESR
    ", or "NONE")
"USRTimeSeries.txt" UserFile        - Name of the file that contains inputs
    for user-defined spectra or time series inputs (used only for "IECKAI" and
     "TIMESR" models)
"1-ED3" IECstandard     - Number of IEC 61400-x standard (x=1,2, or 3 with
    optional 61400-1 edition number (i.e. "1-Ed2") )
17.700  IECturbc        - IEC turbulence characteristic ("A", "B", "C" or the
    turbulence intensity in percent) ("KHTEST" option with NWTCUP model, not
    used for other models)
"NTM"   IEC_WindType        - IEC turbulence type ("NTM"=normal, "xETM"=
    extreme turbulence, "xEWM1"=extreme 1-year wind, "xEWM50"=extreme 50-year
    wind, where x=wind turbine class 1, 2, or 3)
"default"   ETMc        - IEC Extreme Turbulence Model "c" parameter [m/s]
"PL"    WindProfileType     - Velocity profile type ("LOG";"PL"=power law;"JET
    ";"H2L"=Log law for TIDAL model;"API";"PL";"TS";"IEC"=PL on rotor disk,
    LOG elsewhere; or "default")
"unused"    ProfileFile     - Name of the file that contains input profiles
    for WindProfileType="USR" and/or TurbModel="USRVKM" [-]
150.000 RefHt       - Height of the reference velocity (URef) [m]
6.000   URef        - Mean (total) velocity at the reference height [m/s] (or
    "default" for JET velocity profile) [must be 1-hr mean for API model;
    otherwise is the mean over AnalysisTime seconds]
"default"   ZJetMax     - Jet height [m] (used only for JET velocity profile,
    valid 70-490 m)
```

```
0.070   PLExp       - Power law exponent [-] (or "default")
"default"   Z0      - Surface roughness length [m] (or "default")

--------Non-IEC Meteorological Boundary Conditions------------
"default"   Latitude        - Site latitude [degrees] (or "default")
0.05    RICH_NO     - Gradient Richardson number [-]
"default"   UStar       - Friction or shear velocity [m/s] (or "default")
"default"   ZI      - Mixing layer depth [m] (or "default")
"default"   PC_UW       - Hub mean u'w' Reynolds stress [m^2/s^2] (or "default
    " or "none")
"default"   PC_UV       - Hub mean u'v' Reynolds stress [m^2/s^2] (or "default
    " or "none")
"default"   PC_VW       - Hub mean v'w' Reynolds stress [m^2/s^2] (or "default
    " or "none")

--------Spatial Coherence Parameters----------------------------
"default"   SCMod1      - u-component coherence model ("GENERAL","IEC","API","
    NONE", or "default")
"default"   SCMod2      - v-component coherence model ("GENERAL","IEC","NONE",
     or "default")
"default"   SCMod3      - w-component coherence model ("GENERAL","IEC","NONE",
     or "default")
"default"   InCDec1 - u-component coherence parameters for general or IEC
    models [-, m^-1] (e.g. "10.0  0.3e-3" in quotes) (or "default")
"default"   InCDec2 - v-component coherence parameters for general or IEC
    models [-, m^-1] (e.g. "10.0  0.3e-3" in quotes) (or "default")
"default"   InCDec3 - w-component coherence parameters for general or IEC
    models [-, m^-1] (e.g. "10.0  0.3e-3" in quotes) (or "default")
"default"   CohExp      - Coherence exponent for general model [-] (or "
    default")

--------Coherent Turbulence Scaling Parameters-------------------
".\EventData"   CTEventPath     - Name of the path where event data files are
    located
"Random"    CTEventFile     - Type of event files ("LES", "DNS", or "RANDOM")
true    Randomize       - Randomize the disturbance scale and locations? (true
    /false)
1   DistScl     - Disturbance scale [-] (ratio of event dataset height to
    rotor disk). (Ignored when Randomize = true.)
0.5 CTLy        - Fractional location of tower centerline from right [-] (
    looking downwind) to left side of the dataset. (Ignored when Randomize =
    true.)
0.5 CTLz        - Fractional location of hub height from the bottom of the
    dataset. [-] (Ignored when Randomize = true.)
30  CTStartTime     - Minimum start time for coherent structures in RootName.
    cts [seconds]

=======================================================
! NOTE: Do not add or remove any lines in this file!
=======================================================
```

Note regarding the input file above:

- This input file is for FAST.Farm simulations with `Mod_AmbWind=3`.
- `RandSeed1`, `IECturbc`, `URef` and `PLExp` are variables modified throughout the load calculation iterations.
- `NumGrid_Y` and `NumGrid_Z` are also variables conditioned on the mean wind speed according to the modelling guidelines in [95].
- The user-defined file `USRTimeSeries.txt` is also dynamically generated based on the realized low resolution wind files according to the guidelines in [95].

A.4 List of seeds used for random number generators

```
    [508, 199, 889, 582, 162, 763, 899, 580, 356, 762, 328, 196]
```

B

HydroDyn Input File

```
------- HydroDyn v2.03.* Input File
    ------------------------------------------
IEA 15 MW offshore reference model monopile configuration
False            Echo           - Echo the input file data (flag)
---------------------- ENVIRONMENTAL CONDITIONS
    ---------------------------------
        "default"   WtrDens        - Water density (kg/m^3)
        "default"   WtrDpth        - Water depth (meters)
        "default"   MSL2SWL        - Offset between still-water level and mean
     sea level (meters) [positive upward; unused when WaveMod = 6; must be
    zero if PotMod=1 or 2]
---------------------- WAVES
    ------------------------------------------------
             2   WaveMod        - Incident wave kinematics model {0: none=
    still water, 1: regular (periodic), 1P#: regular with user-specified phase
    , 2: JONSWAP/Pierson-Moskowitz spectrum (irregular), 3: White noise
    spectrum (irregular), 4: user-defined spectrum from routine UserWaveSpctrm
     (irregular), 5: Externally generated wave-elevation time series, 6:
    Externally generated full wave-kinematics time series [option 6 is invalid
     for PotMod/=0]} (switch)
             0   WaveStMod      - Model for stretching incident wave kinematics
     to instantaneous free surface {0: none=no stretching, 1: vertical
    stretching, 2: extrapolation stretching, 3: Wheeler stretching} (switch) [
    unused when WaveMod=0 or when PotMod/=0]
          3630   WaveTMax       - Analysis time for incident wave calculations
     (sec) [unused when WaveMod=0; determines WaveDOmega=2Pi/WaveTMax in the
    IFFT]
          0.25   WaveDT         - Time step for incident wave calculations
     (sec) [unused when WaveMod=0; 0.1<=WaveDT<=1.0 recommended; determines
    WaveOmegaMax=Pi/WaveDT in the IFFT]
          4.52   WaveHs         - Significant wave height of incident waves (
    meters) [used only when WaveMod=1, 2, or 3]
          9.45   WaveTp         - Peak-spectral period of incident waves
     (sec) [used only when WaveMod=1 or 2]
"DEFAULT"        WavePkShp      - Peak-shape parameter of incident wave
    spectrum (-) or DEFAULT (string) [used only when WaveMod=2; use 1.0 for
    Pierson-Moskowitz]
       0.15708   WvLowCOff      - Low  cut-off frequency or lower frequency
    limit of the wave spectrum beyond which the wave spectrum is zeroed (rad/s
    ) [unused when WaveMod=0, 1, or 6]
           3.2   WvHiCOff       - High cut-off frequency or upper frequency
    limit of the wave spectrum beyond which the wave spectrum is zeroed (rad/s
    ) [unused when WaveMod=0, 1, or 6]
             0   WaveDir        - Incident wave propagation heading direction
                              (degrees) [unused when WaveMod=0 or 6]
             0   WaveDirMod     - Directional spreading function {0: none, 1:
    COS2S}                    (-)       [only used when WaveMod=2,3, or 4]
             1   WaveDirSpread  - Wave direction spreading coefficient ( > 0 )
                               (-)       [only used when WaveMod=2,3, or 4 and
```

```
    WaveDirMod=1]
              1   WaveNDir       - Number of wave directions
                            (-)       [only used when WaveMod=2,3, or 4 and
    WaveDirMod=1; odd number only]
             90   WaveDirRange   - Range of wave directions (full range:
    WaveDir +/- 1/2*WaveDirRange) (degrees) [only used when WaveMod=2,3,or 4
    and WaveDirMod=1]
      123456789   WaveSeed(1)    - First  random seed of incident waves
    [-2147483648 to 2147483647]    (-)       [unused when WaveMod=0, 5, or 6]
        RANLUX    WaveSeed(2)    - Second random seed of incident waves
    [-2147483648 to 2147483647]    (-)       [unused when WaveMod=0, 5, or 6]
TRUE              WaveNDAmp      - Flag for normally distributed amplitudes
                            (flag)    [only used when WaveMod=2, 3, or 4]
""                WvKinFile      - Root name of externally generated wave data
    file(s)         (quoted string)    [used only when WaveMod=5 or 6]
              1   NWaveElev      - Number of points where the incident wave
    elevations can be computed (-)       [maximum of 9 output locations]
              0   WaveElevxi     - List of xi-coordinates for points where the
    incident wave elevations can be output (meters) [NWaveElev points,
    separated by commas or white space; ususued if NWaveElev = 0]
              0   WaveElevyi     - List of yi-coordinates for points where the
    incident wave elevations can be output (meters) [NWaveElev points,
    separated by commas or white space; ususued if NWaveElev = 0]
---------------------- 2ND-ORDER WAVES
    ---------------------------------------- [unused with WaveMod=0 or 6]
False             WvDiffQTF      - Full difference-frequency 2nd-order wave
    kinematics (flag)
False             WvSumQTF       - Full summation-frequency  2nd-order wave
    kinematics (flag)
              0   WvLowCOffD     - Low  frequency cutoff used in the difference
    -frequencies (rad/s) [Only used with a difference-frequency method]
       3.04292    WvHiCOffD      - High frequency cutoff used in the difference
    -frequencies (rad/s) [Only used with a difference-frequency method]
      0.314159    WvLowCOffS     - Low  frequency cutoff used in the summation-
    frequencies  (rad/s) [Only used with a summation-frequency  method]
            3.2   WvHiCOffS      - High frequency cutoff used in the summation-
    frequencies  (rad/s) [Only used with a summation-frequency  method]
---------------------- CURRENT
    ------------------------------------------------- [unused with WaveMod=6]
              0   CurrMod        - Current profile model {0: none=no current,
    1: standard, 2: user-defined from routine UserCurrent} (switch)
              0   CurrSSV0       - Sub-surface current velocity at still water
    level  (m/s) [used only when CurrMod=1]
"DEFAULT"         CurrSSDir      - Sub-surface current heading direction (
    degrees) or DEFAULT (string) [used only when CurrMod=1]
             20   CurrNSRef      - Near-surface current reference depth
         (meters) [used only when CurrMod=1]
              0   CurrNSV0       - Near-surface current velocity at still water
     level (m/s) [used only when CurrMod=1]
              0   CurrNSDir      - Near-surface current heading direction
       (degrees) [used only when CurrMod=1]
              0   CurrDIV        - Depth-independent current velocity
            (m/s) [used only when CurrMod=1]
              0   CurrDIDir      - Depth-independent current heading direction
       (degrees) [used only when CurrMod=1]
---------------------- FLOATING PLATFORM
    ---------------------------------------- [unused with WaveMod=6]
              0   PotMod         - Potential-flow model {0: none=no potential
    flow, 1: frequency-to-time-domain transforms based on WAMIT output, 2:
    fluid-impulse theory (FIT)} (switch)
         0   ExctnMod       - Wave Excitation model {0: None, 1: DFT, 2: state
    -space} (switch) [only used when PotMod=1; STATE-SPACE REQUIRES *.ssexctn
    INPUT FILE]
         0   RdtnMod        - Radiation memory-effect model {0: no memory-
    effect calculation, 1: convolution, 2: state-space} (switch) [only used
    when PotMod=1; STATE-SPACE REQUIRES *.ss INPUT FILE]
```

```
      60.0  RdtnTMax       - Analysis time for wave radiation kernel
    calculations (sec) [only used when PotMod=1; determines RdtnDOmega=Pi/
    RdtnTMax in the cosine transform; MAKE SURE THIS IS LONG ENOUGH FOR THE
    RADIATION IMPULSE RESPONSE FUNCTIONS TO DECAY TO NEAR-ZERO FOR THE GIVEN
    PLATFORM!]
      0.0   RdtnDT         - Time step for wave radiation kernel calculations
     (sec) [only used when PotMod=1; DT<=RdtnDT<=0.1 recommended; determines
    RdtnOmegaMax=Pi/RdtnDT in the cosine transform]
        1   NBody          - Number of WAMIT bodies to be used (-) [>=1; only
     used when PotMod=1. If NBodyMod=1, the WAMIT data contains a vector of
    size 6*NBody x 1 and matrices of size 6*NBody x 6*NBody; if NBodyMod>1,
    there are NBody sets of WAMIT data each with a vector of size 6 x 1 and
    matrices of size 6 x 6]
        1   NBodyMod       - Body coupling model {1: include coupling terms
    between each body and NBody in HydroDyn equals NBODY in WAMIT, 2: neglect
    coupling terms between each body and NBODY=1 with XBODY=0 in WAMIT, 3:
    Neglect coupling terms between each body and NBODY=1 with XBODY=/0 in
    WAMIT} (switch) [only used when PotMod=1]
"unused"         PotFile        - Root name of potential-flow model data;
    WAMIT output files containing the linear, nondimensionalized, hydrostatic
    restoring matrix (.hst), frequency-dependent hydrodynamic added mass
    matrix and damping matrix (.1), and frequency- and direction-dependent
    wave excitation force vector per unit wave amplitude (.3) (quoted string)
    [MAKE SURE THE FREQUENCIES INHERENT IN THESE WAMIT FILES SPAN THE
    PHYSICALLY-SIGNIFICANT RANGE OF FREQUENCIES FOR THE GIVEN PLATFORM; THEY
    MUST CONTAIN THE ZERO- AND INFINITE-FREQUENCY LIMITS!]
          1   WAMITULEN      - Characteristic body length scale used to
    redimensionalize WAMIT output (meters) [only used when PotMod=1]
      0.0   PtfmRefxt        - The xt offset of the body reference point(s)
    from (0,0,0) (meters) [1 to NBody] [only used when PotMod=1]
      0.0   PtfmRefyt        - The yt offset of the body reference point(s)
    from (0,0,0) (meters) [1 to NBody] [only used when PotMod=1]
      0.0   PtfmRefzt        - The zt offset of the body reference point(s)
    from (0,0,0) (meters) [1 to NBody] [only used when PotMod=1. If NBodyMod
    =2,PtfmRefzt=0.0]
      0.0   PtfmRefztRot     - The rotation about zt of the body reference
    frame(s) from xt/yt (degrees) [1 to NBody] [only used when PotMod=1]
      0.0   PtfmVol0         - Displaced volume of water when the platform is
    in its undisplaced position (m^3) [only used when PotMod=1; USE THE SAME
    VALUE COMPUTED BY WAMIT AS OUTPUT IN THE .OUT FILE!]
        0.0   PtfmCOBxt       - The xt offset of the center of buoyancy (COB
    ) from the platform reference point (meters)  [only used when PotMod=1]
        0.0   PtfmCOByt       - The yt offset of the center of buoyancy (COB
    ) from the platform reference point (meters)  [only used when PotMod=1]
---------------------- 2ND-ORDER FLOATING PLATFORM FORCES
    ---------------------- [unused with WaveMod=0 or 6, or PotMod=0 or 2]
          0   MnDrift          - Mean-drift 2nd-order forces computed
                                   {0: None; [7, 8, 9, 10, 11, or 12]: WAMIT
    file to use} [Only one of MnDrift, NewmanApp, or DiffQTF can be non-zero]
          0   NewmanApp        - Mean- and slow-drift 2nd-order forces
    computed with Newman's approximation {0: None; [7, 8, 9, 10, 11, or 12]:
    WAMIT file to use} [Only one of MnDrift, NewmanApp, or DiffQTF can be non-
    zero. Used only when WaveDirMod=0]
          0   DiffQTF          - Full difference-frequency 2nd-order forces
    computed with full QTF          {0: None; [10, 11, or 12]: WAMIT file to
    use}          [Only one of MnDrift, NewmanApp, or DiffQTF can be non-zero]
          0   SumQTF           - Full summation -frequency 2nd-order forces
    computed with full QTF          {0: None; [10, 11, or 12]: WAMIT file to
    use}
---------------------- PLATFORM ADDITIONAL STIFFNESS AND DAMPING
    --------------
        0.0   AddF0     - Additional preload (N, N-m) [If NBodyMod=1, one
    size 6*NBody x 1 vector; if NBodyMod>1, NBody size 6 x 1 vectors]
        0.0
        0.0
        0.0
```

```
          0.0
          0.0
            0             0             0             0             0
        0   AddCLin  - Additional linear stiffness (N/m, N/rad, N-m/m, N-m/
    rad)
            0             0             0             0             0
        0
            0             0             0             0             0
        0
            0             0             0             0             0
        0
            0             0             0             0             0
        0
            0             0             0             0             0
        0   AddBLin  - Additional linear damping(N/(m/s), N/(rad/s), N-m/(m/s
    ), N-m/(rad/s))
            0             0             0             0             0
        0
            0             0       4389794.6           0             0
        0
            0             0             0             0             0
        0
            0             0             0             0             0
        0
            0             0             0             0             0
        0
            0             0             0             0             0
        0   AddBQuad - Additional quadratic drag(N/(m/s)^2, N/(rad/s)^2, N-m(
    m/s)^2, N-m/(rad/s)^2)
            0             0             0             0             0
        0
            0             0             0             0             0
        0
            0             0             0             0             0
        0
            0             0             0             0             0
        0
            0             0             0             0             0
        0
---------------------- AXIAL COEFFICIENTS
    -------------------------------------
            1   NAxCoef        - Number of axial coefficients (-)
AxCoefID  AxCd     AxCa     AxCp
   (-)    (-)      (-)      (-)
    1     0.00     0.00     1.00
---------------------- MEMBER JOINTS
    ------------------------------------------------
            2   NJoints        - Number of joints (-)   [must be exactly 0 or
     at least 2]
JointID   Jointxi     Jointyi     Jointzi  JointAxID   JointOvrlp   [
    JointOvrlp= 0: do nothing at joint, 1: eliminate overlaps by calculating
    super member]
   (-)     (m)         (m)         (m)        (-)       (switch)
   1      0.00000     0.00000   -30.1000       1            0
   2      0.00000     0.00000    15.0000       1            0
---------------------- MEMBER CROSS-SECTION PROPERTIES
    -------------------------
            1   NPropSets      - Number of member property sets (-)
PropSetID    PropD         PropThck
   (-)        (m)            (m)
   1        10.0            0.055341
---------------------- SIMPLE HYDRODYNAMIC COEFFICIENTS (model 1)
    --------------
```

```
  SimplCd     SimplCdMG     SimplCa     SimplCaMG     SimplCp     SimplCpMG
    SimplAxCd   SimplAxCdMG   SimplAxCa   SimplAxCaMG   SimplAxCp   SimplAxCpMG
    (-)         (-)         (-)         (-)         (-)         (-)
    (-)         (-)         (-)         (-)         (-)         (-)
    1.0         1.0         1.0         1.0         1.0         1.0
    0.0         0.0         1.0         1.0         1.0         1.0
---------------------- DEPTH-BASED HYDRODYNAMIC COEFFICIENTS (model 2)
    ---------
             0   NCoefDpth       - Number of depth-dependent coefficients (-)
   Dpth        DpthCd      DpthCdMG      DpthCa      DpthCaMG      DpthCp
    DpthCpMG     DpthAxCd    DpthAxCdMG    DpthAxCa    DpthAxCaMG    DpthAxCp
    DpthAxCpMG
    (m)         (-)         (-)         (-)         (-)         (-)
    (-)         (-)         (-)         (-)         (-)         (-)
    (-)
---------------------- MEMBER-BASED HYDRODYNAMIC COEFFICIENTS (model 3)
    --------
0           NCoefMembers - Number of member-based coefficients (-)
MemberID_HydC  MemberCd1   MemberCd2  MemberCdMG1 MemberCdMG2  MemberCa1
    MemberCa2  MemberCaMG1 MemberCaMG2  MemberCp1   MemberCp2  MemberCpMG1
    MemberCpMG2 MemberAxCd1 MemberAxCd2 MemberAxCdMG1 MemberAxCdMG2
    MemberAxCa1 MemberAxCa2 MemberAxCaMG1 MemberAxCaMG2 MemberAxCp1
    MemberAxCp2 MemberAxCpMG1 MemberAxCpMG2
    (-)         (-)         (-)         (-)         (-)         (-)
    (-)         (-)         (-)         (-)         (-)         (-)
    (-)         (-)         (-)         (-)         (-)         (-)
    (-)         (-)         (-)         (-)         (-)         (-)
    (-)
--------------------- MEMBERS -----------------------------------------------------
             1   NMembers        - Number of members (-)
MemberID  MJointID1  MJointID2  MPropSetID1  MPropSetID2  MDivSize   MCoefMod
     PropPot   [MCoefMod=1: use simple coeff table, 2: use depth-based coeff
    table, 3: use member-based coeff table] [ PropPot/=0 if member is modeled
    with potential-flow theory]
  (-)        (-)        (-)         (-)          (-)        (m)      (switch)
      (flag)
    1          1          2           1            1         0.5          1
         FALSE
---------------------- FILLED MEMBERS
    ------------------------------------------
             0   NFillGroups     - Number of filled member groups (-) [If
    FillDens = DEFAULT, then FillDens = WtrDens; FillFSLoc is related to
    MSL2SWL]
FillNumM FillMList             FillFSLoc     FillDens
(-)      (-)                   (m)           (kg/m^3)
---------------------- MARINE GROWTH
    ------------------------------------------
             0   NMGDepths       - Number of marine-growth depths specified (-)
MGDpth     MGThck       MGDens
(m)        (m)         (kg/m^3)
---------------------- MEMBER OUTPUT LIST
    --------------------------------------
             0   NMOutputs       - Number of member outputs (-) [must be < 10]
MemberID   NOutLoc    NodeLocs [NOutLoc < 10; node locations are normalized
    distance from the start of the member, and must be >=0 and <= 1] [unused
    if NMOutputs=0]
  (-)        (-)        (-)
---------------------- JOINT OUTPUT LIST
    ---------------------------------------
             2   NJOutputs       - Number of joint outputs [Must be < 10]
   1,2           JOutLst         - List of JointIDs which are to be output (-)[
    unused if NJOutputs=0]
---------------------- OUTPUT
    --------------------------------------------------
False            HDSum           - Output a summary file [flag]
```

```
False            OutAll         - Output all user-specified member and joint
    loads (only at each member end, not interior locations) [flag]
             2   OutSwtch       - Output requested channels to: [1=Hydrodyn.
    out, 2=GlueCode.out, 3=both files]
"ES11.4e2"       OutFmt         - Output format for numerical results (quoted
    string) [not checked for validity!]
"A11"            OutSFmt        - Output format for header strings (quoted
    string) [not checked for validity!]
---------------------- OUTPUT CHANNELS
    -------------------------------------------
END of output channels and end of file. (the word "END" must appear in the
    first 3 columns of this line)
```

Note that in the file above, `WaveHs` and `WaveTp` are variables specified as inputs conditioned on the mean wind speed according to Table 3.6.

C

IEA 15MW OpenFAST Model Input Files

The OpenFAST input files below were retrieved from the GitHub repository of IEA Wind Task 37 [94].

C.1 InflowWind

C.1.1 For Kaimal Wind Files:

```
------- InflowWind v3.01.* INPUT FILE
    ------------------------------------------------------------------------
IEA 15 MW Offshore Reference Turbine
---------------------------------------------------------------------------------------------------

False                   Echo        - Echo input data to <RootName>.ech (flag)
3                       WindType    - switch for wind file type (1=steady; 2=
    uniform; 3=binary TurbSim FF; 4=binary Bladed-style FF; 5=HAWC format; 6=
    User defined; 7=native Bladed FF)
0.0                     PropagationDir - Direction of wind propagation (
    meteoroligical rotation from aligned with X (positive rotates towards -Y)
    -- degrees)
0.0                     VFlowAng    - Upflow angle (degrees) (not used for
    native Bladed format WindType=7)
True                    VelInterpCubic - Use cubic interpolation for velocity
    in time (false=linear, true=cubic) [Used with WindType=2,3,4,5,7]
1                       NWindVel    - Number of points to output the wind
    velocity    (0 to 9)
0.0                     WindVxiList - List of coordinates in the inertial X
    direction (m)
0.0                     WindVyiList - List of coordinates in the inertial Y
    direction (m)
150.0                   WindVziList - List of coordinates in the inertial Z
    direction (m)
================== Parameters for Steady Wind Conditions [used only for
    WindType = 1] =========================
10.0                    HWindSpeed  - Horizontal windspeed
           (m/s)
150.0                   RefHt       - Reference height for horizontal wind
    speed      (m)
0.12                    PLexp       - Power law exponent
           (-)
================== Parameters for Uniform wind file   [used only for WindType
    = 2] ============================
"none"                  Filename_Uni - Filename of time series data for uniform
     wind field.      (-)
150.0                   RefHt_Uni   - Reference height for horizontal wind
    speed                 (m)
```

```
240.0                   RefLength   - Reference length for linear horizontal
    and vertical sheer (-)
================== Parameters for Binary TurbSim Full-Field files   [used only
     for WindType = 3] ==============
"none"                  FileName_BTS - Name of the Full field wind file to use
    (.bts)
================== Parameters for Binary Bladed-style Full-Field files   [used
     only for WindType = 4] =========
"none"                  FilenameRoot - Rootname of the full-field wind file to
    use (.wnd, .sum)
False                   TowerFile   - Have tower file (.twr) (flag)
================== Parameters for HAWC-format binary files  [Only used with
    WindType = 5] ====================
"none"                  FileName_u  - name of the file containing the u-
    component fluctuating wind (.bin)
"none"                  FileName_v  - name of the file containing the v-
    component fluctuating wind (.bin)
"none"                  FileName_w  - name of the file containing the w-
    component fluctuating wind (.bin)
64                      nx          - number of grids in the x direction (in
    the 3 files above) (-)
32                      ny          - number of grids in the y direction (in
    the 3 files above) (-)
32                      nz          - number of grids in the z direction (in
    the 3 files above) (-)
16.0                    dx          - distance (in meters) between points in
    the x direction    (m)
3.0                     dy          - distance (in meters) between points in
    the y direction    (m)
3.0                     dz          - distance (in meters) between points in
    the z direction    (m)
150.0                   RefHt_Hawc  - reference height; the height (in meters)
    of the vertical center of the grid (m)
-------------   Scaling parameters for turbulence
    ---------------------------------------------------------
2                       ScaleMethod - Turbulence scaling method   [0 = none, 1
    = direct scaling, 2 = calculate scaling factor based on a desired standard
     deviation]
1.0                     SFx         - Turbulence scaling factor for the x
    direction (-)   [ScaleMethod=1]
1.0                     SFy         - Turbulence scaling factor for the y
    direction (-)   [ScaleMethod=1]
1.0                     SFz         - Turbulence scaling factor for the z
    direction (-)   [ScaleMethod=1]
1.2                     SigmaFx     - Turbulence standard deviation to
    calculate scaling from in x direction (m/s)    [ScaleMethod=2]
0.8                     SigmaFy     - Turbulence standard deviation to
    calculate scaling from in y direction (m/s)    [ScaleMethod=2]
0.2                     SigmaFz     - Turbulence standard deviation to
    calculate scaling from in z direction (m/s)    [ScaleMethod=2]
-------------   Mean wind profile parameters (added to HAWC-format files)
    ----------------------------------
12.0                    URef        - Mean u-component wind speed at the
    reference height (m/s)
2                       WindProfile - Wind profile type (0=constant;1=
    logarithmic,2=power law)
0.2                     PLExp_Hawc  - Power law exponent (-) (used for PL wind
    profile type only)
0.03                    Z0          - Surface roughness length (m) (used for LG
     wind profile type only)
0                       XOffset     - Initial offset in +x direction (shift of
    wind box) (-)
================== LIDAR Parameters
    ================================================================================
```

```
0                       SensorType          - Switch for lidar configuration (0
     = None, 1 = Single Point Beam(s), 2 = Continuous, 3 = Pulsed)
0                       NumPulseGate        - Number of lidar measurement gates
     (used when SensorType = 3)
30                      PulseSpacing        - Distance between range gates (m)
    (used when SensorType = 3)
0                       NumBeam             - Number of lidar measurement beams
     (0-5)(used when SensorType = 1)
-200                    FocalDistanceX      - Focal distance co-ordinates of
    the lidar beam in the x direction (relative to hub height) (only first
    coordinate used for SensorType 2 and 3) (m)
0                       FocalDistanceY      - Focal distance co-ordinates of
    the lidar beam in the y direction (relative to hub height) (only first
    coordinate used for SensorType 2 and 3) (m)
0                       FocalDistanceZ      - Focal distance co-ordinates of
    the lidar beam in the z direction (relative to hub height) (only first
    coordinate used for SensorType 2 and 3) (m)
0.0 0.0 0.0             RotorApexOffsetPos  - Offset of the lidar from hub
    height (m)
17                      URefLid             - Reference average wind speed for
    the lidar[m/s]
0.25                    MeasurementInterval - Time between each measurement [s]
False                   LidRadialVel        - TRUE => return radial component,
    FALSE => return 'x' direction estimate
1                       ConsiderHubMotion   - Flag whether to consider the hub
    motion's impact on Lidar measurements
====================== OUTPUT
    ==================================================
False                   SumPrint    - Print summary data to <RootName>.IfW.sum
    (flag)
OutList      - The next line(s) contains a list of output parameters.  See
    OutListParameters.xlsx for a listing of available output channels, (-)
Wind1VelX
Wind1VelY
Wind1VelZ
END of input file (the word "END" must appear in the first 3 columns of this
    last OutList line)
---------------------------------------------------------------------------------------
```

C.1.2 For Mann Wind Files:

```
------- InflowWind v3.01.* INPUT FILE
    ------------------------------------------------------------------------
IEA 15 MW Offshore Reference Turbine
---------------------------------------------------------------------------------------------------

False                   Echo        - Echo input data to <RootName>.ech (flag)
7                       WindType    - switch for wind file type (1=steady; 2=
    uniform; 3=binary TurbSim FF; 4=binary Bladed-style FF; 5=HAWC format; 6=
    User defined; 7=native Bladed FF)
0.0                     PropagationDir - Direction of wind propagation (
    meteoroligical rotation from aligned with X (positive rotates towards -Y)
    -- degrees)
0.0                     VFlowAng    - Upflow angle (degrees) (not used for
    native Bladed format WindType=7)
True                    VelInterpCubic - Use cubic interpolation for velocity
    in time (false=linear, true=cubic) [Used with WindType=2,3,4,5,7]
1                       NWindVel    - Number of points to output the wind
    velocity    (0 to 9)
0.0                     WindVxiList - List of coordinates in the inertial X
    direction (m)
0.0                     WindVyiList - List of coordinates in the inertial Y
    direction (m)
```

```
150.0                   WindVziList - List of coordinates in the inertial Z
    direction (m)
================== Parameters for Steady Wind Conditions [used only for
    WindType = 1] ========================
10.0                    HWindSpeed  - Horizontal windspeed
          (m/s)
150.0                   RefHt       - Reference height for horizontal wind
    speed      (m)
0.12                    PLexp       - Power law exponent
          (-)
================== Parameters for Uniform wind file   [used only for WindType
    = 2] ============================
"none"                  Filename_Uni - Filename of time series data for uniform
     wind field.      (-)
150.0                   RefHt_Uni   - Reference height for horizontal wind
    speed                 (m)
240.0                   RefLength   - Reference length for linear horizontal
    and vertical sheer (-)
================== Parameters for Binary TurbSim Full-Field files   [used only
     for WindType = 3] ==============
"none"                  FileName_BTS - Name of the Full field wind file to use
    (.bts)
================== Parameters for Binary Bladed-style Full-Field files   [used
     only for WindType = 4] =========
"BladedScaling.dat"                FilenameRoot - Rootname of the full-field
    wind file to use (.wnd, .sum)
False                   TowerFile   - Have tower file (.twr) (flag)
================== Parameters for HAWC-format binary files  [Only used with
    WindType = 5] ====================
"none"                  FileName_u  - name of the file containing the u-
    component fluctuating wind (.bin)
"none"                  FileName_v  - name of the file containing the v-
    component fluctuating wind (.bin)
"none"                  FileName_w  - name of the file containing the w-
    component fluctuating wind (.bin)
64                      nx          - number of grids in the x direction (in
    the 3 files above) (-)
32                      ny          - number of grids in the y direction (in
    the 3 files above) (-)
32                      nz          - number of grids in the z direction (in
    the 3 files above) (-)
16.0                    dx          - distance (in meters) between points in
    the x direction    (m)
3.0                     dy          - distance (in meters) between points in
    the y direction    (m)
3.0                     dz          - distance (in meters) between points in
    the z direction    (m)
150.0                   RefHt_Hawc  - reference height; the height (in meters)
    of the vertical center of the grid (m)
-------------   Scaling parameters for turbulence
    ---------------------------------------------------------
2                       ScaleMethod - Turbulence scaling method   [0 = none, 1
    = direct scaling, 2 = calculate scaling factor based on a desired standard
     deviation]
1.0                     SFx         - Turbulence scaling factor for the x
    direction (-)   [ScaleMethod=1]
1.0                     SFy         - Turbulence scaling factor for the y
    direction (-)   [ScaleMethod=1]
1.0                     SFz         - Turbulence scaling factor for the z
    direction (-)   [ScaleMethod=1]
1.2                     SigmaFx     - Turbulence standard deviation to
    calculate scaling from in x direction (m/s)    [ScaleMethod=2]
0.8                     SigmaFy     - Turbulence standard deviation to
    calculate scaling from in y direction (m/s)    [ScaleMethod=2]
0.2                     SigmaFz     - Turbulence standard deviation to
    calculate scaling from in z direction (m/s)    [ScaleMethod=2]
```

```
-------------   Mean wind profile parameters (added to HAWC-format files)
    ---------------------------------
12.0                    URef        - Mean u-component wind speed at the
    reference height (m/s)
2                       WindProfile - Wind profile type (0=constant;1=
    logarithmic,2=power law)
0.2                     PLExp_Hawc  - Power law exponent (-) (used for PL wind
    profile type only)
0.03                    Z0          - Surface roughness length (m) (used for LG
     wind profile type only)
0                       XOffset     - Initial offset in +x direction (shift of
    wind box) (-)
================== LIDAR Parameters
    ================================================================================

0                       SensorType          - Switch for lidar configuration (0
     = None, 1 = Single Point Beam(s), 2 = Continuous, 3 = Pulsed)
0                       NumPulseGate        - Number of lidar measurement gates
     (used when SensorType = 3)
30                      PulseSpacing        - Distance between range gates (m)
    (used when SensorType = 3)
0                       NumBeam             - Number of lidar measurement beams
     (0-5)(used when SensorType = 1)
-200                    FocalDistanceX      - Focal distance co-ordinates of
    the lidar beam in the x direction (relative to hub height) (only first
    coordinate used for SensorType 2 and 3) (m)
0                       FocalDistanceY      - Focal distance     co-ordinates
    of the lidar beam in the y direction (relative to hub height) (only first
    coordinate used for SensorType 2 and 3) (m)
0                       FocalDistanceZ      - Focal distance co-ordinates of
    the lidar beam in the z direction (relative to hub height) (only first
    coordinate used for SensorType 2 and 3) (m)
0.0 0.0 0.0             RotorApexOffsetPos  - Offset of the lidar from hub
    height (m)
17                      URefLid             - Reference average wind speed for
    the lidar[m/s]
0.25                    MeasurementInterval - Time between each measurement [s]
False                   LidRadialVel        - TRUE => return radial component,
    FALSE => return 'x' direction estimate
1                       ConsiderHubMotion   - Flag whether to consider the hub
    motion's impact on Lidar measurements
====================== OUTPUT
    ==================================================
False                   SumPrint    - Print summary data to <RootName>.IfW.sum
    (flag)
OutList      - The next line(s) contains a list of output parameters.  See
    OutListParameters.xlsx for a listing of available output channels, (-)
Wind1VelX
Wind1VelY
Wind1VelZ
END of input file (the word "END" must appear in the first 3 columns of this
    last OutList line)
---------------------------------------------------------------------------------------
```

C.1.3 Scaling File for Mann Wind Fields:

```
UBAR  24
REFHT  150
TI  0.062157297618006604
TI_V  0.04351010833260462
TI_W  0.031078648809003302
WDIR  0
FLINC  0
```

```
WINDF  "path_to_Bladed_Mann_wind_file"
WSHEAR  0.1
XOFFSET  0
```

C.2 AeroDyn

```
------- AERODYN v15.03.* INPUT FILE
    ------------------------------------------------
IEA 15 MW Offshore Reference Turbine
======  General Options
    ================================================================================

False                   Echo        - Echo the input to "<rootname>.AD.ech"?  (
    flag)
default                 DTAero      - Time interval for aerodynamic
    calculations {or "default"} (s)
1                       WakeMod     - Type of wake/induction model (switch) {0=
    none, 1=BEMT, 2=DBEMT, 3=OLAF} [WakeMod cannot be 2 or 3 when linearizing]
2                       AFAeroMod   - Type of blade airfoil aerodynamics model
    (switch) {1=steady model, 2=Beddoes-Leishman unsteady model} [AFAeroMod
    must be 1 when linearizing]
1                       TwrPotent   - Type tower influence on wind based on
    potential flow around the tower (switch) {0=none, 1=baseline potential
    flow, 2=potential flow with Bak correction}
1                       TwrShadow   - Calculate tower influence on wind based
    on downstream tower shadow (switch) {0=none, 1=Powles model, 2=Eames model
    }
True                    TwrAero     - Calculate tower aerodynamic loads? (flag)
False                   FrozenWake  - Assume frozen wake during linearization?
    (flag) [used only when WakeMod=1 and when linearizing]
False                   CavitCheck  - Perform cavitation check? (flag) [
    AFAeroMod must be 1 when CavitCheck=true]
False                   Buoyancy    - Include buoyancy effects? (flag)
False                   CompAA      - Flag to compute AeroAcoustics calculation
     [only used when WakeMod=1 or 2]
AeroAcousticsInput.dat AA_InputFile - AeroAcoustics input file [used only when
     CompAA=true]
======  Environmental Conditions
    ================================================================
"default"               AirDens     - Air density (kg/m^3)
"default"               KinVisc     - Kinematic air viscosity (m^2/s)
"default"               SpdSound    - Speed of sound (m/s)
"default"               Patm        - Atmospheric pressure (Pa) [used only when
     CavitCheck=True]
"default"               Pvap        - Vapour pressure of fluid (Pa) [used only
    when CavitCheck=True]
======  Blade-Element/Momentum Theory Options
    ========================================================= [used only when
    WakeMod=1]
2                       SkewMod     - Type of skewed-wake correction model (
    switch) {1=uncoupled, 2=Pitt/Peters, 3=coupled} [unused when WakeMod=0 or
    3]
default                 SkewModFactor - Constant used in Pitt/Peters skewed
    wake model {or "default" is 15/32*pi} (-) [used only when SkewMod=2;
    unused when WakeMod=0 or 3]
True                    TipLoss     - Use the Prandtl tip-loss model? (flag) [
    unused when WakeMod=0 or 3]
True                    HubLoss     - Use the Prandtl hub-loss model? (flag) [
    unused when WakeMod=0 or 3]
True                    TanInd      - Include tangential induction in BEMT
    calculations? (flag) [unused when WakeMod=0 or 3]
True                    AIDrag      - Include the drag term in the axial-
    induction calculation? (flag) [unused when WakeMod=0 or 3]
```

```
True                    TIDrag      - Include the drag term in the tangential-
    induction calculation? (flag) [unused when WakeMod=0,3 or TanInd=FALSE]
default                 IndToler    - Convergence tolerance for BEMT nonlinear
    solve residual equation {or "default"} (-) [unused when WakeMod=0 or 3]
500                     MaxIter     - Maximum number of iteration steps (-) [
    unused when WakeMod=0]
======  Dynamic Blade-Element/Momentum Theory Options
    ==================================================== [used only when
    WakeMod=1]
2                       DBEMT_Mod   - Type of dynamic BEMT (DBEMT) model {1=
    constant tau1, 2=time-dependent tau1} (-) [used only when WakeMod=2]
29.03                   tau1_const  - Time constant for DBEMT (s) [used only
    when WakeMod=2 and DBEMT_Mod=1]
======  OLAF -- cOnvecting LAgrangian Filaments (Free Vortex Wake) Theory
    Options  ================== [used only when WakeMod=3]
../IEA-15-240-RWT-OLAF/IEA-15-240-RWT_OLAF.dat OLAFInputFileName - Input file
    for OLAF [used only when WakeMod=3]
======  Beddoes-Leishman Unsteady Airfoil Aerodynamics Options
    ==================================== [used only when AFAeroMod=2]
3                       UAMod       - Unsteady Aero Model Switch (switch) {1=
    Baseline model (Original), 2=Gonzalez's variant (changes in Cn,Cc,Cm), 3=
    Minnema/Pierce variant (changes in Cc and Cm)} [used only when AFAeroMod
    =2]
True                    FLookup     - Flag to indicate whether a lookup for f'
    will be calculated (TRUE) or whether best-fit exponential equations will
    be used (FALSE); if FALSE S1-S4 must be provided in airfoil input files (
    flag) [used only when AFAeroMod=2]
0.1                     UAStartRad  - Starting radius for dynamic stall (
    fraction of rotor radius) [used only when AFAeroMod=2]
1.0                     UAEndRad    - Ending radius for dynamic stall (fraction
     of rotor radius) [used only when AFAeroMod=2]
======  Airfoil Information
    ==========================================================================
1                       AFTabMod    - Interpolation method for multiple airfoil
     tables {1=1D interpolation on AoA (first table only); 2=2D interpolation
    on AoA and Re; 3=2D interpolation on AoA and UserProp} (-)
1                       InCol_Alfa  - The column in the airfoil tables that
    contains the angle of attack (-)
2                       InCol_Cl    - The column in the airfoil tables that
    contains the lift coefficient (-)
3                       InCol_Cd    - The column in the airfoil tables that
    contains the drag coefficient (-)
4                       InCol_Cm    - The column in the airfoil tables that
    contains the pitching-moment coefficient; use zero if there is no Cm
    column (-)
0                       InCol_Cpmin - The column in the airfoil tables that
    contains the Cpmin coefficient; use zero if there is no Cpmin column (-)
50                      NumAFfiles  - Number of airfoil files used (-)
"Airfoils/IEA-15-240-RWT_AeroDyn15_Polar_00.dat"    AFNames             -
    Airfoil file names (NumAFfiles lines) (quoted strings)
"Airfoils/IEA-15-240-RWT_AeroDyn15_Polar_01.dat"
"Airfoils/IEA-15-240-RWT_AeroDyn15_Polar_02.dat"
"Airfoils/IEA-15-240-RWT_AeroDyn15_Polar_03.dat"
"Airfoils/IEA-15-240-RWT_AeroDyn15_Polar_04.dat"
"Airfoils/IEA-15-240-RWT_AeroDyn15_Polar_05.dat"
"Airfoils/IEA-15-240-RWT_AeroDyn15_Polar_06.dat"
"Airfoils/IEA-15-240-RWT_AeroDyn15_Polar_07.dat"
"Airfoils/IEA-15-240-RWT_AeroDyn15_Polar_08.dat"
"Airfoils/IEA-15-240-RWT_AeroDyn15_Polar_09.dat"
"Airfoils/IEA-15-240-RWT_AeroDyn15_Polar_10.dat"
"Airfoils/IEA-15-240-RWT_AeroDyn15_Polar_11.dat"
"Airfoils/IEA-15-240-RWT_AeroDyn15_Polar_12.dat"
"Airfoils/IEA-15-240-RWT_AeroDyn15_Polar_13.dat"
"Airfoils/IEA-15-240-RWT_AeroDyn15_Polar_14.dat"
"Airfoils/IEA-15-240-RWT_AeroDyn15_Polar_15.dat"
"Airfoils/IEA-15-240-RWT_AeroDyn15_Polar_16.dat"
```

```
"Airfoils/IEA-15-240-RWT_AeroDyn15_Polar_17.dat"
"Airfoils/IEA-15-240-RWT_AeroDyn15_Polar_18.dat"
"Airfoils/IEA-15-240-RWT_AeroDyn15_Polar_19.dat"
"Airfoils/IEA-15-240-RWT_AeroDyn15_Polar_20.dat"
"Airfoils/IEA-15-240-RWT_AeroDyn15_Polar_21.dat"
"Airfoils/IEA-15-240-RWT_AeroDyn15_Polar_22.dat"
"Airfoils/IEA-15-240-RWT_AeroDyn15_Polar_23.dat"
"Airfoils/IEA-15-240-RWT_AeroDyn15_Polar_24.dat"
"Airfoils/IEA-15-240-RWT_AeroDyn15_Polar_25.dat"
"Airfoils/IEA-15-240-RWT_AeroDyn15_Polar_26.dat"
"Airfoils/IEA-15-240-RWT_AeroDyn15_Polar_27.dat"
"Airfoils/IEA-15-240-RWT_AeroDyn15_Polar_28.dat"
"Airfoils/IEA-15-240-RWT_AeroDyn15_Polar_29.dat"
"Airfoils/IEA-15-240-RWT_AeroDyn15_Polar_30.dat"
"Airfoils/IEA-15-240-RWT_AeroDyn15_Polar_31.dat"
"Airfoils/IEA-15-240-RWT_AeroDyn15_Polar_32.dat"
"Airfoils/IEA-15-240-RWT_AeroDyn15_Polar_33.dat"
"Airfoils/IEA-15-240-RWT_AeroDyn15_Polar_34.dat"
"Airfoils/IEA-15-240-RWT_AeroDyn15_Polar_35.dat"
"Airfoils/IEA-15-240-RWT_AeroDyn15_Polar_36.dat"
"Airfoils/IEA-15-240-RWT_AeroDyn15_Polar_37.dat"
"Airfoils/IEA-15-240-RWT_AeroDyn15_Polar_38.dat"
"Airfoils/IEA-15-240-RWT_AeroDyn15_Polar_39.dat"
"Airfoils/IEA-15-240-RWT_AeroDyn15_Polar_40.dat"
"Airfoils/IEA-15-240-RWT_AeroDyn15_Polar_41.dat"
"Airfoils/IEA-15-240-RWT_AeroDyn15_Polar_42.dat"
"Airfoils/IEA-15-240-RWT_AeroDyn15_Polar_43.dat"
"Airfoils/IEA-15-240-RWT_AeroDyn15_Polar_44.dat"
"Airfoils/IEA-15-240-RWT_AeroDyn15_Polar_45.dat"
"Airfoils/IEA-15-240-RWT_AeroDyn15_Polar_46.dat"
"Airfoils/IEA-15-240-RWT_AeroDyn15_Polar_47.dat"
"Airfoils/IEA-15-240-RWT_AeroDyn15_Polar_48.dat"
"Airfoils/IEA-15-240-RWT_AeroDyn15_Polar_49.dat"
======  Rotor/Blade Properties
    ====================================================================
True                    UseBlCm     - Include aerodynamic pitching moment in
    calculations?  (flag)
"IEA-15-240-RWT_AeroDyn15_blade.dat" ADBlFile(1) - Name of file containing
    distributed aerodynamic properties for Blade #1 (-)
"IEA-15-240-RWT_AeroDyn15_blade.dat" ADBlFile(2) - Name of file containing
    distributed aerodynamic properties for Blade #2 (-) [unused if NumBl < 2]
"IEA-15-240-RWT_AeroDyn15_blade.dat" ADBlFile(3) - Name of file containing
    distributed aerodynamic properties for Blade #3 (-) [unused if NumBl < 3]
======  Hub Properties
    ================================================================================
     [used only when Buoyancy=True]
0.0   VolHub             - Hub volume (m^3)
0.0   HubCenBx           - Hub center of buoyancy x direction offset (m)
======  Nacelle Properties
    ================================================================================
     [used only when Buoyancy=True]
0.0   VolNac             - Nacelle volume (m^3)
0,0,0 NacCenB            - Position of nacelle center of buoyancy from yaw
    bearing in nacelle coordinates (m)
======  Tail fin Aerodynamics
    ====================================================================
False         TFinAero          - Calculate tail fin aerodynamics model (flag
    )
"unused"      TFinFile          - Input file for tail fin aerodynamics [used
    only when TFinAero=True]
======  Tower Influence and Aerodynamics
    ========================================================== [used only
    when TwrPotent/=0, TwrShadow/=0, or TwrAero=True]
20                      NumTwrNds   - Number of tower nodes used in the
    analysis  (-) [used only when TwrPotent/=0, TwrShadow/=0, or TwrAero=True]
```

```
TwrElev        TwrDiam        TwrCd         TwrTI      TwrCb !TwrTI used only
    with TwrShadow=2, TwrCb used only with Buoyancy=True
(m)              (m)           (-)           (-)        (-)
  15.000        10.000         0.5           0.1        0.0
  28.000        10.000         0.5           0.1        0.0
  28.001        10.000         0.5           0.1        0.0
  41.000         9.926         0.5           0.1        0.0
  41.001         9.926         0.5           0.1        0.0
  54.000         9.443         0.5           0.1        0.0
  54.001         9.443         0.5           0.1        0.0
  67.000         8.833         0.5           0.1        0.0
  67.001         8.833         0.5           0.1        0.0
  80.000         8.151         0.5           0.1        0.0
  80.001         8.151         0.5           0.1        0.0
  93.000         7.390         0.5           0.1        0.0
  93.001         7.390         0.5           0.1        0.0
 106.000         6.909         0.5           0.1        0.0
 106.001         6.909         0.5           0.1        0.0
 119.000         6.748         0.5           0.1        0.0
 119.001         6.748         0.5           0.1        0.0
 132.000         6.572         0.5           0.1        0.0
 132.001         6.572         0.5           0.1        0.0
 144.386         6.500         0.5           0.1        0.0
======  Outputs
    ======================================================================================

False                   SumPrint    - Generate a summary file listing input
    options and interpolated properties to "<rootname>.AD.sum"?  (flag)
9                       NBlOuts     - Number of blade node outputs [0 - 9] (-)
6, 11, 16, 21, 25, 30, 35, 40, 45 BlOutNd     - Blade nodes whose values will
    be output  (-)
0                       NTwOuts     - Number of tower node outputs [0 - 9]  (-)
0                       TwOutNd     - Tower nodes whose values will be output
    (-)
                    OutList             - The next line(s) contains a list of
    output parameters.  See OutListParameters.xlsx for a listing of available
    output channels, (-)
"RtTSR"
END of input file (the word "END" must appear in the first 3 columns of this
    last OutList line)
====== Outputs for all blade stations (same ending as above for B1N1....
    ========================== [optional section]
   1              BldNd_BladesOut     - Number of blades to output all node
    information at.  Up to number of blades on turbine. (-)
   "All"          BldNd_BlOutNd       - Future feature will allow selecting a
    portion of the nodes to output.  Not implemented yet. (-)
                   OutList             - The next line(s) contains a list of
    output parameters.  See OutListParameters.xlsx for a listing of available
    output channels, (-)
END (the word "END" must appear in the first 3 columns of this last OutList
    line in the optional nodal output section)
```

C.3 ElastoDyn

```
------- ELASTODYN v1.03.* INPUT FILE
    ------------------------------------------
IEA 15 MW offshore reference model monopile configuration
---------------------- SIMULATION CONTROL
    ---------------------------------------
False                   Echo        - Echo input data to "<RootName>.ech" (flag
    )
3                       Method      - Integration method: {1: RK4, 2: AB4, or
    3: ABM4} (-)
```

```
"default"               DT          Integration time step (s)
---------------------- DEGREES OF FREEDOM
    ---------------------------------------
True                    FlapDOF1    - First flapwise blade mode DOF (flag)
True                    FlapDOF2    - Second flapwise blade mode DOF (flag)
True                    EdgeDOF     - First edgewise blade mode DOF (flag)
False                   TeetDOF     - Rotor-teeter DOF (flag) [unused for 3
    blades]
False                   DrTrDOF     - Drivetrain rotational-flexibility DOF (
    flag)
True                    GenDOF      - Generator DOF (flag)
True                    YawDOF      - Yaw DOF (flag)
True                    TwFADOF1    - First fore-aft tower bending-mode DOF (
    flag)
True                    TwFADOF2    - Second fore-aft tower bending-mode DOF (
    flag)
True                    TwSSDOF1    - First side-to-side tower bending-mode DOF
     (flag)
True                    TwSSDOF2    - Second side-to-side tower bending-mode
    DOF (flag)
True                    PtfmSgDOF   - Platform horizontal surge translation DOF
     (flag)
True                    PtfmSwDOF   - Platform horizontal sway translation DOF
    (flag)
True                    PtfmHvDOF   - Platform vertical heave translation DOF (
    flag)
True                    PtfmRDOF    - Platform roll tilt rotation DOF (flag)
True                    PtfmPDOF    - Platform pitch tilt rotation DOF (flag)
True                    PtfmYDOF    - Platform yaw rotation DOF (flag)
---------------------- INITIAL CONDITIONS
    ---------------------------------------
0.0                     OoPDefl     - Initial out-of-plane blade-tip
    displacement (meters)
0.0                     IPDefl      - Initial in-plane blade-tip deflection (
    meters)
11.6                     BlPitch(1)  - Blade 1 initial pitch (degrees)
11.6                     BlPitch(2)  - Blade 2 initial pitch (degrees)
11.6                     BlPitch(3)  - Blade 3 initial pitch (degrees) [unused
    for 2 blades]
0.0                     TeetDefl    - Initial or fixed teeter angle (degrees) [
    unused for 3 blades]
0.0                     Azimuth     - Initial azimuth angle for blade 1 (
    degrees)
7.55                    RotSpeed    - Initial or fixed rotor speed (rpm)
0.0                     NacYaw      - Initial or fixed nacelle-yaw angle (
    degrees)
0.0                     TTDspFA     - Initial fore-aft tower-top displacement (
    meters)
0.0                     TTDspSS     - Initial side-to-side tower-top
    displacement (meters)
0.0                     PtfmSurge   - Initial or fixed horizontal surge
    translational displacement of platform (meters)
0.0                     PtfmSway    - Initial or fixed horizontal sway
    translational displacement of platform (meters)
0.0                     PtfmHeave   - Initial or fixed vertical heave
    translational displacement of platform (meters)
0.0                     PtfmRoll    - Initial or fixed roll tilt rotational
    displacement of platform (degrees)
0.0                     PtfmPitch   - Initial or fixed pitch tilt rotational
    displacement of platform (degrees)
0.0                     PtfmYaw     - Initial or fixed yaw rotational
    displacement of platform (degrees)
---------------------- TURBINE CONFIGURATION
    ------------------------------------
3                       NumBl       - Number of blades (-)
```

```
120.97                  TipRad      - The distance from the rotor apex to the
    blade tip (meters)
3.97                    HubRad      - The distance from the rotor apex to the
    blade root (meters)
-4.0                    PreCone(1)  - Blade 1 cone angle (degrees)
-4.0                    PreCone(2)  - Blade 2 cone angle (degrees)
-4.0                    PreCone(3)  - Blade 3 cone angle (degrees) [unused for
    2 blades]
0.0                     HubCM       - Distance from rotor apex to hub mass [
    positive downwind] (meters)
0.0                     UndSling    - Undersling length [distance from teeter
    pin to the rotor apex] (meters) [unused for 3 blades]
0.0                     Delta3      - Delta-3 angle for teetering rotors (
    degrees) [unused for 3 blades]
0.0                     AzimB1Up    - Azimuth value to use for I/O when blade 1
     points up (degrees)
-12.097571763912535     OverHang    - Distance from yaw axis to rotor apex [3
    blades] or teeter pin [2 blades] (meters)
0.0                     ShftGagL    - Distance from rotor apex [3 blades] or
    teeter pin [2 blades] to shaft strain gages [positive for upwind rotors] (
    meters)
-6.0                    ShftTilt    - Rotor shaft tilt angle (degrees)
-5.125                  NacCMxn     - Downwind distance from the tower-top to
    the nacelle CM (meters)
0.0                     NacCMyn     - Lateral  distance from the tower-top to
    the nacelle CM (meters)
4.315                   NacCMzn     - Vertical distance from the tower-top to
    the nacelle CM (meters)
0.0                     NcIMUxn     - Downwind distance from the tower-top to
    the nacelle IMU (meters)
0.0                     NcIMUyn     - Lateral  distance from the tower-top to
    the nacelle IMU (meters)
0.0                     NcIMUzn     - Vertical distance from the tower-top to
    the nacelle IMU (meters)
4.349459414248071       Twr2Shft    - Vertical distance from the tower-top to
    the rotor shaft (meters)
144.386                 TowerHt     - Height of tower above ground level [
    onshore] or MSL [offshore] (meters)
15.                     TowerBsHt   - Height of tower base above ground level [
    onshore] or MSL [offshore] (meters)
0.0                     PtfmCMxt    - Downwind distance from the ground level [
    onshore] or MSL [offshore] to the platform CM (meters)
0.0                     PtfmCMyt    - Lateral distance from the ground level [
    onshore] or MSL [offshore] to the platform CM (meters)
15.                     PtfmCMzt    - Vertical distance from the ground level [
    onshore] or MSL [offshore] to the platform CM (meters)
15.                     PtfmRefzt   - Vertical distance from the ground level [
    onshore] or MSL [offshore] to the platform reference point (meters)
---------------------- MASS AND INERTIA
    -------------------------------------------
0.0                     TipMass(1)  - Tip-brake mass, blade 1 (kg)
0.0                     TipMass(2)  - Tip-brake mass, blade 2 (kg)
0.0                     TipMass(3)  - Tip-brake mass, blade 3 (kg) [unused for
    2 blades]
69131                   HubMass     - Hub mass (kg)
969952                  HubIner     - Hub inertia about rotor axis [3 blades]
    or teeter axis [2 blades] (kg m^2)
1836784                 GenIner     - Generator inertia about HSS (kg m^2)
644857                  NacMass     - Nacelle mass (kg)
32929058                NacYIner    - Nacelle inertia about yaw axis (kg m^2)
28249                   YawBrMass   - Yaw bearing mass (kg)
0.0                     PtfmMass    - Platform mass (kg)
0.0                     PtfmRIner   - Platform inertia for roll tilt rotation
    about the platform CM (kg m^2)
0.0                     PtfmPIner   - Platform inertia for pitch tilt rotation
    about the platform CM (kg m^2)
```

```
100000000.0             PtfmYIner   - Platform inertia for yaw rotation about
    the platform CM (kg m^2)
---------------------- BLADE
    ------------------------------------------------
50                      BldNodes    - Number of blade nodes (per blade) used
    for analysis (-)
"IEA-15-240-RWT_ElastoDyn_blade.dat" BldFile1    - Name of file containing
    properties for blade 1 (quoted string)
"IEA-15-240-RWT_ElastoDyn_blade.dat" BldFile2    - Name of file containing
    properties for blade 2 (quoted string)
"IEA-15-240-RWT_ElastoDyn_blade.dat" BldFile3    - Name of file containing
    properties for blade 3 (quoted string) [unused for 2 blades]
---------------------- ROTOR-TEETER
    ------------------------------------------
0                       TeetMod     - Rotor-teeter spring/damper model {0: none
    , 1: standard, 2: user-defined from routine UserTeet} (switch) [unused for
     3 blades]
0.0                     TeetDmpP    - Rotor-teeter damper position (degrees) [
    used only for 2 blades and when TeetMod=1]
0.0                     TeetDmp     - Rotor-teeter damping constant (N-m/(rad/s
    )) [used only for 2 blades and when TeetMod=1]
0.0                     TeetCDmp    - Rotor-teeter rate-independent Coulomb-
    damping moment (N-m) [used only for 2 blades and when TeetMod=1]
0.0                     TeetSStP    - Rotor-teeter soft-stop position (degrees)
     [used only for 2 blades and when TeetMod=1]
0.0                     TeetHStP    - Rotor-teeter hard-stop position (degrees)
     [used only for 2 blades and when TeetMod=1]
0.0                     TeetSSSp    - Rotor-teeter soft-stop linear-spring
    constant (N-m/rad) [used only for 2 blades and when TeetMod=1]
0.0                     TeetHSSp    - Rotor-teeter hard-stop linear-spring
    constant (N-m/rad) [used only for 2 blades and when TeetMod=1]
---------------------- DRIVETRAIN
    ------------------------------------------------
100.0                   GBoxEff     - Gearbox efficiency (%)
1.0                     GBRatio     - Gearbox ratio (-)
69737644900.0           DTTorSpr    - Drivetrain torsional spring (N-m/rad)
49418406.0              DTTorDmp    - Drivetrain torsional damper (N-m/(rad/s))
---------------------- FURLING
    ------------------------------------------------
False                   Furling     - Read in additional model properties for
    furling turbine (flag) [must currently be FALSE)
"unused"                FurlFile    - Name of file containing furling
    properties (quoted string) [unused when Furling=False]
---------------------- TOWER
    ------------------------------------------------
20                      TwrNodes    - Number of tower nodes used for analysis
    (-)
"IEA-15-240-RWT-Monopile_ElastoDyn_tower.dat" TwrFile     - Name of file
    containing tower properties (quoted string)
---------------------- OUTPUT
    ------------------------------------------------
False                   SumPrint    - Print summary data to "<RootName>.sum" (
    flag)
1                       OutFile     - Switch to determine where output will be
    placed: {1: in module output file only; 2: in glue code output file only;
    3: both} (currently unused)
True                    TabDelim    - Use tab delimiters in text tabular output
     file? (flag) (currently unused)
"ES10.3E2"              OutFmt      - Format used for text tabular output (
    except time).  Resulting field should be 10 characters. (quoted string) (
    currently unused)
0.0                     TStart      - Time to begin tabular output (s) (
    currently unused)
1                       DecFact     - Decimation factor for tabular output {1:
    output every time step} (-) (currently unused)
```

```
1                       NTwGages    - Number of tower nodes that have strain
    gages for output [0 to 9] (-)
         10   TwrGagNd    - List of tower nodes that have strain gages [1 to
    TwrNodes] (-) [unused if NTwGages=0] TwrGagNd    - List of tower nodes
    that have strain gages [1 to TwrNodes] (-) [unused if NTwGages=0] TwrGagNd
        - List of tower nodes that have strain gages [1 to TwrNodes] (-) [
    unused if NTwGages=0]
2                       NBlGages    - Number of blade nodes that have strain
    gages for output [0 to 9] (-)
         26, 38   BldGagNd    - List of blade nodes that have strain gages [1
    to BldNodes] (-) [unused if NBlGages=0] BldGagNd    - List of blade nodes
    that have strain gages [1 to BldNodes] (-) [unused if NBlGages=0] BldGagNd
        - List of blade nodes that have strain gages [1 to BldNodes] (-) [
    unused if NBlGages=0]
                    OutList             - The next line(s) contains a list of
    output parameters.  See OutListParameters.xlsx for a listing of available
    output channels, (-)

"BldPitch1"               - Blade 1 pitch angle

"RotSpeed"                - Low-speed shaft shaft speed

"RotThrust"       - Rotor Thrust

"RootMEdg1"               - In-plane bending, out-of-plane bending, and
    pitching moments at the root of blade 1
"RootMFlp1"               - In-plane bending, out-of-plane bending, and
    pitching moments at the root of blade 1

"Spn1MLxb1"           - Edge-wise bending at blade 1 midpoint
"Spn1MLyb1"           - Flap-wise bending at blade 1 midpoint

"Spn2MLxb1"           - Edge-wise bending at blade 1 tip
"Spn2MLyb1"           - Flap-wise bending at blade 1 tip

"TwrBsMxt"                - Side-to-side bending at the base of the tower (
    mudline)
"TwrBsMyt"                - Fore-aft bending at the base of the tower (mudline
    )
"TwrBsMzt"                - Yaw bending at the base of the tower (mudline)

"YawBrMxp"        - Yaw bearing (tower top) side-to-side bending moment
"YawBrMyp"        - Yaw bearing (tower top) fore-aft bending moment
"YawBrMzp"        - Yaw bearing (tower top) yaw bending moment

"TwHt1MLxt"           - Side-to-side bending at tower midpoint
"TwHt1MLyt"           - Fore-aft bending at tower midpoint
"TwHt1MLzt"           - Yaw bending at tower midpoint

END of input file (the word "END" must appear in the first 3 columns of this
    last OutList line)
---------------------- NODE OUTPUTS
    --------------------------------------------
          1   BldNd_BladesOut  - Blades to output
         99   BldNd_BlOutNd   - Blade nodes on each blade (currently unused)
              OutList     - The next line(s) contains a list of output
    parameters.  See OutListParameters.xlsx, ElastoDyn_Nodes tab for a listing
     of available output channels, (-)
END of input file (the word "END" must appear in the first 3 columns of this
    last OutList line)
---------------------------------------------------------------------------------
```

C.4 ServoDyn

```
------- SERVODYN v1.05.* INPUT FILE
    ------------------------------------------
IEA 15 MW offshore reference model monopile configuration
---------------------- SIMULATION CONTROL
    --------------------------------------
False                   Echo        - Echo input data to <RootName>.ech (flag)
"default"               DT          - Communication interval for controllers (s
    ) (or "default")
---------------------- PITCH CONTROL
    ------------------------------------------
5                       PCMode      - Pitch control mode {0: none, 3: user-
    defined from routine PitchCntrl, 4: user-defined from Simulink/Labview, 5:
     user-defined from Bladed-style DLL} (switch)
0.0                     TPCOn       - Time to enable active pitch control (s) [
    unused when PCMode=0]
9999.9                  TPitManS(1) - Time to start override pitch maneuver for
     blade 1 and end standard pitch control (s)
9999.9                  TPitManS(2) - Time to start override pitch maneuver for
     blade 2 and end standard pitch control (s)
9999.9                  TPitManS(3) - Time to start override pitch maneuver for
     blade 3 and end standard pitch control (s) [unused for 2 blades]
2.0                     PitManRat(1) - Pitch rate at which override pitch
    maneuver heads toward final pitch angle for blade 1 (deg/s)
2.0                     PitManRat(2) - Pitch rate at which override pitch
    maneuver heads toward final pitch angle for blade 2 (deg/s)
2.0                     PitManRat(3) - Pitch rate at which override pitch
    maneuver heads toward final pitch angle for blade 3 (deg/s) [unused for 2
    blades]
0.0                     BlPitchF(1) - Blade 1 final pitch for pitch maneuvers (
    degrees)
0.0                     BlPitchF(2) - Blade 2 final pitch for pitch maneuvers (
    degrees)
0.0                     BlPitchF(3) - Blade 3 final pitch for pitch maneuvers (
    degrees) [unused for 2 blades]
---------------------- GENERATOR AND TORQUE CONTROL
    ----------------------------
5                       VSContrl    - Variable-speed control mode {0: none, 1:
    simple VS, 3: user-defined from routine UserVSCont, 4: user-defined from
    Simulink/Labview, 5: user-defined from Bladed-style DLL} (switch)
1                       GenModel    - Generator model {1: simple, 2: Thevenin,
    3: user-defined from routine UserGen} (switch) [used only when VSContrl=0]
95.756                  GenEff      - Generator efficiency [ignored by the
    Thevenin and user-defined generator models] (%)
True                    GenTiStr    - Method to start the generator {T: timed
    using TimGenOn, F: generator speed using SpdGenOn} (flag)
True                    GenTiStp    - Method to stop the generator {T: timed
    using TimGenOf, F: when generator power = 0} (flag)
9999.9                  SpdGenOn    - Generator speed to turn on the generator
    for a startup (HSS speed) (rpm) [used only when GenTiStr=False]
0.0                     TimGenOn    - Time to turn on the generator for a
    startup (s) [used only when GenTiStr=True]
9999.9                  TimGenOf    - Time to turn off the generator (s) [used
    only when GenTiStp=True]
---------------------- SIMPLE VARIABLE-SPEED TORQUE CONTROL
    --------------------
7.559987120819503       VS_RtGnSp   - Rated generator speed for simple variable
    -speed generator control (HSS side) (rpm) [used only when VSContrl=1]
19624046.66639          VS_RtTq     - Rated generator torque/constant generator
     torque in Region 3 for simple variable-speed generator control (HSS side)
     (N-m) [used only when VSContrl=1]
343357.4355671095       VS_Rgn2K    - Generator torque constant in Region 2 for
     simple variable-speed generator control (HSS side) (N-m/rpm^2) [used only
     when VSContrl=1]
```

```
2.                      VS_SlPc     - Rated generator slip percentage in Region
     2 1/2 for simple variable-speed generator control (%) [used only when
    VSContrl=1]
---------------------- SIMPLE INDUCTION GENERATOR
    --------------------------------
9999.9                  SIG_SlPc    - Rated generator slip percentage (%) [used
     only when VSContrl=0 and GenModel=1]
9999.9                  SIG_SySp    - Synchronous (zero-torque) generator speed
     (rpm) [used only when VSContrl=0 and GenModel=1]
9999.9                  SIG_RtTq    - Rated torque (N-m) [used only when
    VSContrl=0 and GenModel=1]
9999.9                  SIG_PORt    - Pull-out ratio (Tpullout/Trated) (-) [
    used only when VSContrl=0 and GenModel=1]
---------------------- THEVENIN-EQUIVALENT INDUCTION GENERATOR
    -----------------
9999.9                  TEC_Freq    - Line frequency [50 or 60] (Hz) [used only
     when VSContrl=0 and GenModel=2]
100                     TEC_NPol    - Number of poles [even integer > 0] (-) [
    used only when VSContrl=0 and GenModel=2]
9999.9                  TEC_SRes    - Stator resistance (ohms) [used only when
    VSContrl=0 and GenModel=2]
9999.9                  TEC_RRes    - Rotor resistance (ohms) [used only when
    VSContrl=0 and GenModel=2]
9999.9                  TEC_VLL     - Line-to-line RMS voltage (volts) [used
    only when VSContrl=0 and GenModel=2]
9999.9                  TEC_SLR     - Stator leakage reactance (ohms) [used
    only when VSContrl=0 and GenModel=2]
9999.9                  TEC_RLR     - Rotor leakage reactance (ohms) [used only
     when VSContrl=0 and GenModel=2]
9999.9                  TEC_MR      - Magnetizing reactance (ohms) [used only
    when VSContrl=0 and GenModel=2]
---------------------- HIGH-SPEED SHAFT BRAKE
    ---------------------------------
0                       HSSBrMode   - HSS brake model {0: none, 1: simple, 3:
    user-defined from routine UserHSSBr, 4: user-defined from Simulink/Labview
    , 5: user-defined from Bladed-style DLL} (switch)
9999.9                  THSSBrDp    - Time to initiate deployment of the HSS
    brake (s)
9999.9                  HSSBrDT     - Time for HSS-brake to reach full
    deployment once initiated (sec) [used only when HSSBrMode=1]
9999.9                  HSSBrTqF    - Fully deployed HSS-brake torque (N-m)
---------------------- NACELLE-YAW CONTROL
    ------------------------------------
0                       YCMode      - Yaw control mode {0: none, 3: user-
    defined from routine UserYawCont, 4: user-defined from Simulink/Labview,
    5: user-defined from Bladed-style DLL} (switch)
9999.9                  TYCOn       - Time to enable active yaw control (s) [
    unused when YCMode=0]
0.0                     YawNeut     - Neutral yaw position--yaw spring force is
     zero at this yaw (degrees)
6009291301.0            YawSpr      - Nacelle-yaw spring constant (N-m/rad)
4811254.0               YawDamp     - Nacelle-yaw damping constant (N-m/(rad/s)
    )
9999.9                  TYawManS    - Time to start override yaw maneuver and
    end standard yaw control (s)
0.25                    YawManRat   - Yaw maneuver rate (in absolute value) (
    deg/s)
0.0                     NacYawF     - Final yaw angle for override yaw
    maneuvers (degrees)
---------------------- Aerodynamic Flow Control
    -------------------------------------
0                       AfCmode     - Airfoil control mode {0- none, 1- cosine
    wave cycle, 4- user-defined from Simulink/Labview, 5- user-defined from
    Bladed-style DLL}
0.0                     AfC_Mean    - Mean level for sinusoidal cycling or
    steady value (-) [used only with AfCmode==1]
```

```
0.0                     AfC_Amp     - Amplitude for for cosine cycling of flap
    signal (AfC = AfC_Amp*cos(Azimuth+phase)+AfC_mean) (-) [used only with
    AfCmode==1]
0.0                     AfC_phase   - Phase relative to the blade azimuth (0 is
     vertical) for for cosine cycling of flap signal (deg) [used only with
    AfCmode==1]
---------------------- STRUCTURAL CONTROL
    ----------------------------------------
0                       NumBStC     - Number of blade structural controllers (
    integer)
"unused"                BStCfiles   - Name of the file for blade tuned mass
    damper (quoted string) [unused when CompNTMD is false]
0                       NumNStC     - Number of nacelle structural controllers
    (integer)
"unused"                NStCfiles   - Name of the file for nacelle tuned mass
    damper (quoted string) [unused when CompNTMD is false]
0                       NumTStC     - Number of tower structural controllers (
    integer)
"unused"                TStCfiles   - Name of the file for tower tuned mass
    damper (quoted string) [unused when CompNTMD is false]
0                       NumSStC     - Number of sbustructure structural
    controllers (integer)
"unused"                SStCfiles   - Name of the file for sbustructure tuned
    mass damper (quoted string) [unused when CompNTMD is false]
---------------------- CABLE CONTROL ---------------------------------------
0                       CCmode      - Cable control mode {0- none, 4- user-
    defined from Simulink/Labview, 5- user-defineAfC_phased from Bladed-style
    DLL}
---------------------- BLADED INTERFACE
    ---------------------------------------- [used only with Bladed Interface]
"ServoData/ROSCO.dll"  DLL_FileName - Name/location of the dynamic library {.
    dll [Windows] or .so [Linux]} in the Bladed-DLL format (-) [used only with
     Bladed Interface]
"IEA-15-240-RWT-Monopile_DISCON.IN"   DLL_InFile  - Name of input file sent to
     the DLL (-) [used only with Bladed Interface]
"DISCON"                DLL_ProcName - Name of procedure in DLL to be called
    (-) [case sensitive; used only with DLL Interface]
"default"               DLL_DT      - Communication interval for dynamic
    library (s) (or "default") [used only with Bladed Interface]
False                   DLL_Ramp    - Whether a linear ramp should be used
    between DLL_DT time steps [introduces time shift when true] (flag) [used
    only with Bladed Interface]
9999.9                  BPCutoff    - Cuttoff frequency for low-pass filter on
    blade pitch from DLL (Hz) [used only with Bladed Interface]
0.0                     NacYaw_North - Reference yaw angle of the nacelle when
    the upwind end points due North (deg) [used only with Bladed Interface]
0                       Ptch_Cntrl  - Record 28: Use individual pitch control
    {0: collective pitch; 1: individual pitch control} (switch) [used only
    with Bladed Interface]
0.0                     Ptch_SetPnt - Record  5: Below-rated pitch angle set-
    point (deg) [used only with Bladed Interface]
0.0                     Ptch_Min    - Record  6: Minimum pitch angle (deg) [
    used only with Bladed Interface]
0.0                     Ptch_Max    - Record  7: Maximum pitch angle (deg) [
    used only with Bladed Interface]
0.0                     PtchRate_Min - Record  8: Minimum pitch rate (most
    negative value allowed) (deg/s) [used only with Bladed Interface]
0.0                     PtchRate_Max - Record  9: Maximum pitch rate  (deg/s) [
    used only with Bladed Interface]
0.0                     Gain_OM     - Record 16: Optimal mode gain (Nm/(rad/s)
    ^2) [used only with Bladed Interface]
0.0                     GenSpd_MinOM - Record 17: Minimum generator speed (rpm)
     [used only with Bladed Interface]
0.0                     GenSpd_MaxOM - Record 18: Optimal mode maximum speed (
    rpm) [used only with Bladed Interface]
```

```
0.0                     GenSpd_Dem  - Record 19: Demanded generator speed above
     rated (rpm) [used only with Bladed Interface]
0.0                     GenTrq_Dem  - Record 22: Demanded generator torque
    above rated (Nm) [used only with Bladed Interface]
0.0                     GenPwr_Dem  - Record 13: Demanded power (W) [used only
    with Bladed Interface]
---------------------- BLADED INTERFACE TORQUE-SPEED LOOK-UP TABLE
    -------------
0                       DLL_NumTrq  - Record 26: No. of points in torque-speed
    look-up table {0 = none and use the optimal mode parameters; nonzero =
    ignore the optimal mode PARAMETERs by setting Record 16 to 0.0} (-) [used
    only with Bladed Interface]
GenSpd_TLU               GenTrq_TLU
(rpm)                    (Nm)
---------------------- OUTPUT
    ----------------------------------------------------
False                   SumPrint    - Print summary data to <RootName>.sum (
    flag) (currently unused)
1                       OutFile     - Switch to determine where output will be
    placed: {1: in module output file only; 2: in glue code output file only;
    3: both} (currently unused)
True                    TabDelim    - Use tab delimiters in text tabular output
     file? (flag) (currently unused)
"ES10.3E2"              OutFmt      - Format used for text tabular output (
    except time).  Resulting field should be 10 characters. (quoted string) (
    currently unused)
0.0                     TStart      - Time to begin tabular output (s) (
    currently unused)
              OutList      - The next line(s) contains a list of output
    parameters.  See OutListParameters.xlsx for a listing of available output
    channels, (-)
"GenPwr"
"GenTq"
END of input file (the word "END" must appear in the first 3 columns of this
    last OutList line)
---------------------------------------------------------------------------------------
```

C.5 SubDyn

```
---------- SubDyn v1.01.x MultiMember Support Structure Input File
    ------------
IEA 15 MW offshore reference model monopile configuration
------------------------- SIMULATION CONTROL
    ----------------------------------
False             Echo        - Echo input data to "<rootname>.SD.ech" (flag)
"DEFAULT"        SDdeltaT    - Local Integration Step. If "default", the glue-
    code integration step will be used.
             3   IntMethod   - Integration Method [1/2/3/4 = RK4/AB4/ABM4/AM2
    ].
True             SttcSolve   - Solve dynamics about static equilibrium point
False            GuyanLoadCorrection - Include extra moment from lever arm at
    interface and rotate FEM for floating.
-------------------- FEA and CRAIG-BAMPTON PARAMETERS
    ----------------------------
             3   FEMMod      - FEM switch: element model in the FEM. [1= Euler
    -Bernoulli(E-B);  2=Tapered E-B (unavailable);  3= 2-node Timoshenko;  4=
    2-node tapered Timoshenko (unavailable)]
             1   NDiv        - Number of sub-elements per member
True             CBMod       - [T/F] If True perform C-B reduction, else full
    FEM dofs will be retained. If True, select Nmodes to retain in C-B reduced
     system.
```

```
             0   Nmodes      - Number of internal modes to retain (ignored if
    CBMod=False). If Nmodes=0 --> Guyan Reduction.
             1   JDampings   - Damping Ratios for each retained mode (% of
    critical) If Nmodes>0, list Nmodes structural damping ratios for each
    retained mode (% of critical), or a single damping ratio to be applied to
    all retained modes. (last entered value will be used for all remaining
    modes).
0                       GuyanDampMod - Guyan damping {0=none, 1=Rayleigh
    Damping, 2=user specified 6x6 matrix}.
0.0       , 0.0         RayleighDamp - Mass and stiffness proportional damping
     coefficients (Rayleigh Damping) [only if GuyanDampMod=1].
6                       GuyanDampSize - Guyan damping matrix (6x6) [only if
    GuyanDampMod=2].
           0.0            0.0            0.0            0.0            0.0
            0.0
           0.0            0.0            0.0            0.0            0.0
            0.0
           0.0            0.0            0.0            0.0            0.0
            0.0
           0.0            0.0            0.0            0.0            0.0
            0.0
           0.0            0.0            0.0            0.0            0.0
            0.0
           0.0            0.0            0.0            0.0            0.0
            0.0
---- STRUCTURE JOINTS: joints connect structure members (~Hydrodyn Input File)
    ---
             19   NJoints     - Number of joints (-)
  JointID    JointXss    JointYss    JointZss    JointType   JointDirX
    JointDirY   JointDirZ  JointStiff
    (-)         (m)         (m)         (m)         (-)         (-)
    (-)         (-)      (Nm/rad)
     1      0.00000     0.00000    -30.0000          1          0.0
    0.0         0.0         0.0
     2      0.00000     0.00000    -29.999           1          0.0
    0.0         0.0         0.0
     3      0.00000     0.00000    -25.0000          1          0.0
    0.0         0.0         0.0
     4      0.00000     0.00000    -24.999           1          0.0
    0.0         0.0         0.0
     5      0.00000     0.00000    -20.0000          1          0.0
    0.0         0.0         0.0
     6      0.00000     0.00000    -19.999           1          0.0
    0.0         0.0         0.0
     7      0.00000     0.00000    -15.0000          1          0.0
    0.0         0.0         0.0
     8      0.00000     0.00000    -14.999           1          0.0
    0.0         0.0         0.0
     9      0.00000     0.00000    -10.0000          1          0.0
    0.0         0.0         0.0
    10      0.00000     0.00000     -9.999           1          0.0
    0.0         0.0         0.0
    11      0.00000     0.00000     -5.0000          1          0.0
    0.0         0.0         0.0
    12      0.00000     0.00000     -4.999           1          0.0
    0.0         0.0         0.0
    13      0.00000     0.00000      0.0000          1          0.0
    0.0         0.0         0.0
    14      0.00000     0.00000      0.001           1          0.0
    0.0         0.0         0.0
    15      0.00000     0.00000      5.0000          1          0.0
    0.0         0.0         0.0
    16      0.00000     0.00000      5.001           1          0.0
    0.0         0.0         0.0
    17      0.00000     0.00000     10.0000          1          0.0
    0.0         0.0         0.0
```

```
    18      0.00000     0.00000     10.001          1          0.0
    0.0         0.0         0.0
    19      0.00000     0.00000     15.0000         1          0.0
    0.0         0.0         0.0
------------------- BASE REACTION JOINTS: 1/0 for Locked/Free DOF @ each
    Reaction Node ----------------------
             1   NReact      - Number of Joints with reaction forces; be sure
    to remove all rigid motion DOFs of the structure  (else det([K])=[0])
 RJointID    RctTDXss    RctTDYss    RctTDZss    RctRDXss    RctRDYss
    RctRDZss     SSIfile   [Global Coordinate System]
    (-)       (flag)      (flag)      (flag)      (flag)      (flag)      (
    flag)     (string)
     1           1           1           1           1           1           1
------- INTERFACE JOINTS: 1/0 for Locked (to the TP)/Free DOF @each Interface
    Joint (only Locked-to-TP implemented thus far (=rigid TP)) ---------
             1   NInterf     - Number of interface joints locked to the
    Transition Piece (TP):  be sure to remove all rigid motion dofs
IJointID   ItfTDXss    ItfTDYss    ItfTDZss    ItfRDXss    ItfRDYss
    ItfRDZss     [Global Coordinate System]
  (-)       (flag)      (flag)      (flag)      (flag)      (flag)      (flag)
  10          1           1           1           1           1           1
---------------------------------- MEMBERS
    --------------------------------------
             18   NMembers    - Number of frame members
 MemberID    MJointID1   MJointID2  MPropSetID1 MPropSetID2    MType
    COSMID
    (-)         (-)         (-)         (-)         (-)         (-)
    (-)
     1           1           2           1           1           1
     2           2           3           1           1           1
     3           3           4           2           2           1
     4           4           5           2           2           1
     5           5           6           3           3           1
     6           6           7           3           3           1
     7           7           8           4           4           1
     8           8           9           4           4           1
     9           9          10           5           5           1
    10          10          11           5           5           1
    11          11          12           6           6           1
    12          12          13           6           6           1
    13          13          14           7           7           1
    14          14          15           7           7           1
    15          15          16           8           8           1
    16          16          17           8           8           1
    17          17          18           9           9           1
    18          18          19           9           9           1
------------------ MEMBER X-SECTION PROPERTY data 1/2 [isotropic material for
    now: use this table for circular-tubular elements]
    ------------------------
             9   NPropSets   - Number of structurally unique x-sections (i.e.
    how many groups of X-sectional properties are utilized throughout all of
    the members)
PropSetID     YoungE          ShearG          MatDens          XsecD
     XsecT
  (-)         (N/m2)          (N/m2)          (kg/m3)           (m)
      (m)
   1        2.00000e+11       79.3e9          7800.0           10.0
      0.055341
   2        2.00000e+11       79.3e9          7800.0           10.0
      0.053449
   3        2.00000e+11       79.3e9          7800.0           10.0
      0.051509
   4        2.00000e+11       79.3e9          7800.0           10.0
      0.049527
   5        2.00000e+11       79.3e9          7800.0           10.0
      0.047517
```

```
   6        2.00000e+11       79.3e9          7800.0           10.0
      0.045517
   7        2.00000e+11       79.3e9          7800.0           10.0
      0.043527
   8        2.00000e+11       79.3e9          7800.0           10.0
      0.042242
   9        2.00000e+11       79.3e9          7800.0           10.0
      0.041058
------------------ MEMBER X-SECTION PROPERTY data 2/2 [isotropic material for
    now: use this table if any section other than circular, however provide
    COSM(i,j) below] ------------------------
             0   NXPropSets  - Number of structurally unique non-circular x-
    sections (if 0 the following table is ignored)
 PropSetID     YoungE       ShearG2      MatDens       XsecA       XsecAsx
    XsecAsy      XsecJxx      XsecJyy      XsecJ0
    (-)        (N/m2)       (N/m2)       (kg/m3)       (m2)         (m2)         (m2
    )         (m4)         (m4)         (m4)
--------------------------- CABLE PROPERTIES
    --------------------------------------
0                       NCablePropSets - Number of cable cable properties
 PropSetID       EA         MatDens        T0
    (-)          (N)        (kg/m)         (N)
----------------------- RIGID LINK PROPERTIES
    ------------------------------------
0                       NRigidPropSets - Number of rigid link properties
 PropSetID     MatDens
    (-)        (kg/m)
---------------------- MEMBER COSINE MATRICES COSM(i,j)
    -------------------------
             0   NCOSMs      - Number of unique cosine matrices (i.e., of
    unique member alignments including principal axis rotations); ignored if
    NXPropSets=0   or 9999 in any element below
COSMID    COSM11    COSM12    COSM13    COSM21    COSM22    COSM23    COSM31
      COSM32    COSM33
 (-)       (-)       (-)       (-)       (-)       (-)       (-)       (-)
       (-)       (-)
------------------------ JOINT ADDITIONAL CONCENTRATED MASSES
    ---------------------------
1                       NCmass      - Number of joints with concentrated masses
    ; Global Coordinate System
 CMJointID     JMass        JMXX         JMYY         JMZZ         JMXY
    JMXZ         JMYZ         MCGX         MCGY         MCGZ
    (-)         (kg)       (kg*m^2)     (kg*m^2)     (kg*m^2)     (kg*m^2)     (kg*m
    ^2)     (kg*m^2)        (m)          (m)          (m)
    10        100000.0    1250000.0    1250000.0    2500000.0       0.0
    0.0         0.0          0.0          0.0          0.0
----------------------------- OUTPUT: SUMMARY & OUTFILE
    -------------------------------
False             SumPrint    - Output a Summary File (flag).It contains:
    matrices K,M  and C-B reduced M_BB, M-BM, K_BB, K_MM(OMG^2), PHI_R, PHI_L.
     It can also contain COSMs if requested.
0                 OutCBModes  - Output Guyan and Craig-Bampton modes {0: No
    output, 1: JSON output}, (flag)
0                 OutFEMModes - Output first 30 FEM modes {0: No output, 1:
    JSON output} (flag)
False             OutCOSM     - Output cosine matrices with the selected output
     member forces (flag)
False             OutAll      - [T/F] Output all members' end forces
             2    OutSwtch    - [1/2/3] Output requested channels to: 1=<
    rootname>.SD.out;  2=<rootname>.out (generated by FAST);  3=both files.
True              TabDelim    - Generate a tab-delimited output in the <
    rootname>.SD.out file
             1    OutDec      - Decimation of output in the <rootname>.SD.out
    file
"ES11.4e2"        OutFmt      - Output format for numerical results in the <
    rootname>.SD.out file
```

```
"A11"            OutSFmt     - Output format for header strings in the <
    rootname>.SD.out file
------------------------ MEMBER OUTPUT LIST
    ------------------------------------------
             2   NMOutputs   - Number of members whose forces/displacements/
    velocities/accelerations will be output (-) [Must be <= 9].
MemberID   NOutCnt    NodeCnt [NOutCnt=how many nodes to get output for [<
    10]; NodeCnt are local ordinal numbers from the start of the member, and
    must be >=1 and <= NDiv+1] If NMOutputs=0 leave blank as well.
  (-)        (-)        (-)
   1          1          1
   3          1          1
------------------------ SSOutList: The next line(s) contains a list of
    output parameters that will be output in <rootname>.SD.out or <rootname>.
    out. ------
"-ReactMXss, -ReactMYss, -ReactMZss" - Base reactions: side-to-side, fore-aft
    and yaw moments at the mudline.
END of output channels and end of file. (the word "END" must appear in the
    first 3 columns of this line)
```

D

FAST.Farm Input Files

D.1 FAST.Farm Driver File

```
------- FAST.Farm for OpenFAST INPUT FILE
    ------------------------------------------------
FAST.Farm input file for IEA 15MW simulations with multiple instances of
    InflowWind (Mod_AmbWind=3). 3x3 sqaure wind farm with spacing of 4 rotor
    diameters.
---------------------- SIMULATION CONTROL
    --------------------------------------------------
False          Echo           - Echo input data to <RootName>.ech? (flag)
"SEVERE"        AbortLevel     - Error level when simulation should abort (
    string) {"WARNING", "SEVERE", "FATAL"}
700            TMax           - Total run time (s) [>=0.0] (overrides OpenFAST's
     TMax)
False          UseSC          - Use a super controller? (flag)
3              Mod_AmbWind    - Ambient wind model (-) (switch) {1: high-
    fidelity precursor in VTK format, 2: one InflowWind module, 3: multiple
    instances of InflowWind module}
2              Mod_WaveField - Wave field handling (-) (switch) {1: use
    individual HydroDyn inputs without adjustment, 2: adjust wave phases based
     on turbine offsets from farm origin}
0              Mod_SharedMooring - Shared mooring system model (switch) {0:
    None, 3=MoorDyn}}
--------------------- SUPER CONTROLLER [used only for UseSC=True]
    ----------------------------------------------------
/path/to/SC_DLL.dll SC_FileName   - Name/location of the dynamic library {.dll
     [Windows] or .so [Linux]} containing the Super Controller algorithms (
    quoated string)
---------------------- SHARED MOORING SYSTEM [used only for Mod_SharedMoor>0]
    --------------- -------------------------
""             SharedMoorFile - Name of file containing shared mooring system
    input parameterWs (quoted string) [used only when Mod_SharedMooring > 0]
0.04           DT_Mooring     - Time step for farm-level mooring coupling with
    each turbine (s) [used only when Mod_SharedMooring > 0]
---------------------- AMBIENT WIND: PRECURSOR IN VTK FORMAT [used only for
    Mod_AmbWind=1] --
3.0            DT_Low-VTK     - Time step for low -resolution wind data input
    files; will be used as the global FAST.Farm time step (s) [>0.0]
0.1            DT_High-VTK    - Time step for high-resolution wind data input
    files (s) [>0.0]
"unused"       WindFilePath   - Path name to VTK wind data files from precursor
    (string)
False          ChkWndFiles    - Check all the ambient wind files for data
    consistency? (flag)
---------------------- AMBIENT WIND: INFLOWWIND MODULE [used only for
    Mod_AmbWind=2 or 3] -----------------------------
2.0            DT_Low         - Time step for low -resolution wind data
    interpolation; will be used as the global FAST.Farm time step (s) [>0.0]
```

```
0.5           DT_High       - Time step for high-resolution wind data
    interpolation (s) [>0.0]
78            NX_Low        - Number of low -resolution spatial nodes in X
    direction for wind data interpolation (-) [>=2]
43            NY_Low        - Number of low -resolution spatial nodes in Y
    direction for wind data interpolation (-) [>=2]
13            NZ_Low        - Number of low -resolution spatial nodes in Z
    direction for wind data interpolation (-) [>=2]
-1092.0       X0_Low        - Origin of low -resolution spatial nodes in X
    direction for wind data interpolation (m)
-1512.0       Y0_Low        - Origin of low -resolution spatial nodes in Y
    direction for wind data interpolation (m)
1             Z0_Low        - Origin of low -resolution spatial nodes in Z
    direction for wind data interpolation (m)
52.0          dX_Low        - Spacing of low -resolution spatial nodes in X
    direction for wind data interpolation (m) [>0.0]
72.0          dY_Low        - Spacing of low -resolution spatial nodes in Y
    direction for wind data interpolation (m) [>0.0]
72.0          dZ_Low        - Spacing of low -resolution spatial nodes in Z
    direction for wind data interpolation (m) [>0.0]
22            NX_High       - Number of high-resolution spatial nodes in X
    direction for wind data interpolation (-) [>=2]
44            NY_High       - Number of high-resolution spatial nodes in Y
    direction for wind data interpolation (-) [>=2]
49            NZ_High       - Number of high-resolution spatial nodes in Z
    direction for wind data interpolation (-) [>=2]
"IEA-15-240-RWT_InflowFile.dat" InflowFile    - Name of file containing
    InflowWind module input parameters (quoted string)
---------------------- WIND TURBINES
    ------------------------------------------------------------------------------

9             NumTurbines   - Number of wind turbines (-) [>=1] [last 6
    columns below used only for Mod_AmbWind=2 or 3]
WT_X            WT_Y            WT_Z            WT_FASTInFile   X0_High
      Y0_High         Z0_High         dX_High         dY_High         dZ_High
(m)             (m)             (m)             (string)        (m)
      (m)             (m)             (m)             (m)             (m)
           -960            -960               0 "IEA15MW_Farm_s4_theta0_T1.fst
    "           -1092           -1092               1  1.29200000e+01
          6               6
              0            -960               0 "IEA15MW_Farm_s4_theta0_T2.fst
    " -1.35920000e+02           -1092               1  1.29200000e+01
          6               6
            960            -960               0 "IEA15MW_Farm_s4_theta0_T3.fst
    "  8.20160000e+02           -1092               1  1.29200000e+01
          6               6
           -960               0               0 "IEA15MW_Farm_s4_theta0_T4.fst
    "           -1092            -132               1  1.29200000e+01
          6               6
              0               0               0 "IEA15MW_Farm_s4_theta0_T5.fst
    " -1.35920000e+02            -132               1  1.29200000e+01
          6               6
            960               0               0 "IEA15MW_Farm_s4_theta0_T6.fst
    "  8.20160000e+02            -132               1  1.29200000e+01
          6               6
           -960             960               0 "IEA15MW_Farm_s4_theta0_T7.fst
    "           -1092             828               1  1.29200000e+01
          6               6
              0             960               0 "IEA15MW_Farm_s4_theta0_T8.fst
    " -1.35920000e+02             828               1  1.29200000e+01
          6               6
            960             960               0 "IEA15MW_Farm_s4_theta0_T9.fst
    "  8.20160000e+02             828               1  1.29200000e+01
          6               6
---------------------- WAKE DYNAMICS
    ------------------------------------------------------------------------------
```

```
1             Mod_Wake      - Switch between wake formulations {1:Polar, 2:
    Curl, 3:Cartesian} (-) (switch)
6             dr            - Radial increment of radial finite-difference
    grid (m) [>0.0]
61            NumRadii      - Number of radii in the radial finite-difference
    grid (-) [>=2]
120           NumPlanes     - Number of wake planes (-) [>=2]
0.256         f_c           - Cutoff (corner) frequency of the low-pass time-
    filter for the wake advection, deflection, and meandering model [
    recommended=1.28*U0/R] (Hz) [>0.0] or DEFAULT [DEFAULT=12.5/R, R estimated
     from dr and NumRadii, not recommended]
DEFAULT       C_HWkDfl_O    - Calibrated parameter in the correction for wake
    deflection defining the horizontal offset at the rotor (m ) or DEFAULT [
    DEFAULT= 0.0 ]
DEFAULT       C_HWkDfl_OY   - Calibrated parameter in the correction for wake
    deflection defining the horizontal offset at the rotor scaled with yaw
    error (m/deg) or DEFAULT [DEFAULT= 0.0 if Mod_Wake is 2, 0.3 otherwise]
DEFAULT       C_HWkDfl_x    - Calibrated parameter in the correction for wake
    deflection defining the horizontal offset scaled with downstream distance
    (- ) or DEFAULT [DEFAULT= 0.0 ]
DEFAULT       C_HWkDfl_xY   - Calibrated parameter in the correction for wake
    deflection defining the horizontal offset scaled with downstream distance
    and yaw error (1/deg) or DEFAULT [DEFAULT= 0.0 if Mod_Wake is 2, -0.004
    otherwise]
DEFAULT       C_NearWake    - Calibrated parameter for the near-wake
    correction (-) [>1.0 and <2.5] or DEFAULT [DEFAULT=1.8]
DEFAULT       k_vAmb        - Calibrated parameter for the influence of
    ambient turbulence in the eddy viscosity (-) [>=0.0] or DEFAULT [DEFAULT
    =0.05 ]
DEFAULT       k_vShr        - Calibrated parameter for the influence of the
    shear layer in the eddy viscosity (-) [>=0.0] or DEFAULT [DEFAULT=0.016]
DEFAULT       C_vAmb_DMin   - Calibrated parameter in the eddy viscosity
    filter function for ambient turbulence defining the transitional diameter
    fraction between the minimum and exponential regions (-) [>=0.0 ] or
    DEFAULT [DEFAULT= 0.0 ]
DEFAULT       C_vAmb_DMax   - Calibrated parameter in the eddy viscosity
    filter function for ambient turbulence defining the transitional diameter
    fraction between the exponential and maximum regions (-) [> C_vAmb_DMin ]
    or DEFAULT [DEFAULT= 1.0 ]
DEFAULT       C_vAmb_FMin   - Calibrated parameter in the eddy viscosity
    filter function for ambient turbulence defining the value in the minimum
    region (-) [>=0.0 and <=1.0] or DEFAULT [DEFAULT= 1.0 ]
DEFAULT       C_vAmb_Exp    - Calibrated parameter in the eddy viscosity
    filter function for ambient turbulence defining the exponent in the
    exponential region (-) [> 0.0 ] or DEFAULT [DEFAULT= 0.01]
DEFAULT       C_vShr_DMin   - Calibrated parameter in the eddy viscosity
    filter function for the shear layer defining the transitional diameter
    fraction between the minimum and exponential regions (-) [>=0.0 ] or
    DEFAULT [DEFAULT= 3.0 ]
DEFAULT       C_vShr_DMax   - Calibrated parameter in the eddy viscosity
    filter function for the shear layer defining the transitional diameter
    fraction between the exponential and maximum regions (-) [> C_vShr_DMin ]
    or DEFAULT [DEFAULT=25.0 ]
DEFAULT       C_vShr_FMin   - Calibrated parameter in the eddy viscosity
    filter function for the shear layer defining the value in the minimum
    region (-) [>=0.0 and <=1.0] or DEFAULT [DEFAULT= 0.2 ]
DEFAULT       C_vShr_Exp    - Calibrated parameter in the eddy viscosity
    filter function for the shear layer defining the exponent in the
    exponential region (-) [> 0.0 ] or DEFAULT [DEFAULT= 0.1 ]
DEFAULT       Mod_WakeDiam  - Wake diameter calculation model (-) (switch) {1:
     rotor diameter, 2: velocity based, 3: mass-flux based, 4: momentum-flux
    based} or DEFAULT [DEFAULT=1]
DEFAULT       C_WakeDiam    - Calibrated parameter for wake diameter
    calculation (-) [>0.0 and <0.99] or DEFAULT [DEFAULT=0.95] [unused for
    Mod_WakeDiam=1]
```

```
DEFAULT       Mod_Meander   - Spatial filter model for wake meandering (-) (
    switch) {1: uniform, 2: truncated jinc, 3: windowed jinc} or DEFAULT [
    DEFAULT=3]
DEFAULT       C_Meander     - Calibrated parameter for wake meandering (-)
    [>=1.0] or DEFAULT [DEFAULT=1.9]
--------------- CURLED-WAKE PARAMETERS [only used if Mod_Wake=2 or 3]
    -------------------------------------------------
DEFAULT       Swirl         - Switch to include swirl velocities in wake (-) (
    switch) [DEFAULT=TRUE]
DEFAULT       k_VortexDecay - Vortex decay constant for curl (-) [DEFAULT=0]
DEFAULT       NumVortices   - The number of vortices in the curled wake model
    (-) [DEFAULT=100]
DEFAULT       sigma_D       - The width of the vortices in the curled wake
    model non-dimesionalized by rotor diameter (-) [DEFAULT=0.2]
DEFAULT       FilterInit    - Switch to filter the initial wake plane deficit
    and select the number of grid points for the filter {0: no filter, 1:
    filter of size 1} or DEFAULT [DEFAULT=1] (switch)
DEFAULT       k_vCurl       - Calibrated parameter for scaling the eddy
    viscosity in the curled-wake model (-) [>=0] or DEFAULT [DEFAULT=2.0 ]
DEFAULT       Mod_Projection - Switch to select how the wake plane velocity is
     projected in AWAE {1: keep all components, 2: project against plane
    normal} or DEFAULT [DEFAULT=1: if Mod_Wake is 1 or 3, or DEFAULT=2: if
    Mod_Wake is 2] (switch)
--------------- VISUALIZATION
    ------------------------------------------------------------------------------------------

False         WrDisWind     - Write low- and high-resolution disturbed wind
    data to <RootName>.Low.Dis.t<n>.vtk etc.? (flag)
1             NOutDisWindXY - Number of XY planes for output of disturbed wind
     data across the low-resolution domain to <RootName>.Low.DisXY<n_out>.t<n
    >.vtk (-) [0 to 99]
87.6          OutDisWindZ   - Z coordinates of XY planes for output of
    disturbed wind data across the low-resolution domain (m) [1 to
    NOutDisWindXY] [unused for NOutDisWindXY=0]
2             NOutDisWindYZ - Number of YZ planes for output of disturbed wind
     data across the low-resolution domain to <RootName>/Low.DisYZ<n_out>.t<n
    >.vtk (-) [0 to 99]
10.000000000000014, 640.0 OutDisWindX   - X coordinates of YZ planes for
    output of disturbed wind data across the low-resolution domain (m) [1 to
    NOutDisWindYZ] [unused for NOutDisWindYZ=0]
2             NOutDisWindXZ - Number of XZ planes for output of disturbed wind
     data across the low-resolution domain to <RootName>/Low.DisXZ<n_out>.t<n
    >.vtk (-) [0 to 99]
-315.0, 315.0 OutDisWindY   - Y coordinates of XZ planes for output of
    disturbed wind data across the low-resolution domain (m) [1 to
    NOutDisWindXZ] [unused for NOutDisWindXZ=0]
2.0           WrDisDT       - Time step for disturbed wind visualization
    output (s) [>0.0] or DEFAULT [DEFAULT=DT_Low or DT_Low-VTK] [unused for
    WrDisWind=False and NOutDisWindXY=NOutDisWindYZ=NOutDisWindXZ=0]
--------------- OUTPUT
    ------------------------------------------------------------------------------------------

True          SumPrint      - Print summary data to <RootName>.sum? (flag)
99999.9       ChkptTime     - Amount of time between creating checkpoint files
     for potential restart (s) [>0.0]
100           TStart        - Time to begin tabular output (s) [>=0.0]
1             OutFileFmt    - Format for tabular (time-marching) output file (
    switch) {1: text file [<RootName>.out], 2: binary file [<RootName>.outb],
    3: both}
True          TabDelim      - Use tab delimiters in text tabular output file?
    (flag) {uses spaces if False}
"ES10.3E2"    OutFmt        - Format used for text tabular output, excluding
    the time channel. Resulting field should be 10 characters. (quoted string)
DEFAULT       OutAllPlanes  - Output all wake planes at all time steps. [
    DEFAULT=False]
```

```
7             NOutRadii     - Number of radial nodes for wake output for an
    individual rotor (-) [0 to 20]
0, 2, 5, 11, 17, 21, 39 OutRadii      - List of radial nodes for wake output
    for an individual rotor (-) [1 to NOutRadii] [unused for NOutRadii=0]
9             NOutDist      - Number of downstream distances for wake output
    for an individual rotor (-) [0 to 9 ]
126.0, 189.0, 252.0, 315.0, 378.0, 441.0, 504.0, 630.0, 756.0 OutDist       -
    List of downstream distances for wake output for an individual rotor (m)
    [1 to NOutDist ] [unused for NOutDist =0]
0             NWindVel      - Number of points for wind output (-) [0 to 9]
120.2, 120.2, 750.2, 750.2 WindVelX      - List of coordinates in the X
    direction for wind output (m) [1 to NWindVel] [unused for NWindVel=0]
-315.0, 315.0, -315.0, 315.0 WindVelY      - List of coordinates in the Y
    direction for wind output (m) [1 to NWindVel] [unused for NWindVel=0]
87.6, 87.6, 87.6, 87.6 WsindVelZ     - List of coordinates in the Z direction
    for wind output (m) [1 to NWindVel] [unused for NWindVel=0]
 OutList The next line(s) contains a list of output parameters.  See
    OutListParameters.xlsx for a listing of available output channels (quoted
    string)
"RtPosXT1"
"RtPosYT1"
"YawErrT1"
"YawErrT2"
"YawErrT3"
"YawErrT4"
"RtVAmbT1"
"RtVAmbT2"
"W1VAmbX, W1VAmbY, W1VAmbZ"
"W2VAmbX, W2VAmbY, W2VAmbZ"
"W3VAmbX, W3VAmbY, W3VAmbZ"
"W4VAmbX, W4VAmbY, W4VAmbZ"
"W1VDisX, W1VDisY, W1VDisZ"
"W2VDisX, W2VDisY, W2VDisZ"
"W3VDisX, W3VDisY, W3VDisZ"
"W4VDisX, W4VDisY, W4VDisZ"
END
---------------------------------------------------------------------------------------
```

D.2 FAST.Farm InflowWind File

```
------- InflowWind v3.01.* INPUT FILE
    ------------------------------------------------------------------------
IEA 15 MW Offshore Reference Turbine
---------------------------------------------------------------------------------------

False                   Echo        - Echo input data to <RootName>.ech (flag)
3                       WindType    - switch for wind file type (1=steady; 2=
    uniform; 3=binary TurbSim FF; 4=binary Bladed-style FF; 5=HAWC format; 6=
    User defined; 7=native Bladed FF)
0.0                     PropagationDir - Direction of wind propagation (
    meteoroligical rotation from aligned with X (positive rotates towards -Y)
    -- degrees)
0.0                     VFlowAng    - Upflow angle (degrees) (not used for
    native Bladed format WindType=7)
False                   VelInterpCubic - Use cubic interpolation for velocity
    in time (false=linear, true=cubic) [Used with WindType=2,3,4,5,7]
1                       NWindVel    - Number of points to output the wind
    velocity    (0 to 9)
0.0                     WindVxiList - List of coordinates in the inertial X
    direction (m)
0.0                     WindVyiList - List of coordinates in the inertial Y
    direction (m)
```

```
150.0                   WindVziList - List of coordinates in the inertial Z
    direction (m)
================== Parameters for Steady Wind Conditions [used only for
    WindType = 1] ========================
10.0                    HWindSpeed  - Horizontal windspeed
          (m/s)
150.0                   RefHt       - Reference height for horizontal wind
    speed      (m)
0.12                    PLexp       - Power law exponent
          (-)
================== Parameters for Uniform wind file   [used only for WindType
    = 2] ============================
"none"                  Filename_Uni - Filename of time series data for uniform
     wind field.      (-)
150.0                   RefHt_Uni   - Reference height for horizontal wind
    speed                 (m)
240.0                   RefLength   - Reference length for linear horizontal
    and vertical sheer (-)
================== Parameters for Binary TurbSim Full-Field files   [used only
     for WindType = 3] ==============
"WindData"                  FileName_BTS - Name of the Full field wind file to
    use (.bts)
================== Parameters for Binary Bladed-style Full-Field files   [used
     only for WindType = 4] =========
"none"                  FilenameRoot - Rootname of the full-field wind file to
    use (.wnd, .sum)
False                   TowerFile   - Have tower file (.twr) (flag)
==================  Parameters for HAWC-format binary files  [Only used with
    WindType = 5] =====================
"none"                  FileName_u  - name of the file containing the u-
    component fluctuating wind (.bin)
"none"                  FileName_v  - name of the file containing the v-
    component fluctuating wind (.bin)
"none"                  FileName_w  - name of the file containing the w-
    component fluctuating wind (.bin)
64                      nx          - number of grids in the x direction (in
    the 3 files above) (-)
32                      ny          - number of grids in the y direction (in
    the 3 files above) (-)
32                      nz          - number of grids in the z direction (in
    the 3 files above) (-)
16.0                    dx          - distance (in meters) between points in
    the x direction    (m)
3.0                     dy          - distance (in meters) between points in
    the y direction    (m)
3.0                     dz          - distance (in meters) between points in
    the z direction    (m)
150.0                   RefHt_Hawc  - reference height; the height (in meters)
    of the vertical center of the grid (m)
-------------   Scaling parameters for turbulence
    ---------------------------------------------------------
2                       ScaleMethod - Turbulence scaling method   [0 = none, 1
    = direct scaling, 2 = calculate scaling factor based on a desired standard
     deviation]
1.0                     SFx         - Turbulence scaling factor for the x
    direction (-)   [ScaleMethod=1]
1.0                     SFy         - Turbulence scaling factor for the y
    direction (-)   [ScaleMethod=1]
1.0                     SFz         - Turbulence scaling factor for the z
    direction (-)   [ScaleMethod=1]
1.2                     SigmaFx     - Turbulence standard deviation to
    calculate scaling from in x direction (m/s)    [ScaleMethod=2]
0.8                     SigmaFy     - Turbulence standard deviation to
    calculate scaling from in y direction (m/s)    [ScaleMethod=2]
0.2                     SigmaFz     - Turbulence standard deviation to
    calculate scaling from in z direction (m/s)    [ScaleMethod=2]
```

```
-------------   Mean wind profile parameters (added to HAWC-format files)
    ---------------------------------
12.0                    URef        - Mean u-component wind speed at the
    reference height (m/s)
2                       WindProfile - Wind profile type (0=constant;1=
    logarithmic,2=power law)
0.2                     PLExp_Hawc  - Power law exponent (-) (used for PL wind
    profile type only)
0.03                    Z0          - Surface roughness length (m) (used for LG
     wind profile type only)
0                       XOffset     - Initial offset in +x direction (shift of
    wind box) (-)
================== LIDAR Parameters
    ================================================================================

0                       SensorType          - Switch for lidar configuration (0
     = None, 1 = Single Point Beam(s), 2 = Continuous, 3 = Pulsed)
0                       NumPulseGate        - Number of lidar measurement gates
     (used when SensorType = 3)
30                      PulseSpacing        - Distance between range gates (m)
    (used when SensorType = 3)
0                       NumBeam             - Number of lidar measurement beams
     (0-5)(used when SensorType = 1)
-200                    FocalDistanceX      - Focal distance co-ordinates of
    the lidar beam in the x direction (relative to hub height) (only first
    coordinate used for SensorType 2 and 3) (m)
0                       FocalDistanceY      - Focal distance co-ordinates of
    the lidar beam in the y direction (relative to hub height) (only first
    coordinate used for SensorType 2 and 3) (m)
0                       FocalDistanceZ      - Focal distance co-ordinates of
    the lidar beam in the z direction (relative to hub height) (only first
    coordinate used for SensorType 2 and 3) (m)
0.0 0.0 0.0             RotorApexOffsetPos  - Offset of the lidar from hub
    height (m)
17                      URefLid             - Reference average wind speed for
    the lidar[m/s]
0.25                    MeasurementInterval - Time between each measurement [s]
False                   LidRadialVel        - TRUE => return radial component,
    FALSE => return 'x' direction estimate
1                       ConsiderHubMotion   - Flag whether to consider the hub
    motion's impact on Lidar measurements
====================== OUTPUT
    ==================================================
False                   SumPrint    - Print summary data to <RootName>.IfW.sum
    (flag)
OutList      - The next line(s) contains a list of output parameters.  See
    OutListParameters.xlsx for a listing of available output channels, (-)
Wind1VelX
Wind1VelY
Wind1VelZ
WindDiskVelX
Wind1AngXY
WindHubVelX
WindHubVelY

END of input file (the word "END" must appear in the first 3 columns of this
    last OutList line)
---------------------------------------------------------------------------------------
```

E

Turbulence Intensity Models

The IEC 61400-1 standard [9] recommends two alternative models for calculating the turbulence intensity under normal wind conditions. In both of these models, the turbulence intensity is assumed to be distributed according to a Weibull distribution parameterized by the hub-height mean wind speed (U_{hub}) and the reference turbulence intensity (I_{ref}) as given by Equation E.1. The first alternative suggested by the IEC is to calculate the turbulence intensity as the 90th percentile of this distribution using Equation E.2. This model is referred to as the 90th Percentile Normal Turbulence Model (NTM) in this report. Alternatively, the IEC suggests directly sampling the turbulence intensity value from the Weibull distribution. This approach is referred to as the Distribution NTM in this report.

$$f(I) = \frac{kU_{hub}^{k}}{a}\left(\frac{I}{a}\right)^{k-1} e^{-\left(\frac{U_{hub}I}{a}\right)^{k}} \tag{E.1}$$

where:

$k = 0.27U_{hub} + 1.4$ is the shape parameter

$a = I_{ref}(0.75U_{hub} + 3.3)$ is the scale parameter

$$I = I_{ref}\frac{0.75U_{hub} + 5.6}{U_{hub}} \tag{E.2}$$

To better illustrate the application of these two models in this thesis, first consider Figure E.1, which shows the Weibull distribution $U_{hub} = 10.9$ m/s and for different values of I_{ref}. In the load catalogue of this thesis, both of these parameters are considered as independent input parameters defining the working Weibull distribution for each load calculation run. For each of these runs, the 12 seeds of Section A.4 are employed to sample 12 turbulence intensity values from this Weibull distribution as illustrated in Figure E.2 for $U_{hub} = 10.9$ m/s and $I_{ref} = 12\%$. These values are then used to calculate the DEL corresponding to the Distribution NTM. On the other hand, the 90th percentile value of this same distribution (shown in Figure E.2) is used to compute the DEL corresponding to the 90th Percentile NTM. This process is then repeated for each combination of U_{hub} and I_{ref} in the load catalogue.

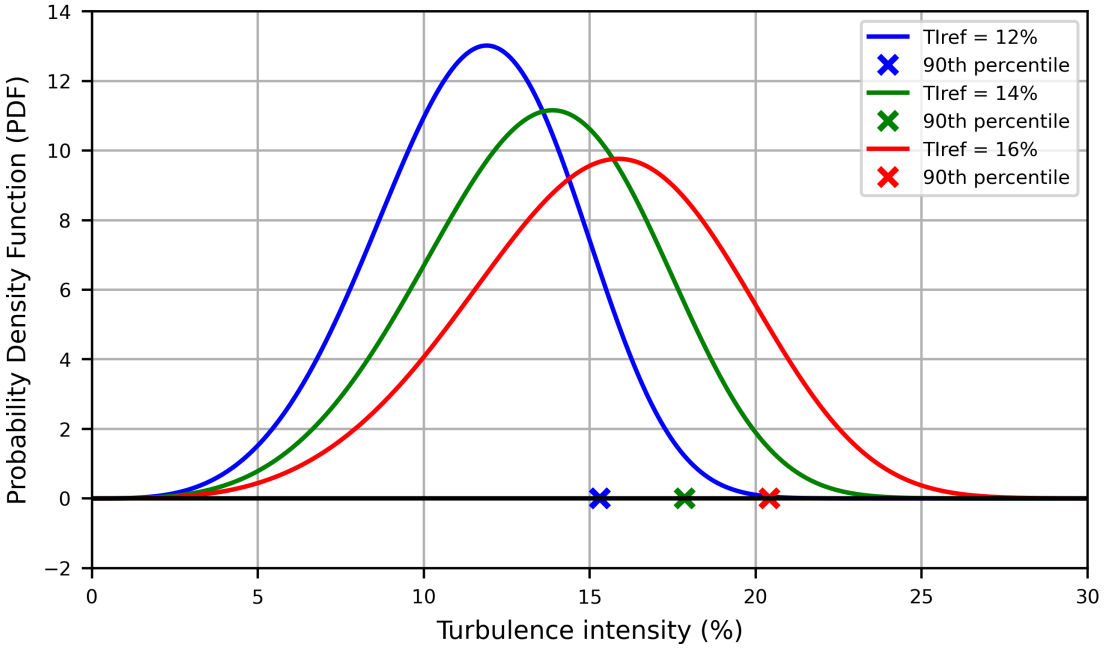

Figure E.1: Weibull distribution for turbulence intensity for $U_{hub} = 10.9$ m/s and for different values of I_{ref}

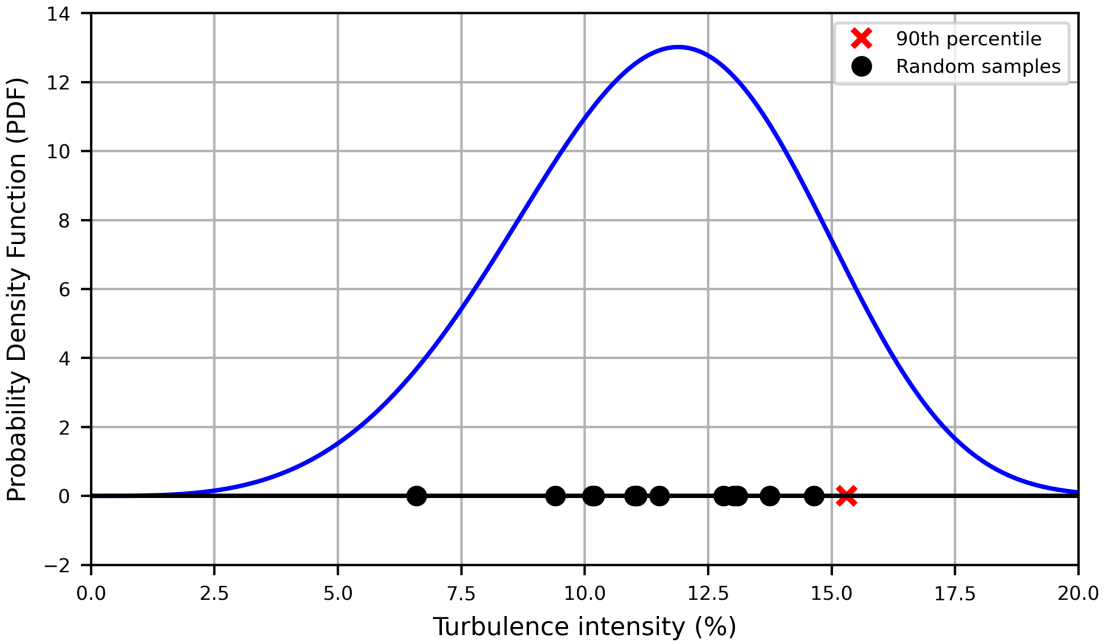

Figure E.2: Weibull Distribution for $U_{hub} = 10.9$ m/s and $I_{ref} = 12\%$ with 90th percentile and 12 random samples